Universidade de Lisboa

Faculdade de Farmácia

Departamento de Bioquímica e Biologia Humana


# Biological membranes – biophysical properties and aquaporin function

*Ana Paula Cavaco da Silva Martins*

Tese orientada pela Professora Doutora Graça Soveral e co-orientada pela Professora Doutora Catarina Prista, elaborada para a obtenção do grau de Doutor em Farmácia, especialidade em Bioquímica.

# Biological membranes – biophysical properties and aquaporin function

# Membranas biológicas – propriedades biofísicas e função das aquaporinas

Dissertação apresentada à Faculdade de Farmácia da Universidade de Lisboa para obtenção do grau de Doutor em Farmácia (especialidade de Bioquímica)

*Ana Paula Cavaco da Silva Martins*

Lisboa

2014

## SUPERVISÃO

Supervisor: Prof. Dr. Graça Soveral

Co-supervisor: Prof. Dr. Catarina Prista

## INSTITUIÇÕES PARTICIPANTES

The studies presented in this thesis were performed at the:

- Research Institute for Medicines (iMed.ULisboa) and Department of Biochemistry and Human Biology, Faculty of Pharmacy, University of Lisbon, Lisbon, Portugal and Requimte, FCT-UNL, 2829-516 Caparica, Portugal, under the supervision of Prof. Dr. Graça Soveral.

- Centro de Botânica Aplicada à Agricultura (CBAA); Laboratório de Bioenergética Microbiana, Instituto Superior de Agronomia, Universidade de Lisboa, Lisboa, Portugal, under the supervision of Prof. Dr. Catarina Prista.

## FINANCIAMENTO

This work was supported by Fundação para a Ciência e Tecnologia, Portugal (SFRH/BD/65046/2009).

## CONTRIBUTO PESSOAL NOS TRABALHOS DE INVESTIGAÇÃO APRESENTADOS NESTA DISSERTAÇÃO

De acordo com o disposto no ponto 1 do artigo nº41 do Regulamento de Estudos Pós-Graduados da Universidade de Lisboa, deliberação nº93/2006, publicada em Diário da República – II série nº153 – 5 de Julho de 2003, a autora desta dissertação declara que participou na concepção e execução do trabalho experimental, interpretação dos resultados obtidos e redação dos manuscritos.

*Aos meus filhos, pais e avó*

# LIST OF ORIGINAL PUBLICATIONS

This thesis is based on the following original publications:

1. Martins AP, Lopes PA, Martins SV, Madeira A, Santos NC, Prates JA, Moura TF, Soveral G. ***Conjugated linoleic acid reduces permeability and fluidity of adipose plasma membranes from obese Zucker rats***. Biochem Biophys Res Commun. 2010 Jul 23;398(2):199-204.
doi: 10.1016/j.bbrc.2010.06.059.

2. Martins AP, Lopes PA, Costa AS, Martins SV, Santos NC, Prates JA, Moura TF, Soveral G. ***Differential mesenteric fat deposition in bovines fed on silage or concentrate is independent of glycerol membrane permeability.*** Animal. 2011 Dec;5(12):1949-56.
doi: 10.1017/S1751731111001091.

3. Martins AP, Lopes PA, Madeira MS, Martins SV, Santos NC, Moura TF, Prates JA, Soveral G. ***Differences in lipid deposition and adipose membrane biophysical properties from lean and obese pigs under dietary protein restriction***. Biochem Biophys Res Commun. 2012 Jun 22;423(1):170-5.
doi: 10.1016/j.bbrc.2012.05.108.

4. Martins AP, Marrone A, Ciancetta A, Galán Cobo A, Echevarría M, Moura TF, Re N, Casini A, Soveral G. ***Targeting aquaporin function: potent inhibition of aquaglyceroporin-3 by a gold-based compound***. PLoS One. 2012;7(5):e37435.
doi: 10.1371/journal.pone.0037435.

5. Martins AP, Ciancetta A, de Almeida A, Marrone A, Re N, Soveral G, Casini A. ***Aquaporin inhibition by gold(III) compounds: new insights***. ChemMedChem. 2013 Jul;8(7):1086-92.
doi: 10.1002/cmdc.201300107.

6. Sabir F, Leandro MJ, Martins AP, Loureiro-Dias MC, Moura TF, Soveral G, Prista C. ***Exploring three PIPs and three TIPs of grapevine for transport of water and atypical substrates through heterologous expression in aqy-null yeast***. PLoS One. 2014 Aug 11;9(8):e102087.
doi: 10.1371/journal.pone.0102087.

7. Noronha H, Agasse A, Martins AP, Berny MC, Gomes D, Zarrouk O, Thiebaud P, Delrot S, Soveral G, Chaumont F, Gerós H. ***The grape aquaporin VvSIP1 transports water across the ER membrane.*** J Exp Bot. 2014 Mar;65(4):981-93.
doi: 10.1093/jxb/ert448.

Other publications

Soveral G, Martins AP, Martins SV, Lopes PA, Alfaia CM, Prates JA, Moura TF. ***Effect of dietary conjugated linoleic acid isomers on water and glycerol permeability of kidney membranes.*** Biochem Biophys Res Commun. 2009 May 22;383(1):108-12.
doi: 10.1016/j.bbrc.2009.03.136.

Abreu-Rodríguez I, Sánchez Silva R, Martins AP, Soveral G, Toledo-Aral JJ, López-Barneo J, Echevarría M. ***Functional and transcriptional induction of aquaporin-1 gene by hypoxia; analysis of promoter and role of Hif-1α.*** PLoS One. 2011;6(12):e28385.
doi: 10.1371/journal.pone.0028385.

# TABLE OF CONTENTS

# ABBREVIATIONS

| | |
|---|---|
| AQP | Aquaporin |
| CLA | Conjugated linoleic acid |
| DHA | Docosahexaenoic acid (22:6*n-3*) |
| DMPC | 1,2-dimiristoyl-sn-3-phosphocholine |
| EPA | Eicosapentaenoic acid (20:5*n-3*) |
| FA | Fatty acid |
| FFA | Free fatty acids |
| LA | Linoleic acid |
| MUFA | Monounsaturated fatty acids |
| OA | Oleic acid |
| PUFA | Polyunsaturated fatty acids |
| RBC | Red blood cells |
| RPD | Reduced protein diet |
| SFA | Saturated fatty acids |

# ABSTRACT

# ABSTRACT

Membranes are barriers that assure the selective communication of the internal media with the external environment, a process that is crucial for life. Membrane components, lipids and proteins, are the main players responsible for the membrane selective permeability and its regulation. The work presented in this thesis encompasses different aspects of biological membranes features.

The first part of this thesis is dedicated to the study of the influence of dietary lipids in membrane biophysical properties, namely fluidity and permeability. We used animal models and designed experiments where the effect of the diet supplementation with fatty acids, PUFA and the conjugated linoleic acid (CLA) on membrane composition, fluidity and permeability, were analysed. In addition, since the animal genetic background is known to have an important contribution to the regulation of several biochemical pathways and resulting in different phenotypes, this variable was included in the study.

Within the same animal species all adipose membranes were found richer in SFA independently of their genetic background or diet. The lipid adipose membrane composition of Zucker rats is highly dependent on the lipid composition of the diet. Regarding the adipose membrane biophysical properties, we were able to correlate a decrease in membrane fluidity and the concomitant decrease on permeability to water and glycerol with the incorporation of t10,c12 CLA isomer into adipose membranes of Zucker rats. Interestingly, this CLA isomer is the one with suggested fat lowering properties in several animal studies. The animal genetic background in obese pigs was also found to play a determinant role on the fluidity of adipose membranes, in accordance with the reported for a wide variety of cell membranes from obese mice and rats. Interestingly, the same increase in membrane fluidity was observed for pigs fed a low protein diet and was correlated with the ratio oleic /linoleic acid. A similar effect was consistently reported in adipose membranes of genetically obese mice pointing to a clear compensatory mechanism to maintain membrane biophysical properties.

The second part of this thesis is dedicated to the study of membrane protein channels, aquaporins, aiming at identifying new modulators with potential pharmacological use. Furthermore, building an experimental cell model able to characterize individual aquaporin activity and selectivity as well as to validate modulators' effect and potency was another goal of this work.

Using the human erythrocyte that expresses one orthodox aquaporin (AQP1) and one aquaglyceroporin (AQP3), we reported on the potent and selective inhibition of human AQP3 by a water-soluble gold(III) coordination compound, Auphen.

From molecular modelling studies and docking approaches, we were able to propose a mechanism of action of Auphen for human AQP3 inhibition, where Cys40 is the crucial residue for binding. Inhibitory assays with other metal complexes, namely phenantroline derivatives of Pt(II) and Cu(II), showed that the AQP3 inhibition potency decreased drastically in the order Au(III) > Cu(II) >> Pt(II). Interestingly, no inhibition effect was achieved when incubating the cells with gold(I) compounds, therefore,

demonstrating the necessity of gold(III)-based scaffolds to achieve protein binding and blockage of the channel. Our mechanistic hypothesis was based on the possibility for Auphen and analogues to bind to certain amino acid residues in the channel close to the selectivity filter domains, thus acting as a “cork” preventing the passage of glycerol.

Given the diversity of pathologies associated with dysfunction of the different aquaporins, these proteins are now emergent drug targets. However, cells and tissues frequently express more than one aquaporin isoform in the plasma membrane and unless a specific isoform is mutated or overexpressed, its function is not easily discriminated. To overcome this difficulty, we developed a yeast heterologous system for expression and functional assessment of aquaporin isoforms. Such a cell system expressing individual AQPs would also be very useful for analysis of function and regulation of aquaporins from the plant kingdom. Plants express numerous aquaporin isoforms, but for most their physiological relevance is still unclear.

Using this approach, grapevine aquaporins VvPIPs, VvTIPs and VvSIPs were expressed in yeast and functionally analysed. We demonstrated that only some isoforms are functional while others are not, and they may transport other small molecules of physiological importance such as ammonia, boron, $CO_2$, hydrogen peroxide and urea. In particular for VvSIP1, we disclosed for the first time its ability to transport water but not glycerol, urea, sorbitol, glucose, or inositol.

SUMÁRIO

# SUMÁRIO

As membranas biológicas comportam-se como barreiras que asseguram a comunicação seletiva do meio interno com o ambiente externo, um processo que é crucial à vida. Os componentes membranares, lípidos e proteínas, são os principais responsáveis pela permeabilidade seletiva das membranas e sua regulação. O estudo apresentado nesta tese abrange diferentes aspetos característicos das membranas biológicas.

A primeira parte desta tese foi dedicada ao estudo da influência dos lípidos da dieta nas propriedades biofísicas das membranas, em particular fluidez e permeabilidade. Foram utilizados modelos animais e concebidos ensaios experimentais onde se analisou o efeito da suplementação da dieta em ácidos gordos, PUFA e ácido linoleico conjugado CLA, na composição lipídica, fluidez e permeabilidade das membranas do tecido adiposo. Ainda, uma vez que a herança genética tem uma contribuição importante para a regulação de vários processos metabólicos resultando em fenótipos diversos, esta variável também foi incluída neste estudo.

Na mesma espécie animal, as membranas de tecido adiposo são mais ricas em ácidos gordos saturados independentemente da sua raça ou dieta. A composição lipídica das membranas de tecido adiposo de ratos Zucker é muito dependente da composição lipídica da dieta. Relativamente às propriedades biofísicas, foi possível correlacionar um decréscimo da fluidez da membrana e concomitante decréscimo da permeabilidade à água e ao glicerol com a incorporação do isómero de CLA t10,c12 nas membranas do tecido adiposo de ratos Zucker. Curiosamente, em diversos estudos animais têm sido atribuídas propriedades de emagrecimento a este isómero CLA.

A herança genética (raça) também tem um papel importante na fluidez das membranas do tecido adiposo, em concordância com o já descrito em vários estudos em membranas celulares de ratinhos e ratos obesos. Também se verificou um aumento da fluidez membranar em porcos alimentados com restrição proteica, o que foi correlacionado com a razão dos ácidos oleico/ linoleico. Um efeito semelhante foi já reportado para membranas de tecido adiposo de ratinhos geneticamente obesos, apontando para um mecanismo compensatório que leva à manutenção das propriedades biofísicas das membranas.

A segunda parte desta tese foi dedicada ao estudo de canais proteicos membranares, as aquaporinas, com o objetivo de identificar novos moduladores com potencial utilização farmacológica. Ainda, pretendemos desenvolver um modelo experimental para a caracterização individual da atividade e seletividade de aquaporinas e para a validação do efeito e da potência de moduladores.

Utilizando eritrócitos humanos que expressam uma aquaporina ortodoxa (AQP1) e uma aquagliceroporina (AQP3), descrevemos a forte inibição seletiva da AQP3 por um composto de coordenação de ouro(III) hidrossolúvel, o Auphen.

Através de estudos de modelação molecular e de *docking*, foi possível propor um mecanismo de ação do Auphen para a inibição da AQP3 onde o resíduo de cisteína cys40 é crucial para a ligação.

Os ensaios de inibição com outros complexos metálicos, nomeadamente derivados da fenantrolina de Pt(II) e de Cu(II), revelaram que a inibição decresce drasticamente na ordem Au(III) > Cu(II) >> Pt(II). Curiosamente, não se observou inibição quando as células foram incubadas com compostos de gold(I), demonstrando assim a importância dos esqueletos dos compostos de gold(III) para a ligação à proteína e bloqueio do canal. Assim, a nossa hipótese de mecanismo é baseada na possibilidade do Auphen e análogos se ligarem a certos resíduos de aminoácidos no canal, perto do filtro de seletividade, atuando deste modo "como uma rolha" que impede a passagem do glicerol.

Devido á diversidade de patologias relacionadas com a disfunção de diferentes aquaporinas, estas proteínas são atualmente consideradas alvos terapêuticos. Contudo, na membrana plasmática das células e tecidos é frequentemente expressa mais do que uma isoforma de aquaporina, pelo que a sua função não é facilmente discriminada a não ser que essa isoforma específica seja mutada ou sobre-expressa. Para ultrapassar esta dificuldade, foi desenvolvido um sistema de expressão heteróloga em leveduras para a expressão e análise funcional de aquaporinas. Tal sistema também é muito útil para a análise da função e regulação de aquaporinas do reino vegetal. As plantas expressam numerosas isoformas de aquaporinas mas na maior parte dos casos, a sua relevância fisiológica ainda não foi estabelecida.

Utilizando esta abordagem, as aquaporinas de uva VvPIPs, VvTIPs e VvSIPs foram expressas em leveduras e a sua função foi analisada. Foi demonstrado que somente algumas isoformas são funcionais, e que algumas podem estar envolvidas no transporte de outras moléculas com importância fisiológica tais como amónia, boro, $CO_2$, peróxido de hidrogénio e ureia. Em particular para a VvSIP1, foi pela primeira vez revelada a sua capacidade para transportar água mas não glicerol, ureia, sorbitol, glucose ou inositol.

# GENERAL AIMS AND THESIS OUTLINE

# GENERAL AIMS AND THESIS OUTLINE

The plasma membrane is the boundary of the cell, separating its content from the environment. This semipermeable membrane is composed of a lipid-bilayer where thousands of different lipid molecules interact dynamically, forming transient or stable structures used by many proteins as platforms for their activity and to enhance their interactions with other proteins. One fundamental cell membrane function is to quickly respond to intra and extracellular events, accomplishing transmembrane fluxes fundamental to the physiology of all living organisms.

Water is the major component of all living organisms. The controlled flow of water through biological membranes not only plays a key role in cellular homeostasis but also contributes to cell survival. Triggered by osmotic and/or pressure gradients, water crosses the membrane both through the lipid-bilayer and specialized membrane channels called aquaporins (AQP), which facilitate highly selective and efficient flow of water and, in some cases, other small solutes such as glycerol and urea.

This work is focused in the study of membrane characteristics that affect the permeability of water or small uncharged solutes such as glycerol. Within this scope, membrane biophysical properties modulated by lipid membrane composition and by the activity of aquaporin channels play a central role.

This work is divided in two parts, Part I (containing chapter 1) and Part II (containing chapter 2 and 3).

The **first part** is dedicated to study the influence of genetic background and diet composition on adipocyte membrane composition and its outcome on membrane biophysical properties such as fluidity and permeability to water and glycerol.

It is known that dietary fatty acids incorporate into cell membrane phospholipids. The health beneficial effects attributed to dietary compounds such as polyunsaturated fatty acids (PUFA) are vast. Examples are their protective effects on hypertension, cardiovascular diseases, and cancer, among others [1]. Albeit several candidate mechanisms have been suggested, the means by which they elicit their effects remain largely unknown. In view of the broad range of effects attributed to these compounds, it is expected that, at least in part, they act at some fundamental cellular level common to all organism.

Our previous results [2] have shown that kidney plasma membranes from Wistar rats, fed with palm oil-based diets supplemented with conjugated linoleic acid (considered a fat lowering fatty acid ), showed altered membrane permeability, an effect that was correlated with the incorporation of this fatty acid into the plasma membrane. With this starting point, this work aims at further understanding the effects of fatty acids and food components on cell membranes and their outcome on membrane composition and biophysical properties such as permeability and fluidity.

In **chapter 1** we present 3 publications where we studied the influence of dietary lipids, protein restriction conditions and genetic background on adipocyte membrane composition and its outcome on membrane biophysical properties such as fluidity and permeability to water and glycerol (publications 1, 2 and 3).

The **second part** is divided in two chapters (chapters 2 and 3) in which human and plant aquaporins were studied.

AQPs are a family of small transmembrane proteins ubiquitous in nature. These proteins form highly selective channels for water and, in the case of the sub-family aquaglyceroporins, other small solutes such as glycerol and urea.

In **chapter 2**, human aquaporins were investigated regarding the screening for specific inhibitors.

Thirteen different mammalian AQPs have been identified so far, present in almost all organs and tissues. It is clear that they play fundamental roles in human physiology and pathophysiology, their dysfunction or aberrant expression is correlated with several diseases such as kidney diseases, brain oedema, obesity and cancer[3]. Numerous reports have highlighted the possible areas where AQP modulators could be useful in treating human diseases. Yet, only a few pharmaceutically relevant compounds have been identified to date and none of them proved to be suitable for clinical trials.

Using a screening system based on permeability assays of human red blood cells (RBC), we investigated modulators of aquaporin activity (publications 4 and 5).

In **chapter 3**, the activity of different isoforms of plant aquaporins natively located in plasma membrane and in intracellular membranes of grapevine, was characterized. To assess their individual activity and contribution to membrane permeability, we used a yeast heterologous expression model that was optimized for the expression and functional analysis of aquaporins and is now suitable to be used as inhibitor screening system (publications 6 and 7).

# PART I – Lipid Bilayer, biophysical properties

# INTRODUCTION

The plasma membrane represents the barrier of life, the structure that separates the cells from their surroundings. This semipermeable membrane is composed of a lipid-bilayer embedded with proteins accomplishing fundamental processes central to the physiology of the cell. In this context, the lipid composition of the cell membrane and the transporters within, play a central role. Part I will deal with the bilayer composition of the membrane and its biophysical properties.

## The Lipid-Bilayer

This part of the work aimed at studying plasma membrane lipid composition and its outcome in biophysical properties such as fluidity and permeability to water and different solutes in response to different dietary compositions, namely, fatty acids (FA) content and protein restriction.

## 1. Composition and properties of the lipid-bilayer.

Biological membranes have a similar general organisation in sheet-like structures, composed of a heterogeneous and asymmetric lipid-bilayer firmly established as the universal basis for cell-membrane function. Herein, thousands of different lipid molecules interact dynamically, forming transient or stable structures used by many proteins as platforms for their activity and to enhance their interactions with other proteins[4,5].

Membrane lipids are divided in three classes of amphipathic lipids: phospholipids, glycolipids, and sterols. The amount of each amphipathic lipid depends upon the type of cell, but in the majority of cases phospholipids are the most abundant, while glycolipids are found exclusively in the outer layer of the membrane. Cholesterol is also abundant in eukaryotic cell membranes - up to one molecule for every phospholipid molecule.

Phospholipids and glycolipids share a similar structure containing a hydrophilic headgroup and one or two hydrophobic tails. Phospholipids are derived from either glycerol (phosphorglycerides) or sphingosine (sphingolipid), having the following components: a glycerol or sphingosine backbone, two or one FA chains, a phosphate group and (usually) an alcohol (e.g. choline, ethanolamine, inositol) (Figure 1). The FA tails can differ in length (containing normally between 14 and 24 carbon atoms) and may be saturated or unsaturated. The number of double bonds present in their hydrocarbon chains can vary from none, saturated fatty acid (SFA), one, monounsaturated fatty acid (MUFA) to several, polyunsaturated fatty acid (PUFA).

Each double bond creates a small bend in the tail. Differences in the length and saturation degree of the FA tails influence their ability to pack against one another, thereby affecting the fluidity and other biophysical properties of the membrane[6].

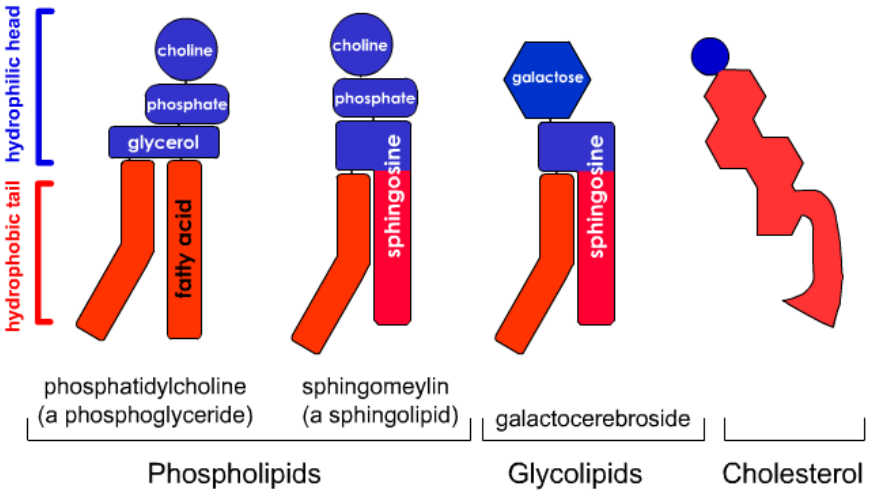


*Figure 1 – **Schematic drawing of common membrane lipids**.*

The variety of headgroups and aliphatic chains allows the existence of more than 1000 different lipid species in any eukaryotic cell[7]. This diversity is only beginning to be characterized while lipidomics is becoming an important tool in cell and developmental biology, molecular medicine and nutrition[8]. The membrane composition differs throughout inner and outer sheets of lipid bilayer, cell organelles and cell type[7] The assortment of lipid species allows to adapt the lipid composition of membranes to fulfil specific functions. How the organism regulates lipid composition and the exact mechanisms of how compositional complexity affects cell homeostasis and its regulation remains poorly understood[8].

The effect of lipid composition on biological membranes points to an extensive list of perturbations induced on membrane lipid structure including changes in membrane fluidity, phase behaviour, permeability, membrane fusion, lateral pressure and flip-flop dynamics[7,5]. In this manner FAs influence the membrane function at several levels including membrane microdomain organization, membrane proteins activity, cell signalling and ultimately human health[5].

## 1.1. The fluidity of a lipid-bilayer depends on lipid composition.

Three main factors, besides temperature and the head group of membrane lipids, contribute to membrane fluidity: membrane lipid tail length, the degree of unsaturation of lipid tails and the amount of cholesterol.

The tail length affects fluidity as lipids with longer tails exhibit more friction when moving around in the membrane. In other words, the longer the tails, the higher the attractive van der Waals forces between them. As a result, membranes with longer lipid tails tend to be less fluid.

The average degree of unsaturation of lipid tails also affects membrane fluidity, as unsaturated tails do not pack as tight as saturated ones, therefore increasing membrane fluidity.

Cholesterol molecules contribute to membrane fluidity enhancing the permeability-barrier properties of the lipid bilayer. They orient themselves in the bilayer

with their hydroxyl group close to the polar head groups of the phospholipid molecules. In this position, their rigid, plate-like steroid rings interact with, and partly immobilize, those regions of the hydrocarbon chains closest to the polar head groups (Figure 2). By decreasing the mobility of the first few $CH_2$ groups of the hydrocarbon chains of the phospholipid molecules, cholesterol makes the bilayer less deformable in this region and thereby decreases its permeability. Although cholesterol tends to make lipid bilayers less fluid, at the high concentrations found in most eukaryotic plasma membranes it also prevents the hydrocarbon chains from coming together and crystallizing. In this way, it inhibits possible phase transitions[6].

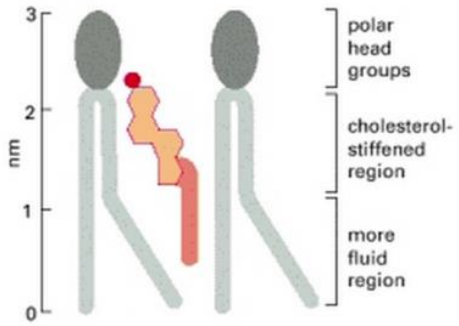


*Figure 2 - **Schematic drawing of a cholesterol molecule interacting with two phospholipid molecules.***

Cholesterol and length and unsaturation degree of fatty acyl chains are not the only players regarding membrane fluidity. The head group of phospholipids also influences membrane behaviour. For example, choline is a bulky headgroup causing phosphatidylcholine (PC) to have a cylindrical molecular geometry. In contrast, ethanolamine is a smaller headgroup, with phosphatidylethanolamine (PE) assuming a conical molecular geometry, allowing a tighter packing of the phospholipids. Thus, when the PE/PC ratio increases there is a reduction in membrane fluidity[7].

## 1.2. Effect of fatty acids on membrane permeability, membrane proteins activity and on micro-domain organization.

FAs can influence membrane permeability, an effect that has been associated with disorder in the membranes' interior and the interaction of the incorporated lipid with the polar head group of phospholipids[9]. It is known that at the gel-to-fluid phase transition of 1,2-dimiristoyl-sn-3-phosphocholine (DMPC) bilayers, when the largest number of defects in the lipid matrix appears, membrane permeability reaches its maximum[10]. It has also been demonstrated that the dietary FA, docosahexaenoic acid (DHA) increases permeability more effectively than its metabolic precursor, linoleic acid (LA) or oleic acid (OA)[11]. DHA is incorporated into lipid membranes either as a FFA or as part of a phospholipid and can increase the permeability of phospholipid vesicles and tumour cells[12].

Since integral membrane proteins are surrounded by lipids, they are affected by this adjacent environment. Effects of lipid structure on membrane protein function can

be described either in terms of molecular interactions or in terms of physical properties of the lipid bilayer such as lipid fluidity, membrane tension, etc[13]. For example, it was proposed that FAs perturb the lipid bilayer and disturb the protein-lipid complementarity of the human erythrocyte membrane[14], inducing changes in the morphology of the membrane and its fluidity, leading to changes in the activity of the human erythrocyte membrane sodium pump[15,16]. It has also been shown that sphingomyelinase activity in red blood cells is modified by membrane bending (surface tension)[17], which in turn, is intimately linked with its shape. Curvature-sensing lipids and proteins localize to curved regions where they accumulate introducing a local curvature[18].

Biological membranes are heterogeneous structures organized in domains and microdomains, characterised by different lipid composition. Proteins may alter the lipid organization via protein-lipid interactions influencing the relative distribution of lipids and proteins in the membrane[18]. It's likely that lipid microdomains form, at least in part, as a consequence of the distinct affinities between lipids[5]. One particular type of lipid domain is the lipid raft. Rafts are sphingolipid- and cholesterol-enriched liquid-ordered domains floating in "a sea" of liquid-disordered phospholipids[19,20]. Building on a wide variety of biophysical studies, it was proposed that a dietary FA with important effects in human health, DHA, is incorporated in membrane phospholipids affecting the organization of plasma membranes, inducing changes in raft and non-raft domains[21,22]. DHA is the longest, most unsaturated FA representing an extreme example of dynamical shape, rapidly interchanging between multiple configurations. The high degree of disorder introduced by DHA severely impacts lipid packing and hence membrane physical properties. Moreover, results obtained with model membranes show that DHA and cholesterol push each other away, leading to segregation of DHA containing phospholipids in highly disordered membrane domains[23,24]. These domains are compositionally and organizationally opposite to lipid rafts that are ordered domains predominantly enriched in sphingolipids "glued" by cholesterol. It was hypothesized that DHA-rich domains formed in the plasma membrane are responsible, at least in part, for the diverse range of health benefits associated with DHA by altering cellular biochemical activity, including essential signalling pathways[21,22].

## 1.3. Regulation of membrane lipid composition.

The incorporation of FFA within membranes may occur quite rapidly. They can be detected either as free entities interlaid between the membrane lipids or as part of the membrane phospholipids after undergoing esterification. For example, OA molecules can be detected embedded within the phospholipids of membrane vesicles under 3 minutes[25,26]. Concerning the esterification of FFA, some examples inculde, LA added to culture media is processed through the endoplasmic reticulum and appears in the plasma membranes phospholipids of neuroblastoma cells between 2–10 min after addition[27]. Another example is eicosapentaenoic acid (EPA) that may be detected as part of phospholipids and triacylglycerols in rat liver, brain and heart within 5 min after intravenous infusion[28]. Moreover, the synthetic FFA, 2-hydroxyoleic acid, has also been detected in phospholipids from U118 human glioma cells 2–24 h after incubation with

this lipid, causing a marked remodelling on the cell membrane FA composition. These changes lead to an important modulation of the cell membrane microdomain structure[29].

As referred above, insertion of FA into membranes and their incorporation in more complex molecules enable these acyl chains to induce changes in the structure of lipid bilayers with the concomitant change in their biophysical properties. Yet, regulation of membrane lipids composition with an appropriate balance between SFA, MUFA, and PUFA phospholipids acyl chains is critical for membrane organization and to maintain membrane biophysical properties tuned to optimize cellular function. That composition is regulated by complex mechanisms involving several transcription factors, such as sterol regulatory element binding proteins, whose activity is in turn modulated by sensitive sensory systems in response to changes in lipid levels[30–32].

## 2. Dietary fatty acids.

The presence of FAs In human diet is essential for healthy growth and organism homeostasis inasmuch as FAs have important functions in energetic metabolism, signal transduction, molecular recognition processes and phospholipid membrane formation[7]. Intake of suitable dietary raw materials is a requirement for endogenous synthesis of appropriate lipids, which in turn is critical for the formation of membrane bilayers.

After ingestion and until the incorporation of new lipids into the membranes, FAs face a complex set of processes involving digestion, absorption, transport, storage and metabolizing. During these processes FAs ingested in the diet are subjected to several alterations according to the body necessities. In the body, FAs derived from the diet and from *de novo* lipogenesis can be further elongated (via *elongases*) and unsaturated (via *desaturases*), generating a variety of lipid species that can then provide a specific lipid composition[30]. This variety of lipids is illustrated by the fact that cells use approximately 5% of their genes to synthesize all of these lipids[7]. Thus, dietary FAs may influence membrane composition, although due to this complex set of processes together with membrane composition regulatory mechanisms, substantial changes in diet are often required for relatively small changes in membrane composition[33].

As some FAs (essential FAs) cannot be endogenously synthesized they have to be provided in diet rendering them important dietary components.

### 2.1. Essential fatty acids.

The *n-3* and *n-6* (or omega-3 and 6) FAs are a family of naturally occurring PUFAs (Figure 3). Since *n*-6 and *n*-3 double bonds cannot be inserted into FAs by animal enzymes allowing their endogenous *de novo* synthesis, the simplest members of *n-6* and *n-3* series, linoleic (18:2*n-6*) and α-linolenic (18:3*n-3*) FAs, are considered essential[34]. Symptoms of essential FA deficiency, similar to other essential nutrient deficiencies, have been reported in mammals[35].

In the cell, linoleic and α-linolenic acids are converted to longer chain FAs upon desaturation and elongation giving rise to the *n-3* and *n-6* series[34](Figure 3).

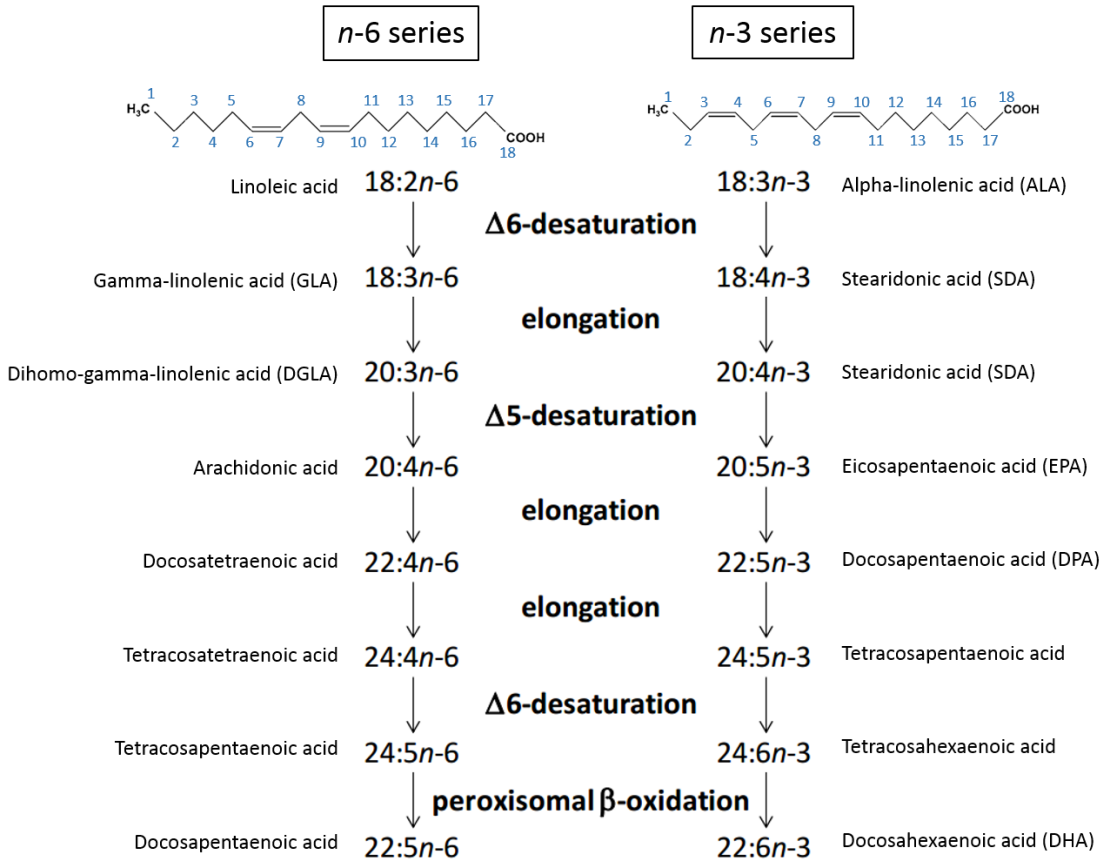


*Figure 3* – Metabolic pathways of essential linoleic (18:2*n-6*) and α-linolenic (18:3*n-3*) fatty acids. Different *n- 3* and *n-6* fatty acids are produced through elongation and desaturation of the essential linoleic and α-linolenic acids, respectively. The addition of double bonds and the elongation of the acyl chains occur in the endoplasmic reticulum, while the final step in the synthesis of the *n-3* DHA and the *n-6* docosopentaenoic acid consists of a single reaction from β-oxidation in the peroxisome. Carbon backbones of linoleic and α-linolenic acids are depicted. Carbons are numbered (in blue) from the first methyl group. Names include: number of carbons : number of double bonds *n*-carbon number of the terminal double bond (i.e. that closest to the methyl end of the hydrocarbon chain).

The PUFAs of the *n-3* and *n-6* series play a significant role in health and disease. Both series are involved in the synthesis of potent modulatory molecules important for inflammatory responses, including eicosanoids (prostaglandins and leukotrienes) and cytokines (interleukins), affecting the gene expression of various bioactive molecules[36,37]. In general, the *n-6* eicosanoids are considered pro-inflammatory while *n-3* are much less so. The *n-6* eicosanoids family of inflammatory mediators is generated from 20 carbon PUFA as the arachidonic acid (20:4*n-6*), liberated from cell membrane phospholipids[37]. Increased consumption of the long chain *n-3* PUFA, such as the EPA (20:5*n-3*) and DHA (22:6*n-3*) acids, decreases the amount of arachidonic acid in cell membranes diminishing arachidonic acid-derived eicosanoids[38].

Since *n-6* and *n-3* PUFAs cannot be synthesised *de novo*, their availability to the composition of cell membranes is ultimately determined by the fraction present in the

diet. Actually, membrane composition was found to be more responsive to *n-6* and *n-3* PUFA levels in the diet and most sensitive to *n-3* PUFA and to the *n-3/n-6* ratio[33,39].

## 2.2. Effect of dietary fatty acids in human health.

A link between diet and disease is being increasingly recognized. Among dietary components, FAs have especially gained recognition in affecting health. The amount and type of FAs consumed are directly involved in the etiology of various diseases. While the ingestion of excessive amounts of SFAs and trans-fatty acids is considered to be a risk factor for cardiovascular diseases, insulin resistance, dyslipidemia, and obesity[1], MUFAs and PUFAs are recommended, for example, for their cardio-protective benefits[40]. In particular, essential FAs from *n-6* and *n-3* series and their derivatives have varied biological actions and seem to be involved in several physiological and pathological processes such as obesity, hypertension, diabetes mellitus, coronary heart disease, schizophrenia, Alzheimer's disease, atherosclerosis, and cancer[41]. For example, numerous studies have shown that high olive oil intake reduces blood pressure; it was proposed that this effect would be caused by its high OA content, increasing OA levels in membranes and thus regulating membrane lipid structure in such a way as to influence the localization and/or activity of signalling proteins involved in hypertension[42,43]. DHA and EPA have also been associated with the prevention of cardiovascular diseases and cancer[44]. Gamma linolenic acid (GLA) (18:3*n-6*), a *n-6* PUFA, has been suggested for potential applications as an anti-inflammatory nutrient or adjuvant[36].

Understanding the mechanisms by which FAs exert their biological effects is important in unravelling the pathogenesis of many disorders, ultimately providing effective preventive measures. Given the large number of processes and health benefits where FAs seem to be involved, it is reasonable to think that they may act at some fundamental level common to the whole organism. Their implications on membrane structure, may explain, at least partially, the modulation exerted by some natural FAs on cell function. In fact there is some evidence that a few metabolic pathologies are related to altered lipid composition. For instance, alterations in the FA composition of membrane phospholipids of human erythrocyte membranes have been linked to obesity and insulin resistance[45]. Another study in rats fed with a diet rich in SFA suggested that intake of the beef tallow diet promotes body fat accumulation by reducing lipolytic activities resulting from lower β-receptor binding and sympathetic activity in adipose tissues. The decreases in β-receptor binding affinities were correlated to changes in membrane fluidity[46].

## 2.3. Conjugated linoleic acid.

Another interesting group of FAs is that formed by the conjugated linoleic acid (CLA). This is a family of 28 naturally occurring isomers of linoleic acid, with 18 carbons and 2 double bonds either on trans or cis configuration. CLA is produced by bio-hydrogenation in ruminants or by bacteria from the gastro-intestinal tract of humans. Although as minor component, consumption of ruminant meat (beef and lamb) and dairy products (milk and cheese) is the main source of dietary CLAs[47]. Where the predominant

isomer formed is cis-9,trans11 (c9,t11) and unlike other trans double bond-containing FAs, it may have beneficial effects on human health[48].

Dietary supplements of CLA have been attracting consumers' interest because of the alleged body fat-lowering effects, together with the perception of a natural compound devoid of harmful effects. These preparations present CLA mostly as a mixture of (c9,t11) and trans-10,cis-12 (t10,c12) isomers (Figure 4).

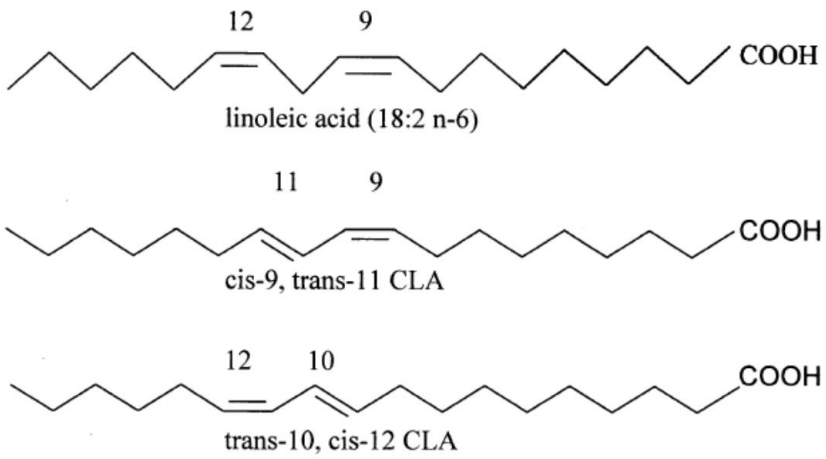


*Figure 4* - Structures of linoleic acid, and CLA isomers (c9,t11) and (t10, c12)

There are several indications that various isoforms might have different biological actions. The c9,t11-isomer was implicated as the active form responsible for the protective effects against tumorigenesis. The t10,c12-isomer seems to be the active form that affects energy metabolism and body fat deposition and composition[49]. Despite numerous studies on CLA their true effect and the mechanism of action in such processes remain unclear[49,50,51,52].

It was reported CLA incorporation into membrane phospholipids of pigs fed with a commercial CLA mixture, where the distribution of CLA isomers in liver phospholipids showed an increase compared to that present in the diet[53].

## 3. Reduced protein diets (RDP).

An equilibrated diet contains 10-15% of the total daily energy provided from protein. Reducing the proportion of protein relative to energy in the diet is known to increase fat deposition. Using pigs as animals models it was shown that plasma cholesterol increased dramatically in lean pigs fed low protein diets[54] and that reduced dietary energy and protein in growing pigs significantly increased intramuscular fat[55], while having a minor effect on the amount of subcutaneous adipose tissue[56,57]. One possible explanation for this effect is that the low protein content restricted muscle growth, resulting in excess energy being converted into intramuscular lipids rather than in endogenous protein synthesis[56].

Since RDP affects FAs deposition in the body it would be interesting to investigate the effect of RDP on membrane composition and biophysical properties.

## 4. Adipose tissue and obesity.

Adipose tissue is a complex organ that regulates and coordinates energy homeostasis. This heterogeneous tissue is primarily composed of adipocytes surrounded by fibroblasts, fibroblastic preadipocytic cells, endothelial cells, nerves and immune cells. Although adipose tissue was originally thought to just be an energy storage site, studies in recent years have revealed that it carries out many key endocrine functions. Indeed, dysfunction of the adipose compartment is central to the pathology associated with metabolic diseases such as obesity, type 2 diabetes, cancer cachexia and lipodystrophies[58].

There are two main types of adipose tissue in mammals, white adipose tissue (WAT) and brown adipose tissue (BAT). Adipocytes from WAT are optimized to store energy and are characterized by containing a large single cytoplasmic lipid droplet and a "squeezed" nucleus. BAT adipocytes dissipate energy for thermogenesis and are characterized by being polygonal cells with a roundish nucleus and several cytoplasmic lipid droplets. Thus, white and brown adipocytes are quite different in their morphology and physiology: white adipocytes store energy for the metabolic needs of the organism, whereas brown adipocytes burn energy for thermogenesis[59]. WAT is the main type of adipose tissue found in adult humans and is distributed throughout the body in subcutaneous regions, surrounding visceral organs and in the face. It is an active endocrine organ that mostly regulates insulin sensitivity, lipid metabolism and satiety[58].

During caloric excess periods, adipocytes readily convert glucose into FAs storing them along with those collected from the extracellular space. During periods of caloric deficit, stored triacylglycerols are hydrolysed to FFAs and glycerol[60], which then leave the cell towards other tissues.

Obesity is characterized by excess body fat, which is predominantly stored in the adipose tissue leading to adipose cells expansion. As adipose cells expand, more phospholipids have to be incorporated into cellular membranes. The specific mechanisms that may lead from obesity towards the higher risk of metabolic complications such as insulin resistance and type 2 diabetes remain elusive. One hypothesis is the adipose tissue expandability that states that adipose tissue has a limited maximal capacity to increase in mass. When the adipose tissue expansion limit is reached, it stops storing lipids appropriately. The excess lipid accumulates in organs such as muscle, liver, and pancreas, causing metabolic disease with insulin resistance[61].

While the idea that lean and very obese people may develop insulin resistance through the same pathogenic paradigm of exhaustion of adipose tissue expandability is controversial[61], it is actually well supported in rodent models; for example, studies in mouse have demonstrated that even in overweight or obese mice, a genetic limit on adipose tissue expansion can exacerbate insulin resistance[62,63]. In humans, lipidomic analyses of adipose tissue of lean and obese (but metabolically healthy) individuals, identified multiple changes in membrane phospholipids. Using computer modeling, it was shown that "lean" and "obese" membrane lipid compositions have the same physical

properties despite their different compositions[64]. These changes in lipid membrane composition were suggested to occur in order to protect the physical properties of the membranes.

The expandability limit is determined on an individual basis by environmental and genetic factors[61]. Since dietary FAs may incorporate into the membranes and/or serve as precursors to other FAs they may also have a role in the expansion capacity of adipocyte cell membranes.

## 5. Genetic background and animal models.

It is well accepted that the genotype influences the metabolism of nutrients in particular lipid metabolism. How the membrane biophysical properties are affected by the genetic background and regulated to match the specific needs of the individual is still obscure.

Considering problems in collecting tissue samples and the multifactorial etiology of obesity in human patients, suitable animal models are essential for a better understanding of the metabolic onset of obesity. Pigs display several anatomical-physiological and metabolic similarities to humans[65]. Additionally, taking advantage of pigs genetic background (fat or lean, genetic or diet induced obesity), pigs are considered a valuable animal model. Zucker rats are also commonly used as a genetic model for human obesity[66]. The fa/fa Zucker rat is a strain of laboratory animal descendent from the wild model rodent Rattus norvegicus[67], used often to study genetic obesity problems. This animal model develops morbid obesity, through the fa/fa mutation in the extracellular domain of the leptin receptor, which inhibits completely leptin action. This leads to an appetite increase promoting severe insulin resistance[68]. The rat is a highly valuable model for the investigation of cardiovascular diseases, metabolic disorders (*e.g.* lipid metabolism, diabetes), cancers, renal dysfunctions, neurologic pathologies, and so many other diseases.

In addition, in these studies we also used bovines that are models for animal production studies. This approach allows investigating the possible correlation of dietary fats with membrane features and possible outcome on meat quality.

## Aim of part I:

The work presented in part I - chapter 1 of this thesis includes publications 1, 2 and 3 that are focused on the study of the influence of genetic background and diet on adipocyte membrane composition and its outcome on membrane biophysical properties such as fluidity and permeability to water and glycerol.

# CHAPTER 1 - Influence of diet on cell membrane composition and biophysical properties

# CHAPTER 1 - Influence of diet on cell membrane composition and biophysical properties

The information contained in this chapter is included in the following original publications:

*Publication1*

Martins AP, Lopes PA, Martins SV, Madeira A, Santos NC, Prates JA, Moura TF, Soveral G.
*Conjugated linoleic acid reduces permeability and fluidity of adipose plasma membranes from obese Zucker rats.*
Biochem Biophys Res Commun. 2010 Jul 23;398(2):199-204.
doi: 10.1016/j.bbrc.2010.06.059.

*Publication 2*

Martins AP, Lopes PA, Costa AS, Martins SV, Santos NC, Prates JA, Moura TF, Soveral G.
*Differential mesenteric fat deposition in bovines fed on silage or concentrate is independent of glycerol membrane permeability.*
Animal. 2011 Dec;5(12):1949-56.
doi: 10.1017/S1751731111001091.

*Publication 3*

Martins AP, Lopes PA, Madeira MS, Martins SV, Santos NC, Moura TF, Prates JA, Soveral G.
*Differences in lipid deposition and adipose membrane biophysical properties from lean and obese pigs under dietary protein restriction.*
Biochem Biophys Res Commun. 2012 Jun 22;423(1):170-5.
doi: 10.1016/j.bbrc.2012.05.108.

Biochemical and Biophysical Research Communications 398 (2010) 199–204

Contents lists available at ScienceDirect

Biochemical and Biophysical Research Communications

journal homepage: www.elsevier.com/locate/ybbrc

# Conjugated linoleic acid reduces permeability and fluidity of adipose plasma membranes from obese Zucker rats

Ana P. Martins [a], Paula A. Lopes [b], Susana V. Martins [b], Ana Madeira [a,c], Nuno C. Santos [d], José A.M. Prates [b], Teresa F. Moura [a], Graça Soveral [a,e,*]

[a] REQUIMTE, Dep. Química, FCT-UNL, 2829-516 Caparica, Portugal
[b] CIISA, Faculdade de Medicina Veterinária, TULisbon, 1300-477 Lisboa, Portugal
[c] Institute for Research in Biomedicine (IRB, Barcelona), C/Baldiri Reixac 10, Barcelona, Spain
[d] Instituto de Medicina Molecular, Faculdade de Medicina, Universidade de Lisboa, 1649-028 Lisboa, Portugal
[e] Faculdade de Farmácia, Universidade de Lisboa, 1649-003 Lisboa, Portugal

ARTICLE INFO

*Article history:*
Received 10 June 2010
Available online 17 June 2010

*Keywords:*
Conjugated linoleic acid
Adipose plasma membrane
Glycerol permeability
Water permeability
Membrane fluidity
Obese Zucker rats

*Abstract:* Conjugated linoleic acid (CLA) is a dietary fatty acid frequently used as a body fat reducing agent whose effects upon cell membranes and cellular function remain unknown. Obese Zucker rats were fed atherogenic diets containing saturated fats of vegetable or animal origin with or without 1% CLA, as a mixture of *cis*(*c*)9,*trans*(*t*)11 and *t*10,*c*12 isomers. Plasma membrane vesicles obtained from visceral adipose tissue were used to assess the effectiveness of dietary fat and CLA membrane incorporation and its outcome on fluidity and permeability to water and glycerol. A significant decrease in adipose membrane fluidity was correlated with the changes observed in permeability, which seem to be caused by the incorporation of the *t*10,*c*12 CLA isomer into membrane phospholipids. These results indicate that CLA supplementation in obese Zucker rats fed saturated and cholesterol rich diets reduces the fluidity and permeability of adipose membranes, therefore not supporting CLA as a body fat reducing agent through membrane fluidification in obese fat consumers.



## 1. Introduction

Increased consumption of highly energetic food with high levels of saturated fats have led to a threefold increase of obesity rates in industrialized societies contributing to human premature morbidity and mortality [1]. Facing this worldwide health problem, new compounds that might prevent or even reverse such scenario have attracted scientific attention. One of the natural compounds most studied in the last decades as a body fat reducing agent is the conjugated linoleic acid (CLA). CLA is a generic term for a mixture of geometrical and positional isomers of linoleic acid (18:2$n-6$) with conjugated double bonds in either *cis* (*c*) or *trans* (*t*) configuration, found mainly in ruminant-derived foods [2]. Being a dietary fatty acid, CLA reveals an impressive range of promising health benefits including reduction of body fat mass [2] but the mechanisms by which CLA elicits its promising effects remain unknown. It is known that CLA isomers rapidly incorporate into cell membrane lipids [3,4], but their outcome on cell membranes and changes in cellular function is still unexploited. Due to the potential anti-adipogenic effect attributed to CLA, it would be interesting to gain insights on its effect on adipose tissue and specifically on adipose membrane composition, permeability and fluidity. It has been reported that incorporation of polyunsaturated fatty acids (PUFA) into cellular membranes increases fluidity and permeability [5]. Moreover, the effect of diet supplementation with CLA has been shown to modify lipid composition and glycerol permeability of rat kidney membranes [4]. Glycerol is a key substrate involved in lipogenesis and lipolysis of adipose tissue; glycerol release and uptake from the adipocyte is mediated by aquaporin 7 (AQP7), a glycerol-channel that regulates glycerol accumulation [6].

The present study aimed at assessing the effect of dietary CLA on adipose membrane lipid composition and further correlate it with changes in permeability and fluidity. In order to reproduce the most frequent human group consuming CLA as a promoter of body fat mass reduction, our experimental design included obese Zucker rats fed atherogenic diets containing saturated fats of vegetable and animal origins (palm oil and ovine fat) and with or without 1% CLA mixture. An enriched preparation of plasma membrane vesicles, osmotically responsive and suitable for transport experiments, has been obtained from rat white adipose tissue. Membrane vesicles were analyzed regarding their total lipid profile and CLA incorporation into membrane phospholipids. Permeabilities to glycerol and water were assessed and used to estimate the activa-

* Corresponding author at: REQUIMTE, Dep. Química, FCT-UNL, 2829-516 Caparica, Portugal. Fax: +351 212948550.
*E-mail addresses:* gsoveral@ff.ul.pt, soveral@dq.fct.unl.pt (G. Soveral).

0006-291X/$ - see front matter © 2010 Elsevier Inc. All rights reserved.
doi:10.1016/j.bbrc.2010.06.059

tion energy of transport, a valuable parameter indicating the relative contribution of specific transport proteins for membrane permeation. The relationship between membrane composition and fluidity was further characterized by fluorescence anisotropy, a method sensitive to the packing density induced by cholesterol and membrane lipids incorporation.

## 2. Materials and methods

### 2.1. Experimental design: animals and diets

The experimental protocol was reviewed by the Ethics Commission of CIISA/FMV and approved by the Animal Care Committee of the National Veterinary Authority following European Union guidelines (N. 86/609/EEC).

Male obese Zucker (*fa/fa*) rats ($n = 32$) were obtained from Harlan Interfauna Iberia (Barcelona, Spain), aging 5 weeks old. Animals were housed individually and after 1 week of adaptation, rats were fed semi-purified atherogenic diets (Provimi Kliba, SA, Switzerland), with 2% (w/w) cholesterol (plus 0.5% (w/w) sodium cholate to improve cholesterol absorption) and 15% (w/w) of fat with distinct fatty acid composition [7]. Rats were divided into four groups with eight animals each, according to the dietary fat: group P – 11.3% palm oil (w/w) plus 3.8% (w/w) sunflower oil; group PCLA – 11.3% (w/w) palm oil plus 2.5% sunflower oil (w/w) plus 1.2% (w/w) CLA; group O – 11.3% (w/w) ovine fat plus 3.8% (w/w) sunflower oil; group OCLA – 11.3% (w/w) ovine fat plus 2.5% (w/w) sunflower oil plus 1.2% (w/w) CLA. The CLA oil contained similar proportions of *c*9,*t*11 and *t*10,*c*12 isomers with a purity level of 80% (PharmaNutrients Inc., USA). After 14 weeks of trial, rats were fasted for 12 h and sacrificed by decapitation under light isofluorane anaesthesia (Abbott, USA). The epididymal fat pads were removed, washed with saline, weighted and stored at −80 °C for subsequent analysis.

### 2.2. Preparation of membrane vesicles from epididymal fat

Membrane vesicles were prepared from rat's epididymal fat by differential centrifugation with buffer without detergents. Approximately 4 g of epididymal white fat tissue from each rat was chopped into small pieces, removing visible endothelial tissue, and homogenized in mannitol-Hepes buffer (100 mM mannitol, 10 mM Tris–Hepes, pH 7.4) in a warring blender for 2 min. The homogenate was filtered through a 70 μm nylon mesh to further separate the vascular stroma from fat. The filtrate was centrifuged at 1800*g* for 10 min and the supernatant, consisting in intracellular fat, was discarded. The infranatant was centrifuged at 46,000*g* for 45 min at 10 °C to obtain a pellet of crude membranes, and further washed in the same buffer. The membrane pellet was resuspended in mannitol-Hepes buffer, transferred to a syringe and sheared by vigorously passing it 10 times through a 21-gauge needle and immediately used for transport experiments. Protein content was determined by the Bradford technique [8].

### 2.3. Vesicle size determination

Vesicle size of all the membrane preparations was determined by the Quasi-Elastic Light Scattering (QELS) technique (Brookhaven Instruments BI-90).

### 2.4. Immunoblot analysis

Proteins were resolved in 12.5% (w/v) SDS–PAGE and transferred to PVDF membrane (Immobilon-P membrane; Millipore). After blocking with 10% nonfat powder milk in PBS for 1 h at room temperature, the membrane was incubated overnight at 4 °C with primary rabbit antibodies against GLUT4 (BD Transduction Laboratories, Canada), caveolin (Dept. Bioquímica i Biologia Molecular, Facultat de Biologia, Universitat de Barcelona, Spain) and AQP7 (Millipore). Immunoblot analysis was performed with the enhanced chemiluminescence system and horseradish peroxidase conjugated with anti-rabbit IgG (Amersham).

### 2.5. Fatty acid composition and cholesterol content of adipose membranes

After membrane vesicle lyophilisation, fatty acids were converted to methyl esters (FAME) according to [9]. The resulting FAME were analyzed by gas chromatography (GC), using a capillary column (Omegawax 250; Supelco, USA), equipped with a flame-ionization detector. The fatty acid composition was expressed as g/100 g of total fatty acids identified.

Total cholesterol was extracted from lyophilised membrane vesicles through a direct saponification with saturated methanolic KOH solution [10]. Cholesterol was separated and identified using a high performance liquid chromatography (HPLC) equipment (Agilent 1100 Series, Agilent Technologies Inc., USA) by normal phase (Zorbax Rx-Sil column, Agilent Technologies Inc.). Total cholesterol content was calculated, in triplicate, based on the external standard technique, from a standard curve for peak area *versus* cholesterol concentration and expressed as mg/g vesicles.

### 2.6. Stopped-flow experiments on water and glycerol permeability

Stopped-flow experiments were performed on a HI-TECH Scientific PQ/SF-53 apparatus, which has a 2 ms dead time, temperature controlled and interfaced with a PC microcomputer. Experiments were performed at temperatures from 14 °C to 37 °C. Five runs were usually stored and analysed in each experimental condition. For the measurement of osmotic water permeability, membrane vesicles (0.2 mg protein/ml) resuspended in mannitol-Hepes buffer (120 mOsM) were mixed with an equal amount of isosmotic or hyperosmotic (240 mOsM) mannitol solutions to reach an inwardly directed gradient of the impermeant solute. The kinetics of vesicle shrinkage was measured from the time course of scattered light intensity at 400 nm until a stable light scatter signal was attained. The osmotic water permeability coefficient ($P_f$) was estimated by fitting the light scatter signal to a single exponential curve and using the linear relation between $P_f$ and the exponential time constant $k$ [11], $P_f = k\,(V_o/A)(1/V_w(osm_{out})_\infty)$, where $V_w$ is the molar volume of water, $V_0/A$ is the initial volume to area ratio of the vesicle preparation, and $(osm_{out})_\infty$ is the final medium osmolarity after the applied osmotic gradient. For glycerol permeability, membrane vesicles equilibrated in 120 mOsM mannitol-Hepes buffer were confronted to an external solution where the impermeant solute was partially replaced by glycerol (60 mOsM mannitol plus 180 mOsM glycerol, creating an inwardly directed glycerol gradient). After the first fast vesicle shrinkage due to water outflow, glycerol influx in response to its chemical gradient was followed by water influx with subsequent vesicle reswelling. Glycerol permeability was calculated as $P_{gly} = k\,(V_o/A)$, where $k$ is the single exponential time constant fitted to the light scattering signal of glycerol influx [12]. For inhibitor assays, vesicles were incubated for 5 min with 0.5 mM $HgCl_2$ immediately prior to stopped flow injection. All solution osmolarities were determined from freezing point depression on a semi-micro osmometer (Knauer GmbH, Germany) using standards of 100 and 400 mOsM.

The activation energy $E_a$ of water and glycerol transport was calculated from the slope of the Arrhenius plot ($\ln P_f$ or $\ln P_{gly}$ as a function of $1/T$) multiplied by the gas constant $R$.

### 2.7. Membrane fluidity measurements

Membrane fluidity was studied by a fluorescence polarization method, which measures the fluorescence anisotropy of two probes incorporated in the membrane: 1,6-diphenyl-1,3,5-hexatriene (DPH), or 1-(4-(trimethylamino)-phenyl)-6-phenyl-1,3,5-hexatriene (TMA-DPH), (Molecular Probes, USA). DPH is incorporated inside the membrane, at the fatty acyl group's level, while TMA–DPH is anchored by its cationic part at the membrane/water interface, probing the membrane region closer to the phospholipids head groups [13]. DPH 1 mM in acetone or TMA–DPH 0.5 mM in dimetylformamide were diluted 1:180 in mannitol-Hepes buffer, vigorously stirred for 1 min, mixed with an aliquot of the vesicle suspension (final protein 20 μg/ml) and incubated 30 min in the dark, at 37 °C for DPH and at room temperature for TMA–DPH. Blank samples were prepared replacing the probes by identical volumes of their solvents. As the fluorescent probes reach equilibrium between the aqueous and lipid phases and the unincorporated probes almost do not fluoresce [14], no washing was needed. Membrane fluidity was assessed by fluorescence anisotropy ($r$) defined by the equation $r = (I_{VV} - GI_{VH})/(I_{VV} + 2GI_{VH})$, where $I_{VV}$ and $I_{VH}$ are the fluorescence intensities and the subscripts indicate the vertical ($V$) or horizontal ($H$) orientations of the excitation and emission polarizers, and $G = I_{HV}/I_{HH}$ is the instrumental factor [15]. DPH fluorescence was measured at an excitation wavelength ($\lambda_{exc}$) of 357 nm and an emission wavelength ($\lambda_{em}$) of 428 nm. For TMA–DPH, $\lambda_{exc}$ = 343 nm and $\lambda_{em}$ = 427 nm. The fluorescence intensity data used for calculations were the average of three identical aliquots (after blank subtraction) measured on a Varian Cary Eclipse fluorescence spectrophotometer (Mulgrave, Australia).

### 2.8. Statistics

Statistical analysis was performed using the statistical analysis system (SAS) software package, v9.1 (SAS Institute, USA). Data were mean and standard error of the mean (SEM). The procGLM procedure was used to perform a 2 × 2 factorial analysis to determine significant effects of CLA, fat origin and their respective interaction (CLA × fat). In the case of interaction, significant differences between groups were identified using Tukey's *post-hoc* test at $P < 0.05$.

## 3. Results

### 3.1. Characterization of membrane vesicles from epididymal fat

Vesicle size of membrane preparations within each dietary treatment ($n = 8$) revealed homogeneous populations with monomodal distributions, showing a mean diameter of (303 ± 42, 297 ± 54, 319 ± 50 and 276 ± 44) nm for P, PCLA, O and OCLA groups, respectively.

Western blots of aliquots from the initial fat tissue homogenate and from the final adipose membrane preparations were incubated with antibody anti-GLUT4 and anti-caveolin. Additionally, membrane preparations were incubated with anti-AQP7. An intense band of GLUT4, the insulin-stimulated glucose transporter [16], was depicted in the membrane vesicles but was almost absent in the homogenate fraction (Fig. 1). Likewise, the band for caveolin, a constitutive protein of plasma membranes of mature adipocytes [16], was stronger in the final vesicle preparation. AQP7 was also detected in the adipose membranes, despite in a fainter band than caveolin. Altogether, these results assure purified and homogeneous adipose plasma membrane preparations.

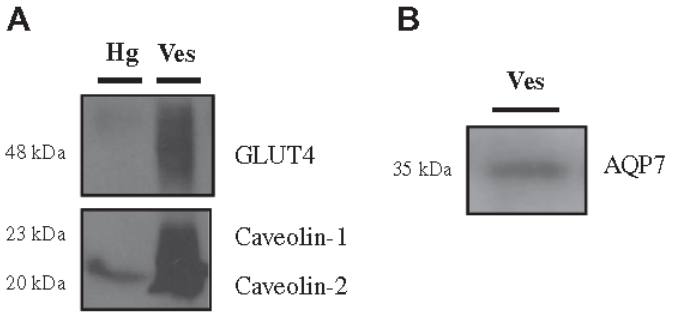


**Fig. 1.** (A) GLUT4 and caveolin proteins in the initial fat tissue homogenate (Hg, lane 1) and in the final adipose membrane vesicles (Ves, lane 2) (10 μg protein). (B) AQP7 in the final adipose membrane vesicles (Ves, 50 μg protein).

### 3.2. Fatty acid membrane composition depends on dietary fat and CLA supplementation

The fatty acid composition of membrane vesicles from the four dietary treatments is shown in Table 1. Total cholesterol content was higher in membranes from palm oil groups and not affected by CLA supplementation. The deposition of total saturated fatty acids (SFA) was not different among groups. However, while the 16:0 incorporation was greater in palm oil groups, the 18:0 and 20:0 fatty acids were enhanced in ovine fat groups. The differences found for monounsaturated fatty acids (MUFA) were related to the dietary fat origin, being consistently higher in palm oil groups, with and without CLA. Yet, the incorporation of 18:1 fatty acid was affected by both CLA and fat origin effects in separate, being higher in ovine fat diets.

The sum of PUFA and specifically $n - 6$ fatty acids, was not affected by CLA, fat origin or their respective interaction. However, the $n - 3$ sum was influenced by the fat origin. Regarding the CLA isomeric profile, major differences were observed between the four dietary groups. The sum of CLA isomers increased by CLA mixture supplementation and was higher in diets based on animal fat. However, isomeric incorporation in adipose membranes was distinct. The *t*10,*c*12 isomer was detected only by CLA supplementation, while *c*9,*t*11 deposition was influenced by both CLA and fat origin and was significantly larger in both fat based diets.

### 3.3. CLA decreases permeability and fluidity of adipose membrane vesicles

For water transport experiments, vesicles in isotonic buffer were subjected to a hyperosmotic gradient with mannitol, as depicted in Fig. 2A. Fig. 2B shows a typical trace where a glycerol gradient was imposed. Fast vesicle shrinkage due to water outflow (first part of the trace) is followed by vesicle reswelling; as glycerol enters due to its chemical gradient, vesicles progressively swell until they reach equilibrium. The time courses of vesicle volume changes are used to calculate $P_f$ and $P_{gly}$.

Fig. 3 shows the water and glycerol permeability coefficients obtained at 23 °C for the various membrane preparations (for each group, $n = 8$). Average $P_f \pm$ SEM were $(1.88 \pm 0.113,\ 1.59 \pm 0.260,\ 2.08 \pm 0.080$ and $1.75 \pm 0.080) \times 10^{-3}$ cm s$^{-1}$ for P, PCLA, O and OCLA groups, respectively. For the same groups, $P_{gly} \pm$ SEM were $(4.77 \pm 0.274,\ 4.16 \pm 0.275,\ 5.22 \pm 0.183$ and $4.43 \pm 0.348) \times 10^{-7}$ cm s$^{-1}$. A significant CLA effect was detected for both permeabilities as dietary groups with CLA presented lower values in relation to their counterparts ($P < 0.01$ for $P_f$ and $P < 0.05$ for $P_{gly}$).

The activation energy values ($E_a$) for water and glycerol transport were similar among dietary groups, ranging from 24.4 ± 0.36

**Table 1**
Cholesterol content (mg/g vesicles) and fatty acid (% of total FAME) profile of membrane vesicles from the dietary treatments tested.

| | Dietary treatments | | | | | Significance level | | |
|---|---|---|---|---|---|---|---|---|
| | P | PCLA | O | OCLA | SEM | CLA | Fat | CLA × Fat |
| Cholesterol content | 0.044 | 0.040 | 0.027 | 0.036 | 0.004 | ns | * | ns |
| *Fatty acid profile* | | | | | | | | |
| 14:0 | 0.867[b] | 1.05[a] | 1.02[a] | 1.07[a] | 0.033 | ** | * | * |
| 15:0 | 0.114 | 0.140 | 0.237 | 0.247 | 0.010 | ns | *** | ns |
| 16:0 | 23.6 | 24.1 | 18.7 | 18.8 | 0.380 | ns | *** | ns |
| 16:1 | 0.564 | 0.657 | 0.693 | 0.698 | 0.027 | ns | ** | ns |
| 16:1*c*9 | 4.39 | 4.81 | 4.05 | 3.81 | 0.197 | ns | ** | ns |
| 17:0 | 0.300 | 0.357 | 0.644 | 0.659 | 0.029 | ns | *** | ns |
| 18:0 | 10.9[b] | 10.1[b] | 13.4[a] | 14.9[a] | 0.451 | ns | *** | * |
| 18:1 | 3.46 | 3.94 | 5.42 | 5.84 | 0.075 | *** | *** | ns |
| 18:1*c*9 | 28.5 | 26.4 | 24.1 | 22.9 | 0.868 | ns | ** | ns |
| 18:2*n* − 6 | 11.4 | 11.9 | 12.2 | 12.1 | 0.247 | ns | * | ns |
| CLA-*c*9*t*11 | 0.273 | 1.15 | 1.59 | 2.35 | 0.063 | *** | *** | ns |
| CLA-*t*10*c*12 | n.d. | 0.369 | n.d. | 0.439 | 0.028 | *** | ns | ns |
| Σ CLA *tt* | n.d. | 0.178 | 0.049 | 0.226 | 0.016 | *** | ** | ns |
| 18:3*n* − 3 | 0.113 | 0.109 | 0.343 | 0.294 | 0.022 | ns | *** | ns |
| 20:0 | 0.293 | 0.305 | 0.409 | 0.376 | 0.040 | ns | * | ns |
| 20:1*n* − 9 | 0.233 | 0.187 | 0.146 | 0.109 | 0.007 | *** | *** | ns |
| 20:3*n* − 6 | 0.536 | 0.508 | 0.597 | 0.498 | 0.037 | ns | ns | ns |
| 20:4*n* − 6 | 6.84 | 7.12 | 7.71 | 7.09 | 0.693 | ns | ns | ns |
| 20:5*n* − 3 | n.d. | 0.062 | 0.142 | 0.160 | 0.014 | ** | *** | ns |
| 21:0 | 0.672 | 0.730 | 0.953 | 0.916 | 0.117 | ns | ns | ns |
| 23:0 | 0.344 | 0.143 | 0.187 | 0.157 | 0.055 | * | ns | ns |
| 22:4*n* − 6 | 0.930 | 0.848 | 0.811 | 0.621 | 0.100 | ns | ns | ns |
| 22:5*n* − 3 | 0.096[c] | 0.109[b,c] | 0.362[a] | 0.215[b] | 0.029 | * | *** | ** |
| 22:6*n* − 3 | 0.119 | 0.073 | 0.208 | 0.180 | 0.024 | ns | *** | ns |
| Σ Unidentified | 5.51 | 4.74 | 5.99 | 5.42 | 0.397 | ns | ns | ns |
| Σ SFA | 37.0 | 36.9 | 35.5 | 37.1 | 0.424 | ns | ns | ns |
| Σ MUFA | 37.2 | 36.0 | 34.5 | 33.4 | 1.06 | ns | * | ns |
| Σ PUFA | 20.0 | 20.7 | 22.4 | 21.1 | 0.911 | ns | ns | ns |
| Σ CLAs | 0.273 | 1.70 | 1.64 | 3.01 | 0.080 | *** | *** | ns |
| Σ *n* − 3 | 0.328 | 0.352 | 1.05 | 0.849 | 0.061 | ns | *** | ns |
| Σ *n* − 6 | 19.7 | 20.4 | 21.4 | 20.3 | 0.874 | ns | ns | ns |

Dietary treatments: P = palm oil diet; PCLA = palm oil diet + 1 % conjugated linoleic acid; O = ovine fat diet; OCLA = ovine fat diet + 1 % conjugated linoleic acid. n.d. = not detected. Significance level: ns, not significant, $P > 0.05$; *$P < 0.05$; **$P < 0.01$; ***$P < 0.001$. [a–c]Mean values within the same row with different superscript letters are significantly different (Tukey's *post-hoc* test, $P < 0.05$). FAME = fatty acid methyl esters. Σ SFA, saturated fatty acids = sum of 14:0, 15:0, 16:0, 17:0, 18:0, 20:0, 21:0 and 23:0; Σ MUFA, monounsaturated fatty acids = sum of 16:1,16:1*c*9, 18:1, 18:1*c*9 and 20:1*n* − 9; Σ PUFA, polyunsaturated fatty acids = sum of 18:2*n* − 6, 18:3*n* − 3, 20:3*n* − 6, 20:4*n* − 6, 20:5*n* − 3, 22:4*n* − 6, 22:5*n* − 3 and 22:6*n* − 3; Σ CLA = sum of CLA-*c*9,*t*11, CLA-*t*10,*c*12 and CLAtt; Σ *n* − 3 = sum of 18:3*n* − 3, 20:5*n* − 3, 22:5*n* − 3 and 22:6*n* − 3; Σ *n* − 6 = sum of 18:2*n* − 6, 20:3*n* − 6, 20:4*n* − 6 and 22:4*n* − 6.

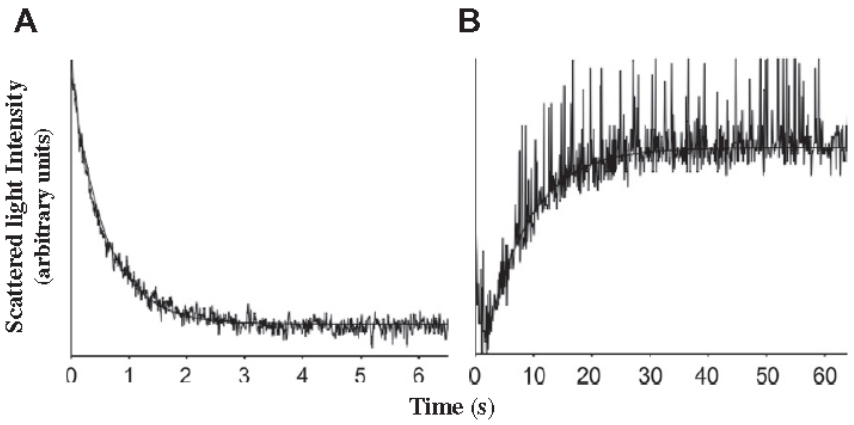


**Fig. 2.** Representative stopped flow light scatter of adipose membrane vesicles permeability to water and glycerol at 23 °C. (A) Vesicle shrinkage due to water outflow after an hyperosmotic shock with 120 mOsM mannitol gradient. (B) Fast shrinkage followed by vesicle reswelling due to glycerol uptake after an inwardly directed 180 mOsM glycerol gradient.

to 24.9 ± 0.35 kcal mol $^{-1}$ (102.1 ± 1.51 to 104.1 ± 1.46 kJ mol $^{-1}$) for glycerol and from 14.7 ± 0.24 to 15.1 ± 0.23 kcal mol $^{-1}$ (61.5 ± 0.98 to 63.2 ± 1.96 kJ mol $^{-1}$) for water. Neither CLA nor fat origin had any effect on $E_a$ of water and glycerol transport. These relative high $E_a$ values suggest a lipid- rather than a channel-mediated pathway for both transports. While selective water channels have not been described in adipose membranes, the AQP7 glycerol channel was found in adipose tissue from mice [6]. In our study, we also detected AQP7 in adipose membranes, although in a residual amount. This low level of AQP7 channel expression or incorporation in the plasma membrane may be responsible for the observed high $E_a$ value for glycerol permeation, indicating that glycerol permeates the membrane mainly by passive diffusion through the lipid bilayer and that the channel pathway is unimportant. Down-regulation

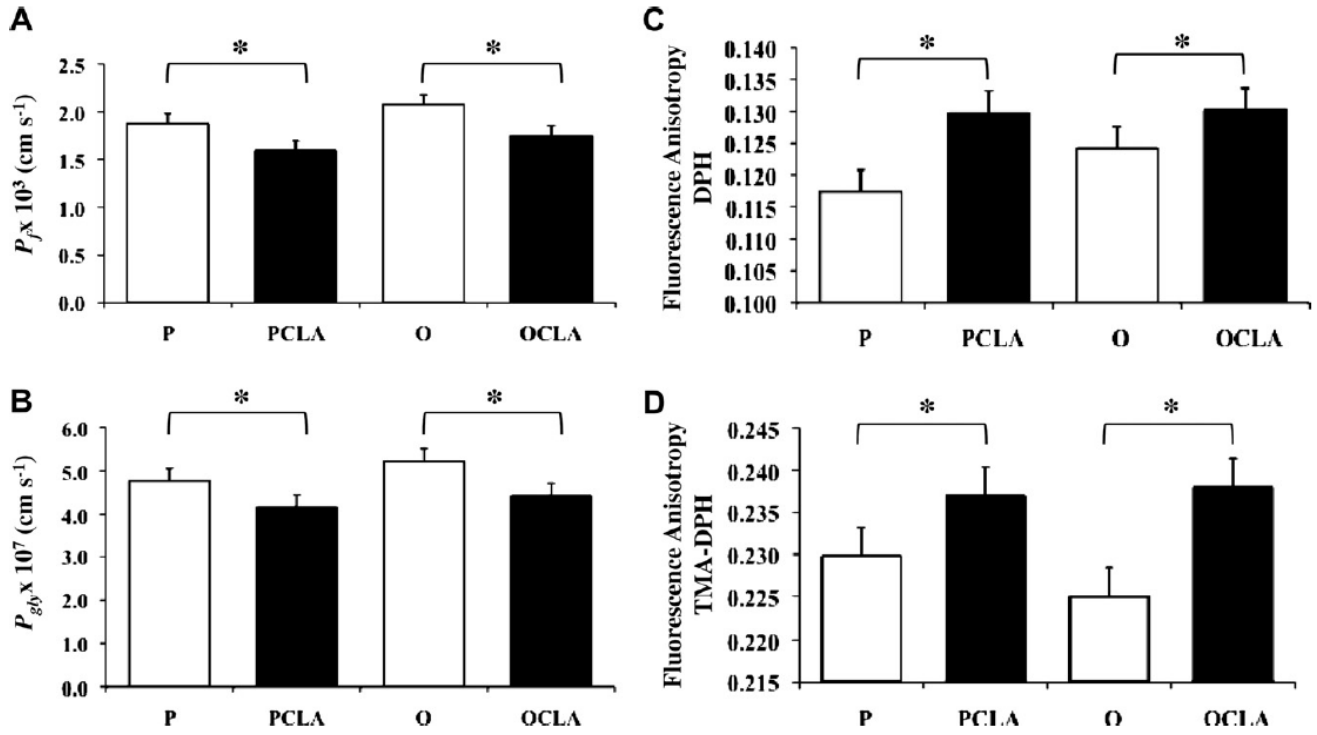


**Fig. 3.** Permeabilities of water (A) and glycerol (B) at 23 °C, and fluorescence anisotropy of DPH (C) and TMA-DPH (D) in adipose membrane vesicles from dietary groups (P = palm oil; PCLA = palm oil + 1% conjugated linoleic acid; O = ovine fat; OCLA = ovine fat + 1% conjugated linoleic acid). Values are mean ± SEM. *Significant CLA effect detected by two-way ANOVA ($P < 0.01$ for $P_f$, $P < 0.05$ for $P_{gly}$, and $P < 0.01$ for both fluidity measurements).

of the AQP7 gene in adipose tissue of obese individuals has been reported and correlated with the susceptibility to obesity of obese high fat consumers [17]. To confirm the lipid bilayer as the main pathway for water and glycerol permeation, adipose membrane vesicles were pre-incubated with $HgCl_2$, a known inhibitor of aquaporin function [18], before permeability assays. Results of $P_f$ or $P_{gly}$ did not change after $HgCl_2$ treatment ($P > 0.05$; Fig. 4), suggesting a non-channel mediated water and glycerol transport.

The relative changes in fluorescence anisotropy of DPH and TMA–DPH in membrane vesicles from each dietary treatment are shown in Fig. 3. With both fluorescence probes, a significant increase in the viscosity was observed for groups with CLA. Being viscosity inversely related to fluidity, adipose membrane vesicles from dietary groups with CLA are therefore less fluid than without CLA, regardless the fat origin. The membrane rigidification effect associated with CLA supplementation is evident and significant at both membrane depths probed by the two different fluorophores used.

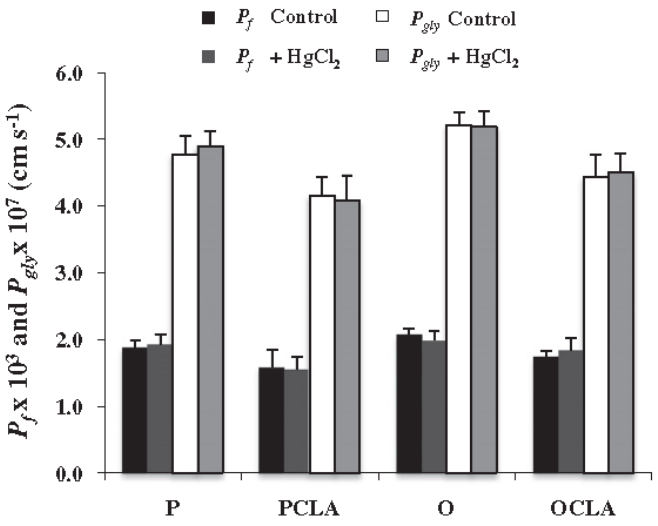


**Fig. 4.** Permeabilities of water and glycerol at 23 °C in adipose membrane vesicles from dietary groups (P = palm oil; PCLA = palm oil + 1% conjugated linoleic acid; O = ovine fat; OCLA = ovine fat + 1% conjugated linoleic acid) before and after $HgCl_2$ treatments. Values are mean ± SEM. No significant effects were detected between control and $HgCl_2$ treatments ($P > 0.05$).

## 4. Discussion

The human health effects of CLA, including the potential to reduce body fat mass, became the subject of widespread research for nearly three decades. Still, its efficiency remains controversial [19]. Depending on the country, estimation of CLA daily intake varies from 15 to 1000 mg [20] thus representing a large range of consumption values. It has been suggested that a consumption of 0.8–3.0 g CLA *per day* might provide significant health benefits [21], a dosage that in most cases is only achievable through diet supplementation. Besides being the dosage most commonly used in animal research, 1% CLA is meant to mimic nutritional supplement use.

We thought it might be interesting to look at CLA supplementation effects on adipose membranes obtained from visceral fat of obese Zucker rats. These animals were fed atherogenic and saturated fat diets with distinct origins, vegetable (palm oil) and animal (ovine fat), and the effectiveness of CLA isomers incorporation, the changes of adipose membrane lipid profile and its outcome on fluidity and permeability were assessed in plasma membrane vesicles from visceral adipose tissue. The membrane vesicles obtained herein were homogeneous and enriched in the adipocyte plasma membrane fraction, showed to be osmotically responsive and therefore suitable for transport experiments.

The increase in cholesterol content of a membrane in the liquid disordered state leads to a decrease in its fluidity. On biomem-

brane model systems of certain lipid compositions and on different cell membranes, cholesterol leads to the formation of lipid rafts, microdomains on the liquid ordered state [22] with decreased fluidity that are enriched in cholesterol, sphingolipids and specific proteins [23]. The lipid profile analysis of adipose membranes from the distinct dietary groups has shown that, despite cholesterol content had been influenced by the fat origin, CLA supplementation did not affect cholesterol membrane incorporation. In a similar way, the deposition of SFA, MUFA and PUFA $n-3$ fatty acids were dependent on the fat origin, not presenting any relation to CLA supplementation. As for total PUFA, their total incorporation was not affected by the fat origin or by CLA supplementation. It is known that incorporation of unsaturated fatty acids into cellular membranes increases its fluidity. PUFA acyl chains are extremely flexible and can rapidly change conformational states. The acyl chain flexibility differs substantially between $n-3$ and $n-6$ fatty acids and the number of double bonds significantly alters membrane fluidity. In fact, membrane incorporation of eicosapentaenoic acid EPA (20:5$n-3$) and docosahexaenoic acid DHA (22:6$n-3$), to which numerous health effects have been attributed [24], was significantly dependent on the dietary fat, whereby the effect of CLA was almost negligible. This fact excludes the decrease in DHA or EPA content as responsible for the decrease in adipose membrane fluidity observed in this study, supporting the idea that changes at the fluidity level should be accounted to CLA supplementation rather than to dietary fat. Accordingly, permeability values were consistently lower in adipose membranes when obese Zucker rats were fed CLA, not showing any dependence on the dietary fat origin. Given that the activation energy for both water and glycerol transports was high and relatively stable in all cases, indicating that permeation occurs via the lipid bilayer, the decrease in permeability correlates well with the decrease in membrane fluidity which seems to be caused by CLA incorporation into membrane phospholipids. Despite the same concentration of both CLA isomers in the oil mixture, the *c*9,*t*11, which is the natural occurring isomer in ruminant fat, was detected in a larger amount than the *t*10,*c*12 in all dietary groups, independently of dietary fat. This result *per se* might suggest that *c*9,*t*11 isomer could be accountable for the changes in the membrane properties reported here. However, given that changes in permeability and fluidity are only observed for CLA supplemented groups and do not depend on the fat origin, the *c*9,*t*11 isomer can be discarded since its concentration is much higher in ovine than in vegetable fat. Therefore, the *t*10,*c*12 isomer may be suggested as the most probable membrane component affecting adipose plasma membrane fluidity and permeability. Interestingly, this CLA isomer is the one with suggested body fat lowering properties in several animal studies [19].

In conclusion, this study suggests that CLA supplementation in obese Zucker rats fed saturated fat and cholesterol rich diets, through its incorporation in membrane phospholipids, has an effect on the fluidity of adipose membranes by increasing membrane rigidity both at the centre of the bilayer (hydrocarbon core) and at a shallow position, closer to the water/lipid interface. This effect could be explained by the geometric structure of the *t*10,*c*12 CLA isomer, where a considerable bending in the fatty acid chain induces a decrease in the average chain length that, similarly to cholesterol, may affect lipid packing within cellular membranes. This isomer and particularly its conformation may promote the formation of other type of raft-like structure, different from the cholesterol and sphingolipids rich microdomains, contributing to the experimentally observed decrease on the average membrane fluidity and permeability of the system. Consequently, our results do not point out to membrane fluidification as a possible mechanism supporting CLA effect as a body fat reducing agent in obese fat consumers.

## Acknowledgments

This study was supported by FCT grants PTDC/CVT/2006/66114 and PTDC/CVT/2008/99210 and individual fellowships SFRH/BPD/2009/63019 and SFRH/BD/45930/2008. We wish to thank PharmaNutrients Inc. (Gurnee, IL, USA). We acknowledge Rui Bessa and Susana Alves (L-INIA-REQUIMTE) for fatty acid analysis, Pedro Matos and Teresa Freitas (IMM, FMUL) for assistance in fluidity measurements, and Marta Camps (IRB, Spain) for support in immunoassays.

## References

[1] K.F. Adams, A. Schatzkin, T.B. Harris, V. Kipnis, T. Mouw, R. Ballard-Barbash, A. Hollenbeck, M.F. Leitzmann, Overweight, obesity, and mortality in a large prospective cohort of persons 50–71 years old, N. Engl. J. Med. 355 (2006) 763–778.
[2] J.A.M. Prates, R.B. Bessa, Trans and $n-3$ fatty acids, in: L.M.L. Nollet, F. Toldrá (Eds.), Handbook of Muscle Food Analysis, CRC Press, New York, 2009, pp. 399–417.
[3] C.J. Field, P.D. Schley, Evidence for potential mechanisms for the effect of conjugated linoleic acid on tumor metabolism and immune function: lessons from $n-3$ fatty acids, Am. J. Clin. Nutr. 79 (2004) 1190S–1198S.
[4] G. Soveral, A.P. Martins, S.V. Martins, P.A. Lopes, C.M. Alfaia, J.A. Prates, T.F. Moura, Effect of dietary conjugated linoleic acid isomers on water and glycerol permeability of kidney membranes, Biochem. Biophys. Res. Commun. 383 (2009) 108–112.
[5] W. Stillwell, S.R. Wassall, Docosahexaenoic acid: membrane properties of a unique fatty acid, Chem. Phys. Lipids 126 (2003) 1–27.
[6] K. Kishida, H. Kuriyama, T. Funahashi, I. Shimomura, S. Kihara, N. Ouchi, M. Nishida, H. Nishizawa, M. Matsuda, M. Takahashi, K. Hotta, T. Nakamura, S. Yamashita, Y. Tochino, Y. Matsuzawa, Aquaporin adipose, a putative glycerol channel in adipocytes, J. Biol. Chem. 275 (2000) 20896–20902.
[7] S.V. Martins, P.A. Lopes, C.M. Alfaia, P.O. Rodrigues, S.P. Alves, R.M. Pinto, M.F. Castro, R.J. Bessa, J.A. Prates, Serum adipokine profile and fatty acid composition of adipose tissues are affected by conjugated linoleic acid and saturated fat diets in obese Zucker rats, Br. J. Nutr. 103 (2010) 869–878.
[8] M.M. Bradford, A rapid and sensitive method for the quantitation of microgram quantities of protein utilizing the principle of protein-dye binding, Anal. Biochem. 72 (1976) 248–254.
[9] W.W. Christie, G. Dobson, R.O. Adlof, A practical guide to the isolation, analysis and identification of conjugated linoleic acid, Lipids 42 (2007) 1073–1084.
[10] E.D. Naeemi, N. Ahmad, T.K. Al-Sharrah, M. Behbahani, Rapid and simple method for determination of cholesterol in processed food, J. AOAC Int. 78 (1995) 1522–1525.
[11] M.P. van Heeswijk, C.H. van Os, Osmotic water permeabilities of brush border and basolateral membrane vesicles from rat renal cortex and small intestine, J. Membr. Biol. 92 (1986) 183–193.
[12] J.A. Dix, D.A. Ausiello, C.Y. Jung, A.S. Verkman, Target analysis studies of red cell water and urea transport, Biochim. Biophys. Acta 821 (1985) 243–252.
[13] E. Pebay-Peyroula, E.J. Dufourc, A.G. Szabo, Location of diphenyl-hexatriene and trimethylammonium-diphenyl-hexatriene in dipalmitoylphosphatidylcholine bilayers by neutron diffraction, Biophys. Chem. 53 (1994) 45–56.
[14] Z.J. Huang, R.P. Haugland, Partition coefficients of fluorescent probes with phospholipid membranes, Biochem. Biophys. Res. Commun. 181 (1991) 166–171.
[15] J.R. Lakowicz, Principles of fluorescence spectroscopy, Kluwer Academic/Plenum, New York, 1999.
[16] K.V. Kandror, J.M. Stephens, P.F. Pilch, Expression and compartmentalization of caveolin in adipose cells: coordinate regulation with and structural segregation from GLUT4, J. Cell. Biol. 129 (1995) 999–1006.
[17] M.P. Marrades, F.I. Milagro, J.A. Martinez, M.J. Moreno-Aliaga, Differential expression of aquaporin 7 in adipose tissue of lean and obese high fat consumers, Biochem. Biophys. Res. Commun. 339 (2006) 785–789.
[18] R.I. Macey, R.E. Farmer, Inhibition of water and solute permeability in human red cells, Biochim. Biophys. Acta 211 (1970) 104–106.
[19] Y. Park, M.W. Pariza, Mechanisms of body fat modulation by conjugated linoleic acid, Food Res. Int. 40 (2007) 311–323.
[20] S.V. Martins, P.A. Lopes, C.M. Alfaia, V.S. Ribeiro, T.V. Guerreiro, C.M. Fontes, M.F. Castro, G. Soveral, J.A. Prates, Contents of conjugated linoleic acid isomers in ruminant-derived foods and estimation of their contribution to daily intake in Portugal, Br. J. Nutr. (2007) 1–8.
[21] F.C.J. Parrish, B.R. Wiegand, D.C. Beitz, D.U. Ahn, M. Du, A.H. Trenkle, Use of dietary CLA to improve composition and quality of animal-derived foods, in: J.L. Sébédio, W.W. Christie, R. Adlof (Eds.), Advances in Conjugated Linoleic Acid Research, AOCS Press, Champaign, IL, 2003, pp. 189–217.
[22] D. Marsh, Cholesterol-induced fluid membrane domains: a compendium of lipid-raft ternary phase diagrams, Biochim. Biophys. Acta 1788 (2009) 2114–2123.
[23] D. Lingwood, K. Simons, Lipid rafts as a membrane-organizing principle, Science 327 (2010) 46–50.
[24] J.J. Li, C.J. Huang, D. Xie, Anti-obesity effects of conjugated linoleic acid, docosahexaenoic acid, and eicosapentaenoic acid, Mol. Nutr. Food Res. 52 (2008) 631–645.

*Animal* (2011), **5:12**, pp 1949–1956 © The Animal Consortium 2011
doi:10.1017/S1751731111001091

animal

# Differential mesenteric fat deposition in bovines fed on silage or concentrate is independent of glycerol membrane permeability

A. P. Martins[1a], P. A. Lopes[2a], A. S. H. Costa[2], S. V. Martins[2], N. C. Santos[3], J. A. M. Prates[2], T. F. Moura[1] and G. Soveral[1,4†]

[1]*REQUIMTE, Dep. Química, FCT-UNL, 2829-516 Caparica, Portugal;* [2]*CIISA, Faculdade de Medicina Veterinária, Universidade Técnica de Lisboa, 1300-477 Lisboa, Portugal;* [3]*Instituto de Medicina Molecular, Faculdade de Medicina, Universidade de Lisboa, 1649-028 Lisboa, Portugal;* [4]*Faculdade de Farmácia, Universidade de Lisboa, 1649-003 Lisboa, Portugal*

(Received 16 March 2011; Accepted 13 June 2011; First published online 15 July 2011)

*In the meat industry, the manipulation of fat deposition in cattle is of pivotal importance to improve production efficiency, carcass composition and ultimately meat quality. There is an increasing interest in the identification of key factors and molecular mechanisms responsible for the development of specific fat depots. This study aimed at elucidating the influence of breed and diet on adipose tissue membrane permeability and fluidity and their interplay on fat deposition in bovines. Two Portuguese autochthonous breeds, Alentejana and Barrosã, recognized as late- and early-maturing breeds, respectively, were chosen to examine the effects of breed and diet on fat deposition and on adipose membrane composition and permeability. Twenty-four male bovines from these breeds were fed on silage-based or concentrate-based diets for 11 months. Animals were slaughtered to determine their live slaughter and hot carcass weights, as well as weights of subcutaneous and visceral adipose depots. Mesenteric fat depots were excised and used to isolate adipocyte membrane vesicles where cholesterol content, fatty acid profile as well as permeability and fluidity were determined. Total accumulation of neither subcutaneous nor visceral fat was influenced by breed. In contrast, mesenteric and omental fat depots weights were higher in concentrate-fed bulls relative to silage-fed animals. Membrane fluidity and permeability to water and glycerol in mesenteric adipose tissue were found to be independent of breed and diet. Moreover, the deposition of cholesterol and unsaturated fatty acids, which may influence membrane properties, were unchanged among experimental groups. Adipose membrane lipids from the mesenteric fat depot of ruminants were rich in saturated fatty acids, and unaffected by polyunsaturated fatty acids dietary levels. Our results provide evidence against the involvement of cellular membrane permeability to glycerol on fat accumulation in mesenteric fat tissue of concentrate-fed bovines, which is consistent with the unchanged membrane lipid profile found among experimental groups.*

**Keywords:** adipose membrane, glycerol permeability, membrane fluidity, lipid composition, bovine breeds

## Implications

Visceral fat deposition has been considered an important factor in cattle finishing. As maturing proceeds, large amounts of mesenteric fat can be deposited leading to production inefficiencies, which can jeopardize meat quality. Yet, no studies addressing fatty acid incorporation at the cell membrane and its outcome on membrane physical properties, including rigidity and permeability to water and solutes, are available for ruminants. This study exploits the membrane fluidity and permeability to glycerol, a key substrate involved in lipogenesis, while an underlying mechanism for differential visceral fat deposition in bovines that may be influenced by breed or diet.

## Introduction

Traditional meats with Protected Designation of Origin, derived from local extensive production systems and autochthonous breeds, have the certification of European Union legislation due to their supposed quality and sensory traits, which have been associated with their specific lipid fraction properties (Council Regulation No. 2081/92 of 14 July, European Economic Community). Curiously, the scientific information available to sustain the claimed quality, mainly dependent on its lipid composition, is scarce. On the other hand, the

[a] These authors have contributed equally to this article.
† E-mail: gsoveral@ff.ul.pt; soveral@dq.fct.unl.pt

manipulation of adipose tissue deposition in cattle has represented for many years a major breeding goal as a future guarantee for the improvement of production efficiency, visceral fat partitioning, carcass composition and meat quality (De Smet *et al.*, 2004). The identification of key factors and molecular mechanisms responsible for the development of specific fat depots (Azain, 2004) in autochthonous bovine breeds is necessary, in particular, mechanisms underlying visceral fat accumulation in young bulls with distinct precociousness, Alentejana and Barrosã, known as late- and early-maturing breeds, respectively (da Silva *et al.*, 1998). Precociousness is intimately related to adipose tissue deposition in meat-producing animals, as early-maturing breeds deposit noticeable amounts of marbling fat before late-maturing breeds (Hocquette *et al.*, 2010).

The degree of saturation of plasma membrane acyl chains might be among the primary events in adipocyte differentiation (Stubbs and Smith, 1984). Nevertheless, literature addressing bovines' fatty acid deposition at the cell membrane level and its outcome on membrane physical properties is unavailable. Given that the membrane bilayer permeability to water and solutes is tightly related to phospholipid composition and membrane fluidity (Lande *et al.*, 1995), it seems reasonable that distinct fat depots with specific metabolic characteristics would affect membrane physical properties. Fatty acid incorporation into cellular membranes is known to affect permeability to water and, most importantly, to glycerol (Soveral *et al.*, 2009; Martins *et al.*, 2010). It is well established that glycerol is a key substrate for lipogenesis and lipolysis in adipose tissues of ruminants. The concept of membrane permeability and fluidity could therefore be critical for understanding membrane structure–function.

Specific genetic characteristics have been also described, with the purebred Alentejana breed considered phylogenetically distant from the purebred Barrosã breed (Beja-Pereira *et al.*, 2003). Large differences in the levels of intramuscular fat in Alentejana and Barrosã bovines were previously reported by our group, with values of Alentejana breed (1.2%) nearly half of the other (2.3%) (Alfaia *et al.*, 2007 and 2009). Studies in humans and mice (Field and Clandinin, 1984; Field *et al.*, 1988) demonstrated that dietary fat can alter adipose cell membrane composition. Thus, the structure and physiological properties of the adipocyte membrane may be changed. The goal of the present study was to assess the effect of breed and diet on fat deposition, as well as on the lipid composition, permeability and fluidity of adipocyte membranes.

## Material and methods

*Experimental design: animals and diets*

The experimental design included 24 male bovines from two phylogenetically distant autochthonous breeds, the late-maturing breed, Alentejana, and the early-maturing breed, Barrosã, allocated to silage-based or concentrate-based diets (four experimental groups of six animals each) from January to November 2009. At the beginning of the experiment, Alentejana bulls were 332 ± 10.2 days old (initial weight of 275 ± 15.6 kg) and Barrosã bulls were 268 ± 2.96 days old (initial weight of 217 ± 4.57 kg). Bulls were fed two experimental diets composed of 70/30% and 30/70% of corn silage and concentrate, respectively. The proximate composition and fatty acid profile in both experimental diets ($n = 3$) are shown in Table 1.

Bulls were slaughtered at 18 months of age at the INRB Experimental Abattoir by exsanguination after stunning with a cartridge-fired captive bolt stunner. The amount of subcutaneous fat was determined by dissection of the leg joint. The former has been suggested to be representative of the overall bovine carcass composition in these particular breeds (Simões and Mendes, 2003). Mesenteric, omental and kidney knob and channel fat (KKCF) depots were excised and weighed. Samples from the mesenteric fat were collected,

**Table 1** *Diet composition*

| | Silage† | Concentrate‡ | s.e.m. | Significance level |
|---|---|---|---|---|
| Gross energy (MJ/kg DM) | 19.1 | 18.6 | 0.417 | 0.391 |
| Proximate composition (g/kg DM) | | | | |
| Crude protein | 14.2 | 12.5 | 0.632 | 0.130 |
| Crude fat | 2.87 | 3.17 | 0.033 | 0.003 |
| Crude fiber | 19.8 | 15.0 | 1.14 | 0.041 |
| Ash | 5.53 | 6.17 | 0.307 | 0.219 |
| Starch | 28.5 | 37.6 | 1.51 | 0.013 |
| Fatty acid composition (g/100 g fatty acids) | | | | |
| 16:0 | 20.2 | 24.1 | 0.677 | 0.016 |
| 18:0 | 5.11 | 9.44 | 1.05 | 0.043 |
| 20:0 | 6.51 | 3.66 | 0.567 | 0.024 |
| 18:1*c*9 | 15.1 | 16.0 | 0.345 | 0.154 |
| 18:2n-6 | 43.9 | 40.9 | 0.399 | 0.006 |
| 18:3n-3 | 9.16 | 5.96 | 0.716 | 0.034 |

DM = dry matter.
$n = 3$; values are mean + s.e.m.
†Silage-based diet = 30/70% of concentrate and silage, respectively.
‡Concentrate-based diet = 70/30% of concentrate and silage, respectively.

flash-frozen in liquid nitrogen and stored at −80°C for subsequent analysis.

The entire experiment was conducted under the guidelines for the care and use of experimental animals in the Unidade de Produção Animal, L-INIA, INRB (Fonte Boa, Vale de Santarém, Portugal).

*Preparation of membrane vesicles from bovine's mesenteric fat*

Membrane vesicles from bovine's mesenteric fat were prepared by differential centrifugation with buffer without detergents, according to Martins *et al.* (2010). Briefly, approximately 20 g of fat tissue from each bovine was chopped into small pieces, removing visible blood vessels, and homogenized in 200 ml of mannitol-Hepes buffer (100 mM mannitol, 10 mM Tris-Hepes, pH 7.4) in a Warring blender for 2 min. The homogenate was filtered through a 70 μm nylon mesh to separate the vascular stroma and intracellular fat retained in the filter. The filtrate was centrifuged at 46 000 × **g** for 45 min at 10°C to obtain a pellet of crude membranes and further washed in the same buffer. The membrane pellet was then resuspended in mannitol-Hepes buffer, transferred to a syringe and sheared by vigorously passing it 10 times through a 21-gauge needle and immediately used for transport experiments. Protein content was determined by the Bradford method (Bradford, 1976). The vesicle size of all membrane preparations was determined by Dynamic Light Scattering; Brookhaven Inst. BI-90.

*Fatty acid composition and cholesterol concentration of adipose membranes*

After membrane vesicle lyophilisation (at −60°C and 2.0 hPa), fatty acids were converted to methyl esters (FAME) (Raes *et al.*, 2001; Christie *et al.*, 2007). The resulting FAME were then analysed by gas chromatography, using a capillary column (30 m × 0.25 mm i.d., Omegawax 250; 0.25 mm film thickness; Supelco, Bellefont, CA, USA), equipped with a flame-ionization detector. The chromatographic conditions were described in detail elsewhere (Alves and Bessa, 2009). The fatty acid composition was expressed as g/100 g of total fatty acids identified.

Total cholesterol was extracted from lyophilized adipose membrane vesicles through a direct saponification with saturated methanolic KOH solution (Naeemi *et al.*, 1995). Cholesterol was separated and identified using high-performance liquid chromatography (HPLC) equipment (Agilent 1100 Series, Agilent Technologies Inc., Palo Alto, CA, USA) by normal phase (Zorbax Rx-Sil column, 250 mm × 4.6 mm i.d., 5 μm particle size, Agilent Technologies Inc.). HPLC was equipped with a diode array detector set at 206 nm and the solvent (30 ml/l isopropanol in *n*-hexane) flowed at 1 ml/min. Total cholesterol concentration was calculated, in duplicate, based on the external standard technique, from a standard curve for peak area *v.* cholesterol concentration and expressed as mg/mg vesicles.

*Water and glycerol permeability experiments*

Stopped-flow experiments were performed on a HI-TECH Scientific PQ/SF-53 apparatus with 2 ms dead time, temperature controlled and interfaced with a PC microcomputer. Experiments were performed at temperatures ranging from 14°C to 37°C. Typically, five runs were stored and analyzed in each experimental condition. For the measurement of osmotic water permeability, membrane vesicles (0.3 mg protein/ml) resuspended in mannitol-Hepes buffer (120 mOsM) were mixed with an equal amount of isosmotic or hyperosmotic (240 mOsM) mannitol solutions to reach an inwardly directed gradient of the impermeant solute. The kinetics of vesicle shrinkage was monitored from the time course of scattered light intensity at 400 nm until a stable light scatter signal was attained. The osmotic water permeability coefficient ($P_f$) was estimated by fitting the light scatter signal to a single exponential curve and using the linear relation between $P_f$ and the exponential time constant $k$ (van Heeswijk and van Os, 1986), $P_f = k(V_o/A)(1/V_w(\text{osm}_{out})_\infty)$, where $V_w$ is the molar volume of water, $V_o/A$ is the initial volume to area ratio of the vesicles and $(\text{osm}_{out})_\infty$ is the final medium osmolarity after the applied osmotic gradient. For glycerol permeability, membrane vesicles equilibrated in 120 mOsM mannitol-Hepes buffer were exposed to an external solution where the impermeant solute was partially replaced by glycerol (60 mOsM mannitol plus 180 mOsM glycerol, creating an inwardly directed glycerol gradient). After the first fast vesicle shrinkage due to water outflow, glycerol influx in response to its chemical gradient was followed by water influx with subsequent vesicle reswelling. Glycerol permeability was calculated as $P_{gly} = k(V_o/A)$, where $k$ is the single exponential time constant fitted to the light scatter signal of glycerol influx (Dix *et al.*, 1985). All solution osmolarities were determined from freezing point depression on a semimicro osmometer (Knauer GmbH, Germany) using standards of 100 and 400 mOsM.

The activation energy $E_a$ of water and glycerol transport was calculated from the slope of the Arrhenius plot (ln $P_f$ or ln $P_{gly}$ as a function of $1/T$) multiplied by the gas constant $R$.

*Membrane fluidity measurements*

Membrane fluidity was studied by a fluorescence polarization method, which measures the fluorescence anisotropy ($r$) of two probes incorporated in the membrane: 1,6-diphenyl-1,3,5-hexatriene (DPH), or 1-(4-(trimethylamino)phenyl)-6-phenyl-1,3,5-hexatriene (TMA–DPH; Molecular Probes, Junction City, OR, USA), as previously described (Martins *et al.*, 2010). Membrane fluidity was assessed based on the fluorescence anisotropy values, calculated by the equation $r = (I_{VV} - GI_{VH})/(I_{VV} + 2GI_{VH})$, where $I_{VV}$ and $I_{VH}$ are the fluorescence intensities and the subscripts indicate the vertical ($V$) or horizontal ($H$) orientations of the excitation and emission polarizers, and $G = I_{HV}/I_{HH}$ is the instrumental factor (Lakowicz, 1999). DPH fluorescence measurements were performed with an excitation wavelength ($\lambda_{exc}$) of 357 nm and an emission wavelength ($\lambda_{em}$) of 428 nm. For TMA–DPH, $\lambda_{exc} = 343$ nm and $\lambda_{em} = 427$ nm. The fluorescence intensity data points used for calculations were the average of three replicate aliquots (after blank subtraction) measured on a Varian Cary Eclipse fluorescence spectrophotometer (Varian Scientific Instruments, Mulgrave, Victoria, Australia).

*Statistics*

Statistical analysis was performed using the Statistical Analysis System (SAS) software package, version 9.1 (SAS Institute, USA). Data were expressed as mean and standard error of the mean. The GLM procedure was used to perform a $2 \times 2$ factorial analysis to determine significant main effects of breed (Alentejana or Barrosã), diet (silage or concentrate) and their respective interaction (breed × diet). In the case of interaction, significant differences between groups were identified using Fisher's *post-hoc* test at $P < 0.05$.

## Results

*Mesenteric and omental fat weights are affected by diet but not by breed*

Some of the growth performance parameters, including live slaughter weight, hot carcass weight and subcutaneous and visceral fat depots weights are shown in Table 2. An effect of breed was observed for live slaughter and hot carcass weights, as Alentejana bulls had higher values of both variables in relation to Barrosã bulls ($P < 0.0001$).

The subcutaneous fat weight obtained through the dissection of the leg was unchanged across the experimental groups ($P > 0.05$). The same occurred for total visceral fat ($P > 0.05$). Mesenteric and omental fat weights were increased ($P < 0.05$ and $P < 0.01$, respectively), by feeding a concentrate-based diet. An interaction between breed and diet was observed for KKCF depot weight ($P < 0.05$). Regarding this adipose depot weight, and for concentrate-fed bovines, Alentejana bulls had lower values, whereas Barrosã bulls had the opposite.

*Membrane-saturated fatty acids but not cholesterol concentration is influenced by diet and not by breed*

Table 3 depicts the lipid composition of membrane vesicles from mesenteric fat from the four experimental groups. Total cholesterol concentration was unaffected by breed or diet ($P > 0.05$). The distribution of the main fatty acid classes showed a highest occurrence of saturated fatty acids (SFA), followed by monounsaturated fatty acids (MUFA), then polyunsaturated fatty acids (PUFA) and lastly *trans* fatty acids (TFA). The diet affected the sum of SFA ($P < 0.05$), including the 18:0 fatty acid, being the values higher in silage-fed animals than in concentrate-fed bulls ($P < 0.05$). For this former fatty acid, a breed effect was also observed, as overall Barrosã breed showed a lower concentration ($P < 0.05$). In contrast, the 22:0 fatty acid was enhanced in Barrosã bulls, regardless of the diet ($P < 0.05$). Even if the sum of MUFA was not influenced by the factors under study ($P > 0.05$), 16:1*c*9 and 17:1*c*9 fatty acids were affected by diet, showing consistently higher concentrations in concentrate-fed bulls ($P < 0.05$). Moreover, the breed had a notorious effect in the 14:1*c*9 fatty acid concentration, with Barrosã bulls showing higher values than Alentejana ($P < 0.05$). The same effect was observed for 18:1*t*11 fatty acid ($P < 0.05$). In addition, an interaction between breed and diet was found for 18:1*c*11 and 18:1*c*12 fatty acids ($P < 0.05$), because significant differences on these concentrations were observed for the diet factor for Alentejana breed, but not for Barrosã. Hence, for Alentejana bulls, 18:1*c*11 fatty acid concentration was higher in concentrate-based than in silage-based diets; the opposite was observed for 18:1*c*12 fatty acid. Apart from these changes, no other significant variations regarding the sum or the individual fatty acids promoted by breed, diet or their respective interaction were observed.

*Permeability and fluidity of adipose membranes are independent of breed or diet*

Membrane vesicles obtained from mesenteric fat revealed a unimodal size distribution, showing a mean diameter of $371 \pm 57$ nm for all tested groups. These membrane preparations were subsequently used to assess water and glycerol permeability by stopped-flow spectroscopy, as well as membrane fluidity by fluorescence anisotropy.

Figure 1 depicts typical stopped-flow light scatter signals of vesicle volume changes when gradients of mannitol (water permeability, panel A) and glycerol (panel B) were imposed. The time courses of vesicle volume changes are

**Table 2** *Slaughter weight, hot carcass weight, subcutaneous and visceral adipose depots weights from Alentejana and Barrosã bulls fed silage- and concentrate-based diets*

| | Alentejana | | Barrosã | | | Significance level | | |
|---|---|---|---|---|---|---|---|---|
| | Sil | Conc | Sil | Conc | s.e.m. | Breed | Diet | Breed × diet |
| Performance traits | | | | | | | | |
| Live slaughter weight (kg) | 640 | 655 | 447 | 485 | 24.4 | <0.0001 | 0.286 | 0.640 |
| Hot carcass weight (kg) | 368 | 382 | 252 | 275 | 14.2 | <0.0001 | 0.213 | 0.774 |
| Carcass traits | | | | | | | | |
| Subcutaneous fat (g/kg leg) | 41.3 | 49.5 | 45.8 | 50.7 | 6.47 | 0.663 | 0.325 | 0.800 |
| Visceral fat (g/kg carcass) | 62.6 | 61.5 | 53.7 | 77.5 | 6.19 | 0.576 | 0.082 | 0.058 |
| Mesenteric fat (g/kg carcass) | 16.2 | 17.7 | 14.7 | 22.7 | 2.03 | 0.396 | 0.028 | 0.121 |
| Omental (g/kg carcass) | 21.7 | 24.4 | 18.2 | 29.4 | 2.35 | 0.747 | 0.008 | 0.087 |
| KKCF (g/kg carcass) | 24.8 | 19.4 | 20.8 | 25.3 | 2.28 | 0.666 | 0.852 | 0.042 |

KKCF = kidney knob and channel fat.
Dietary treatments: Sil = silage diet based on 30/70% of concentrate and silage, respectively; Conc = concentrate diet based on 70/30% of concentrate and silage, respectively. Values are mean + s.e.m.

**Table 3** *Cholesterol concentration (mg/mg vesicles) and fatty acid profile (g/100 g fatty acids) in mesenteric adipose tissue membrane vesicles from Alentejana and Barrosã bulls fed silage- and concentrate-based diets*

| | Alentejana | | Barrosã | | | Significance level | | |
|---|---|---|---|---|---|---|---|---|
| | Sil | Conc | Sil | Conc | s.e.m. | Breed | Diet | Breed × diet |
| Cholesterol | 0.014 | 0.014 | 0.011 | 0.017 | 0.004 | 0.922 | 0.380 | 0.345 |
| Fatty acid profile | | | | | | | | |
| 14:0 | 2.23 | 2.22 | 2.48 | 2.20 | 2.74 | 0.508 | 0.399 | 0.280 |
| 14:1*c*9 | 0.265 | 0.212 | 0.325 | 0.513 | 0.092 | 0.034 | 0.404 | 0.143 |
| 15:0 | 0.579 | 0.405 | 0.614 | 0.530 | 0.073 | 0.222 | 0.056 | 0.488 |
| 16:0 | 18.5 | 18.7 | 19.1 | 19.4 | 0.668 | 0.251 | 0.607 | 0.975 |
| 16:1*c*7 | 0.387 | 0.290 | 0.362 | 0.383 | 0.163 | 0.507 | 0.463 | 0.252 |
| 16:1*c*9 | 1.32 | 1.68 | 1.57 | 1.82 | 0.185 | 0.124 | 0.023 | 0.679 |
| 17:0 | 1.09 | 1.06 | 1.01 | 0.950 | 0.152 | 0.501 | 0.737 | 0.891 |
| 17:1*c*9 | 0.476 | 0.680 | 0.485 | 0.535 | 1.68 | 0.219 | 0.028 | 0.163 |
| 18:0 | 25.5 | 22.7 | 23.0 | 21.5 | 2.11 | 0.030 | 0.014 | 0.437 |
| 18:1*t*6 + *t*8 | 0.408 | 0.288 | 0.382 | 0.440 | 0.168 | 0.428 | 0.699 | 0.269 |
| 18:1*t*9 | 0.335 | 0.243 | 0.258 | 0.462 | 0.092 | 0.423 | 0.526 | 0.105 |
| 18:1*t*10 | 0.222 | 0.618 | 0.275 | 0.399 | 0.134 | 0.521 | 0.054 | 0.296 |
| 18:1*t*11 | 1.44 | 1.00 | 2.00 | 1.56 | 1.91 | 0.018 | 0.055 | 0.988 |
| 18:1*t*12 | 0.548 | 0.428 | 0.475 | 0.535 | 0.083 | 0.828 | 0.703 | 0.253 |
| 18:1*c*9 | 24.0 | 26.5 | 26.0 | 25.9 | 2.67 | 0.593 | 0.345 | 0.325 |
| 18:1*c*11 | 1.16[a] | 1.63[b] | 1.40[ab] | 1.44[ab] | 0.154 | 0.803 | 0.018 | 0.045 |
| 18:1*c*12 | 0.529[a] | 0.332[b] | 0.383[ab] | 0.493[ab] | 0.114 | 0.912 | 0.517 | 0.030 |
| 18:1*t*16 + *c*14 | 0.321 | 0.176 | 0.302 | 0.252 | 0.055 | 0.577 | 0.072 | 0.365 |
| 18:2n-6 | 3.72 | 3.82 | 3.76 | 4.17 | 2.28 | 0.719 | 0.629 | 0.775 |
| 18:3n-3 | 0.551 | 0.396 | 0.520 | 0.504 | 0.071 | 0.529 | 0.173 | 0.265 |
| 20:0 | 0.509 | 0.501 | 0.491 | 0.500 | 0.116 | 0.924 | 0.996 | 0.928 |
| 20:2n-6 | 0.134 | 0.130 | 0.219 | 0.128 | 0.046 | 0.324 | 0.259 | 0.303 |
| 20:4n-6 | 3.49 | 3.42 | 3.54 | 3.29 | 0.701 | 0.951 | 0.792 | 0.884 |
| 22:0 | 1.14 | 1.13 | 1.32 | 1.77 | 0.279 | 0.018 | 0.187 | 0.170 |
| 22:5n-3 | 0.464 | 0.332 | 0.550 | 0.562 | 0.120 | 0.174 | 0.597 | 0.526 |
| ΣSFA | 49.5 | 46.8 | 48.0 | 46.9 | 4.19 | 0.449 | 0.041 | 0.394 |
| ΣMUFA | 28.1 | 31.4 | 30.5 | 31.1 | 2.90 | 0.448 | 0.182 | 0.356 |
| ΣTFA | 3.28 | 2.75 | 3.69 | 3.65 | 0.625 | 0.138 | 0.517 | 0.576 |
| ΣPUFA | 8.36 | 8.10 | 8.59 | 8.65 | 1.32 | 0.706 | 0.924 | 0.876 |
| Σn-3 | 1.02 | 0.728 | 1.07 | 1.07 | 4.21 | 0.199 | 0.336 | 0.350 |
| Σn-6 | 7.34 | 7.37 | 7.52 | 7.59 | 2.53 | 0.840 | 0.962 | 0.984 |
| ΣUnidentified | 10.8 | 11.0 | 9.17 | 9.70 | 1.42 | 0.179 | 0.718 | 0.888 |

SFA = saturated fatty acids; MUFA = monounsaturated fatty acids; TFA = *trans* fatty acids; PUFA = polyunsaturated fatty acids.
Dietary treatments: Sil = silage diet based on 30/70% of concentrate and silage, respectively; Conc = concentrate diet based on 70/30% of concentrate and silage, respectively. Values are mean + s.e.m.
[a,b]Mean values within the same row with different superscript letters are significantly different (Fisher's *post-hoc* test, $P<0.05$).
FAME = fatty acid methyl esters. ΣSFA = sum of 14:0, 15:0, 16:0, 17:0, 18:0, 20:0 and 22:0; ΣMUFA = sum of 14:1*c*9, 16:1*c*7, 16:1*c*9, 17:1*c*9, 18:1*c*9, 18:1*c*11 and 18:1*c*12; ΣTFA = sum of 18:1*t*6 + *t*8, 18:1*t*9, 18:1*t*10, 18:1*t*11, 18:1*t*12 and 18:1*t*16 + *c*14; ΣPUFA = sum of 18:2n-6, 18:3n-3, 20:2n-6, 20:4n-6 and 22:5n-3; Σn-6 = sum of 18:2n-6, 20:2n-6 and 20:4n-6; Σn-3 = sum of 18:3n-3 and 22:5n-3.

used to calculate $P_f$ and $P_{gly}$, as described in the section 'Material and Methods'.

The permeability values obtained for the two bovine breeds fed silage- or concentrate-based diets are shown in Table 4. Neither breed nor diet affected the permeability of adipose membrane vesicles to water ($P_f$) and glycerol ($P_{gly}$) ($P > 0.05$). Accordingly, the activation energy values ($E_a$) for water and glycerol permeation were similar among experimental groups, ranging from 14.5 ± 0.3 to 15.0 ± 0.2 kcal/mol (60.7 ± 1.3 to 62.8 ± 0.8 kJ/mol) for water ($P > 0.05$) and 23.7 ± 0.3 to 24.3 ± 0.2 kcal/mol (99.2 ± 1.4 to 102 ± 1.0 kJ/mol) for glycerol ($P > 0.05$). These relative high $E_a$ values suggest that permeation occurs mainly through the lipid bilayer with no contribution of specific protein channels for transport.

The fluorescence anisotropy of DPH and TMA–DPH in membrane vesicles from each experimental group are also shown in Table 4. Following the same pattern, no significant effects of breed or diet were detected among experimental groups ($P > 0.05$) for both fluorescence probes.

## Discussion

The manipulation of adipose tissue growth, deposition and metabolism has important economic implications for the

livestock industry, because it can improve production efficiency, carcass composition and meat quality.

Two underlying processes are responsible for increased adiposity in beef cattle: hypertrophy (larger adipocyte size) and hyperplasia (larger number of adipocytes) (Novakofski, 2004), which are affected by factors such as genetics, sex, age, feeding regimen, food supply and the specific adipose tissue depot (Vernon and Houseknecht, 1991). However, an understanding of the mechanisms of body fat deposition in farm animals and its outcome in adipocyte physiology is far from well established. Consequently, this study was designed to elucidate the contribution of breed and diet to adipose tissue membrane permeability and fluidity as possible key players on fat deposition in bovines. The morphological features between these breeds reflect differences in mature size and, consequently, fat accumulation (da Silva *et al.*, 1998). Following on our previous results, in which the mesenteric fat depot had smaller adipocytes but a greater number of cells than subcutaneous fat (Costa ASH *et al.*, unpublished data), the aforementioned visceral fat was selected for analysis due to its unique properties, regarding lipogenic activity and immune-response potential (Mukesh *et al.*, 2010).

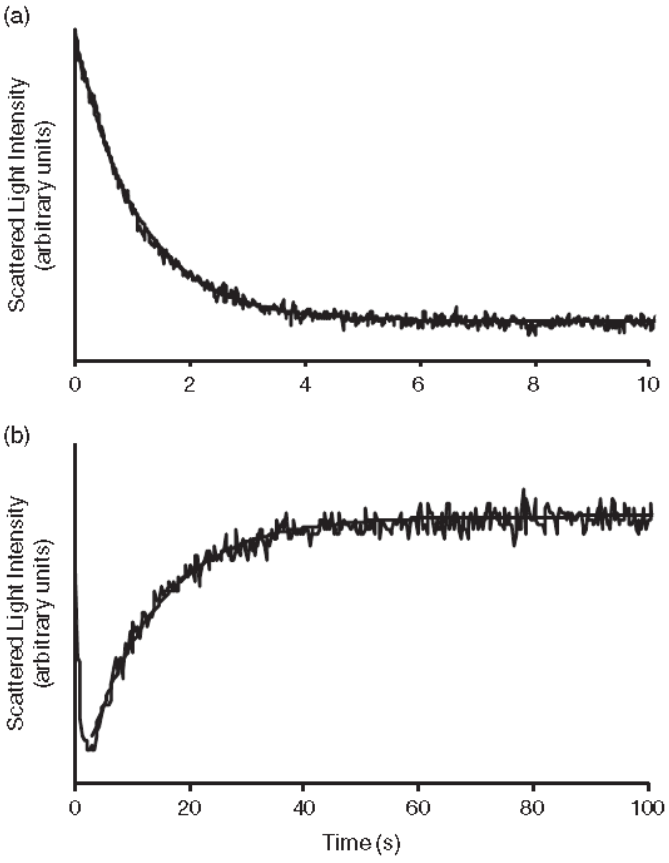


**Figure 1** Representative stopped flow light scatter of adipose membrane vesicles permeability to water and glycerol at 23°C. Time course of (a) vesicle shrinkage due to water outflow after an hyperosmotic shock with 120 mOsM mannitol gradient or (b) vesicle reswelling due to glycerol uptake after an inwardly directed 180 mOsM glycerol gradient.

As expected, a clear effect of breed was observed for some growth performance parameters, with Alentejana displaying higher values for live slaughter and hot carcass weights (da Silva *et al.*, 1998; Reis *et al.*, 2001).

Regarding lipid deposition, all fat depots under study were unaffected by breed. However, diet appeared to play a significant role in determining mesenteric and omental fat depots weight, which were consistently higher in concentrate-fed bovines. The chosen silage- and concentrate-based diets provided significant differences in their composition. The concentrate-based diet exhibited higher fat and starch concentrations, whereas the silage-based diet exhibited higher fiber concentration. These differences extend to the detailed fatty acid composition, in particular to the sums of SFA and PUFA classes. The proportions for SFA were higher in concentrate-based diets (silage 31.9 *v.* concentrate 37.2) at the expenses of 16:0, 18:0 and 20:0 fatty acids. The inverse trend was observed for PUFA (silage 53.0 *v.* concentrate 46.8), determined by 18:2n-6 and 18:3n-3 fatty acids.

There is convincing evidence in animal models that dietary fat influences cell membrane phospholipid composition (Clandinin *et al.*, 1985; Jenkins, 1994). Typically, ruminant diets are low in fat but high in PUFA contents. Nevertheless, unsaturated fatty acids in the diet undergo an extensive biohydrogenation in the rumen, with consequently high levels of SFA being absorbed in the intestine and deposited in the tissues (Wachira *et al.*, 2002). In agreement, adipose membranes from visceral fat were found to be richer in SFA, displaying concomitantly a lower proportion of PUFA.

**Table 4** *Permeability values for water ($P_f$) and glycerol ($P_{gly}$), and fluorescence anisotropy of DPH and TMA–DPH in mesenteric adipose tissue membrane vesicles from Alentejana and Barrosã bulls fed silage- and concentrate-based diets*

| | Alentejana | | Barrosã | | | Significance level | | |
|---|---|---|---|---|---|---|---|---|
| | Sil | Conc | Sil | Conc | s.e.m. | Breed | Diet | Breed × diet |
| Permeability | | | | | | | | |
| $P_f \times 10^{-4}$ cm/s | 1.42 | 1.41 | 1.45 | 1.42 | 0.053 | 0.766 | 0.681 | 0.894 |
| $P_{gly} \times 10^{-7}$ cm/s | 4.47 | 4.57 | 4.26 | 4.55 | 0.213 | 0.593 | 0.370 | 0.673 |
| Fluorescence anisotropy | | | | | | | | |
| DPH | 0.159 | 0.148 | 0.168 | 0.169 | 0.010 | 0.118 | 0.617 | 0.524 |
| TMA–DPH | 0.274 | 0.266 | 0.271 | 0.270 | 0.005 | 0.943 | 0.364 | 0.525 |

DPH = 1,6-diphenyl-1,3,5-hexatriene; TMA–DPH = 1-(4-(trimethylamino)phenyl)-6-phenyl-1,3,5-hexatriene.
Dietary treatments: Sil = silage diet based on 30/70% of concentrate and silage, respectively; Conc = concentrate diet based on 70/30% of concentrate and silage, respectively. Values are mean + s.e.m.

Cholesterol is a biomembrane-rigidifying component. When cholesterol is aligned in parallel array with the phospholipid fatty acyl chains, it reduces membrane fluidity (Stubbs and Smith, 1984; Onuki *et al.*, 2008), but inversely, increases rigidity. Our results indicate that total cholesterol concentration was unchanged by any factor under study. Accordingly, neither breed nor diet affected the permeability of adipose membranes to water or glycerol. The activation energy for both water and glycerol transport was high and relatively stable in all cases, thus indicating that permeation is not protein-mediated and occurs mainly via the lipid bilayer where permeability correlates with fluidity. Accordingly, no variations for adipose membrane fluidity were found with DPH or TMA–DPH probes, which assess fluidity at different depths in the bilayer (TMA–DPH assessing a region closer to the lipid–water interface). Altogether, these results corroborate the stability found in permeability data.

Besides cholesterol, fatty acids strongly influence membrane fluidity. With an increase in unsaturated fatty acids concentration, membrane fluidity increases because PUFA acyl chains are extremely flexible and can rapidly change conformational states. The fatty acid profile in adipose membranes from mesenteric fat of Alentejana and Barrosã bovines fed silage- and concentrate-based diets showed no variations in PUFA sum and, foremost important, included none of the n-3 fatty acids, EPA (20:5n-3) and DHA (22:6n-3), well known for their impressive range of health benefits, the latter being recognized as a potent membrane fluidizer agent (Stillwell and Wassall, 2003). These results are in accordance to Wachira *et al.* (2002), who found residual concentration of both n-3 fatty acids in subcutaneous fat of sheep, even after the intake of feeding regimens enriched in linseed and fish oils. Dietary lipids do not directly affect the fatty acid composition of ruminant adipose tissues, as they do in non-ruminants (Sarkkinen *et al.*, 1994). Raising the PUFA content of ruminant tissues by PUFA feeding is rather complex due to the extensive hydrogenation of dietary unsaturated fatty acids by rumen microorganisms (Pond, 1999; Jambrenghi *et al.*, 2007). Nevertheless, the few changes observed for the general fatty acid profile in adipose membranes appear to reflect the dietary treatment imposed, instead of a breed-related effect. The same pattern had already been observed for the fatty acid profile in mesenteric fat, with diet determining the proportions of the major fatty acids as well as their partial sums (Costa ASH *et al.*, unpublished data). Although the sum of MUFA was kept similar across experimental groups, the 16:1*c*9 and 17:1*c*9 fatty acids were under the influence of diet, with higher concentration in concentrate-fed bulls. This is in line with previous reports stating that concentrate promotes higher expression or activity levels of delta-9 desaturase enzyme, responsible for the conversion of SFA to MUFA (Daniel *et al.*, 2004). Nevertheless, these differences relate to residual concentration of these fatty acids, ranging from 0.48% to 1.82% and, therefore we believe, play an irrelevant physiological role. Similarly, total SFA was affected by the diet factor, being the difference observed largely determined by stearic acid (18:0) concentration in Alentejana bulls fed on silage. More 18:2n-6 fatty acid in the silage feeding regimen results in more 18:0 in adipose plasma membranes, as reported formerly (Jenkins, 1994). High stearic levels are also in accordance to the reported values in the adipose tissue of lambs (Enser *et al.*, 1996).

Finally, a breed effect was observed for 22:0, 14:1*c*9 and 18:1*t*11. All three fatty acids concentration were higher in Barrosã bulls when compared with Alentejana bulls. The long-chain fatty acids (LCFA) occurred at very low levels in the adipose membranes of bovines, either Alentejana or Barrosã, fed any of the dietary treatments. Low levels of LCFA in ruminant's adipose tissue have already been reported and were attributed to the low incorporation of these fatty acids into the triacylglycerol fraction, as well as to the low proportion of phospholipid in the adipose tissue (Enser *et al.*, 1996; Wachira *et al.*, 2002). Concerning the difference observed between breeds for the 22:0 fatty acid, it might be due to a higher elongase expression, or enzymatic activity, in the Barrosã than in the Alentejana breed. Genetic background also appeared to dictate a differential expression, or activity, of delta-9 desaturase enzyme, responsible for the conversion of 14:0 to 14:1*c*9 (Keating *et al.*, 2006). These hypotheses remain to be tested. In relation to the 18:1*t*11 fatty acid, commonly known as vaccenic acid, it is metabolized into the *c*9,*t*11-conjugated linoleic acid (CLA) isomer (Lock *et al.*, 2004), to which numerous health claims have been attributed (Bhattacharya *et al.*, 2006), and for this reason has been considered as beneficial or neutral.

## Conclusions

This study reports that adipose membranes from ruminant's mesenteric fat depot were rich in SFA due to ruminal biohydrogenation of dietary PUFA. Membrane fluidity and permeability to glycerol were found to be independent of breed (Alentejana or Barrosã) and diet (based on 70/30% or 30/70% of corn silage and concentrate, respectively). Re-enforcing these findings, cholesterol, the main biomembrane-rigidifying component, and in particular, unsaturated fatty acid concentration were unchanged among experimental groups.

## Acknowledgements

This study was supported by Fundação para a Ciência e a Tecnologia (FCT) through grant PTDC/CVT/2006/66114 and individual fellowships to Ana P. Martins (SFRH/BD/2009/65046), Ana S. H. Costa (SFRH/BD/2009/61068) and Susana V. Martins (SFRH/BPD/2009/63019). Paula A. Lopes is a researcher from the program "Ciência 2008" from FCT. We wish to express our gratitude to Rui Bessa and Susana Alves (L-INIA-REQUIMTE) for providing fatty acid profiles.

## References

Alfaia CMM, Castro MLF, Martins SIV, Portugal APV, Alves SPA, Fontes CMGA, Bessa RJB and Prates JAM 2007. Effect of slaughter season on fatty acid composition, conjugated linoleic acid isomers and nutritional value of intramuscular fat in Barrosã-PDO veal. Meat Science 75, 44–52.

Alfaia CPM, Alves SP, Martins SIV, Costa ASH, Fontes CMGA, Lemos JPC, Bessa RJB and Prates JAM 2009. Effect of the feeding system on intramuscular fatty acids and conjugated linoleic acid isomers of beef cattle, with emphasis on their nutritional value and discriminatory ability. Food Chemistry 114, 939–946.

Alves SP and Bessa RJ 2009. Comparison of two gas–liquid chromatograph columns for the analysis of fatty acids in ruminant meat. Journal of Chromatography A 1216, 5130–5139.

Azain MJ 2004. Role of fatty acids in adipocyte growth and development. Journal of Animal Science 82, 916–924.

Beja-Pereira A, Alexandrino P, Bessa I, Carretero Y, Dunner S, Ferrand N, Jordana J, Laloe D, Moazami-Goudarzi K, Sanchez A and Canon J 2003. Genetic characterization of southwestern European bovine breeds: a historical and biogeographical reassessment with a set of 16 microsatellites. Journal of Heredity 94, 243–250.

Bhattacharya A, Banu J, Rahman M, Causey J and Fernandes G 2006. Biological effects of conjugated linoleic acids in health and disease. Journal of Nutritional Biochemistry 17, 789–810.

Bradford MM 1976. A rapid and sensitive method for the quantitation of microgram quantities of protein utilizing the principle of protein–dye binding. Analytical Biochemistry 72, 248–254.

Christie WW, Dobson G and Adlof RO 2007. A practical guide to the isolation, analysis and identification of conjugated linoleic acid. Lipids 42, 1073–1084.

Clandinin MT, Field CJ, Hargreaves K, Morson L and Zsigmond E 1985. Role of diet fat in subcellular structure and function. Canadian Journal of Physiology and Pharmacology 63, 546–556.

da Silva MF, Lemos JPC, Monteiro LS and Portugal AV 1998. Studies on growth and form: multivariate analysis of distribution of muscle and fat in Portuguese cattle breeds. Livestock Production Science 55, 261–271.

Daniel ZCTR, Wynn RJ, Salter AM and Buttery PJ 2004. Differing effects of forage and concentrate diets on the oleic acid and conjugated linoleic acid content of sheep tissues: the role of stearoyl-CoA desaturase. Journal of Animal Science 82, 747–758.

De Smet S, Raes K and Demeyer D 2004. Meat fatty acid composition as affected by fatness and genetic factors: a review. Animal Research 53, 81–98.

Dix JA, Ausiello DA, Jung CY and Verkman AS 1985. Target analysis studies of red cell water and urea transport. Biochimica et Biophysica Acta 821, 243–252.

Enser M, Hallett K, Hewitt B, Fursey GAJ and Wood JD 1996. Fatty acid content and composition of English beef, lamb and pork at retail. Meat Science 42, 443–456.

Field CJ and Clandinin MT 1984. Modulation of adipose-tissue fat composition by diet – a review. Nutrition Research 4, 743–755.

Field CJ, Ryan EA, Thomson ABR and Clandinin MT 1988. Dietary-fat and the diabetic state alter insulin binding and the fatty acyl composition of the adipocyte plasma-membrane. Biochemical Journal 253, 417–424.

Hocquette JF, Gondret F, Baeza E, Medale F, Jurie C and Pethick DW 2010. Intramuscular fat content in meat-producing animals: development, genetic and nutritional control, and identification of putative markers. Animal 4, 303–319.

Jambrenghi AC, Paglialonga G, Gnoni A, Zanotti F, Giannico F, Vonghia G and Gnoni GV 2007. Changes in lipid composition and lipogenic enzyme activities in liver of lambs fed omega-6 polyunsaturated fatty acids. Comparative Biochemistry and Physiology B – Biochemistry & Molecular Biology 147, 498–503.

Jenkins TC 1994. Regulation of lipid-metabolism in the rumen. The Journal of Nutrition 124, S1372–S1376.

Keating AF, Kennelly JJ and Zhao FQ 2006. Characterization and regulation of the bovine stearoyl-CoA desaturase gene promoter. Biochemical and Biophysical Research Communications 344, 233–240.

Lakowicz JR 1999. Principles of fluorescence spectroscopy. Kluwer Academic/Plenum, New York.

Lande MB, Donovan JM and Zeidel ML 1995. The relationship between membrane fluidity and permeabilities to water, solutes, ammonia, and protons. Journal of General Physiology 106, 67–84.

Lock AL, Corl BA, Barbano DM, Bauman DE and Ip C 2004. The anticarcinogenic effect of trans-11 18:1 is dependent on its conversion to cis-9, trans-11 CLA by delta 9-desaturase in rats. The Journal of Nutrition 134, 2698–2704.

Martins AP, Lopes PA, Martins SV, Madeira A, Santos NC, Prates JA, Moura TF and Soveral G 2010. Conjugated linoleic acid reduces permeability and fluidity of adipose plasma membranes from obese Zucker rats. Biochemical and Biophysical Research Communications 398, 199–204.

Mukesh M, Bionaz M, Graugnard DE, Drackley JK and Loor JJ 2010. Adipose tissue depots of Holstein cows are immune responsive: inflammatory gene expression in vitro. Domestic Animal Endocrinology 38, 168–178.

Naeemi ED, Ahmad N, al-Sharrah TK and Behbahani M 1995. Rapid and simple method for determination of cholesterol in processed food. Journal of AOAC International 78, 1522–1525.

Novakofski J 2004. Adipogenesis: usefulness of in vitro and in vivo experimental models. Journal of Animal Science 82, 905–915.

Onuki Y, Hagiwara C, Sugibayashi K and Takayama K 2008. Specific effect of polyunsaturated fatty acids on the cholesterol-poor membrane domain in a model membrane. Chemical & Pharmaceutical Bulletin 56, 1103–1109.

Pond CM 1999. Physiological specialisation of adipose tissue. Progress in Lipid Research 38, 225–248.

Raes K, De Smet S and Demeyer D 2001. Effect of double-muscling in Belgian Blue young bulls on the intramuscular fatty acid composition with emphasis on conjugated linoleic acid and polyunsaturated fatty acids. Animal Science 73, 253–260.

Reis C, Navas D, Pereira M and Cravador A 2001. Growth hormone *ALUI* polymorphism analysis in eight Portuguese bovine breeds. Archivos de Zootecnia 50, 41–48.

Sarkkinen ES, Agren JJ, Ahola I, Ovaskainen ML and Uusitupa MIJ 1994. Fatty-acid composition of serum-cholesterol esters, and erythrocyte and platelet membranes as indicators of long-term adherence to fat-modified diets. American Journal of Clinical Nutrition 59, 364–370.

Simões JA and Mendes I 2003. Distribution of tissues in carcasses at the same proportion of total fat in Portuguese cattle breeds. Animal Research 52, 287–298.

Soveral G, Martins AP, Martins SV, Lopes PA, Alfaia CM, Prates JA and Moura TF 2009. Effect of dietary conjugated linoleic acid isomers on water and glycerol permeability of kidney membranes. Biochemical and Biophysical Research Communications 383, 108–112.

Stillwell W and Wassall SR 2003. Docosahexaenoic acid: membrane properties of a unique fatty acid. Chemistry and Physics of Lipids 126, 1–27.

Stubbs CD and Smith AD 1984. The modification of mammalian membrane polyunsaturated fatty-acid composition in relation to membrane fluidity and function. Biochimica et Biophysica Acta 779, 89–137.

van Heeswijk MP and van Os CH 1986. Osmotic water permeabilities of brush border and basolateral membrane vesicles from rat renal cortex and small intestine. Journal of Membrane Biology 92, 183–193.

Vernon RG and Houseknecht KL 1991. Adipose tissue: beyond an energy reserve. In Ruminant physiology: digestion, metabolism, growth and reproduction (ed. PB Cronjé), pp. 171–186. CAB International, London.

Wachira AM, Sinclair LA, Wilkinson RG, Enser M, Wood JD and Fisher AV 2002. Effects of dietary fat source and breed on the carcass composition, n-3 polyunsaturated fatty acid and conjugated linoleic acid content of sheep meat and adipose tissue. British Journal of Nutrition 88, 697–709.

Biochemical and Biophysical Research Communications 423 (2012) 170–175

Contents lists available at SciVerse ScienceDirect

Biochemical and Biophysical Research Communications

journal homepage: www.elsevier.com/locate/ybbrc

# Differences in lipid deposition and adipose membrane biophysical properties from lean and obese pigs under dietary protein restriction

Ana P. Martins [a,1], Paula A. Lopes [b,1], Marta S. Madeira [b], Susana V. Martins [b], Nuno C. Santos [c], Teresa F. Moura [a], José A.M. Prates [b], Graça Soveral [a,d,*]

[a] REQUIMTE, Dep. Química, FCT-UNL, 2829-516 Caparica, Portugal
[b] CISA, Faculdade de Medicina Veterinária, Universidade Técnica de Lisboa, 1300-477 Lisboa, Portugal
[c] Instituto de Medicina Molecular, Faculdade de Medicina, Universidade de Lisboa, 1649-028 Lisboa, Portugal
[d] Dep. Bioquímica e Biologia Humana, Faculdade de Farmácia, Universidade de Lisboa, 1649-003 Lisboa, Portugal

ARTICLE INFO

*Article history:*
Received 17 May 2012
Available online 26 May 2012

*Keywords:*
Adipocyte membranes
Lipid composition
Membrane fluidity
Permeability
Pigs
Reduced protein diet

ABSTRACT

Obesity consists in fat accumulation leading to increase in adipose cells number and size. Adipocyte membrane biophysical properties are critical to maintain cellular viability in metabolically healthy obesity. This study investigated the effect of the genetic background and dietary protein restriction on fat tissue lipid composition, adipocyte membrane fluidity and water permeability using the pig as experimental model.

Twenty-four male pigs from distinct genotypes, lean and obese, were fed on normal and reduced protein diets within a 2 × 2 factorial arrangement (two genotypes and two diets). Backfat thickness was two-fold higher in obese than in lean pigs but unrelated to dietary protein level. In contrast, total fatty acids in the subcutaneous adipose tissue were dependent on both breed and diet, with increased lipid content promoted by the fatty genotype and by the restriction of dietary protein. Adipose membranes isolated from obese pig's subcutaneous fat tissue showed higher permeability to water, in line with an increased fluidity. Moreover, the reduced content of dietary protein influenced positively the fluidity of adipose membranes. Neither genotype nor diet affected total cholesterol concentration in the adipose membranes. Membrane-saturated fatty acids' content was influenced by genotype, while membrane-polyunsaturated fatty acids, particularly from the *n*-6 family, was influenced by diet. The ratio of oleic (18:1c9)/linoleic (18:2*n*-6) acids was positively correlated with membrane fluidity. All together, these findings reinforce the genetic background as a determinant player on adipose membrane biophysical properties and point to the dietary protein level as an important factor for subcutaneous lipid deposition as well as for regulation of membrane function, factors that may have impact on human obesity and metabolic syndrome.



## 1. Introduction

Obesity is characterized by increased accumulation of triacylglycerols in the adipose tissue from subcutaneous and visceral depots, but also in surrounding organs as kidney, epicardium, skeletal muscle, and blood vessels as the result of hypertrophy and hyperplasia of adipocytes [1]. The adipose tissue is a highly dynamic endocrino-metabolic organ capable of efficient storage and mobilization of lipids to fulfill bioenergetic demands [2]. Lipids are involved in a wide array of processes, not only providing efficient energy storage and specific substrates for cell signaling, but also building membranes within the cell, thus providing compartmentalization.

Cell membranes are primarily composed of lipids and different lipids can alter membrane physical properties such as fluidity and passive permeability. Depending on their composition, cell membranes play an important role in regulating many cellular functions, such as signal transduction, receptor mobility, lipid trafficking, channels and transporters and cell adhesion. Moreover, membrane fluidity and lipid composition have been shown to affect the specific binding of a variety of hormones to their receptors [3].

It is well known that dietary fats can affect the types of lipids present in the organism. In the body, fatty acids derived from the diet and from *de novo* lipogenesis can be further elongated and unsaturated via elongases and desaturases thus generating a variety of lipid species that can then maintain a specific lipid composition [4]. This adaptation, enabling to preserve membrane function as the adipose

* Corresponding author at: REQUIMTE, Dep. Química, FCT-UNL, 2829-516 Caparica, Portugal. Fax: +351 212948550.
*E-mail address:* gsoveral@ff.ul.pt (G. Soveral).
[1] These authors have contributed equally to this article.

0006-291X/$ - see front matter © 2012 Elsevier Inc. All rights reserved.
http://dx.doi.org/10.1016/j.bbrc.2012.05.108

cells expand, is eventually disrupted in morbidly obese individuals, with an outcome favoring secondary diseases such as the metabolic syndrome [5]. How the membrane biophysical properties are regulated to match the specific needs of the membrane expansion is still obscure.

Another aspect related to tissue lipid redistribution was reported using pigs as an experimental model. It has been shown that plasma cholesterol increased dramatically in lean pigs fed low protein diets [6] and that reduced dietary energy and protein in growing pigs significantly increased intramuscular fat [7], while having a minor effect on the amount of subcutaneous adipose tissue [8,9]. Reducing the proportion of protein relative to energy in the diet consistently increases fat deposition. One possible explanation for this effect is that the low protein content restricted muscle growth, resulting in excess energy being converted into intramuscular lipids [8]. Another possibility is that restricted growth from the reduced protein diet (RPD) led to fat redistribution, resulting in an increase of intramuscular fat [7,10].

Considering problems in collecting tissue samples and the multifactorial etiology of obesity in human patients, suitable animal models are essential for a better understanding of the metabolic onset of obesity. Pigs display several anatomical-physiological and metabolic similarities to humans of special interest for the study of genetic or dietary induced obesity [11].

In the present study, pigs with distinct genetic backgrounds, Crossbred (commercial pigs resulting from Large White, Landrace and Pietrain inbreeding) and Alentejana purebred, were selected because they mimic genetically lean and obese animal models respectively, thus providing a valuable comparative model for human obesity. The effect of genotype (lean *versus* obese) as well as the restriction of dietary protein (control or reduced protein diets) on subcutaneous fat deposition was investigated. Additionally, the impact of genotype and RPD at the cell membrane level was determined by assessing adipose membrane lipid composition and biophysical properties such as fluidity and permeability.

## 2. Materials and methods

### 2.1. Experimental design: Animals and diets

This trial was conducted at the facilities of L-INIA (INRB, Vale de Santarem, Portugal) under the guidelines for the care and use of experimental animals, following EU directive 86/609/EEC.

Twenty-four Crossbred (50% Large White, 25% Landrace and 25% Pietrain) and Alentejano purebred entire male pigs with an initial average weight of 60 ± 2 kg were selected. Animals were fed a commercial concentrate diet from weaning until the beginning of the experiment. Thereafter, six animals from each genotype were randomly assigned to one of two diets in a 2 × 2 factorial arrangement (two genotypes and two diets). Pigs were fed individually twice a day whilst water was freely available. Throughout the experiment, pigs were weighted weekly just before feeding. Diets were isoenergetically formulated (16 MJ ME/kg) and differed in crude protein and lysine contents: the control diet contained 17.5% of crude protein and 0.7% of lysine; and the RPD contained 13.1% of crude protein and 0.4% of lysine. The proximate and fatty acid composition of the diets is presented in Table 1.

**Table 1**
Proximate and fatty acid composition of control and reduced protein diets (RPD).

| | Control | RPD |
|---|---|---|
| *Chemical composition (% diet)* | | |
| Dry matter | 89.1 | 89.0 |
| Ash | 4.4 | 4.0 |
| Crude fiber | 4.9 | 4.0 |
| Crude fat | 3.1 | 2.9 |
| Crude protein | 17.5 | 13.1 |
| Calcium | 0.82 | 0.84 |
| Phosphorus | 0.37 | 0.37 |
| Lysine | 0.7 | 0.4 |
| *Fatty acid composition (% total fatty acids)* | | |
| 14:0 | 0.1 | 0.2 |
| 16:0 | 17.3 | 19.6 |
| 16:1c9 | 0.8 | 0.2 |
| 18:0 | 2.6 | 2.6 |
| 18:1c9 | 19.0 | 19.3 |
| 18:1c11 | 1.5 | 1.6 |
| 18:2n-6 | 52.5 | 50.2 |
| 18:3n-3 | 4.9 | 4.3 |
| 20:0 | 0.3 | 0.3 |
| 20:1c11 | 0.4 | 0.5 |

### 2.2. Pigs' tissue sampling

Feed was removed 17–19 h before slaughter. Pigs were slaughtered at a live weight of 93 ± 2 kg (L-INIA experimental abattoir). After electrical stunning and exsanguination, samples from subcutaneous adipose tissue were collected from the right carcass side directly above *longissimus lumborum* muscle. At 24 h postmortem, the backfat thickness was measured in the left carcass side at the last rib position (P2).

### 2.3. Total fatty acids in the subcutaneous adipose tissue

Subcutaneous adipose tissue samples were lyophilized (−60 °C and 2.0 hPa) to constant weight, kept dry at −20 °C, and analyzed within two weeks. Total fatty acids were extracted from the lyophilized samples (ca. 250 mg) [12] using dichloromethane:methanol 2:1 (v/v), converted to methyl esters (FAME) [13] and were determined using a gas chromatograph HP6890A (Hewlett–Packard, PA, USA), equipped with a flame ionization detector and a CP-Sil 88 capillary column (100 m; 0.25 mm i.d.; 0.20 m film thickness; Chrompack, Varian Inc., Walnut Creek, CA, USA) with the chromatographic conditions described [14]. The quantification of total FAME was done using nonadecanoic acid (19:0) from Supelco (Bellefonte, PA, USA), as internal standard.

### 2.4. Isolation of membranes from subcutaneous adipose tissue

Membrane vesicles were prepared from subcutaneous adipose tissue by differential centrifugation with buffer without detergents, using a previously described method [15,16] optimized for pig fat tissue. Crude membranes re-suspended in mannitol–Hepes buffer (100 mM mannitol, 10 mM Tris–Hepes, pH 7.4) were immediately used for experiments. Protein content was determined by the Bradford technique [17].

Vesicle size of all membrane preparations was determined by Quasi-Elastic Light Scattering (Brookhaven Instruments) [18], revealing homogenous populations with monomodal distributions, with a mean hydrodynamic diameter of 342 ± 46 nm.

### 2.5. Fatty acid composition and cholesterol concentration of adipose membranes

Membranes were lyophilized and fatty acids were converted to FAME [19]. The resulting FAME were analyzed by gas chromatography as described in detail [15].

Total cholesterol was extracted from lyophilized membranes as described [15] and was calculated, in triplicate, based on the external standard technique, from a standard curve for peak area versus cholesterol concentration.

### 2.6. Assessment of membrane fluidity

Membrane fluidity was evaluated by measuring the fluorescence anisotropy of two probes incorporated in the membrane: 1,6-diphenyl-1,3,5-hexatriene (DPH), or 1-(4-(trimethylamino)-phenyl)-6-phenyl-1,3,5-hexatriene (TMA-DPH), from Molecular Probes (Eugene, OR, USA). DPH is incorporated inside the membrane at the fatty acyl group's level, while TMA-DPH is anchored by its cationic moiety at the membrane/water interface probing the membrane region closer to the phospholipids head groups [20]. Measurements of fluorescence anisotropy ($r$) were conducted as previously described [15] and calculated using the equation $r = (I_{VV} - GI_{VH})/(I_{VV} + 2\,GI_{VH})$, where $I_{VV}$ and $I_{VH}$ are the fluorescence intensities; the subscripts indicate the vertical ($V$) or horizontal ($H$) orientations of the excitation and emission polarizers, and $G = I_{HV}/I_{HH}$ is the instrumental factor. The fluorescence intensity data points used for calculations were the average of three identical aliquots (after blank subtraction) measured on a Varian Cary Eclipse fluorescence spectrophotometer (Mulgrave, Australia).

### 2.7. Evaluation of membrane water permeability

Water permeability of membrane vesicles was assessed using the stopped-flow technique (HI-TECH Scientific PQ/SF-53) [21]. Experiments were done at 23 °C for single measurements and from 12 to 37 °C for evaluation of the activation energy, as described [15]. The kinetics of vesicle shrinkage after a hyperosmotic shock (120 mOsM mannitol gradient) was monitored from the time course of scattered light intensity at 400 nm until a stable light scatter signal was attained (Fig. 3A). The osmotic water permeability coefficient ($Pf$) was estimated by fitting the light scatter signal to a single exponential curve and using the equation $Pf = k\,(V_o/A)(1/V_w(\mathrm{osm}_{out})_\infty)$, where $k$ is the exponential time constant, $V_w$ is the molar volume of water, $V_0/A$ is the initial volume to area ratio of the vesicle preparation, and $(osm_{out})_\infty$ is the final medium osmolarity after the applied osmotic gradient. All solution osmolarities were determined from freezing point depression on a semi-micro osmometer (Knauer GmbH, Germany). The activation energy of water transport was obtained from the slope of an Arrhenius plot ($\ln P_f$ as a function of $1/T$) multiplied by the gas constant $R$.

### 2.8. Statistical analysis

Statistical analysis was performed using the Statistical Analysis System (SAS) software package, version 9.1 (SAS Institute, USA). All data were presented as mean and standard error (SE). Data were analyzed using PROC MIXED with variance heterogeneity to determine the significance of the main effects, genotype (lean or obese) and diet (control or RPD), and their respective interaction (genotype × diet). If significant effects were obtained ($P < 0.05$), least squares means were determined using the LSMEANS option and compared using the probability difference procedure (PDIFF option). Pearson's correlation coefficients were calculated with the CORR procedure to establish linear relationships among lipid composition, membrane fluidity and permeability.

## 3. Results

### 3.1. Backfat thickness and fatty acids are increased in obese pigs

Fig. 1 displays the P2 backfat thickness and total fatty acids in the subcutaneous adipose tissue from lean and obese pigs fed on control and RPDs. A clear genotype effect was observed for both parameters. Bakfat thickness at the P2 position was twofold higher in obese than in lean pigs (Panel A; $P < 0.001$) but unrelated to dietary protein level ($P > 0.05$). In a similar manner, obese pigs had a higher amount of total fatty acids in the subcutaneous fat (Panel B; $P < 0.01$). Moreover, a diet effect was also observed with pigs fed on reduced protein showing higher content of total fatty acids in the same tissue ($P < 0.05$). Following these results, we next isolated adipose membranes from pig's subcutaneous adipose tissue in

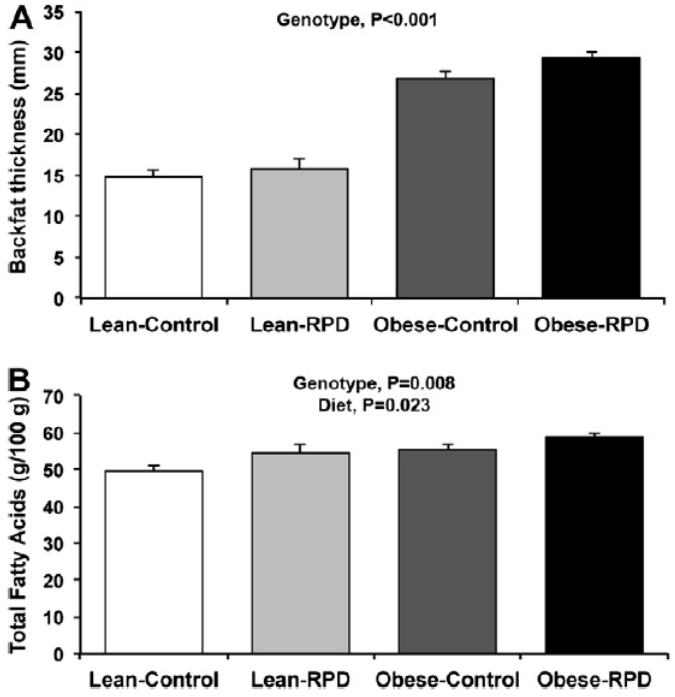


**Fig. 1.** Analysis of subcutaneous adipose tissue. (A) Backfat thickness measured at P2 level, and (B) total fatty acids of lean and obese pigs fed on control and reduced protein (RPD) diets. Statistical significances are shown for the effects of genotype (lean *versus* obese pigs) and diet (control *versus* reduced protein diets) at $P < 0.05$.

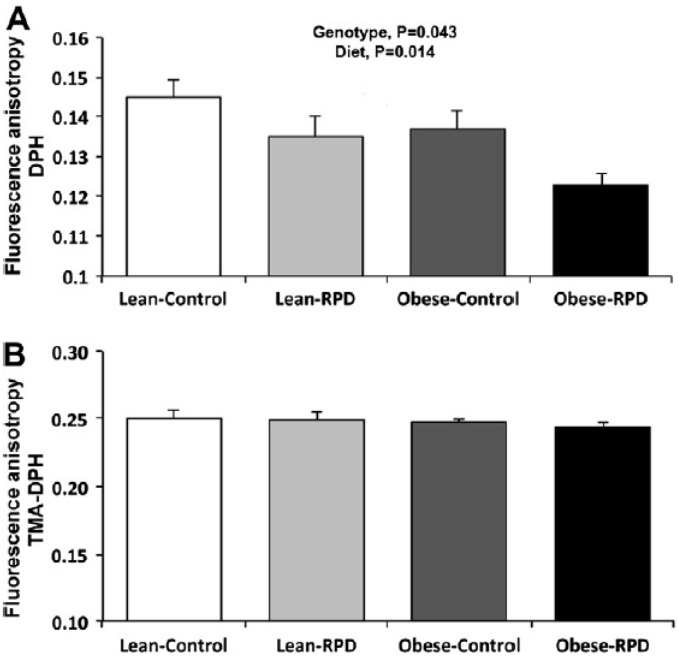


**Fig. 2.** Membrane fluidity measured by fluorescence anisotropy. (A) DPH and (B) TMA-DPH, in adipose membrane vesicles from lean and obese pigs fed on control and reduced protein (RPD) diets. Statistical significances are shown for the effects of genotype (lean *versus* obese pigs) and diet (control *versus* reduced protein diets) at $P < 0.05$.

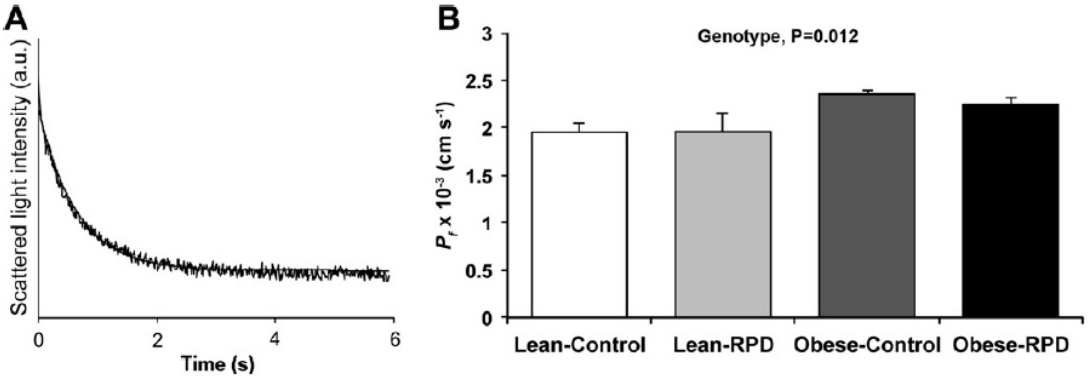


**Fig. 3.** Water permeability of adipose tissue membranes. (A) Typical stopped flow light scatter signal showing membrane vesicles shrinkage due to water outflow after a hyperosmotic shock (gradient 120 mOsM). (B) Water permeability (*Pf*) at 23 °C from lean and obese pigs fed on control and reduced protein (RPD) diets. Statistical significances are shown for the effect of genotype (lean *versus* obese pigs) at $P < 0.05$.

**Table 2**
Cholesterol concentration (mg/g membrane) and fatty acid (% of total FAME) profile of adipose membranes from lean and obese pigs fed on control and reduced protein (RPD) diets.

| | Lean | | Obese | | Significance level | | |
|---|---|---|---|---|---|---|---|
| | **Control** | **RPD** | **Control** | **RPD** | **Genotype** | **Diet** | **Genotype × Diet** |
| Cholesterol | 0.019 ± 0.001 | 0.021 ± 0.004 | 0.018 ± 0.0010 | 0.020 ± 0.004 | 0.688 | 0.453 | 0.863 |
| *Fatty acid profile* | | | | | | | |
| 14:0 | 0.693 ± 0.129 | 0.756 ± 0.108 | 0.780 ± 0.117 | 0.808 ± 0.082 | 0.536 | 0.688 | 0.873 |
| 16:0 | 16.8 ± 1.29 | 17.4 ± 1.44 | 18.1 ± 0.295 | 19.9 ± 0.660 | 0.129 | 0.343 | 0.628 |
| 16:1c7 | 0.278 ± 0.039 | 0.262 ± 0.024 | 0.224 ± 0.008 | 0.204 ± 0.024 | 0.052 | 0.500 | 0.931 |
| 16:1c9 | 1.22 ± 0.225 | 1.06 ± 0.150 | 1.07 ± 0.128 | 1.26 ± 0.095 | 0.894 | 0.917 | 0.289 |
| 17:0 | 0.508 ± 0.044 | 0.402 ± 0.048 | 0.433 ± 0.024 | 0.374 ± 0.045 | 0.231 | 0.063 | 0.577 |
| 17:1c9 | 0.376 ± 0.034 | 0.343 ± 0.034 | 0.288 ± 0.009 | 0.269 ± 0.025 | 0.011 | 0.358 | 0.808 |
| 18:0 | 19.0 ± 0.686 | 18.6 ± 1.01 | 20.9 ± 1.25 | 20.6 ± 0.814 | 0.058 | 0.740 | 0.973 |
| 18:1c9 | 29.9 ± 0.380 | 30.7 ± 1.49 | 31.4 ± 1.03 | 32.7 ± 1.32 | 0.140 | 0.369 | 0.827 |
| 18:1c11 | 2.40 ± 0.158 | 2.15 ± 0.128 | 2.18 ± 0.072 | 2.29 ± 0.056 | 0.725 | 0.540 | 0.132 |
| 18:2*n*-6 | 14.5 ± 1.29 | 11.5 ± 1.32 | 13.8 ± 0.940 | 11.8 ± 0.484 | 0.816 | 0.031 | 0.632 |
| 18:3*n*-3 | 0.526 ± 0.079 | 0.371 ± 0.077 | 0.463 ± 0.072 | 0.356 ± 0.034 | 0.571 | 0.071 | 0.729 |
| 20:0 | 0.244 ± 0.046 | 0.261 ± 0.031 | 0.225 ± 0.026 | 0.301 ± 0.030 | 0.757 | 0.190 | 0.404 |
| 20:1c11 | 0.818 ± 0.102 | 0.905 ± 0.105 | 0.844 ± 0.060 | 0.969 ± 0.098 | 0.636 | 0.271 | 0.841 |
| 20:2*n*-6 | 0.750 ± 0.037 | 0.612 ± 0.045 | 0.511 ± 0.037 | 0.445 ± 0.043 | <0.001 | 0.021 | 0.384 |
| 20:3*n*-3 | 0.346 ± 0.028 | 0.206 ± 0.024 | 0.369 ± 0.041 | 0.318 ± 0.025 | 0.043 | 0.007 | 0.162 |
| 20:4*n*-6 | 2.46 ± 0.383 | 1.20 ± 0.283 | 2.45 ± 0.371 | 1.58 ± 0.112 | 0.558 | 0.004 | 0.546 |
| 20:5*n*-3 | 0.110 ± 0.024 | 0.130 ± 0.033 | 0.102 ± 0.016 | 0.055 ± 0.021 | 0.113 | 0.588 | 0.192 |
| 22:5*n*-3 | 0.044 ± 0.044 | 0.117 ± 0.039 | 0.175 ± 0.043 | 0.117 ± 0.030 | 0.113 | 0.851 | 0.113 |
| *Partial sums* | | | | | | | |
| ΣSFA | 37.2 ± 1.04 | 37.5 ± 1.90 | 40.5 ± 1.44 | 42.0 ± 1.12 | 0.014 | 0.538 | 0.659 |
| ΣMUFA | 35.0 ± 0.549 | 35.4 ± 1.75 | 36.1 ± 1.20 | 37.7 ± 1.45 | 0.221 | 0.440 | 0.649 |
| ΣPUFA | 18.8 ± 1.71 | 14.7 ± 1.82 | 17.8 ± 1.41 | 15.4 ± 0.239 | 0.924 | 0.041 | 0.588 |
| Σ*n*-6 | 17.7 ± 1.62 | 13.8 ± 1.75 | 16.7 ± 1.31 | 14.5 ± 0.578 | 0.925 | 0.039 | 0.526 |
| Σ*n*-3 | 1.03 ± 0.123 | 0.971 ± 0.153 | 1.11 ± 0.111 | 0.846 ± 0.074 | 0.848 | 0.193 | 0.404 |
| Unidentified | 9.02 ± 2.79 | 12.4 ± 4.20 | 5.63 ± 2.10 | 5.47 ± 1.43 | 0.092 | 0.583 | 0.546 |
| *Ratios* | | | | | | | |
| PUFA/SFA | 0.501 ± 0.037 | 0.392 ± 0.039 | 0.443 ± 0.039 | 0.353 ± 0.017 | 0.178 | 0.009 | 0.774 |
| *n*-6/*n*-3 | 18.1 ± 1.69 | 15.4 ± 1.95 | 15.3 ± 0.689 | 17.1 ± 0.738 | 0.750 | 0.807 | 0.176 |
| 18:1c9/18:2*n*-6 | 2.15 ± 0.220 | 2.82 ± 0.301 | 2.34 ± 0.188 | 2.82 ± 0.216 | 0.697 | 0.025 | 0.698 |

FAME = fatty acid methyl esters; SFA = saturated fatty acids; MUFA = monounsaturated fatty acids; PUFA = polyunsaturated fatty acids.
Σ SFA = sum of 14:0, 16:0, 17:0, 18:0 and 20:0; Σ MUFA = sum of 16:1*c*7, 16:1c9, 17:1c9, 18:1c9, 18:1c11 and 20:1c11; Σ PUFA = sum of 18:2*n*-6, 18:3*n*-3, 20:2*n*-6, 20:3*n*-3, 20:4*n*-6, 20:5*n*-3 and 22:5*n*-3; Σ*n*-6 = sum of 18:2*n*-6, 20:2*n*-6 and 20:4*n*-6; Σ *n*-3 = sum of 18:3*n*-3, 20:3*n*-3, 20:5*n*-3 and 22:5*n*-3.

order to study their lipid profile and further correlate those findings with membrane biophysical properties such as fluidity and permeability.

### 3.2. Membrane-saturated fatty acids are influenced by genotype

The lipid composition of adipose membranes from lean and obese genotypes fed on control and reduced protein diets is depicted in Table 2.

Total cholesterol concentration was unaffected by genotype or by diet ($P > 0.05$). The distribution pattern of the main fatty acid classes across groups showed a highest occurrence of saturated fatty acids (SFA) from 37% to 42%, closely followed by monounsaturated fatty acids (MUFA) from 35% to 38% and lastly, polyunsaturated fatty acids (PUFA) from 14% to 19%. The genotype affected the sum of SFA ($P < 0.05$), being the values higher in obese pigs. As for MUFA, only the 17:1c9 fatty acid was affected by genotype ($P < 0.05$) with decreased content in obese pigs. Whereas PUFA sum was not affected by the genotype, the 20:2*n*-6 fatty acid was reduced ($P < 0.001$) and the 20:3*n*-3 was increased ($P < 0.05$) in the obese genotype.

### 3.3. Membrane-polyunsaturated fatty acids are influenced by diet

The most important factor affecting the fatty acid profile of adipose membranes was the diet. In fact, the diet influenced the sum

of PUFA, in particular from the *n*-6 family, most at the expenses of 18:2*n*-6 fatty acid ($P < 0.05$) and in a smaller magnitude of 20:2*n*-6 ($P < 0.05$) and 20:4*n*-6 ($P < 0.01$) fatty acids (Table 2), the former in lower amounts in pigs fed a reduced protein diet. In addition, and following the same trend, the 20:3*n*-3 fatty acid was greatly affected by diet ($P < 0.01$). Regarding the fatty acids indexes, diet affected the ratios of PUFA/SFA and 18:1*c*9/18:2*n*-6 in opposite directions. While PUFA/SFA was diminished in reduced protein diets ($P < 0.01$), the 18:1*c*9/18:2*n*-6 was increased ($P < 0.05$), regardless of the genotype.

### 3.4. Fluidity of adipose membranes is dependent on genotype and affected by diet

The relative changes in fluorescence anisotropy of DPH and TMA-DPH in adipose membranes from each group are shown in Fig. 2. With the DPH probe, a significant decrease in fluorescence anisotropy was observed in obese pigs relatively to lean (panel A; $P < 0.05$). Moreover, reduced anisotropy was observed for pigs with reduced protein diets facing their controls (Panel A; $P < 0.05$). Being fluorescence anisotropy inversely related to membrane fluidity, adipose membranes from obese pigs are therefore more fluid. As for TMA-DPH probe, the values observed were similar across groups (Panel B; $P > 0.05$) indicating that the fluidity is mostly changed due to adjustments at the fatty acyl groups' level rather than at the membrane surface.

### 3.5. Permeability of adipose membranes is dependent on genotype

For permeability experiments, membrane vesicles in isotonic buffer were subjected to a hyperosmotic gradient with mannitol and the time course of vesicle volume change was used to calculate membrane water permeability (*Pf*) (Fig. 3A). As shown in Fig. 3B, a significant genotype effect was detected, obese pigs' membranes showing higher permeability values ($P < 0.05$). To investigate whether membrane water channels were involved in this permeability, we assessed the activation energy for water transport (*Ea*) by measuring *Pf* at different temperatures. The *Ea* obtained were similar among groups, ranging from 13.1 ± 0.6 to 14.7 ± 0.8 kcal/mol (54.8 ± 2.4 to 61.5 ± 3.2 kJ/mol) ($P > 0.05$). These relative high *Ea* values suggest that water permeation occurs mainly by diffusion through the lipid bilayer with no contribution of specific protein channels for transport and may therefore correlate with fluidity [22].

### 3.6. Correlation between lipid composition and fluidity

Some interesting Pearson's correlation coefficients were found between membrane's fatty acid composition and fluidity. The correlation of the fluorescence anisotropy obtained by the fluorescent probes among themselves was not significant ($r = -0.082$, $P = 0.731$), pointing to independent membrane biophysical measurements. In contrast, the fluorescence anisotropy from the DPH probe was positively correlated with 18:2*n*-6 fatty acid ($r = 0.442$, $P = 0.035$), PUFA/SFA ratio ($r = 0.483$, $P = 0.020$) and negatively with 18:1*c*9/18:2*n*-6 ratio (r = -0.461, P = 0.027). PUFA/SFA and 18:1*c*9/18:2*n*-6 were found strongly but inversely correlated ($r = -0.840$, $P < 0.001$).

## 4. Discussion

In this study, feeding pigs on a RPD increased the total fatty acid content of the subcutaneous adipose tissue, which is consistent with previous results [9,23]. In contrast, the P2 backfat thickness was not affected by the RPD, which is in agreement with numerous reports [6,8,24,25]. In addition, P2 fat thickness revealed clearly genetic effects on the pattern of fat deposition [6]. As expected, backfat was thicker in the genetically obese than in lean pigs, in accordance with the fact that traditional pig breeds, growing much slower than modern breeds, display higher backfat thickness [8].

Our results evidenced a difference in dietary protein requirement between the two genetic backgrounds. Protein and energy metabolism of growing pigs are markedly dependent on pig's genotype [24,26]. The nutritional requirements of the Alentejano pig, a slow growing, obese porcine breed, seem to differ from those of conventional or high-performing pigs with lower dietary protein requirements [6]. It has been suggested that fast-growing genotypes, such as the lean Crossbred, having a high capacity for muscle growth can use high protein and energy diets without accumulating fat [8]. This is in accordance with the herein results.

Contrary to the reported results on genetically obese mice and rats [3,27], it was recently proposed that the membrane lipid composition of obese healthy humans is different from lean but the fluidity remains unaltered [5]. These notions led us to investigate how adipose membranes from genetically obese pigs could be compared to a lean genotype regarding lipid composition, permeability and membrane fluidity. Furthermore, to our best knowledge, the effect of RPD on membrane lipid composition and biophysical properties has never been investigated.

Overall, all adipose membranes were found to be richer in SFA independently of breed or diet. The distribution pattern of the main fatty acid classes follows the trend SFA > MUFA > PUFA, which is similar to our previous results on fat depots from obese Zucker rats [15] and bovines [16].

An increase in membrane fluidity was observed in the adipose membranes from obese pigs, in accordance with the reported for a wide variety of cell membranes from obese mice and rats [3,27], which was explained by a lower total cholesterol concentration. Yet, in this study, the total cholesterol was unchanged by any factor under study. In addition, membrane incorporation of eicosapentaenoic acid (EPA, 20:5*n*-3) and docosahexaenoic acid (DHA, 22:6*n*-3) that have been demonstrated to significantly alter many basic properties of membranes, including acyl chain order [28], were detected in residual amounts thus not explaining the increased membrane fluidity and permeability. However, this variation may eventually be explained based on the observation that obese pigs had a significantly higher amount of total fatty acids (Fig. 1B). Therefore, even considering that there are no alterations in the total amount of cholesterol, a higher (phospho)lipids to cholesterol ratio may occur on the adipocytes membranes, inducing a decrease on the cholesterol-induced membrane ordering effect and leading to the increased membrane fluidity at the membrane core (lower DPH fluorescence anisotropy) observed for the obese pigs.

Regarding the adipose membrane lipid composition of pigs fed with different protein diets, as previously reported [25], no major differences were observed for the contents of 16:0, 18:0, 18:1*c*9 fatty acids, nor there were differences in the subsequent sums of SFA or MUFA. However, lower contents of linoleic (18:2*n*-6) and arachidonic acids (20:4*n*-6) were detected in pigs fed on RPDs, resulting in a lower PUFA sum, in particular from the *n*-6 family. Since dietary linoleic acid is the precursor for the synthesis of arachidonic acid, it was predictable that both fatty acids vary proportionally and in the same direction.

One consistent change reported in adipose membranes of genetically obese mice was an increase in the ratio oleic (18:1*c*9)/linoleic (18:2*n*-6) acids, a result probably due to an increased desaturation of linoleic acid [3]. This explanation fits well with the increased membrane fluidity observed in pigs fed on RPDs, for which this ratio reached the highest value. In addition, and re-enforcing this finding, membrane fluidity was correlated with 18:1*c*9/18:2*n*-6 ratio,

pointing to a clear compensatory mechanism to maintain membrane biophysical properties. Pigs fed on RPDs also shown a significantly higher content of total fatty acids (Fig. 1B), without changes on the total cholesterol levels. As previously discussed on the context of the comparison between lean and obese animals, this variation profile can also be the main reason for the increased membrane fluidity observed for animals fed on RPD when compared with their controls.

In conclusion, this study demonstrates that the genetic background clearly influences the backfat thickness in pigs, and that the restriction of dietary protein independently increases the total fatty acid content of the subcutaneous adipose tissue. Moreover, the genetic background in obese pigs plays a determinant role on the fluidity of adipose membranes by decreasing membrane rigidity at the core of the bilayer but not at a shallow position, closer to the water/lipid interface. Interestingly, the same effect was observed for pigs fed a RPD. Since relatively small changes in the concentration of membrane lipids, in the order of 10%, are significant enough to alter biophysical properties of the membrane [29], one can speculate that minor concentrations of some fatty acids, due to their geometric structure, may affect lipid packing within cellular membranes thus contributing to the experimentally observed increase in membrane fluidity and permeability. These findings likely reflect membrane adaptation to preserve optimal cellular function.

## Acknowledgments

This study was supported by Fundação para a Ciência e a Tecnologia (FCT), grant PTDC/CVT/2008/99210 and fellowships to A.P. Martins (SFRH/BD/2009/65046), M. Madeira (SFRH/BD/2008/48240) and S.V. Martins (SFRH/BPD/2009/63019). P.A. Lopes is a researcher from the FCT program "Ciência 2008".

## References

[1] J.P. Montani, J.F. Carroll, T.M. Dwyer, V. Antic, Z. Yang, A.G. Dulloo, Ectopic fat storage in heart, blood vessels and kidneys in the pathogenesis of cardiovascular diseases, Int. J. Obes. Relat. Metab. Disord. 28 (Suppl. 4) (2004) S58–S65.
[2] P. Wang, E. Mariman, J. Renes, J. Keijer, The secretory function of adipocytes in the physiology of white adipose tissue, J. Cell Physiol. 216 (2008) 3–13.
[3] D.A. York, Alterations in membrane function, organization and composition in the obese ob/ob mouse, Proc. Nutr. Soc. 44 (1985) 189–200.
[4] R.M. Hagen, S. Rodriguez-Cuenca, A. Vidal-Puig, An allostatic control of membrane lipid composition by SREBP1, FEBS Lett. 584 (2010) 2689–2698.
[5] K.H. Pietilainen, T. Rog, T. Seppanen-Laakso, S. Virtue, P. Gopalacharyulu, J. Tang, S. Rodriguez-Cuenca, A. Maciejewski, J. Naukkarinen, A.L. Ruskeepaa, P.S. Niemela, L. Yetukuri, C.Y. Tan, V. Velagapudi, S. Castillo, H. Nygren, T. Hyotylainen, A. Rissanen, J. Kaprio, H. Yki-Jarvinen, I. Vattulainen, A. Vidal-Puig, M. Oresic, Association of lipidome remodeling in the adipocyte membrane with acquired obesity in humans, PLoS Biol. 9 (2011) e1000623.
[6] W.G. Pond, J.T. Yen, H.J. Mersmann, W.M. Haschek, Comparative effects of dietary protein and cholesterol-fat content on genetically lean and obese pigs, J. Nutr. 116 (1986) 1116–1124.
[7] J.L. Hornick, C. Van Eenaeme, O. Gerard, I. Dufrasne, L. Istasse, Mechanisms of reduced and compensatory growth, Domest. Anim. Endocrinol. 19 (2000) 121–132.
[8] J.D. Wood, G.R. Nute, R.I. Richardson, F.M. Whittington, O. Southwood, G. Plastow, R. Mansbridge, N. da Costa, K.C. Chang, Effects of breed, diet and muscle on fat deposition and eating quality in pigs, Meat Sci. 67 (2004) 651–667.
[9] O. Doran, S.K. Moule, G.A. Teye, F.M. Whittington, K.G. Hallett, J.D. Wood, A reduced protein diet induces stearoyl-CoA desaturase protein expression in pig muscle but not in subcutaneous adipose tissue: relationship with intramuscular lipid formation, Br. J. Nutr. 95 (2006) 609–617.
[10] N. da Costa, C. McGillivray, Q. Bai, J.D. Wood, G. Evans, K.C. Chang, Restriction of dietary energy and protein induces molecular changes in young porcine skeletal muscles, J. Nutr. 134 (2004) 2191–2199.
[11] M.E. Spurlock, N.K. Gabler, The development of porcine models of obesity and the metabolic syndrome, J. Nutr. 138 (2008) 397–402.
[12] J. Folch, M. Lees, G.H. Sloane Stanley, A simple method for the isolation and purification of total lipides from animal tissues, J. Biol. Chem. 226 (1957) 497–509.
[13] K. Raes, S. De Smet, D. Demeyer, Effect of dietary fatty acids on incorporation of long chain polyunsaturated fatty acids and conjugated linoleic acid in lamb, beef and pork meat: a review, Anim. Feed Sci. Tech. 113 (2004) 199–221.
[14] S.P. Alves, R.J. Bessa, Comparison of two gas-liquid chromatograph columns for the analysis of fatty acids in ruminant meat, J. Chromatogr. A 1216 (2009) 5130–5139.
[15] A.P. Martins, P.A. Lopes, S.V. Martins, A. Madeira, N.C. Santos, J.A. Prates, T.F. Moura, G. Soveral, Conjugated linoleic acid reduces permeability and fluidity of adipose plasma membranes from obese Zucker rats, Biochem. Biophys. Res. Commun. 398 (2010) 199–204.
[16] A.P. Martins, P.A. Lopes, A.S.H. Costa, S.V. Martins, N.C. Santos, J.A.M. Prates, T.F. Moura, G. Soveral, Differential mesenteric fat deposition in bovines fed on silage or concentrate is independent of glycerol membrane permeability, Animal 5 (2011) 1949–1956.
[17] M.M. Bradford, A rapid and sensitive method for the quantitation of microgram quantities of protein utilizing the principle of protein-dye binding, Anal. Biochem. 72 (1976) 248–254.
[18] G. Soveral, R.I. Macey, T.F. Moura, Mechanical properties of brush border membrane vesicles from kidney proximal tubule, J. Membr. Biol. 158 (1997) 209–217.
[19] W.W. Christie, G. Dobson, R.O. Adlof, A practical guide to the isolation, analysis and identification of conjugated linoleic acid, Lipids 42 (2007) 1073–1084.
[20] E. Pebay-Peyroula, E.J. Dufourc, A.G. Szabo, Location of diphenyl-hexatriene and trimethylammonium-diphenyl-hexatriene in dipalmitoylphosphatidylcholine bilayers by neutron diffraction, Biophys. Chem. 53 (1994) 45–56.
[21] G. Soveral, R.I. Macey, T.F. Moura, Water permeability of brush border membrane vesicles from kidney proximal tubule, J. Membr. Biol. 158 (1997) 219–228.
[22] E. Campos, T.F. Moura, A. Oliva, P. Leandro, G. Soveral, Lack of Aquaporin 3 in bovine erythrocyte membranes correlates with low glycerol permeation, Biochem. Biophys. Res. Commun. 408 (2011) 477–481.
[23] J. Mourot, M. Kouba, P. Peiniau, Comparative study of in vitro lipogenesis in various adipose tissues in the growing domestic pig (*Sus domesticus*), Comp. Biochem. Physiol. B Biochem. Mol. Biol. 111 (1995) 379–384.
[24] R. Barea, R. Nieto, J.F. Aguilera, Effects of the dietary protein content and the feeding level on protein and energy metabolism in Iberian pigs growing from 50 to 100 kg body weight, Animal 1 (2007) 357–365.
[25] V. Alonso, M. Campo Mdel, L. Provincial, P. Roncales, J.A. Beltran, Effect of protein level in commercial diets on pork meat quality, Meat Sci. 85 (2010) 7–14.
[26] R. Nieto, A. Miranda, M.A. Garcia, J.F. Aguilera, The effect of dietary protein content and feeding level on the rate of protein deposition and energy utilization in growing Iberian pigs from 15 to 50 kg body weight, Br. J. Nutr. 88 (2002) 39–49.
[27] M. Guerre-Millo, P. Guesnet, C. Guichard, G. Durand, M. Lavau, Alteration in membrane lipid order and composition in metabolically hyperactive fatty rat adipocytes, Lipids 29 (1994) 205–209.
[28] W. Stillwell, S.R. Wassall, Docosahexaenoic acid: membrane properties of a unique fatty acid, Chem. Phys. Lipids. 126 (2003) 1–27.
[29] M. Oresic, V.A. Hanninen, A. Vidal-Puig, Lipidomics: a new window to biomedical frontiers, Trends Biotechnol. 26 (2008) 647–652.

# PART II – Aquaporins

# INTRODUCTION

One of the fundamental tasks of the plasma membrane is to quickly respond to intra and extracellular events. Water is the major component of living organisms, thus controlled flow of water into and out of cells is central for cell homeostasis. Although water can cross biological membranes through the lipid bilayer, membrane water permeability can be greatly enhanced by specific proteins called aquaporins (AQPs). These transmembrane proteins enable the fine-tuning of water permeation and in some cases also small solutes. Part II of this thesis will focus on different aspects of these proteins.

## Aquaporins

AQPs are a family of small transmembrane channels ubiquitous in nature. These proteins form highly selective channels that, in response to osmotic or solute gradients, facilitate bidirectional flow of water and in the case of aquaglyceroporins, other small solutes such as glycerol and urea, enabling the adjustment of these flows to the organism necessities.

The existence of water channels was predicted long before aquaporin discovery. The first studies on water transport started in the late 1950s on mammalian red blood cells (RBC)[69–72] and later on renal epithelia[73] and demonstrated that water permeability in these cells was much higher than predicted by simple water diffusion through the bilayer. Evidence for their existence was based mainly on measures of high osmotic water permeability, on their inhibition by mercurial reagents[69,70], on the low activation energy for transport[74] and finally on the ratio of osmotic to diffusion water permeabilities[75] leading to the proposed single-file mechanism of transport within the channel[76]. In 1984 it was identified a major intrinsic protein in bovine lens cells that was suggested to participate in the formation of an aqueous channel[77]. But only in the 1990s, using a Xenopus oocyte expression assay, Agre and co-workers[78] demonstrated that a 28-kDa membrane protein that is abundant in RBC and renal proximal tubules [79] was water permeable. The 28-kDa membrane protein was later named aquaporin-1 (AQP1).

Ever since their discovery, more than 300 homologues from many phyla, including bacteria, plant, and animal have been identified[80]. In prokaryotic and other microorganisms, AQPs are believed to aid survival by providing protection against osmotic shocks and rapid freezing[81,82]. In Escherichia coli there are two MIP family proteins: one is the glycerol facilitator (GlpF)[83] and the other is the water channel (AQPZ)[84]. More AQP genes are present in the genomes of multicellular organisms: Arabidopsis thaliana contains 35 putative AQP genes[85] while in humans, 13 AQPs isoforms, distributed in specific organs, tissues and with different cellular localization have been identified so far[3]. The identification and study of mammalian AQPs have provided insight at the molecular level into the fundamental physiology of water balance, regulation and the pathophysiology of water balance disorders[3,86].

Furthermore, aside from water and glycerol, numerous studies have pointed out a broader range of AQPs' substrates, these include polyols, hydrogen peroxide, ammonia, nitrate, arsenite, antimonite, small ions, and gases[87].

The widespread distribution of this ancient family of channels in all kingdoms of life points to their fundamental significance in biology.

## 1. Aquaporin classification and selectivity.

Thirteen mammalian AQPs, have been described so far. These can be divided in three sub-groups mainly determined by their transport capabilities: *i)* orthodox or classical AQPs (AQP0, AQP1, AQP2, AQP4, AQP5, AQP6 and AQP8), primarily water selective facilitating water movement across cell membranes in response to osmotic or pressure gradients and, *ii)* aquaglyceroporins (AQP3, AQP7, AQP9 and AQP10) which transport some small uncharged solutes such as glycerol and urea in addition to water. A third sub-group, named *iii)* S-aquaporins (AQP11 and AQP12), was defined based primarily on their subcellular location and on the lower sequence similarity to the other mammalian AQPs (Figure 5).

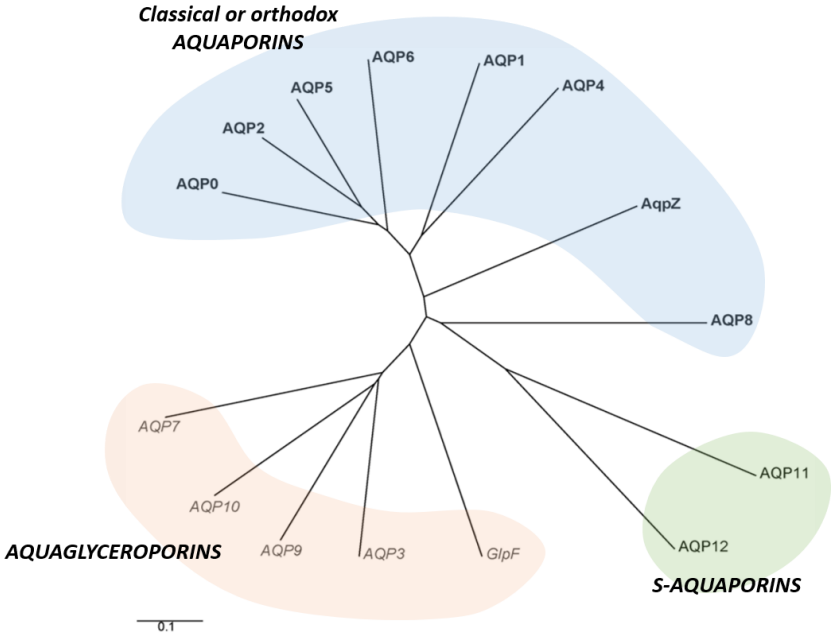


*Figure 5* - ***Phylogenetic tree of the human Aquaporin gene family*** *(Adapted from [88]).* Water permeable AQPs (AQP0, 1, 2, 4, 5, 6, 8, AqpZ) are shown in blue background. Glycerol permeable aquaglyceroporins (AQP3, 7, 9, 10, GlpF) are in orange background. AqpZ and GlpF are the E. coli homologues. S-Aquaporins (AQP11 and 12) is on the bottom right with green background. The scale bar represents genetic distance between homologues.

Numerous studies have revealed the diverse permeation characteristics of AQPs. In addition to water and glycerol, a diverse set of solutes including small ions, urea, hydrogen peroxide, ammonia, nitrate, arsenite, antimonite and gases[87], has been shown to permeate through specific AQPs. Aquaglyceroporins AQP3, AQP7, AQP9 and AQP10 transport glycerol and urea[89–92] , while both AQP7 and AQP9 are permeable for arsenite[93].

In addition, AQP9 also permeates a wide range of non-charged solutes like mannitol, sorbitol, purines and pyrimidines[94]. AQP6 has low water permeability and seems to function primarily as an anion transporter[95,96]. In addition, AQPs have also been proposed to transport gases, including carbon dioxide, ammonia, nitric oxide and hydrogen peroxide[97–99]. However, some of these permeability characteristics are still controversial and subject of intense debate[100,101].

## 2. Aquaporin structure.

The three dimensional structures of several AQPs has enabled the conceptualization of a general structure, revealing the structural determinants that are essential for AQPs selectivity and extraordinary permeation rates. The atomic model of mammalian AQP1 derived from a 3.8 Å resolution potential map obtained by electron crystallography was the first atomic structure of a human membrane protein to be solved, and gave the first insight into AQP's water specificity[102]. Medium and high-resolution structures of several AQPs belonging to different subfamilies have been ever since determined, namely, from archaea[103], bacteria[104,105], yeast[106], protozoa[107], plants[108] and mammals[109–112]. More recently, molecular dynamics (MD) simulations have complemented the experimental data, by providing the progression of the biomolecular system at atomic resolution[101].

The reported structures have revealed that AQPs are grouped as homotetramers embedded in the bilayer[113], consisting of four independent monomers, each behaving as an independent channel[114] (Figure 6) and sharing a conserved overall typical hourglass fold[102,115].

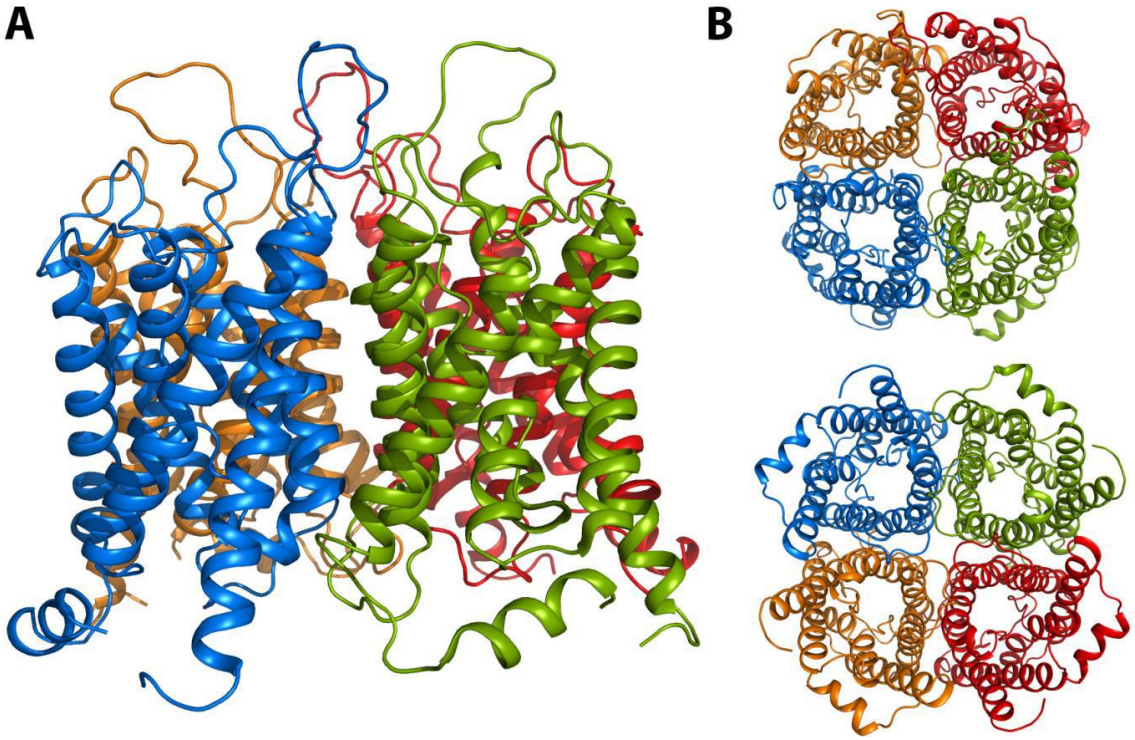


*Figure 6* - ***Tetrameric structure of bovine AQP1***. (A) side view, (B) top and bottom views. Reprinted with author's permission[116].

Each monomer interact with two of its neighbours, forming the tetramer central pore. It has been suggested that this pore, which is not involved in water conductance[102], may permeate gases[99,117,118] and function as a gated cation channel[119,120]. Each AQP monomer is a small protein with usually fewer than 300 amino acids, organized in six transmembrane α-helices (H1-6) arranged in a right-handed helical bundle and connected by five loops (A-E), with both amino and carboxyl termini located in the cytoplasm side[121,122] (Figure 7A). The angle at which the transmembrane α-helices are oriented gives rise to funnel-shaped cytoplasmic and extracellular vestibules connected by the conduction pore. The latter is formed by two small α-helical segments, loop B, entering from exoplasmatic side and connecting H2 and H3, while loop E enters from the cytoplasmatic side and connects H5 and H6, called HB and HE respectively[123].

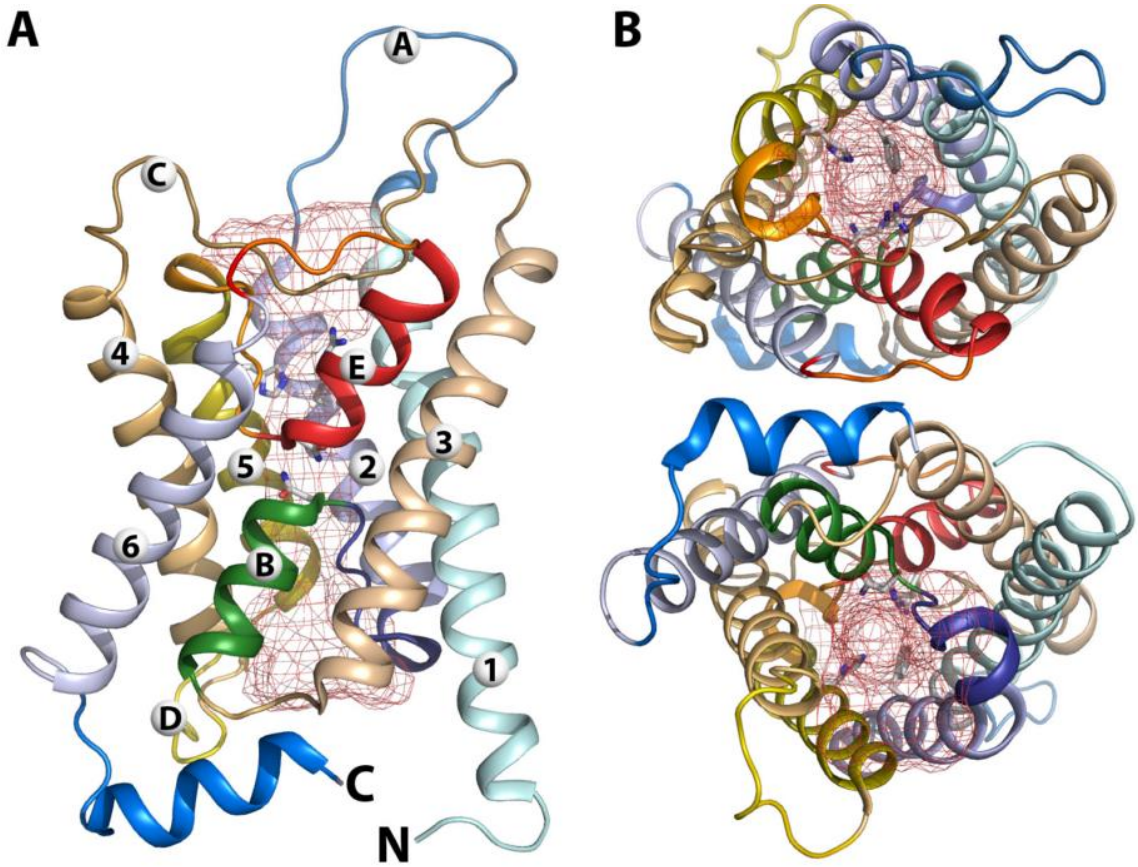


*Figure 7* - ***Monomeric structure of bovine AQP1***. (A) side view, (B) top and bottom views. The red mesh indicates the pore region. Reprinted with author's permission[116].

Aquaporins have important characteristics (two filters) that provide selectivity for water and some small solutes, preventing protons and solutes above a certain size and charged solutes to permeate (Figure 8). The amino acid residues of the first selective filter is for most AQPs composed of two highly conserved asparagine-proline-alanine (NPA), called signature motifs, located at the end of the loops (HB and HE). These motifs are oriented 180 degrees toward each other, forming part of the surface of the aqueous pathway at the centre of the pore. The chemical/structural characteristics of this region, mostly due to the presence of these residues and the dipole behaviour of the two half

helices HB, generates an electric field[124] that induces upon the interaction with the asparagines, a rotation of the water molecule, thus disrupting any H-bonds between adjacent water molecules and preventing the Grottus mechanism for protons permeation[102,104,109,115,125,126,127]. The second important selective filter located at the extracellular side, the aromatic/arginine (ar/R) constriction region, prevents permeation of solutes above 2.8 Å and of charged solutes[109]. Within this region a hydrophobic phenylalanine residue side chain (Phe 58 in bAQP1) orients the water molecules such as to enforce strong hydrogen bonds to an arginine and a histidine (Arg 197 and His 182 in bAQP1) (Figure 8A). Besides these selective filters in the pore, the channel has in the vestibules at the entrance of either side, in the vestibules, different residues, mainly carbonyl groups that interact with water molecules[82,109]. Furthermore, the wall regions of the pore have different hydrophobic/hydrophilic characteristics determining, conduction rate and the open/closed state of the channel[82].

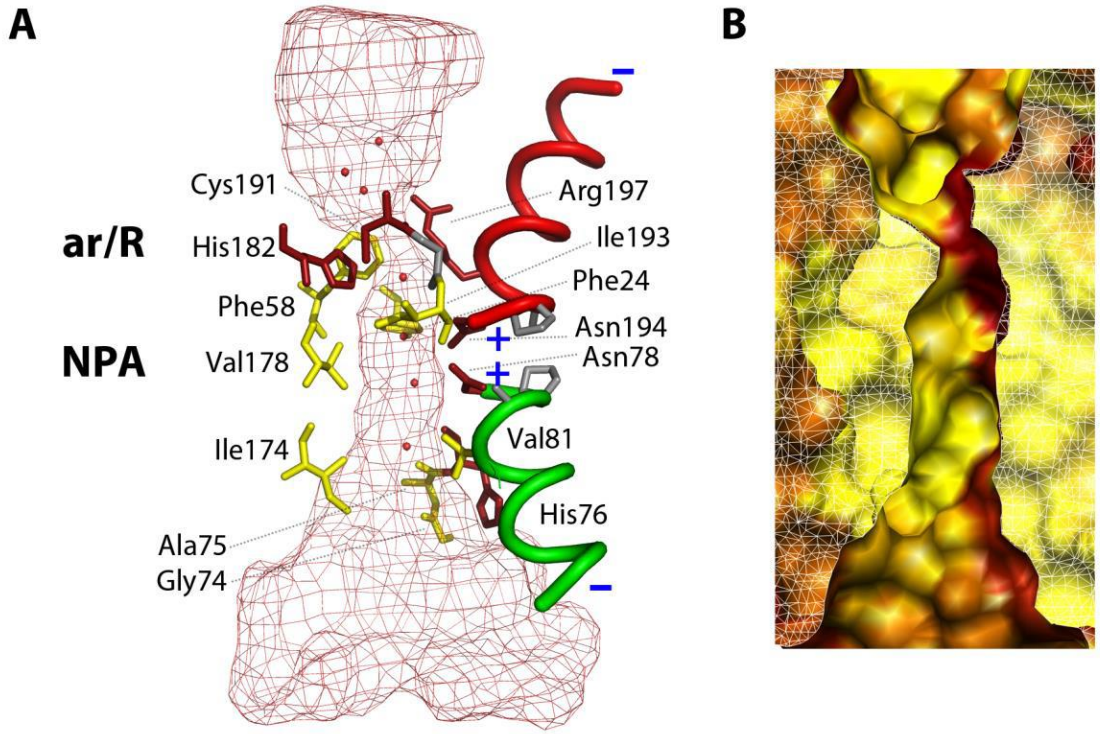


*Figure 8* - ***Detailed view of bovine AQP1 pore region***. (A) Half helices dipoles and the hydrophilic and hydrophobic residues lining the pore are depicted in red and yellow, respectively; the ar/R and NPA selective filters are shown as well; (B) Inside view of the pore surface (hydrophilic and hydrophobic properties are painted red and yellow, respectively). Reprinted with author's permission[116].

In the highly dielectric (ε = 80) bulk water, protons are well solvated by surrounding water molecules. Upon moving the proton across the AQP pore, the solvation shell needs to be removed from the proton thus creating an electrostatic barrier[128,129]. Inside the pore, the hydronium ion is only partially solvated by few close water molecules, and the surrounding protein medium (ε ≈ 4) stabilizes the hydronium only to a fraction of the solvation in the bulk. Thus, a large energetic cost results for moving the hydronium from the water into the pore. Inside the pore, water molecules move in single file, so whenever and wherever bulk water-water hydrogen bonds have to

be ruptured to allow the water molecule to squeeze through the narrow NPA or ar/R regions (so preventing protons to permeate AQPs), the protein offers replacement interactions, which largely compensate for the energetic cost of water-water bond rupture. This remarkable complementarity to bulk water lowers the activation barrier to a large extent. Furthermore, the high permeation rates are observed both experimentally and in simulations[101,109]. The high permeation rate is thought to be partially due to the hydrophobic nature of some pore regions, where water molecules have to pass rapidly, while they slowdown in hydrophilic regions upon interactions with residues. The conduction rate is so, modulated by the hydrophobicity/hydrophilic characteristics of the pore and is often referred as saltatory conduction (named after the saltatory ion conduction in axons).

## 3. Aquaglyceroporin structure.

The structure of Escherichia coli glycerol facilitator GlpF revealed that the AQP general fold topology is conserved among orthodox AQPs and aquaglyceroporins[104,130]. Yet GlpF permeability to water is substantially less than that measured for its bacterial AQP counterpart AqpZ[83,131].

The ar/R constriction region of GlpF has Trp48, Gly191, Phe200, and Arg205[109] instead of Phe56, His180, Cys189 and Arg195 in AQP1. Among the water-specific AQPs, the histidine residue, which is preserved among water-specific AQPs, together with the highly conserved arginine residue providing a hydrophilic edge in juxtaposition to an aromatic residue[123]. On the other hand, for GlpF, the replacement of this histidine by glycine significantly increases the size of this constriction region and sterically allows a second residue change, replacing the cysteine by a phenylalanine[109,123,132]. These substitutions have two critical effects on the characteristics of the GlpF ar/R constriction region: they increase its size, making it wider than AQP1 (3.4Å and 2.8Å, respectively) and also increase its hydrophobicity[109]. It seems that the more hydrophobic nature of GlpF is the primary factor responsible for its relatively reduced ability to transport water[109,133]. Moreover, the ladder of aromatic residues (Phe and Trp) in GlpF constriction region forms a greasy slide that allows the efficient conduction of glycerol, small linear polyols, and urea, while making it less efficient for water passage[123].

The GlpF channel lining is strongly amphipathic, with oxygens and nitrogens lined up on one side and carbons on the opposite side of the lumen surface. This amphipathic channel uniquely matches the chemical structure of glycerol, which is a composite of the polar hydroxyl group arranged on a non-polar alkyl backbone[104]. The glycerol permeation through the selectivity filter of GlpF depends on the orientation of the glycerol molecule inside the pore. In the narrow ar/R selectivity filter of the channel all three hydroxyl groups of glycerol are able to form hydrogen bonds to polar protein groups or to the nearby water molecules[134]. Two consecutive OH groups of the glycerol molecule are oriented with ideal geometry with respect to donor and acceptor atoms from within the channel[104].

## 4. Aquaporin regulation.

One important aspect regarding AQPs is that they are tightly regulated. Eukaryotic AQPs are frequently regulated post-translationally either by gating, which controls of the channels' rate of flux, or by trafficking, whereby AQPs are shuttled from intracellular storage sites to the plasma membrane[135]. Within the gating mechanisms, it is well established that eukaryotic AQPs are often directly regulated by pH, phosphorylation, divalent cations[136] and membrane tension[137,138,139]. These regulatory mechanisms directly affect the protein conformation, which in turn impacts its transport capacity.

AQPs pore structure dictates both the permeation rate and the channel specificity and so, changes in its structure resulting from changes in pH or from other external factors will affect water and solute fluxes[140]. Since the specificity of the pore is high, only small changes of a few or even a single residue are required to produce the gating phenomenon. Small changes of critical residues at the pore entrances may obstruct the pore as well[123]. For some AQPs, the mechanism of the conformational transition from a closed state to an open one has already been elucidated[140]. High-resolution structures of gated AQPs show that the cytoplasmic entry contains another very narrow constriction site, which significantly hinders the movement of water molecules[135]. Three eukaryotic AQP structures solved at high-resolution reveal the presence of this second constriction site: mammalian AQP0 found in the eye lens[110,111,141], SoPIP2;1 a plant plasma membrane AQP[108], and Aqy1 a yeast plasma membrane AQP[106]. From these structural results, two distinct pictures of 'capping' and 'pinching' have emerged to describe how transmembrane water channels are gated[140]. From this perspective SoPIP2;1 and Aqy1 are ''cappers" that dramatically reduce their water transport activity through gating[135]. Both loop D in SoPIP2;1 and the N-terminus in Aqy1 cap the channel within the cytoplasmic side, leading to the repositioning of a key residue that ends up blocking the movement of water[135]. In this context AQP0 represents a special case since its cytoplasmic entrance appears to be always blocked by Tyr149; yet this channels' activity seems to be further adjusted by small conformational changes that ''pinch" on either constriction region of the pore[135].

## 5. Physiological relevance.

Mammalian AQPs are widely expressed in the body. They are differently distributed in several organs and tissues involved in fluid transport, such as epithelia (the wall of tubular organs), as well as in other tissues that do not have an obvious role in fluid transport, such as adipocytes[3]. For example: kidneys express eight AQPs isoforms (AQP1, 2, 3, 4, 6, 7, 8 and 11) along the water-permeable segments, of which five have been shown to play a role in body water balance (AQP1, 2, 3, 4 and 7)[142]; in brain cells of rodents and primates, eight isoforms have been described (AQP1, 3, 4, 5, 6, 8, 9 and 12) from which AQP4 is the most abundant[143]. Additionally, one type of cell may have more than one isoform, for example RBC express the orthodox AQP1 and the aquaglyceroporin AQP3.

The AQP channels are involved in numerous physiological processes as well as in several pathological conditions, such as: ***Transepithelial fluid*** *transport* in the kidney where several regions of tubules and microvessels must own a high water permeability necessary to achieve its urine-concentrating function[142]. ***Epithelial fluid secretion*** (eg. saliva secretion in salivary glands and insulin and pancreatic fluid secretion in pancreas)[144]. ***Cell migration*** where AQPs are necessary to enhance formation of membrane protrusion at the leading end of a migrating cell, which is critical for cell motility thus facilitating wound healing processes[145] as well as tumour cell infiltration and metastasis[146]. ***Brain water transport*** where water permeation across the blood–brain barrier and the blood–cerebrospinal fluid barrier facilitates the movement of water into and out of the brain[3]. Most brain diseases (e.g. stroke, traumatic brain injury, brain tumors, brain inflammation) present the hallmark of oedema, that consists in water accumulation resulting from brain osmotic homeostasis dysfunctions[143]. ***Neuroexcitation***, where AQP4-facilitated water transport in astrocytes during potassium reuptake following neuroexcitation causes contraction of the extracellular space, maintaining the driving force for potassium reuptake[3]. ***Skin hydration***, AQP3 expressed in epidermal cells facilitates skin hydration by maintaining high glycerol levels in the stratum corneum, which acts as a humectant to retain water[147,148]. ***Cell proliferation*** where AQP3 expressed in epidermal cells enhances the proliferation rate of basal keratinocytes[149] by maintaining high cellular glycerol levels necessary for ATP formation and lipid biosynthesis, leading to cellular proliferation[3]. Another example is AQP5 that might interact in signalling pathways switching on other proteins that ultimately turn on genes involved in cell growth in colon cancer[150] and lung cancer[151]. These interactions may represent novel AQP functions, which are unrelated to water or solutes transport[146]. ***Glycerol metabolism***, where the interplay between two AQPs, AQP7 expressed in adipocytes (that enables the efflux of glycerol, thus preventing intracellular accumulation of glycerol and triglycerides involved in the pathophysiology of diabetes) and AQP9 expressed in liver (which facilitate the uptake of glycerol and thereby the availability of glycerol for *de novo* synthesis of glucose and triglyceride), have an important role in controlling glycerol metabolism in both adipose tissue and liver[152].

The physiological relevance of AQPs is well documented by studies of the phenotypes of AQP-knockout mice that have provided most of the information on AQP physiology as well as by the discovery of humans with non-functioning mutations[3,153] or altered AQP distribution and expression in pathological situations[154]. These and other studies point to a broad potential for AQP based therapies.

### 5.1.AQP3 as drug target.

AQPs are involved in several pathological conditions, and since their discovery they have been increasingly singled out as important drug targets useful in the treatment of several pathologies. Depending on the AQP isoform, location, function, and on the particular pathological condition several therapeutic approaches have been proposed by many authors[3,154,155]. In this work, the AQP3 potential role for therapy will be addressed.

AQP3 is normally expressed in ***renal collecting duct epithelial cells.*** Together with AQP4, it is constitutively active as water channel on the basolateral membrane while, on apical membrane, water transport is mediated by a vasopressin-induced trafficking of AQP2 from an intracellular compartment[142]. AQP3 levels of expression are regulated on a long term basis, where prolonged water deprivation increases AQP3 protein and mRNA levels[156] which was mainly attributed to the increased vasopressin levels observed[157]. Additionally, phenotypes of AQP-null mice revealed defects in urine-concentrating function[158]. Hence inhibition of these AQPs would produce an aquaretic response similar to that produced by vasopressin V2 receptor antagonists[3].

AQP3 is also expressed in the basal layer of proliferating ***epidermal keratinocytes.*** AQP3-deficient mice exhibited impaired skin hydration[148], reduced skin elasticity, delayed wound healing recovery[147]. Thus AQP3 activators are expected to enhance skin hydration, elasticity and wound healing mechanisms. However there is also an established link between AQP3 expression in the epidermis and skin cancer. AQP3 is known to be overexpressed in skin tumours[159]. In addition, AQP3-null mice showed to be remarkably resistant to the development of skin tumours probably due to impaired glycerol uptake by tumour cells[160]. This association between AQP3 expression levels and skin cancer appeals for caution in the use of activators of AQP3 activity[161]. Due to AQP3 involvement in skin tumour cell proliferation and probably also cell migration, an AQP3 inhibitor would have a therapeutical role in this type of cancer both as anti-proliferative and anti-metastatic agent.

AQP3 is also present in the ***conjunctiva*** and ***corneal epithelium*** of rat, dog, and mouse[162–165]. The transepithelial water flow in the corneal endothelium is mainly paracellular and less transcellular, thus the role of AQPs in cell membranes is to allow the fast cellular osmotic equilibration, which is necessary to maintain optimal rates of fluid movement[166]. Also, as seen in many cell types, AQPs in the cornea are found to be involved in cell migration and proliferation. In mouse, AQP3 deficiency was associated with impaired wound healing (reduced corneal re-epithelialization and delayed restoration of full-thickness epithelia after scraping) what was related to a defect in cell migration and cell proliferation arising from AQP3 deletion[164]. Thus it was suggested that AQP3 induction might provide a possible therapy to accelerate the resurfacing of corneal defects. In corneal endothelial diseases such as pseudophakic bullous keratopathy (BK), whose clinical hallmark is the chronic corneal oedema, it was reported an altered expression of AQPs including increased AQP3[165]. AQP changes in BK corneas suggest future BK therapies including treatments that can suppress AQP3 expression or function in order to control cornea oedema.

AQP1, 4, 3 and 5 are expressed in ***lacrimal glands***[165,167]. AQP3 is located on the basolateral membranes of acinar cells. However, knockout mice lacking AQP3 (and also AQP1, 4 and 5) showed unaltered tear secretion[167]. This finding does not support an essential role for AQPs in lacrimal gland fluid secretion. It was proposed that the requirement for AQPs in salivary but not lacrimal gland secretion, may involve the substantially slower fluid secretion rate across lacrimal gland acinar cells. However, another study showed that in patients with Sjögren's syndrome (an autoimmune disorder characterized by decreased lacrimal and salivary gland secretions, resulting in severe dry eye and dry mouth), AQP5 is localized in the cytoplasm and not in its normal location, the apical membranes[168]. This defect in lacrimal gland AQP5 trafficking was related to decreased lacrimation and dry eye in these patients, thus supporting AQPs essential role

in fluid secretion rate across lacrimal glands of humans. Clearly, additional work is needed for a better understanding of AQPs function in the lacrimal gland in order to understand the therapeutic potential of AQPs in this cells.

AQP3 is also expressed in ***Immune cells***. T cells were reported to expressed AQP3. Based on AQP3-deficient mice phenotypes, it was proposed to regulate T cells trafficking in cutaneous immune reactions where, T cell migration toward chemokines would be dependent on AQP3-mediated hydrogen peroxide uptake and not on the water/glycerol transport[169]. The authors proposed that AQP3 should be considered a target for T cell–mediated diseases. For example, inflammatory skin diseases, such as atopic dermatitis and psoriasis, are characterized by the infiltration of T cells into both the dermis and the epidermis of affected skin[170]. Thus, impairing AQP3 function would be useful in the treatment of inflammatory skin diseases.

AQP3 is expressed in resident peritoneal macrophages' plasma membrane[171]. AQP3-deficient mice showed significantly greater mortality than wild-type mice in a model of bacterial peritonitis, linking AQP3 as a novel determinant in macrophage immune function by a cellular mechanism involving water and glycerol transport, and consequent phagocytic and migration activity[171]. This AQP3 involvement in key macrophage function suggested AQP3 as a novel therapeutic target in modulating the immune response in various infectious and inflammatory conditions.

AQP3 is expressed at the ***Intestinal epithelium*** in the basolateral membrane of colonic epithelial cells. However little is known regarding the details of the physiological role of AQP3 in gastrointestinal tract[172]. AQP3 null mice developed severe colitis with colonic haemorrhage, marked epithelial cell loss and death[173]. The results suggested a novel role for AQP3 in enterocyte proliferation that is probably related to its glycerol-transporting function. AQP3 is thus a potential target for therapy of intestinal diseases associated with enterocyte destruction, such as Crohn's disease, that are associated with enterocyte hyper- or hypoproliferation[173].

AQP3 is also expressed in ***red blood cells***[174]. On the other hand, the life-cycle of some parasites such as Plasmodium falciparum (the infectious agent of malaria a devastating worldwide disease) outlines additional opportunities for pharmacological intervention in the treatment of human pathologies. Host AQPs are also potential drug targets in some parasitosis. For example, the malarial parasite, dwelling within erythrocytes, relies on human-AQP3 or mouse-AQP9 in the erythrocyte membrane to obtain glycerol[175].

Finally, ***tumour*** generally overexpress AQPs including isoforms that are normally found in their cell of origin as well as others not originally present. AQPs role in cancer may be related to tissue water balance, cell migration, cell proliferation and cell adhesion[146] leading to tumour angiogenesis, invasion, metastasis and growth[3]. AQP3 have been reported to be over expressed in a wide range of carcinomas (e.g. liver cancer[176], oesophageal cancer[177], pituitary adenomas, salivary gland tumours, thymic tumours, adenocarcinoma of the lung and prostate, squamous cell carcinomas of the skin, oesophagus and uterine cervix, apocrine carcinoma of the breast, germinal cell tumours of the ovary and testis and urothelial carcinoma of the bladder[159], collecting duct carcinoma[178], among others). Still there is much to know about the mechanisms underlying AQPs relevance in tumours physiology. AQP3, however, is considered as having a great potential as a drug target in cancer therapy and thus AQP3 inhibitors will certainly be of broad utility.

Additionally to drug targeting, since the levels of AQPs expression are altered in many pathological conditions, AQPs detection are now being considered as biomarkers for diagnosis.

## 5.2.Aquaporin modulators.

The current knowledge about AQP pathophysiology outlines great potential in treatments targeting AQP function. AQPs based modulator drugs are predicted to be of broad utility in the treatment of several disorders, such as cerebral oedema, cancer, obesity, wound healing, epilepsy, glaucoma and malaria[3,154].

Search for AQP based therapies has become a thriving topic. AQPs are now the focus of pharmaceutical sciences. However, finding inhibitors suitable for use in humans has turned out to be unexpectedly challenging and elusive.

The inhibition of water permeation in RBCs (which express AQP1) by sulfhydryl-reactive heavy metal ions and organomercurial compounds, such as pCMBS (p-chloromercuribenzene sulphonate), has been known since the 70s[179]. Later on the thiol group of Cys189 residue of the loop E was identified as the biding site responsible for $HgCl_2$ inhibition[114]. The mercury (II) sterically occlude the water pore through a covalent bond with Cys189 residue that projects inside the pore while other AQPs (such as AQP4) that lack a cysteine residue at this position are resistant to inhibition by mercurial compounds[180]. However, recent molecular dynamic studies have suggested that mercury disrupts the water pore of AQP1 through local conformational changes in the ar/R region[181]. Other heavy metals such as Gold (HAuCl4)[182], Silver ($AgNO_3$ and silver-sulphadiazine)[182], Nickel ($NiCl_2$), Copper ($CuCl_2$) and Zinc ($ZnCl_2$)[183] have also been shown to inhibit water and/or glycerol permeability in different AQPs.

Small molecules, not containing metals have also been reported to inhibit water permeation. One example is the non-selective ion channel blocker tetra-ethylammonium (TEA+), a blocker of voltage-gated potassium channels, calcium-dependent potassium channels and the nicotinic acetylcholine receptor. TEA+ was reported to inhibit AQP1, AQP2 and AQP4[184,185]. However, this effect was not corroborated by other studies, which indicated little or no AQP inhibition by TEA at concentrations up to 10mM[186,187].

In general, all the compounds mentioned so far are valuable for gaining insight into the effect of AQP modulation on a cellular level, but they are not suitable for therapeutic applications due to their toxic side effects and lack of selectivity.

The diuretic carbonic anhydrase inhibitor, acetazolamide[188–190] and other related sulfonamides[191] as well as several anti-epileptic drugs[192] were reported as efficient reversible blockers of AQP1 and AQP4. However, these effects were not confirmed by other studies[186,187,193]. and the utility of these antiepileptic drugs as AQP inhibitors has been questioned, since they are known to interact with multiple relevant targets[194].

Recently, the loop diuretic bumetanide as well as a synthesized analogue (AqB013) and furosemide were reported to inhibit water fluxes of both human AQP1 and rat AQP4[194,195], while an analogue of furosemide (AqF026) was reported to slightly increase AQP1 activity[196].

AQP4–IgG (immunoglobulin G) autoantibodies in NMO were found to impair water transport in AQP4 expressing *X. laevis* oocytes[197], although other studies reported that AQP4–IgG autoantibodies does not inhibit AQP4 water permeability[198,199].

More recently, organic small-molecule compounds have been described as modulators of orthodox AQPs[154]. TGN-020 (2-nicotinamido-1,3,4-thiadiazole), an AQP4 inhibitor[200], was also shown to reduce cerebral oedema in rodent models[201], a radio-labeled version of which has been developed to study AQP distribution in vivo using positron emission tomography (PET)[202]. In addition, a recent report identified some compounds containing carboxylic groups and an aromatic moiety, acting as inhibitors of human AQP1[203]. In another study, as a result of a screening assay, four molecules were identified as effective inhibitors of mediated water transport of both AQP1 and AQP4[204], but the mechanism by which they interact with the water channels is still unknown.

Concerning aquaglyceroporin's activity regulation by organic modulators, up to date, not much is known. Phloretin was found to be effective in inhibiting AQP9[94], but it has been also reported to inhibit solute transporters, as well as ion channels, and thus exerts profound effects on osmotic gradients in multiple ways[205]. More recently some small-molecule inhibitors of mice AQP9 glycerol permeability have been reported[206], but given their poor water solubility, these compounds are not yet suitable for in vivo experimentation.

## 6. Plant aquaporins.

Comparatively with other organisms, plants have a remarkable large number of AQPs homologues, ubiquitously expressed. Genome sequencing revealed the presence of 35 MIP-encoding genes in Arabidopsis, 36 in maize and 33 in rice[207].

Based on their sub-cellular localization and sequence similarity, plant AQPs are classified into seven subfamilies: PIPs (plasma membrane intrinsic proteins), TIPs (tonoplast intrinsic proteins), NIPs (nodulin26-like intrinsic proteins), SIPs (small basic intrinsic proteins), XIPs (x intrinsic proteins), HIPs (hybrid intrinsic proteins) and GIPs (GlpF-like intrinsic proteins)[208–211].

Besides water, plants AQPs are reported to transport a broad range of subtracts including other small molecules and/or gases of physiological relevance in plant development and adaptation under stress conditions[212,213,211].

The wide range of substrates for these proteins as well as their complex regulation levels and pathways together with some emerging aspects of their functionalities[207], make them behave more like multifunctional, highly adapted channels rather than simple water and solute pores.

Plant growth and development are dependent on the tight regulation of water uptake and transport across cellular membranes and tissues[214]. Therefore, it is crucial that plant AQPs are subjected to a fine-tuned regulation according to cell/tissue type, environmental conditions as well as plant developmental stages. Besides regulation of gene expression, the activity of AQPs protein is regulated by various posttranslational modifications such as methylation, glycosylation, phosphorylation, membrane trafficking, heteromerization. Their gating can also be regulated by pH, divalent ions and membrane

tension[215,137]. Various stress conditions like anoxia, salt and water stress have also been reported to affect the activity of aquaporins in plants[213,215].

## 7. Aquaporin heterologous expression in yeast

The yeast *Saccharomyces cerevisiae* constitutes a valuable system for numerous studies on the basic cellular and molecular mechanisms, processes that are well conserved between yeast and higher eukaryotes, including mammals. Due to the functional similarity to higher eukaryotes, the ease of genetic manipulation and the existence of a collection of yeast gene deletion strains, the yeast model has been considered an attractive organism to study AQP physiology and to screen for compounds of potential pharmacological use[216]. AQP from several organisms including mammals and plants has been successfully expressed in yeast, allowing channel analysis either using whole yeast cells[217] or vesicles containing the expressed AQP[218].

## 8. Functional studies to assess aquaporin activity.

Water/solute transport assays have been performed using isolated cells from different organisms, such as bacteria[219], yeast[220,221], and animal cells[222]. Intracellular vesicles[223] as well as plasma membrane vesicles obtained from animal tissues (mainly kidney or intestinal epithelia) were used to evaluate AQP functionality either in intracellular organelles[224] or in transepithelial water fluxes[225]. Other widely used approach consists in aquaporin heterologous expression in Xenopus laevis oocytes, which have very low intrinsic water permeability, to functionally characterize novel AQP isoforms[78]. In addition to oocytes, yeast cells lacking endogenous AQPs have also been used as a system for heterologous expression[217].

Cell volume changes induced by osmotic gradients are used to study membrane permeability allowing the evaluation of the osmotic water permeability (Pf) and/or solute permeability (Ps) coefficients, the activation energy of water and/or solute transport (Ea). High Pf and/or Ps and low Ea values indicate the existence of functional water and/or solute channels while low permeabilities and high Ea indicates permeation occurs mostly through lipids. Pf is the proportionality constant between the measured volume change and the pressure gradient applied (osmotic and/or hydrostatic) and can be attained by following the time course of cell volume change (dV/dt) during an osmotic shock with an impermeant solute. Ps is the proportionality constant between the measured volume change and the solute gradient applied and can also be attained by following dV/dt, during the application of a permeant solute gradient. If the osmotic shock is applied with a permeant solute, fluxes of water and solute occur simultaneously, but at different rates, and both movements are responsible for volume changes and must be taken into account when evaluating both permeabilities. These measurements can be obtained using volume dependent physical parameters based in optical properties such as light transmission or absorbance, light scattering and fluorescence of volume sensitive dyes.

A commonly used method to follow rapid volume changes is the stopped flow spectroscopy. In the stopped flow device, cell/vesicles suspensions are subjected to osmotic challenges by rapid mixing with an equal volume of hypo or hyperosmotic solution. For vesicle or cell suspensions, light of a chosen wavelength is directed to the observation chamber through an optical fiber and the change in 90º light scattered is followed until a stable signal is attained. An alternative approach uses cell/vesicles loaded with fluorescent dyes and the changes in fluorescence intensity of the suspension are monitored by stopped-flow fluorescence. Signals are calibrated into volumes and used for permeability evaluation.

Stopped-flow experiments can be done in plasma membrane vesicles from AQP-expressing cells, in reconstituted proteoliposomes or in small cells such as erythrocytes. For larger cells, kinetics of cell volume change due to osmotic gradients is followed by microscopy. This is the case of Xenopus oocytes expressing AQPs (by cRNA injection) where swelling kinetics is determined by image analysis of oocyte cross-sectional area[205]. In another configuration, cells are grown as monolayer cultures, loaded with a fluorescent dye, mounted on the stage of an epifluorescence microscope and subjected to osmotic challenges by extracellular addition osmotic solutions. Fluorescence signals resulting from cell volume changes together with cell image analysis are used to evaluate kinetics of cell volume changes and Pf and/or PS.

Regulation of AQP function by pH, phosphorylation or specific inhibitors, can be screened through simple measurements of Pf and/or PS and Ea. However, AQP gating by physical parameters such as membrane surface tension implies the design of specific protocols that can only be applied to vesicle systems[139,226] or walled cells[220] that can sustain membrane tensions without rupture.

## Aim of part II

Part II aims at screening for AQPs modulators with potential utility for drug development. Chapter 2 encloses two publications (publications 4 and 5) where human erythrocytes were used as a cell model to screen the inhibitory effect of gold coordinated compounds, accessing their effects in human AQP1 (an orthodox AQP) and human AQP3 (an aquaglyceroporin).

Chapter 3 encloses 2 publications (publications 6 and 7), where *S. cerevisiae* was used as a heterologous expression system for studying the activity of individual plant AQPs. Plant cells express numerous AQPs isoforms whose function is still unclear; the development of a cell model where they can be individually characterized is crucial for functional assays. Yeast cells deleted in their endogenous AQPs thus having low intrinsic water permeability, were used to express and functionally assess grapevine AQPs.

# CHAPTER 2 – Aquaporins as Drug Targets

# CHAPTER 2 – Aquaporins as Drug Targets

The information contained in this chapter is included in the following original publications:

*Publication 4*

Martins AP, Marrone A, Ciancetta A, Galán Cobo A, Echevarría M, Moura TF, Re N, Casini A, Soveral G
*Targeting aquaporin function: potent inhibition of aquaglyceroporin-3 by a gold-based compound.*
PLoS One. 2012;7(5):e37435.
doi: 10.1371/journal.pone.0037435.

*Publication 5*

Martins AP, Ciancetta A, de Almeida A, Marrone A, Re N, Soveral G, Casini A.
*Aquaporin inhibition by gold(III) compounds: new insights.*
ChemMedChem. 2013 Jul;8(7):1086-92.
doi: 10.1002/cmdc.201300107.

OPEN ACCESS Freely available online

PLoS one

# Targeting Aquaporin Function: Potent Inhibition of Aquaglyceroporin-3 by a Gold-Based Compound

**Ana Paula Martins[1], Alessandro Marrone[2], Antonella Ciancetta[2], Ana Galán Cobo[3], Miriam Echevarría[3], Teresa F. Moura[1], Nazzareno Re[2], Angela Casini[4]*, Graça Soveral[1,5]***

**1** REQUIMTE, Departamento de Química, Faculdade de Ciências e Tecnologia, Universidade Nova de Lisboa, Caparica, Portugal, **2** Dipartimento di Scienze del Farmaco, Università G. d'Annunzio, Chieti, Italy, **3** Instituto de Biomedicina de Sevilla (IBiS), Hospital Universitario Virgen del Rocío/CSIC/Universidad de Sevilla, Seville, Spain, **4** Pharmacokinetics, Toxicology and Targeting, Research Institute of Pharmacy, University of Groningen, Groningen, The Netherlands, **5** Departamento de Bioquímica e Biologia Humana, Faculdade de Farmácia, Universidade de Lisboa, Lisbon, Portugal

## Abstract

Aquaporins (AQPs) are membrane channels that conduct water and small solutes such as glycerol and are involved in many physiological functions. Aquaporin-based modulator drugs are predicted to be of broad potential utility in the treatment of several diseases. Until today few AQP inhibitors have been described as suitable candidates for clinical development. Here we report on the potent inhibition of AQP3 channels by gold(III) complexes screened on human red blood cells (hRBC) and AQP3-transfected PC12 cells by a stopped-flow method. Among the various metal compounds tested, Auphen is the most active on AQP3 ($IC_{50} = 0.8 \pm 0.08$ μM in hRBC). Interestingly, the compound poorly affects the water permeability of AQP1. The mechanism of gold inhibition is related to the ability of Au(III) to interact with sulphydryls groups of proteins such as the thiolates of cysteine residues. Additional DFT and modeling studies on possible gold compound/AQP adducts provide a tentative description of the system at a molecular level. The mapping of the periplasmic surface of an homology model of human AQP3 evidenced the thiol group of Cys40 as a likely candidate for binding to gold(III) complexes. Moreover, the investigation of non-covalent binding of Au complexes by docking approaches revealed their preferential binding to AQP3 with respect to AQP1. The high selectivity and low concentration dependent inhibitory effect of Auphen (in the nanomolar range) together with its high water solubility makes the compound a suitable drug lead for future *in vivo* studies. These results may present novel metal-based scaffolds for AQP drug development.

**Citation:** Martins AP, Marrone A, Ciancetta A, Galán Cobo A, Echevarría M, et al. (2012) Targeting Aquaporin Function: Potent Inhibition of Aquaglyceroporin-3 by a Gold-Based Compound. PLoS ONE 7(5): e37435. doi:10.1371/journal.pone.0037435

**Editor:** Immo A. Hansen, New Mexico State University, United States of America

**Received** January 13, 2012; **Accepted** April 19, 2012; **Published** May 18, 2012



**Funding:** This work was supported from Fundação para a Ciência e a Tecnologia, Portugal, through a Ph.D. fellowship to APM (SFRH/BD/65046/2009). A. Casini thanks the University of Groningen (Rosalind Franklin fellowship). The authors thank COST CM0902 for financial support. The funders had no role in study design, data collection and analysis, decision to publish, or preparation of the manuscript.

**Competing Interests:** The authors have declared that no competing interests exist.

* E-mail: gsoveral@ff.ul.pt (GS); a.casini@rug.nl (AC)

## Introduction

AQPs belong to a highly conserved group of membrane proteins called the major intrinsic proteins (MIPs) present in all type of organisms and involved in the transport of water and small solutes such as glycerol, nitrate and urea [1]. The 13 human AQP isoforms (AQP0-12) are differentially expressed in many types of cells and tissues in the body and can be divided into two major groups: those strictly selective for water (called orthodox aquaporins) and those that besides water are also permeable to small solutes including glycerol (called "aquaglyceroporins") [2]. Both groups of channels are involved in many pathophysiological conditions [3,4]. There is considerable potential for transferring knowledge of AQP structure, function and physiology to the clinic, and certainly there is great translational potential in aquaporin-based therapeutics. AQP-based modulator drugs are predicted to be of broad potential utility in the treatment of several diseases such as kidney diseases, cancer, obesity, glaucoma, brain edema and epilepsy [5]. In particular, recent studies have correlated AQP3 glycerol permeation with skin tumorigenesis [6] and identified it as being aberrantly expressed in melanoma [7], suggesting that AQP3 might be a novel target for skin tumor prevention and therapy.

There are at present very few reported AQP inhibitors that are suitable candidates for clinical trials and none of them showed specificity for AQP3 so far. Though various AQPs are inhibited by mercurial compounds, such as $HgCl_2$ [8], these substances are non-selective in their action and extremely toxic. Other inorganic salts such as $AgNO_3$ and $HAuCl_4$, that are prone to interact with sulfhydryl groups of proteins as mercurials, have been also shown to inhibit water permeability in plasma membrane from roots, and in particular $AgNO_3$ has been reported to efficiently inhibit water permeability in human red blood cells ($EC_{50} = 3.9$ μM) [9]. Various other candidate blockers of AQP1 have been also reported, including tetraethyl-ammonium [10], acetazolamide [11] and DMSO [12]; however, other studies indicated little or no AQP1 inhibition by tetraethylammonium salts or acetazolamide [13] and apparently inhibition by DMSO results from an osmotic clamp effect rather than true inhibition [14]. Several papers reported AQP4 inhibition by a series of arylsulfonamides, antiepileptic drugs and related molecules, with strong inhibition at low micromolar concentrations [15,16]; yet, these results could not

be confirmed, with no inhibition activity found even at high concentrations of any of the putative AQP4 inhibitors [17]. An AQP4 inhibitor (2-nicotinamido-1,3,4-thiadiazole) was also shown to reduce cerebral edema in rodent models [18], a radio-labeled version of which has been developed to study AQP distribution *in vivo* using PET [19]. Migliati et al. reported on AQP1 and AQP4 inhibition by an analogue of the sulfonamide Bumetamide [20], that was also recently found to reduce cerebral edema in rodent models [21] via AQP4 inhibition. Recently, Jelen et al. identified novel small molecule inhibitors of AQP9 glycerol permeability; however, since their solubility in aqueous solution is very limited, these compounds are currently not suitable for *in vivo* experiments [22].

Within this frame, we decided to reconsider metal-based compounds as possible AQP inhibitors, and we report here the inhibitory effect on the water and glycerol permeability mediated by AQP1 and AQP3 of a series of metal complexes based on different transition metals. The selected compounds are metal-based drugs already known to possess different therapeutic properties as anticancer, antirheumatic and antibacterial agents. Among them were the anticancer drug *cis*-[$PtCl_2(NH_3)_2$] (cisplatin) [23], the antimetastatic trans-[Ru(dmso)(Him)Cl4] (dmso = dimethylsulfoxide, Him = imidazole, NAMI-A) [24], the antibacterial Ag(I) sulfadiazine (AgSDZ) [25], and the antirheumatic agent aurothioglucose (AuTG) [26] (Figure 1). In addition, the gold(III) compound [Au(phen)$Cl_2$]Cl (phen = 1,10-phenatroline, Auphen) [27,28,29] showing antiproliferative properties on cancer cells *in vitro*, was also selected. For most of these compounds, the mechanisms of pharmacological actions are still poorly understood [30]. Therefore, AQPs also appeared to be interesting to investigate as putative targets for metal-based drugs.

The effect of the compounds was tested by a stopped-flow method on human red blood cells (hRBC) that specifically express large amount of AQP1 and AQP3 [31,32], and confirmed on transfected PC12 cell lines with overexpression of either AQP1 or AQP3. In all cases, the gold(III) complex Auphen was the most potent inhibitor and showed selectivity towards AQP3. Further studies on a selected series of gold(III) complexes supported the idea of the necessity of direct binding of gold ions to the protein to achieve glycerol permeability inhibition. Additional DFT calculations on the interactions of gold(III) complexes with model amino acids side chains, as well as docking studies investigating the non-covalent binding of gold(III) complexes with both the known structure of AQP1 and a homology model of AQP3, allowed to provide a tentative description of the putative mechanisms of inhibition and to explain the compounds' selectivity for AQP3.

## Results

### Inhibition of water and glycerol permeability by metal compounds

The effect of different metallo-drugs based on Pt(II), Ru(III), Ag(I), Au(I,III) (Figure 1) was tested on water and glycerol permeability of hRBCs. For this purpose hRBCs incubated in isotonic phosphate buffered saline (PBS) solution were challenged with hypertonic sucrose solution (impermeant solute, inducing cell shrinkage) or hypertonic glycerol solution (permeant solute, cells shrink due to the hyper-osmotic gradient and re-swell due to glycerol entrance). Since hRBCs were shown to express large amount of AQP1 and AQP3 accountable for membrane permeability to water and glycerol [32,33,34], this assay allows the direct evaluation of these aquaporins activity and is thus a promising screening assay for modulators of aquaporin function. From the rate of cell volume changes (shrinkage and re-swelling) after imposed osmotic shocks, the membrane permeability for water and for glycerol can be calculated [34].

Figure 2A shows the effect induced by the metal complexes (0.1 mM concentration or higher) on AQP1 and AQP3 (10 min incubation at room temperature) in comparison to $HgCl_2$, a well-known inhibitor of aquaporin activity, tested in the same conditions. The obtained results demonstrated that the Au(III) complex Auphen is the most effective of the series on glycerol permeability, and far more effective than the mercurial compound (with a statistical significance of $P<0.001$). For control hRBCs, the osmotic water ($P_f$) and glycerol ($P_{gly}$) permeability values were respectively $(4.2\pm0.4)\times10^{-2}$ cm $s^{-1}$ (n = 5) at 10°C and

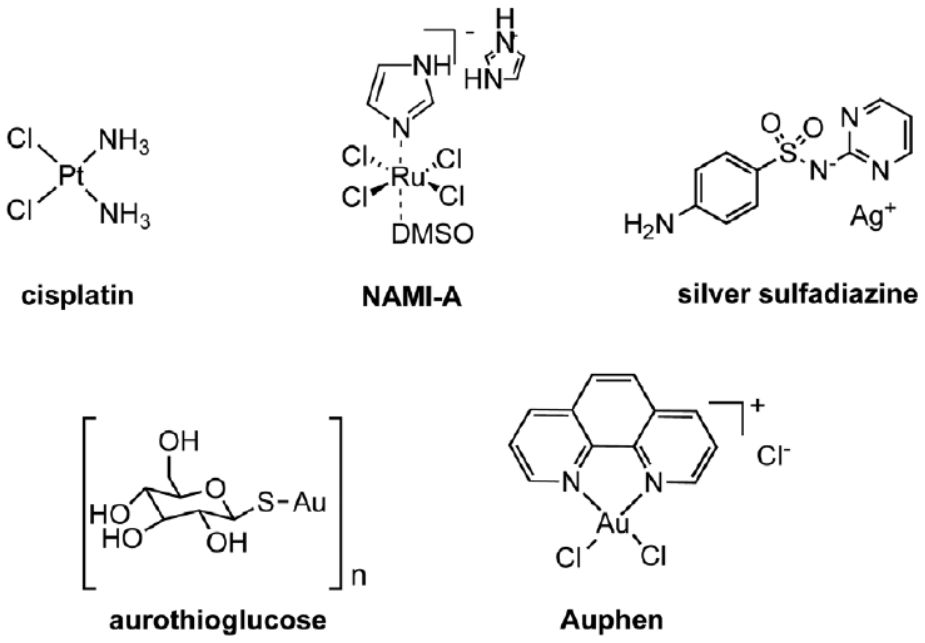


**Figure 1. Metal compounds used in this study.**
doi:10.1371/journal.pone.0037435.g001

$(1.8\pm0.2)\times10^{-5}$ cm $s^{-1}$ (n = 5) at 23°C. As shown in Figure 2A, Auphen showed a modest effect on water permeability (ca. 20% inhibition), while being able to drastically reduce glycerol transport with a residual permeability of ca. 11% (90% inhibition). The smaller effect obtained for water permeability points to a more potent effect on AQP3, which itself is also a water-transporting channel [35,36] but with a smaller contribution to the total bulk of water flow through hRBC membranes where AQP1 is the main water channel [32].

Representative traces of stopped-flow experiments with control and hRBCs treated with even lower concentration of Auphen (5 μM, incubated 30 min at room temperature) showing the inhibition of the osmotic water flux or glycerol flux are reported in Figure 2B and 2C, respectively.

To assure the compound selectivity, the effect of Auphen was also tested on urea transport. Notably, no significant effect could be observed for both concentrations tested in comparison to the controls (P>0.05, n = 5) (Figure 2D). The ability of AQP3 to transport urea has been debated [37,38]. In the erythrocyte, the urea transporter UT-B [39] accounts for a very high urea permeability reducing osmotic shrinkage of RBCs while passing through the kidney. Therefore, compared to urea transporters, urea permeability through AQP3 may have only a negligible contribution and thus its inhibition would not be enough to observe decreased urea permeability. Since Auphen did not affect

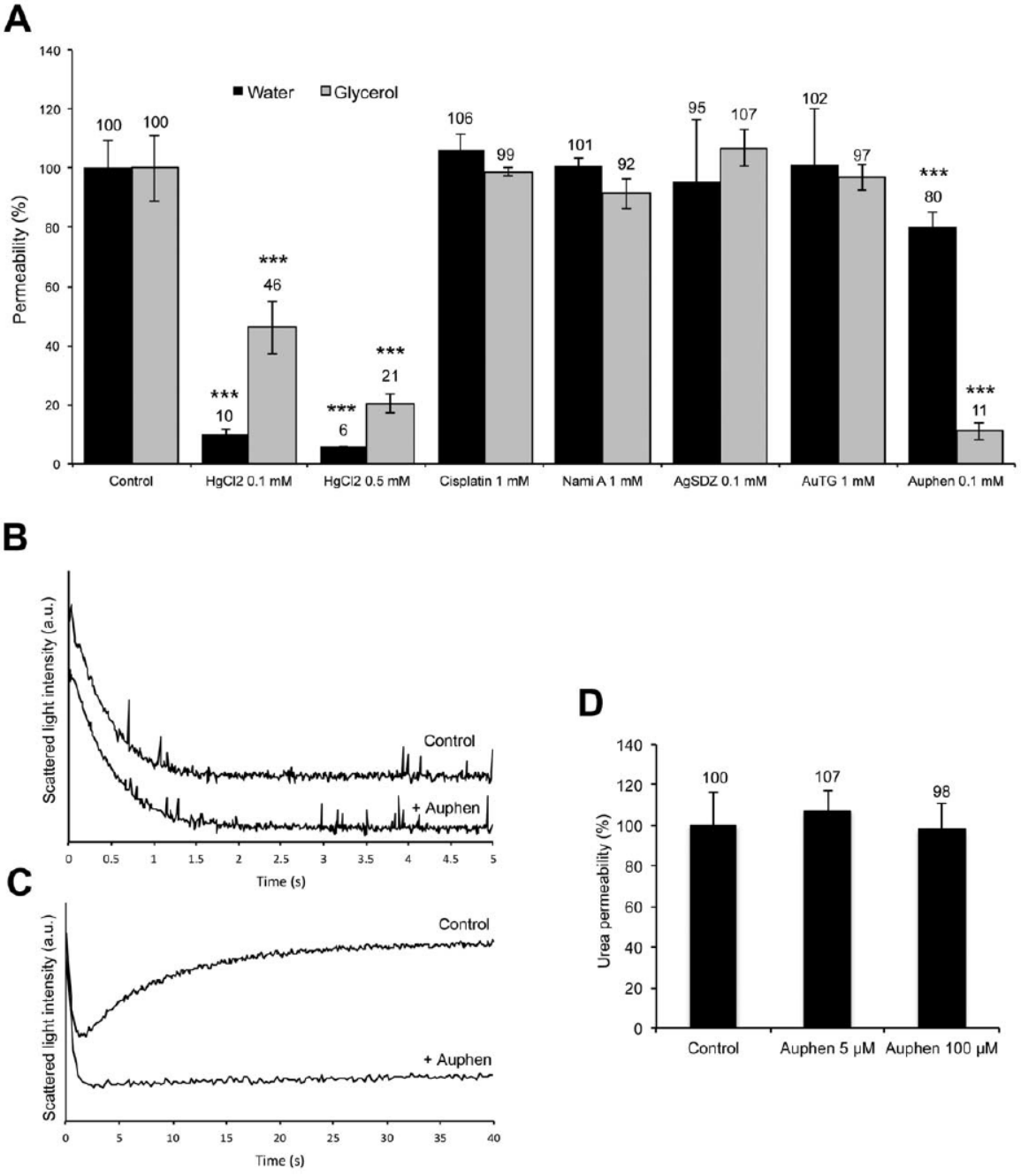


**Figure 2. Effect of compounds on hRBC permeability.** (A) Water and glycerol permeabilities (% of control) after treatment with the compounds under study and with $HgCl_2$ (10 min at r.t.) A marked effect of Auphen (100 μM) is depicted (***P<0.001). (B) Stopped flow representative traces of water and (C) of glycerol permeability (control and after incubation with 5 μM Auphen, 30 min at r.t.). (D) Urea permeability showing no significant effect of Auphen treatment (5 and 100 μM, 30 min at r.t.; P>0.05).
doi:10.1371/journal.pone.0037435.g002

urea permeability, this result indicates that this metallodrug is specific for AQP3 not having any effect on UT-B.

Following these promising results we further investigated the inhibition of glycerol transport through AQP3 evaluating the effect of the incubation time of hRBCs with Auphen. Figure 3A shows the inhibitory effect of a fixed concentration of Auphen (5 μM) where a maximum inhibition, after an exponential decay of activity, could be observed after 30 min incubation of the samples at r.t. It is worth mentioning that no cell hemolysis was detected even after 4 hours incubation with the compound, pointing to a non-toxic inhibitory effect. Subsequently, the concentration dependent inhibition of glycerol transport in hRBC by Auphen incubated 30 min at r.t. was assessed (Figure 3B). According to the obtained results the $IC_{50}$ value for Auphen was calculated as 0.8±0.08 μM.

The activation energy ($E_a$) for water and glycerol transport, a valuable parameter indicating the contribution of protein channels to permeation, was also estimated from an Arrhenius plot (Figure S1). Upon treatment of hRBC with 5 μM Auphen, similar $E_a$ values for water transport were obtained for control (3.9±0.4 kcal $mol^{-1}$) and Auphen treated hRBCs (4.1±1.0 kcal $mol^{-1}$). However, the $E_a$ for glycerol permeation increased ca. 54% when Auphen was present (8.5±0.8 to 13.2±1.1 kcal $mol^{-1}$). Since the Auphen concentration used in the assay was higher than the $IC_{50}$ (corresponding approximately to 80% inhibition), the increase in $E_a$ is in accordance with a blockage of the AQP3 channel. Regarding water transport, the observed variation on the $E_a$ was not significant (P>0.05); indeed, in hRBC the contribution of the channel pathway to the total water permeability is usually considered to be 90% while the bilayer adds the remaining 10% [40]. The total 20% inhibition observed with Auphen (Figure 2) would exclusively reduce the contribution of the aquaporin (AQP1+AQP3) pathway maintaining the lipid pathway intact, thus reflecting a decrease of the total permeability only to ca. 87.5% of its initial value. Since the channel contribution for the total permeability still remains very large, the $E_a$ for water transport is predicted not to be significantly affected.

## Recovery of aquaporin activity by mercaptoethanol

In order to assess the reversibility of inhibition by Auphen, hRBCs pre-treated with 2 μM Auphen for 30 min r.t. were subsequently washed with PBS or with the reducing agent 2-mercaptoethanol (EtSH, 1 mM in PBS). As seen in Figure 3C, washing the sample twice with PBS had a limited effect in the recovery of Auphen inhibition of glycerol permeability. Conversely, incubation of the Auphen-treated hRBC sample with EtSH for 30 min produced an almost complete recovery of glycerol permeability (ca. 90%), suggesting that EtSH effect on cysteine residues is competing with Auphen binding to the pore [9].

The results obtained with EtSH, as well as the known affinity of gold ions for binding to sulfhydryl groups of proteins, suggest that AQP3 inhibition by Auphen might involve direct protein binding of the Au centre to Cys residues as it has already been reported for $HgCl_2$. Indeed, mercury inhibition is likely to occur both via covalent modification to Cys189 located immediately after the extracellular entrance of the water pore of hAQP1 [41] and also to other regions of the protein, causing either blockage or conformational changes with a resultant inhibition of water transport [42].

## Selectivity of AQP3 inhibition in transfected cell lines

To further confirm the specific effect of Auphen on AQP3 glycerol transport, the inhibition of glycerol permeation by Auphen was also assessed on PC12 cells stably transfected with

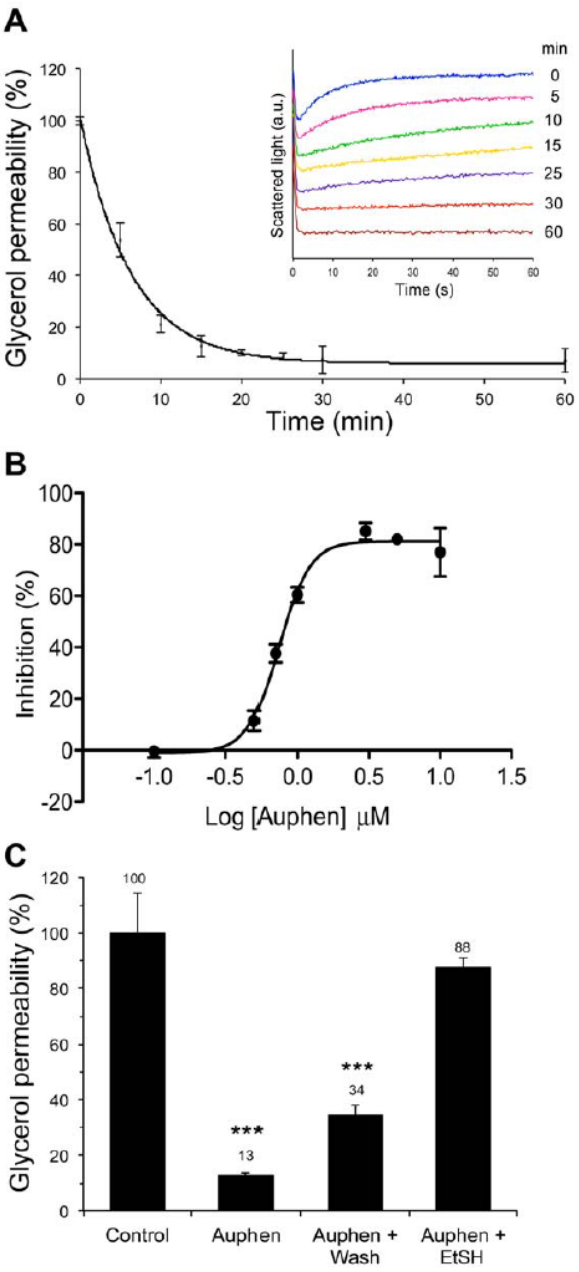


**Figure 3. Effect of Auphen on hRBC glycerol permeability.** (A) Time dependent inhibition of glycerol permeability by 5 μM Auphen. The inset shows the progressive decrease of glycerol permeability observed in the assays where the increase in cell volume due to glycerol entrance decreases drastically with the incubation time. (B) Concentration dependent inhibition of glycerol permeability in hRBC by Auphen (compound concentrations in the range 0.1–10 μM; $IC_{50}$ = 0.8+0.08 μM). (C) Inhibition of glycerol permeability (% of control) of hRBCs after Auphen treatment (2 μM, 30 min at r.t.), and reversibility by washing with PBS or incubation with 2-mercaptoethanol (1 mM for 30 min) (***P<0.001).
doi:10.1371/journal.pone.0037435.g003

rat AQP1 or AQP3 (Table 1) [43]. Cell permeability for water and glycerol was analyzed by stopped-flow experiments and results are depicted in Figure 4A. The enhancement of water permeability for AQP1 overexpressing cells (2.7 -folds) and that of glycerol permeability for AQP3 overexpressing cells (1.8 -folds) correlates well with their respective protein level of expression (Table 1). When treated with Auphen (10 to 1000 μM, 30 min incubation at r.t.) a decrease in glycerol permeability was only observed for the PC12-AQP3 cell line, reaching 72% inhibition (Figure 4B); none

of the other two cell lines (wild type and PC12-AQP1) were affected regarding glycerol. As for water permeability, only the PC12-AQP1 showed an inhibition of ca. 25% for 100 μM Auphen. It must be noted that higher concentrations of Auphen were needed to produce the same inhibitory effect observed in hRBCs. Besides the fact that Auphen might have a lower affinity for rat AQP3 than for human AQP3, the possibility of Auphen binding to other reactive groups within the whole cell membrane decreasing its effective concentration in the media and therefore leading to an underestimation of the $IC_{50}$ should not be disregarded. The PC12 cells are much larger than RBCs; hence, the presence of a larger number of these bias reactive groups may eventually contribute to a higher decrease in the effective Auphen concentration available for AQP3 blockage.

## Analysis of the mechanisms of AQP3 inhibition by gold(III) compounds

In order to evaluate our mechanistic hypothesis that sees the gold centre as responsible for AQP3 inhibition, the ligand Phen, as well as the Au(III) complexes $[Au(dien)Cl]Cl_2$ [28], (dien = diethylentriamine, Audien) and $[Au(cyclam)](ClO_4)_2Cl$ [28] (cyclam = 1,4,8,11-tetraazacyclotetradecane, Aucyclam) (Figure 5A) were tested for glycerol transport inhibition in hRBCs. It must be noted that Auphen and Audien, with $AuN_2Cl_2$ and $AuN_3Cl$ cores, can undergo substitution of the chlorides with other nucleophiles present in physiological environment. Instead, Aucyclam is a gold(III) complex with a $AuN_4$ chromophore which lacks of chemical activation resulting into poor reactivity and scarce biological (e.g. anticancer) effects [28]. The obtained results, plotted in Figure 5B, confirm that while Audien at a concentration of 50 μM reaches an inhibition of 80% (lower than the 90% inhibition observed for Auphen at the same concentration), its $IC_{50}$ is 20-fold higher than observed for Auphen ($IC_{50} = 16.6 \pm 1.6$ μM, Figure 5C). Notably, similarly to Auphen, the inhibition of AQP3 by Audien reached its maximum at 30 min incubation. On the other hand, Aucyclam and Phen are completely inactive at any tested concentrations and incubation times.

## DFT calculations

The inhibition of AQP3 by Auphen and Audien is believed to be related to the coordination of the Au(III) centre to a protein residue in the pore, presumably cysteine, methionine or histidine side-chains [44]. In order to establish the possibility of such a mechanism and to elucidate possible structure-activity relationships, DFT studies were performed to determine the molecular geometry and the binding energy of these two selected Au(III) compounds with several models of soft metal ion-binding protein sites (Figure S2). A large body of knowledge on Au(III) chemistry in water solutions [27] indicates that Auphen, and presumably also Audien, is predominantly in its intact or hydroxo forms at neutral pH, the diaquo form of Auphen being essentially negligible (Table S1). Thus, both chloro and monohydroxo species, namely $[Au(phen)Cl_2]^+$ or $[Au(phen)Cl(OH)]^+$, and $[Au(dien)Cl]^{2+}$ or $[Au(dien)(OH)]^{2+}$), were taken into account for the DFT evaluation of the Auphen and Audien binding at putative protein target residues through the calculation of thermodynamics of the ligand exchange process (Figure S3, Table S1) between Cl/OH and suitable models of the side chains of Cys ($L = CH_3SH$, $CH_3S^-$), Met ($L = CH_3SCH_3$), and His residues ($L = CH_3$-Im), in different polarity media.

The trend in Au L binding strength estimated at this level of theory (see Table S1) was $CH_3S > CH_3Im > CH_3SCH_3 > CH_3SH$ indicating the thiolate form of Cys as the most stable binding site for Au(III) complexes, and the only one showing a favorable reaction free energy with both $Cl^-$ and $OH^-$ ligands, together with the $CH_3Im$ which, however, show a much smaller reaction free energy. It must be noted that, while at physiological pH cysteine residues are predominantly in their neutral form, therefore appearing the least favorable target of Au(III) binding, calculations on the acidic dissociation of thioalcohol complexes gave negative free energy values and very low $pK_a$'s (below zero), indicating the facile deprotonation at neutral and even acidic pH with formation of a metal-thiolate complex (Figure S3 and Figure S4).

It is worth noting that the reaction free energy for $Cl^-$ substitution by thiolate is much more favorable than for $OH^-$, thus suggesting that the ligand reactivity for Au(III) complexes is different from that for cisplatin and other Pt(II) complexes where the aqua-species are well known to be more reactive. This could be due to the differences in redox properties of the Au(III) compounds with respect to the Pt(II) complexes. Finally, the free energy for $Cl^-$ substitution by thiolate is slightly but significantly, 10 20 kJ $mol^{-1}$, more favorable for Auphen than for Audien, suggesting a stronger binding of Aupen to Cys, in agreement with its experimentally observed higher AQP3 inhibition.

## Construction of the homology model of AQP3 and comparison with AQP1 structure

Three homology models of human AQP3, namely hmod1, hmod2 and hmod3, were obtained by the use of freely available web-servers SWISS-MODEL, Phyre, and ESyPred, respectively, based on the structurally characterized *Escherichia coli* glycerol facilitator (GlpF) [45], the bacterial homolog of human AQP3, or on its W48F, F200T mutant [46] as templates. The obtained models (Dataset S1) were characterized by a high degree of structure similarity, as evidenced by the overall good superimposition of helix domains and by the small values of RMSD of Cα backbones. In addition, a moderate degree of structure similarity was detected by the comparison of either side chain or loop conformations, thus suggesting that the three homology models may actually be characterized by similar binding properties. We thus selected the hmod1 structure because it was characterized by a slightly more favored ratio of model completeness: 250/292 residues for hmo1 with respect to 249/292 for both hmod2 and hmod3.

The family of the aquaporins and the aquaglyceroporin subfamily are known to share a common protein fold. It comprises six membrane-spanning helices plus two half-helices with their positive, N-terminal ends located at the centre of the protein and their C-terminal ends pointing towards either side of the membrane. The helices surround the 20-Å-long and 3 4-Å-wide amphipathic AQP channel. AQPs are identified by two asparagine-proline-alanine (NPA) sequence motifs located at the ends of the two quasi 2-fold related half-spanning helices. The selectivity filter, a constricted region formed by four residues near the periplasmic/extracellular entrance, provides distinguishing features that identify the subfamilies. In water selective AQPs this region is smaller and more polar and contains a conserved histidine residue, while in aquaglyceroporins it is larger and more hydrophobic with two conserved aromatic residues [47]. Two conserved constriction sites are present in the channel. An aromatic/Arg (ar/R) constriction is located at the extracellular pore mouth. Its diameter determines whether or not solutes, such as glycerol and methylamine, can pass the AQP in addition to water [48,49,50]. Furthermore, the positively charged residues in this region form an energy barrier for protons. The second constriction resides in the centre of the channel, where the positive

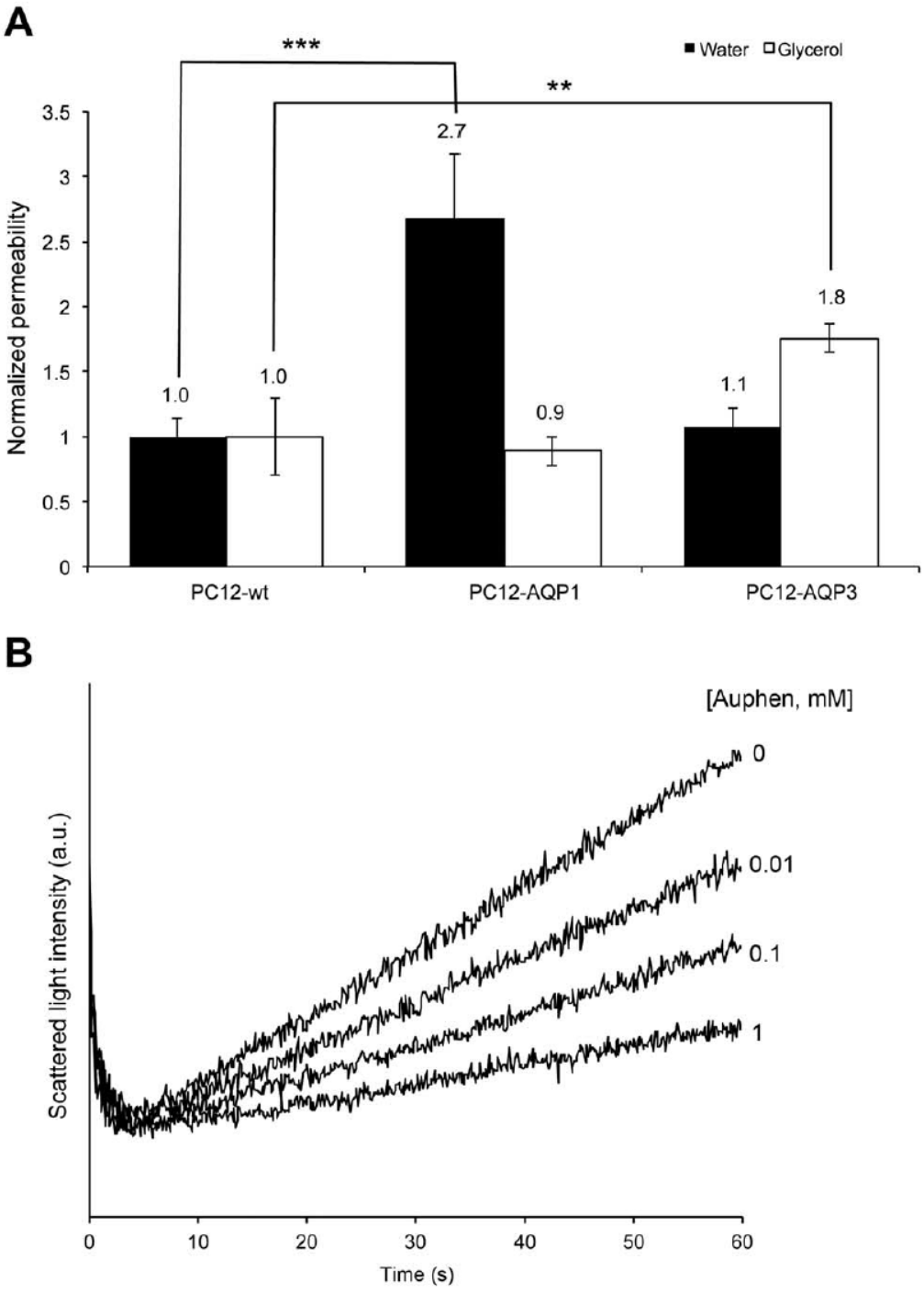


**Figure 4. PC12 cell lines assays.** (A) Permeability to water and glycerol of wild type PC12 cells and PC12 transfected with either AQP1 or AQP3. Significant differences were found for the PC12-AQP3 clones (**P<0.01) for glycerol permeability, and for the PC12-AQP1 for water permeability (***P<0.001) when compared to PC12-wt. (B) Effect of Auphen on glycerol permeability of PC12-AQP3 transfected cells (30 min incubation at r.t.).
doi:10.1371/journal.pone.0037435.g004

**Table 1.** Folds of expression and permeabilities of PC12 cells.

| Clone | Expression level | $P_{Gly} \times 10^{-7}$ (cm $s^{-1}$) | $P_f \times 10^{-2}$ (cm $s^{-1}$) |
|---|---|---|---|
| PC12wt | 1.0 | 2.16±0.64 | 3.76±0.50 |
| AQP1 | 4.0 | 1.91±0.25 | 10.11±1.84 |
| AQP3 | 2.0 | 3.78±0.24 | 4.00±0.52 |

Folds of mRNA expression were determined by Northern blot analysis and are normalized relative to the clone PC12wt.
doi:10.1371/journal.pone.0037435.t001

ends of the two half-helices meet. The helix dipole moments add up to a full positive charge, and the resulting electrostatic field poses another energy barrier for cations [51].

The structure of our homology model of AQP3 was analyzed in detail and compared with the crystal structure of human AQP1 to characterize the different propensity of both proteins for the binding of the considered Au(III) complexes. Thus, the two AQP1 and AQP3 structures were analyzed by the SiteMap module of Maestro for the identification and characterization of protein binding pockets. Two major binding pockets were observed in both AQP1 and AQP3, and, as expected, the mapping retraced

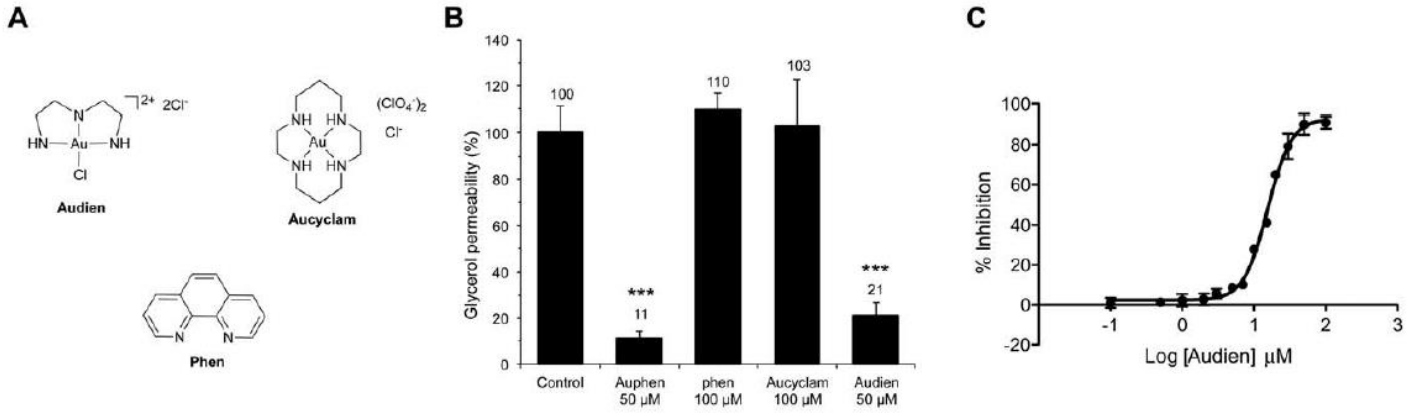


**Figure 5. AQP3 inhibition by Au(III) compounds in hRBC.** (A) Structures of the Au(III) complexes Audien and Aucyclam, and of the ligand phen. (B) Effect of Auphen, phen, Aucyclam and Audien on glycerol permeability (% of control) after 30 min incubation at r.t. (***P<0.001). (C) Dose response curve of Audien ($IC_{50}$ = 16.62±1.61 μM).
doi:10.1371/journal.pone.0037435.g005

the cavities corresponding to the water channels identifying a binding pocket for each side of the protein, namely a periplasmic and a cytoplasmic pocket separated by the selectivity filter (SF) domain (Figure 6) [47].

The SiteMap comparison of periplasmic pockets of AQP1 and AQP3 evidenced the main distinctive features of these protein surfaces. In particular, an extended hydrophobic region was detected in proximity of the SF of AQP3, but not in AQP1, the latter showing a markedly higher hydrophilic character. This result is in agreement with several literature evidences suggesting the different hydrophilic/hydrophobic balance on the periplasmic pocket as the major difference between orthodox aquaporin and

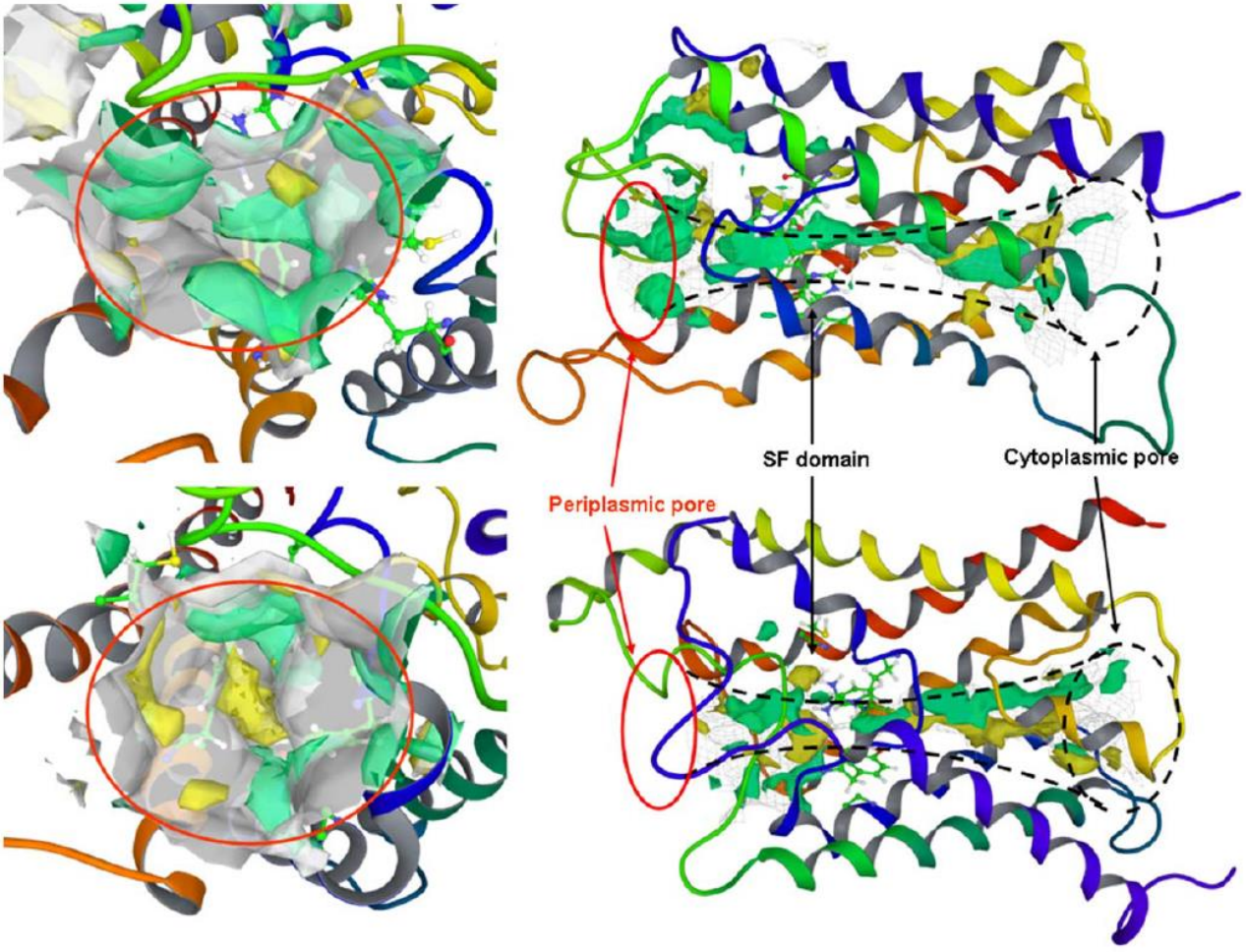


**Figure 6. Identification of protein binding pockets.** Ribbon view of the whole protein channel (left) and periplasmic pocket (right) with molecular surfaces displayed for AQP1 (top) and AQP3 (bottom). Hydrophilic and hydrophobic isosurfaces are also shown in light green and yellow, respectively.
doi:10.1371/journal.pone.0037435.g006

aquaglycerolporin subfamilies, including AQP1 and AQP3, respectively [52].

Afterwards, the position and the chemical environment of the most suitable soft-metal ion protein binding sites, such as cysteine, methionine and histidine side chain residues, was analyzed in detail. First of all, it must be noted that AQP3 is characterized by a higher content of these residues (5 Cys, 5 Met and 6 His) in comparison to AQP1 (4 Cys, 1 Met and 5 His). The mapping of the periplasmic surface provided a valuable assessment of these possible gold-binding sites location and exposure on both aquaporin isoforms. In AQP1, Cys189 and His180 resulted to be the only residues proximal to the periplasmic pore, therefore, directly accessible to gold complexes. However, the exposure of these residues is quite scarce and, being part of the SF domain, they are located in the narrowest section of the membrane filter, which can be easily approached only by small molecules. Moreover, being the size filter function a conserved property of SF [47], the transition to a "more open" conformation with enhanced exposure of Cys189 and His180 is very unlikely.

On the other hand, AQP3 is characterized by the presence of a MxxC motif located on the H1 domain, close enough to the periplasmic pocket to be potentially targeted by metal complexes. In this homology model, while Met37 is projected toward the outer space of the protein (quite far from the pore surface and probably in close contact with the membrane phospholipidic layer), the thiol group of Cys40 is projected toward the periplasmic space approaching the channel pore (Figure 7). The proximity of Cys40 to the SF domain is further indicated by the partial burying of this residue's side chain by the guanidine moiety of Arg218. Thus, among the possible gold binding sites available on AQP3, the side chain of Cys40 is the most favorable, being very close to the SF domain and in the right orientation.

## Docking study of the non-covalent adducts of Au complexes with AQP1 and AQP3

Although the Auphen and Audien inhibition is essentially irreversible, a preliminary docking calculation has been carried out to evaluate the accessibility of the proposed cysteine binding side of AQP1 and AQP3, trying to identify non-covalent binding poses and possible steric crashes. Thus, we considered the same species assumed in the DFT calculations, *i.e.* Auphen and Audien and their monohydroxo derivatives, and through the calculation of the docking poses and their corresponding scoring we made a preliminary estimation of both the affinity and accessibility of these metal complexes to the targeted pores. In particular, the molecular geometries of the Au(III) complexes obtained at DFT level of theory were rigidly docked into the periplasmic pocket of both AQP1 and AQP3 by using the Glide algorithm. The results of docking studies are summarized in Table S2, and the most representative calculated poses are depicted in Figure 8. In general, docking calculations showed that the non-covalent interaction of both Au(III) complexes is favored in the periplasmic pocket of both AQP1 and AQP3. On the other hand, the interaction of both Au(III) complexes with AQP3 is slightly stronger as indicated by both the scoring of top ranked poses and average score values (Table S2). Additionally, the analysis of the docking poses indicated the AQP3 periplasmic pocket as the most sterically accessible to the interaction of the considered Au(III) complexes. Indeed, as shown in Figure 8, the top ranked poses of both Au(III) complexes approached closer to the SF domain when docked at AQP3, thus favoring the binding of these species at a protein site closer to the constriction pore.

It is also worth noting that the Cys40 thiol group in AQP3 is in proximity (9 10 Å) and well-oriented with respect to the gold

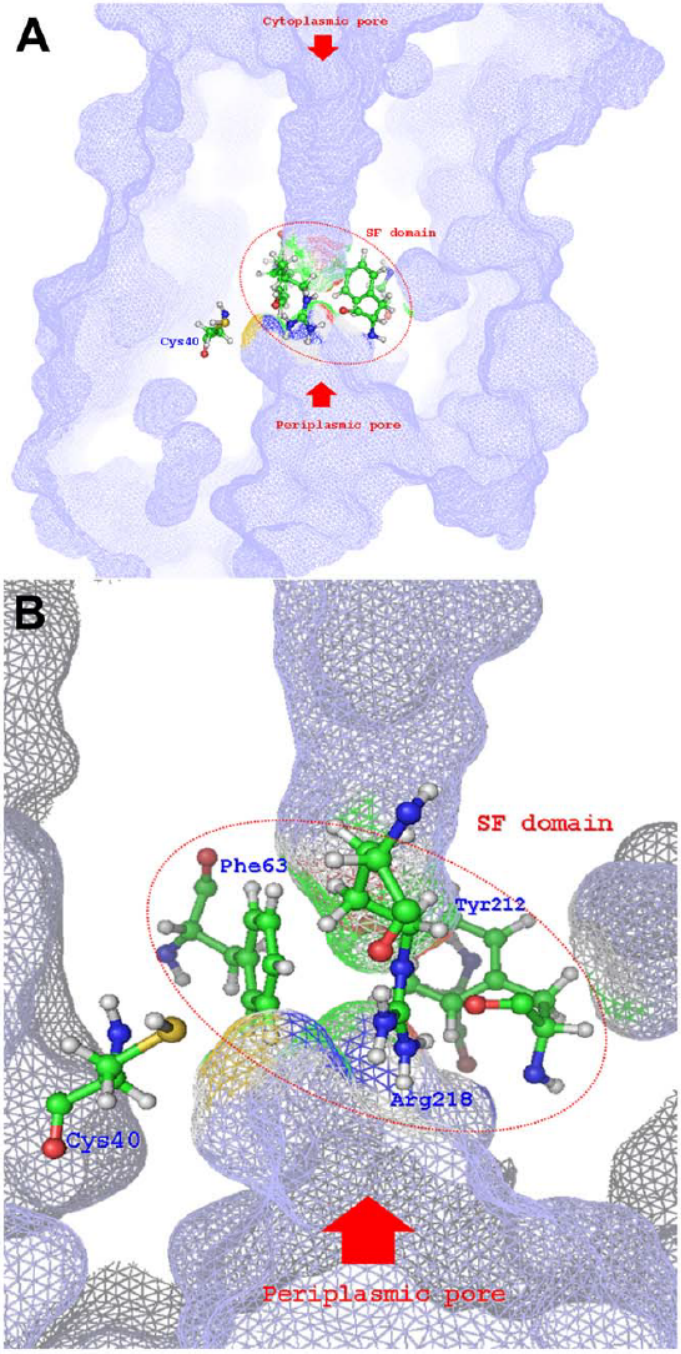


**Figure 7. Molecular surface of AQP3 periplasmic pocket.** (A) SF domain residues together with Cys40 side chain are displayed. (B) Colour scheme representing the contributor atoms to the molecular surface is also shown.
doi:10.1371/journal.pone.0037435.g007

centre of top ranked poses (Figure 8), thus confirming to be a suitable metal binding site upon minimal adaptation of the protein structure. On the other hand, the side chains of Cys189 and His180, the only two possible metal sites at AQP1, are more distant from the gold ion (12 14 Å) and not favorably oriented to be easily bound by Auphen and Audien.

## Discussion

While AQP1 is a selective water channel, AQP3 permeates both water and glycerol on human erythrocytes. In spite of being also a water-transporting channel [35,36] its contribution to the total

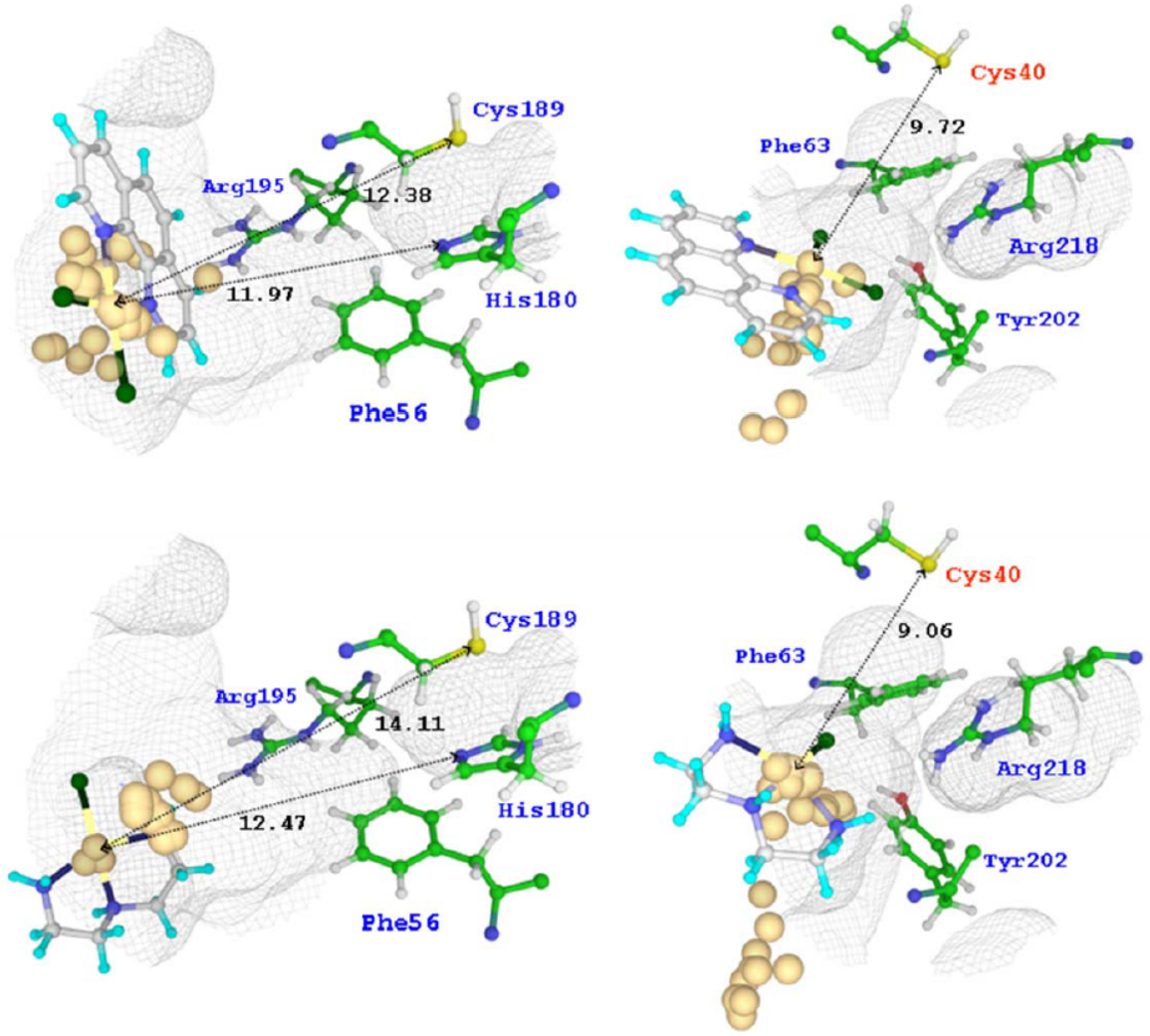


**Figure 8. Docking of Auphen and Audien on AQP1 and AQP3.** Top ranked poses of Auphen (top) and Audien (bottom) at periplasmic pocket of AQP1 (left) and AQP3 (right). Positions of metal centre for the other calculated poses are also displayed in golden yellow. SF domain residues are labelled in blue. Au–S and Au–N distances are reported in Å.
doi:10.1371/journal.pone.0037435.g008

bulk of water flow through hRBC membranes is minimal compared to AQP1 [32]. Conversely, AQP3 has been shown to mediate most of the glycerol movements across RBCs membranes [32,34]. In addition to its expression in hRBCs, AQP3 has a wide tissue distribution in the epithelial cells of kidney, airways and skin, suggesting a role in water reabsorption, mucosal secretions, skin hydration and cell volume regulation [53]. Moreover, a recent study reported an aberrant AQP3 expression in melanoma and proved that it significantly increases chemoresistance to arsenite treatment [7].

In the present study we report on the screening of different known metallodrugs, with various therapeutic applications, for the inhibition of AQP1 and AQP3. Thus, the potent and selective inhibition of the glycerol permeability through AQP3 in hRBC by water soluble gold(III) complexes, namely Auphen and Audien, was observed, while the other metal complexes were completely ineffective as AQPs inhibitors. Both the effective compounds are tetracoordinated gold(III) complexes with square planar geometry in which the Au(III) oxidation state, at variance with the case of $NaAuCl_4$, is stabilized by the presence of nitrogens on the phenantroline and diethylentriamine ligands. Auphen and Audien resulted to inhibit glycerol transport in hRBC with an $IC_{50} = 0.8 \pm 0.08$ μM and $IC_{50} = 16.6 \pm 1.6$ μM, respectively, while having only a modest inhibitory effect on water permeability. Moreover, the gold(III) compounds also resulted to be ineffective as inhibitor of urea transport on hRBC.

The observed increase in the $E_a$ for glycerol transport in hRBC with no concomitant $E_a$ change for water transport upon treatment with Auphen, points to a potent blockage of the AQP3 channel with a much lower effect on AQP1. A similar effect has already been reported in the case of $Cu^{2+}$ and $Ni^{2+}$ ions, which were shown to inhibit selectively AQP3 in transfected human cell lines, although at higher concentrations in the mM range [54,55]. Notably, the Au(III) compounds are also much more effective on AQP3 than the non-specific inhibitor of aquaporins $HgCl_2$, and most importantly they are not toxic for the cells in the entire range of investigated concentrations as suggested by the absence of hemolysis and by the recovery of activity after treatment with EtSH.

The specificity of Auphen towards AQP3 was further confirmed by assessing glycerol transport on PC12 cell lines transfected with either AQP1 or AQP3 from rat. The marked inhibitory effect of the compound for the PC12-AQP3 cell clone denotes its higher affinity for AQP3 residues.

The time-dependent inhibition of AQP3 by Auphen is in accordance with the typical reactivity pattern of this gold(III)

complex in aqueous solution. It is worth mentioning that, as commonly found for several other metallodrugs, gold(III) compounds behave as *"prodrugs"* [56]. In other words, their adducts with biomolecular targets are often the result of a specific chemical transformation (e.g. ligand substitution, redox processes, hydrolysis) of the compounds. In the case of Auphen, AQP3 binding is most likely achieved through substitution of at least one halide ligand from the tetracoordinated gold(III) chromophore $AuN_2Cl_2$ [28]. Similarly, Audien can bind AQP3 after replacement of the unique chloride ligand, but slightly less efficiently than Auphen as demonstrated by its higher $IC_{50}$ value. Conversely, the chemically stable Au(III) complex Aucyclam shows lack of inhibition properties supporting the hypothesis that the gold centre is essential for inhibition and most likely is involved in protein binding.

The mechanism of gold inhibition is probably due to the ability of Au(III) to interact with sulphydryl groups of proteins such as the thiolate of cysteine. This hypothesis is partly confirmed by the almost complete recovery of AQP3 activity upon treatment of hRBC with EtSH. However, other modes of Auphen binding might also occur (e.g. with histidine groups). In order to shed light on the putative binding modes of gold complexes to AQPs we used DFT analysis. Thus, DFT calculations on the reactions of Auphen and Audien with model side chain residues indicated the thiolate form of Cys as the most favorable binding site for Au(III) complexes both in the intact or mono-hydroxo species.

To further investigate the mechanisms of AQP inhibition by gold compounds at a molecular level, we undertook molecular modeling studies. Initially, a homology model of human AQP3 was built and compared to the structure of human AQP1 via molecular modeling SiteMap analysis, allowing the identification and characterization of protein binding pockets. Our model confirmed the well-established presence of an extended hydrophobic area in the periplasmic region of AQP3, while a marked hydrophilic character was evidenced in the same region of AQP1. This important difference might account for a higher binding affinity of the Auphen complex for AQP3 with respect to Audien, resulting in higher inhibition potency, being the phenantroline ligand likely to establish hydrophobic interactions at the entrance of the glyceroporin channel. Most importantly, the mapping of the periplasmic surface allowed establishing the possible gold binding sites and their exposure on both aquaporin isoforms. In AQP1 none of the cysteine, methionine or histidine residues appear to be accessible for gold binding, including Cys189 previously reported to be the binding site of mercurial AQP inhibitors [42]. Conversely, in AQP3 the thiol group of Cys40 is projected towards the periplasmic space approaching the channel pore and, therefore, it is proposed here as a likely candidate for binding to gold(III) complexes.

The investigation of non-covalent binding of Auphen and Audien and their monohydroxo species at AQP1 and AQP3 by docking approaches allowed to ascertain the possibility for the gold complexes to reach the SF domain of AQP3 in closer proximity with respect to AQP1, therefore allowing the compounds to bind at protein sites closer to the constriction pore of the aquaglyceroporin such as the side chain of Cys40. Indeed, it is known that the AQP1 channel cross-section size is the major determinant of selectivity for larger amphipathic molecules such as glycerol [47]. Thus, the same steric restrictions which account for the poor glycerol permeation by pure water channels with respect to aquaglyceroporins, might also apply to gold(III) complexes. In addition, the analysis of docking scores evidenced a slightly higher affinity of the two compounds for the AQP3 periplasmatic pore, characterized by a higher extent of hydrophobic sites with respect to AQP1. The highest docking scores for the approach of Auphen at the targeted periplasmic pore, together with the strongest binding of Auphen to Cys shown by our DFT calculations, can explain the slightly higher inhibitory potency demonstrated by Auphen.

Interestingly, both Auphen and Audien have been previously reported to possess anticancer properties *in vitro* [28,29]. Indeed, in recent years several gold(III) compounds have shown promising anticancer effects related to the inhibition of different protein targets, such as the proteasome and specific zinc finger proteins [57,58,59,60]. In this context, we cannot exclude that inhibition of AQP3 might influence the biological effects of the compounds towards cancer cells, although other studies need to be performed to validate such a hypothesis.

In conclusion, metal compounds, in particular mercurial salts, have already been reported as inhibitors of AQPs, but have major drawbacks such as poor selectivity and extreme toxicity, which hamper their development as therapeutic agents. We described here the selective and potent inhibitory effect (in the nanomolar range) of two Au(III) complexes bearing nitrogen donor ligands on AQP3, which together with their limited toxicity and high water solubility makes them suitable candidates for future *in vivo* studies. These results may present novel metal-based scaffolds for AQP drug development.

## Methods

### Chemistry

Gold compounds and NAMI-A were prepared according to literature procedures (see references throughout the text). The purity of the compounds was confirmed by elemental analysis, and all of them showed purity greater than 98%. Cisplatin, silver sulfadiazine, aurothioglucose and 2-Mercaptoethanol were from Sigma.

### Ethics Statement

Venous blood samples were obtained from healthy human volunteers following a protocol approved by the Ethics Committee of the Faculty of Pharmacy of the University of Lisbon. Informed written consent was obtained from all participants. Rat adrenal medulla pheochromocytoma cells (PC12) were kindly provided by Dr. M. Eschevarria, Virgen del Rocio University Hospital, Seville [33].

### Erythrocyte sampling and preparation

Venous blood samples, collected in citrate anticoagulant (2.7% citric acid, 4.5% trisodium citrate and 2% glucose). Fresh blood was centrifuged at 750×*g* for 5 min at 4°C and plasma and buffy coat were discarded. Packed erythrocytes were washed three times in PBS (KCl 2.7 mM, $KH_2PO_4$ 1.76 mM, $Na_2HPO_4$ 10.1 mM, NaCl 137 mM, pH 7.4), diluted to 0.5% haematocrit and immediately used for experiments [34].

### Cell Culture and Transfections

To obtain stable clones of PC12 (cell line derived from a pheochromocytoma of rat adrenal medulla) that overexpress either rat AQP1 or rat AQP3, twenty micrograms of pcDNA3-AQP1 or pcDNA3-AQP3 were transfected into wild type PC12 by electroporation. After selection with geneticin sulphate (GIBCO) 40 clones were analyzed for levels of expression of either AQP1 or AQP3. Out of 20 positive clones with variable levels of AQPs expression, for each AQP those with higher expression were selected. PC12 cells were cultured in Dulbecco's modified Eagle's medium (Invitrogen) supplemented with 5% foetal bovine serum,

10% horse serum, and 1% penicillin/streptomycin (Invitrogen) in a $CO_2$ (10%) incubator at 37°C. Geneticin at 0.2 mg/ml was added to culture AQP-overexpressing clones. Levels of AQP overexpression were determined by Northern blot analysis and expressed relative to wild type PC12. RNA analysis and functional characterization of these clones have been described in detail previously [43].

## Cell volume measurements

hRBC mean volume in isotonic solution was determined using a CASY-1 Cell Counter (Schärfe System GmbH, Reutlingen, Germany) and was calculated as 82 fL. Equilibrium volumes of PC12 cells were obtained by phase contrast microscopy on an inverted microscope (Axiovert Zeiss 100M) equipped with a digital camera.

Plated cells were dislodged by mechanical aspiration with pipette, washed and re-suspended in PBS. For each measured set of data, an aliquot of cell suspension was placed on a microscope slide and an average of 6 pictures with 4 6 cells each were taken and analyzed using NIH ImageJ software. Cells were assumed to have a spherical shape with a diameter calculated as the average of the maximum and minimum dimensions of each cell. Calculated volumes were 1076±123 $\mu m^3$ for all the clones measured.

## Stopped-flow light scattering experiments

Stopped-flow experiments were performed on a HI-TECH Scientific PQ/SF-53 apparatus, with 2 ms dead time, temperature controlled and interfaced with a microcomputer. Experiments were performed at 23°C for glycerol permeability and at 10°C for water and urea permeability; for activation energy measurements temperatures were ranged from 10°C to 37°C. For each experimental condition, 5 7 replicates were analyzed. For measuring the osmotic water permeability ($P_f$), 100 µL of a suspension of fresh erythrocytes (0.5%) or PC12 cells ($1.5\times10^3$ to $3.5\times10^3$ cells/$mm^3$) was mixed with an equal volume of PBS containing 200 mM sucrose as a non-permeable osmolyte to produce a 100 mM inwardly directed sucrose gradient [34]. The kinetics of cell shrinkage was measured from the time course of 90° scattered light intensity at 400 nm until a stable light scatter signal was attained.

$Pf$ was estimated by $Pf = k\,(V_o/A)(1/V_w(osm_{out})_\infty)$, where $V_w$ is the molar volume of water, $V_o/A$ is the initial cell volume to area ratio and $(osm_{out})_\infty$ is the final medium osmolarity after the applied osmotic gradient and $k$ is the single exponential time constant fitted to the light scattering signal of erythrocyte shrinkage. For PC12 cells, a double exponential function was used instead and the weighted averaged rate constant $k_{de} = (\Delta I_1 k_1 + \Delta I_2 k_2)/(\Delta I_1 + \Delta I_2)$, where $\Delta I_1$ and $\Delta I_2$ correspond to the signal changes with either a slow rate constant $k_1$ or a fast one $k_2$, was alternatively used to calculate $P_f$ [61].

For glycerol permeability ($P_{gly}$), 100 µL of erythrocyte or PC12 cell suspension was mixed with an equal volume of hyperosmotic PBS containing 200 mM glycerol creating a 100 mM inwardly directed glycerol gradient. After the first fast cell shrinkage due to water outflow, glycerol influx in response to its chemical gradient was followed by water influx with subsequent cell reswelling. $P_{gly}$ was calculated as $Pgly = k\,(V_o/A)$, where $k$ is the single exponential time constant fitted to the light scattering signal of glycerol influx in erythrocytes [34]. The same protocol was performed for urea permeability, but using instead a hyperosmotic PBS solution containing 200 mM urea. For PC12 cells, the rate of re-swelling due to glycerol influx was measured as the slope of a linear regression fit.

For inhibition experiments cells were incubated with different concentrations of complexes, from freshly prepared stock aqueous solutions, for various times at room temperature before stopped-flow experiments. A time dependent inhibition assay for Auphen over several hours incubation with hRBC and PC12 cells showed no further increase of inhibition after 30 min at r.t. A similar time dependent inhibition assay was performed for all the compounds up to 4 hours incubation at r.t. except for the highly toxic $HgCl_2$ (10 min, r.t.). The inhibitor concentration necessary to achieve 50% inhibition ($IC_{50}$) was calculated by nonlinear regression of dose-response curves (Graph Pad Prism, Inc) to the equation: $y = y_{min} + (y_{max} - y_{min})/(1 + 10^{((LogIC50 - [Inh])\ H)})$, where y is the percentage inhibition obtained for each concentration of inhibitor [Inh] and H is the Hill slope. The activation energy ($E_a$) of water and glycerol transport was calculated from the slope of the Arrhenius plot ($\ln P_f$ or $\ln P_{gly}$ as a function of $1/T$) multiplied by the gas constant $R$. All solution osmolarities were determined from freezing point depression on a semi-micro osmometer (Knauer GmbH, Berlin, Germany) using standards of 100 and 400 mOsM.

## Statistic analysis

Data were presented as mean ± standard error of the mean (SEM) of at least four independent experiments, and were analyzed with either the paired Student's t-test or one-way analysis of variance (ANOVA) followed by Tukey's test. A value of $P \leq 0.01$ was considered to be statistically significant.

## QM calculations

The structures of Au(III) complexes, i.e. Auphen and Audien, and their respective hydrolyzed forms were investigated at DFT level of theory with the B3LYP hybrid functional [62,63], which is known to give good descriptions of transition metal-containing compounds [64,65]. The core electrons of the chloride and metal atoms were described with the Hay and Wadt core-valence relativistic effective core-potential (ECP) leaving the outer electrons to be treated explicitly through the basis set denoted as LACV3P* in Jaguar [66], while for the remaining atoms the 6-311G** basis set was used [67]. Each structure was optimized in the gas phase ($\varepsilon = 0$) and frequency calculations were performed to verify the correct nature of the stationary points and to estimate zero point energy (ZPE) and vibrational entropy corrections at room temperature. Single point energies of all stationary points were calculated by using the larger 6-311++G** set for the main group elements, and the LACV3P++** set for the metal and the chloride atoms. The Poisson-Boltzmann (PB) continuum solvent method was employed to simulate $\varepsilon > 0$ environments, namely a low-polarity medium resembling the inner protein with $\varepsilon = 4$ and an aqueous medium with $\varepsilon = 80$ [68].

The thermodynamics of Auphen and Audien aquation (I) and acidity of the corresponding aquo (II) and methanethiol (III) complexes was investigated by means of the thermodynamic cycles depicted in Figure S2. The reaction free energy for the exchange processes involving metallodrug species was first calculated at DFT level of theory while the free energy values for the processes of interest, i.e. $\Delta G^\circ_{\mathrm{I}}$, $\Delta G^\circ_{\mathrm{II}}$ and $\Delta G^\circ_{\mathrm{III}}$, were obtained as reported in Figure S2. The $\Delta G^\circ$ values obtained by this indirect procedure are expectedly subjected to less approximations than those calculated for the respective direct processes because the inclusion of empirical parameters such as the solvation energy of proton and chloride ion, characterized by large and negative values (and thus affected by larger approximation), is avoided. The corresponding values of $pK_a$ for the acidic dissociation reaction II and III were calculated by the equation $pK_a = \Delta G^\circ_{rea}/2.303\,RT$, where $R$ is the ideal gas constant and $T$ is 298.15 K.

The Jaguar 7.7 quantum chemistry package was used for all calculations [69].

### Molecular modeling

The crystal structure of AQP1 was downloaded from the PDB archive (entry code 1H6I) [70] and processed in the Maestro environment [71]. Thus, the pdb structure of AQP1 underwent the Protein Preparation workflow to remove water and other co-crystallized molecules, to assign the most plausible formal charge to the ionisable protein residues and to eventually add hydrogen atoms. After these steps, the protein structure was relaxed in a OPLS2001 [72,73] force field through a conjugate-gradient minimization algorithm and a gradient-based convergence threshold of 0.3 kJ $mol^{-1}$ $Å^{-1}$, allowing to preserve the main features of the parent crystal conformation in the final structure of AQP1.

The 3D structure of AQP3, not yet resolved, was obtained by homology modeling on accessible web-servers as follow. Initially, possible AQP3 homologues were searched using the HHmod web-server [74,75]. Among the top ranked homologues 1LDA and 1LDF [46] were selected as templates for subsequent homology modeling on the above cited web-servers. However, the homology models obtained by 1LDF as template were either incomplete or presenting structural misfolding, so that only the three models generated by 1LDA were considered afterwards, namely hmod1, hmod2 and hmod3 from Swiss-Model, Phyre, and ESyPred, respectively.

The three homology models were subjected to a Protein Preparation procedure by the same treatment employed for AQP1 (see above). After this step, the structures of AQP1 and hmod1-3 were superimposed in the Maestro workspace by using the protein alignment tool and then processed by the SiteMap module [76]. This tool adopts a grid-based procedure to map the space surrounding the protein structure by employing volumetric, electrostatic and hydrophobic probes. By the identification and characterization of protein cavities, SiteMap is able to retrace the possible binding pockets from a protein structure. The molecular surface, the hydrophobic and hydrophilic isosurfaces of each identified site are measured and used to calculate the corresponding site score.

The SiteMap calculation on AQP1 was performed by essentially using the default parameters with the exception of the mapping resolution set to 0.3 to gain the maximum mapping accuracy.

Docking calculations were carried out with Glide 3.5 that makes use of a series of hierarchical filters to calculate the ligand binding poses in the active-site region of the target [77]. The periplasmic pore of AQP1 and AQP3 was selected as docking active region through a 30×30×30 grid centered on to the center of mass of SF domain residues for each protein structure, namely residues 56, 180 189 and 195 for AQP1 and residues 63, 203 212 and 218 for AQP3. The positional space of Au(III) complexes was instead limited to a 15×15×15 box centered as already mentioned; these settings are default for grid calculation with Glide3.5 [77]. Docking was performed using the standard parameters set-up for rigid docking in which only the roto-translational degrees of freedom were explored and metal complexes kept the corresponding DFT geometry. The evaluation of binding pose quality was performed in terms of GlideScore as function of ligand-target molecular mechanics interaction energy and ligand strain energy. A maximum of 30 docking poses per metal complex were searched in each docking run.

## Supporting Information

**Figure S1** Arrhenius plots showing the water and glycerol permeability of hRBS, in the absence (control) or presence of 5 μM Auphen (30 min incubation at r.t. previous to permeability measurements). Activation energy ($E_a$) values for water transport were not affected by Auphen treatment (3.9±0.4 kcal $mol^{-1}$ for control and 4.1±1.0 kcal $mol^{-1}$ for Auphen treated hRBCs). The $E_a$ for glycerol permeation increased ca. 54% when Auphen was present (8.5±0.8 to 13.2±1.1 kcal $mol^{-1}$).
(TIF)

**Figure S2** Reaction of Au(III) complexes with soft-metal protein sites investigated at DFT level of theory.
(TIF)

**Figure S3** Two-step formation of the Au thiolate adduct between Auphen and Cys side chain.
(TIF)

**Figure S4** Calculation of reaction free energies in water for the I) aquation of Audien (X = $NH_2$) and Auphen (X = Cl), II) acidic dissociation of their respective aquo forms and III) acidic dissociation of corresponding thiol adducts, and the corresponding *pKa* values of the two latter processes. All free energy values were reported in kJ $mol^{-1}$. Values of $K_{hyd}^{Pt}$ and $K_{a1}^{Pt}$, referred to the cisplatin first hydrolysis and to the acidity of the corresponding monaquo form, respectively, were taken from B. Lippert, "Cisplatin" 1999, Wiley-VCH, Weinheim, Germany, pp 184, 186.
(TIF)

**Table S1** Calculated enthalpies and free energies for the reaction of Auphen and Audien with soft-metal protein sites in different polarity media. All values are in kJ $mol^{-1}$.
(DOC)

**Table S2** Docking score of Auphen and Audien at periplasmic pocket of AQP1 and AQP3.
(DOC)

**Dataset S1** Calculated homology modelling structures (pdb format) of AQP3. Available at http://www.ff.ul.pt/fct/dataset_s1.pdf.
(PDF)

## Author Contributions

Conceived and designed the experiments: GS A. Casini. Performed the experiments: APM AM A. Ciancetta AGC GS. Analyzed the data: ME TFM GS A. Casini NR. Contributed reagents/materials/analysis tools: GS A. Casini ME NR. Wrote the paper: GS A. Casini NR.

## References


1. Carbrey JM, Agre P (2009) Discovery of the aquaporins and development of the field. In: Beitz E, ed. Handb Exp Pharmacol: Springer. pp 3 28.
2. Takata K, Matsuzaki T, Tajika Y (2004) Aquaporins: water channel proteins of the cell membrane. Prog Histochem Cytochem 39: 1 83.
3. Verkman AS (2011) Aquaporins at a glance. J Cell Sci 124: 2107 2112.
4. Ishibashi K, Kondo S, Hara S, Morishita Y (2011) The evolutionary aspects of aquaporin family. Am J Physiol Regul Integr Comp Physiol 300: R566 576.
5. Verkman AS (2009) Knock-out models reveal new aquaporin functions. In: Beitz E, ed. Handb Exp Pharmacol 2008/12/20 ed: Spinger. pp 359 381.
6. Hara-Chikuma M, Verkman AS (2008) Prevention of skin tumorigenesis and impairment of epidermal cell proliferation by targeted aquaporin-3 gene disruption. Mol Cell Biol 28: 326 332.
7. Gao L, Gao Y, Li X, Howell P, Kumar R, et al. (2011) Aquaporins mediate the chemoresistance of human melanoma cells to arsenite. Mol Oncol.

8. Preston GM, Jung JS, Guggino WB, Agre P (1993) The mercury-sensitive residue at cysteine 189 in the CHIP28 water channel. J Biol Chem 268: 17 20.
9. Niemietz CM, Tyerman SD (2002) New potent inhibitors of aquaporins: silver and gold compounds inhibit aquaporins of plant and human origin. FEBS Lett 531: 443 447.
10. Brooks HL, Regan JW, Yool AJ (2000) Inhibition of Aquaporin-1 Water Permeability by Tetraethylammonium: Involvement of the Loop E Pore Region. Mol Pharmacol 57: 1021 1026.
11. Ma B, Xiang Y, Mu SM, Li T, Yu HM, et al. (2004) Effects of acetazolamide and anordiol on osmotic water permeability in AQP1-cRNA injected Xenopus oocytel. Acta Pharmacol Sin 25: 90 97.
12. Vanhoek AN, Vanos CH (1990) Inhibition of water channels in isolated rat renal cortical plasma-membranes by dimethylsulfoxide and mercuric sulfhydryl-reagents. J Physiol-London 420: P142 P142.
13. Sogaard R, Zeuthen T (2008) Test of blockers of AQP1 water permeability by a high-resolution method: no effects of tetraethylammonium ions or acetazolamide. Pflug Arch Eur J Phy 456: 285 292.
14. Yang B, Kim JK, Verkman AS (2006) Comparative efficacy of HgCl2 with candidate aquaporin-1 inhibitors DMSO, gold, TEA+ and acetazolamide. FEBS Lett 580: 6679 6684.
15. Tanimura Y, Hiroaki Y, Fujiyoshi Y (2009) Acetazolamide reversibly inhibits water conduction by aquaporin-4. J Struct Biol 166: 16 21.
16. Huber VJ, Tsujita M, Yamazaki M, Sakimura K, Nakada T (2007) Identification of arylsulfonamides as Aquaporin 4 inhibitors. Bioorg Med Chem Lett 17: 1270 1273.
17. Yang BX, Zhang H, Verkman AS (2008) Lack of aquaporin-4 water transport inhibition by antiepileptics and arylsulfonamides. Bioorgan Med Chem 16: 7489 7493.
18. Igarashi H, Huber VJ, Tsujita M, Nakada T (2011) Pretreatment with a novel aquaporin 4 inhibitor, TGN-020, significantly reduces ischemic cerebral edema. Neurol Sci 32: 113 116.
19. Nakamura Y, Suzuki Y, Tsujita M, Huber VJ, Yamada K, et al. (2011) Development of a novel ligand, [C]TGN-020, for Aquaporin 4 positron emission tomography imaging. ACS Chem Neurosci 2: 568 571.
20. Migliati E, Meurice N, DuBois P, Fang JS, Somasekharan S, et al. (2009) Inhibition of aquaporin-1 and aquaporin-4 water permeability by a derivative of the loop diuretic bumetanide acting at an internal pore-occluding binding site. Mol Pharmacol 76: 105 112.
21. Migliati ER, Amiry-Moghaddam M, Froehner SC, Adams ME, Ottersen OP, et al. (2010) Na(+)-K (+)-2Cl (−) cotransport inhibitor attenuates cerebral edema following experimental stroke via the perivascular pool of aquaporin-4. Neurocrit Care 13: 123 131.
22. Jelen S, Wacker S, Aponte-Santamaria C, Skott M, Rojek A, et al. (2011) Aquaporin-9 is the primary route of hepatocyte glycerol uptake for glycerol gluconeogenesis in mice. J Biol Chem.
23. Reedijk J (2003) New clues for platinum antitumor chemistry: kinetically controlled metal binding to DNA. Proc Natl Acad Sci U S A 100: 3611 3616.
24. Bergamo A, Gaiddon C, Schellens JH, Beijnen JH, Sava G (2012) Approaching tumour therapy beyond platinum drugs: status of the art and perspectives of ruthenium drug candidates. J Inorg Biochem 106: 90 99.
25. Tsipouras N, Rix CJ, Brady PH (1995) Solubility of silver sulfadiazine in physiological media and relevance to treatment of thermal burns with silver sulfadiazine cream. Clin Chem 41: 87 91.
26. Messori L, Marcon G (2004) Metal ions and their complexes in medication. Met Ions Biol Syst 41: 2799.
27. Abbate F, Orioli P, Bruni B, Marcon G, Messori L (2000) Crystal structure and solution chemistry of the cytotoxic complex 2,2-dichloro(o-phenantroline)gold(III) chloride. Inorg Chim Acta 311: 1 5.
28. Messori L, Abbate F, Marcon G, Orioli P, Fontani M, et al. (2000) Gold(III) complexes as potential antitumor agents: Solution chemistry and cytotoxic properties of some selected gold(III) compounds. J Med Chem 43: 3541 3548.
29. Casini A, Kelter G, Gabbiani C, Cinellu MA, Minghetti G, et al. (2009) Chemistry, antiproliferative properties, tumor selectivity, and molecular mechanisms of novel gold(III) compounds for cancer treatment: a systematic study. J Biol Inorg Chem 14: 1139 1149.
30. Casini A (2012) Exploring the mechanisms of metal-based pharmacological agents via an integrated approach. J Inorg Biochem 109: 97 106.
31. Denker BM, Smith BL, Kuhajda FP, Agre P (1988) Identification, purification, and partial characterization of a novel Mr 28,000 integral membrane protein from erythrocytes and renal tubules. J Biol Chem 263: 15634 15642.
32. Roudier N, Verbavatz JM, Maurel C, Ripoche P, Tacnet F (1998) Evidence for the presence of aquaporin-3 in human red blood cells. J Biol Chem 273: 8407 8412.
33. Preston GM, Carroll TP, Guggino WB, Agre P (1992) Appearance of water channels in Xenopus oocytes expressing red cell CHIP28 protein. Science 256: 385 387.
34. Campos E, Moura TF, Oliva A, Leandro P, Soveral G (2011) Lack of Aquaporin 3 in bovine erythrocyte membranes correlates with low glycerol permeation. Biochem Biophys Res Commun 408: 477 481.
35. Echevarria M, Windhager EE, Tate SS, Frindt G (1994) Cloning and expression of AQP3, a water channel from the medullary collecting duct of rat kidney. Proc Natl Acad Sci U S A 91: 10997 11001.
36. Ishibashi K, Sasaki S, Fushimi K, Uchida S, Kuwahara M, et al. (1994) Molecular cloning and expression of a member of the aquaporin family with permeability to glycerol and urea in addition to water expressed at the basolateral membrane of kidney collecting duct cells. Proc Natl Acad Sci U S A 91: 6269 6273.
37. Meinild AK, Klaerke DA, Zeuthen T (1998) Bidirectional water fluxes and specificity for small hydrophilic molecules in aquaporins 0 5. J Biol Chem 273: 32446 32451.
38. Rojek A, Praetorius J, Frokiaer J, Nielsen S, Fenton RA (2008) A current view of the mammalian aquaglyceroporins. Annu Rev Physiol 70: 301 327.
39. Bagnasco SM (2006) The erythrocyte urea transporter UT-B. J Membr Biol 212: 133 138.
40. Moura TF, Macey RI, Chien DY, Karan D, Santos H (1984) Thermodynamics of all-or-none water channel closure in red cells. J Membr Biol 81: 105 111.
41. de Groot BL, Grubmuller H (2001) Water permeation across biological membranes: mechanism and dynamics of aquaporin-1 and GlpF. Science 294: 2353 2357.
42. Savage DF, Stroud RM (2007) Structural basis of aquaporin inhibition by mercury. J Mol Biol 368: 607 617.
43. Echevarria M, Munoz-Cabello AM, Sanchez-Silva R, Toledo-Aral JJ, Lopez-Barneo J (2007) Development of cytosolic hypoxia and hypoxia-inducible factor stabilization are facilitated by aquaporin-1 expression. J Biol Chem 282: 30207 30215.
44. Shaw CF (1989) The protein chemistry of anti-arthritic gold (I) thiolates and related complexes. Comment Inorg Chem 8: 233 267.
45. Fu D, Libson A, Miercke LJ, Weitzman C, Nollert P, et al. (2000) Structure of a glycerol-conducting channel and the basis for its selectivity. Science 290: 481 486.
46. Tajkhorshid E, Nollert P, Jensen MO, Miercke LJ, O'Connell J, et al. (2002) Control of the selectivity of the aquaporin water channel family by global orientational tuning. Science 296: 525 530.
47. Savage DF, O'Connell JD, 3rd, Miercke LJ, Finer-Moore J, Stroud RM (2010) Structural context shapes the aquaporin selectivity filter. Proc Natl Acad Sci U S A 107: 17164 17169.
48. Beitz E, Wu BH, Holm LM, Schultz JE, Zeuthen T (2006) Point mutations in the aromatic/arginine region in aquaporin 1 allow passage of urea, glycerol, ammonia, and protons. Proc Natl Acad Sci U S A 103: 269 274.
49. Wu B, Beitz E (2007) Aquaporins with selectivity for unconventional permeants. Cell Mol Life Sci 64: 2413 2421.
50. Hub JS, de Groot BL (2008) Mechanism of selectivity in aquaporins and aquaglyceroporins. Proc Natl Acad Sci U S A 105: 1198 1203.
51. Chen H, Ilan B, Wu Y, Zhu F, Schulten K, et al. (2007) Charge delocalization in proton channels, I: the aquaporin channels and proton blockage. Biophys J 92: 46 60.
52. Park JH, Saier MH, Jr. (1996) Phylogenetic characterization of the MIP family of transmembrane channel proteins. J Membr Biol 153: 171 180.
53. Hara M, Verkman AS (2003) Glycerol replacement corrects defective skin hydration, elasticity, and barrier function in aquaporin-3-deficient mice. Proc Natl Acad Sci U S A 100: 7360 7365.
54. Zelenina M, Bondar AA, Zelenin S, Aperia A (2003) Nickel and extracellular acidification inhibit the water permeability of human aquaporin-3 in lung epithelial cells. J Biol Chem 278: 30037 30043.
55. Zelenina M, Tritto S, Bondar AA, Zelenin S, Aperia A (2004) Copper inhibits the water and glycerol permeability of aquaporin-3. J Biol Chem 279: 51939 51943.
56. Casini A, Hartinger C, Gabbiani C, Mini E, Dyson PJ, et al. (2008) Gold(III) compounds as anticancer agents: Relevance of gold-protein interactions for their mechanism of action. J Inorg Biochem 102: 564 575.
57. Aldinucci D, Lorenzon D, Stefani L, Giovagnini L, Colombatti A, et al. (2007) Antiproliferative and apoptotic effects of two new gold(III) methylsarcosine-dithiocarbamate derivatives on human acute myeloid leukemia cells in vitro. Anticancer Drugs 18: 323 332.
58. Zhang X, Frezza M, Milacic V, Ronconi L, Fan Y, et al. (2010) Inhibition of tumor proteasome activity by gold-dithiocarbamato complexes via both redox-dependent and -independent processes. J Cell Biochem 109: 162 172.
59. Serratrice M, Edafe F, Mendes F, Scopelliti R, Zakeeruddin SM, et al. (2012) Cytotoxic gold compounds: synthesis, biological characterization and investigation of their inhibition properties of the zinc finger protein PARP-1. Dalton Trans 41: 3287 3293.
60. Mendes F, Groessl M, Nazarov AA, Tsybin YO, Sava G, et al. (2011) Metal-based inhibition of poly(ADP-ribose) polymerase the guardian angel of DNA. J Med Chem 54: 2196 2206.
61. van Heeswijk MP, van Os CH (1986) Osmotic water permeabilities of brush border and basolateral membrane vesicles from rat renal cortex and small intestine. J Membr Biol 92: 183 193.
62. Becke AD (1993) Density-functional thermochemistry. III. The role of exact exchange. J Chem Phys 98: 5648 5652.
63. Becke AD (1988) Density-functional exchange-energy approximation with correct asymptotic behavior. Physical Review A 38: 3098 3100.
64. Niu SQ, Hall MB (2000) Theoretical studies of reactions of transition-metal complexes. Chem Rev 100: 353 405.
65. Nielsen RJ, Keith JM, Stoltz BM, Goddard WA, 3rd (2004) A computational model relating structure and reactivity in enantioselective oxidations of secondary alcohols by (-)-sparteine-Pd(II) complexes. J Am Chem Soc 126: 7967 7974.

66. Hay PJ, Wadt WR (1985) Ab initio effective core potentials for molecular calculations - potentials for the transition-metal atoms Sc to Hg. J Chem Phys 82: 299 310.
67. Hariharan P, Pople JA (1972) The effect of d-functions on molecular orbital Chem Phys Lett 16: 217 219.
68. Tannor DJ, Marten B, Murphy R, Friesner RA, Sitkoff D, et al. (1994) Accurate first principles calculation of molecular charge distributions and solvation energies from Ab initio quantum mechanics and continuum dielectic theory. J Am Chem Soc 116: 11875 11882.
69. Schrodinger LLC (2009) Jaguar 7.7, 7.5. New York.
70. de Groot BL, Engel A, Grubmuller H (2001) A refined structure of human aquaporin-1. FEBS Lett 504: 206 211.
71. Schrodinger LLC (2008) Maestro 8.5. New York.
72. Jorgensen WL, Maxwell DS, Tirado-Rives J (1996) Development and testing of the OPLS all-atom force field on conformational energetics and properties of organic liquids. J Am Chem Soc 118: 11225 11236.
73. Kaminski G, Friesner RA, Tirado-Rives J, Jorgensen WL (2001) Evaluation and reparametrization of the OPLS-AA force field for proteins via comparison with accurate quantum chemical calculations on peptides. J Phys Chem B 105: 6474 6487.
74. Soding J (2005) Protein homology detection by HMM-HMM comparison. Bioinformatics 21: 951 960.
75. Soding J, Biegert A, Lupas AN (2005) The HHpred interactive server for protein homology detection and structure prediction. Nucleic Acids Res 33: W244 248.
76. Schrodinger LLC (2008) Sitemap 2.2. New York.
77. Friesner RA, Banks JL, Murphy RB, Halgren TA, Klicic JJ, et al. (2004) Glide: a new approach for rapid, accurate docking and scoring. 1. Method and assessment of docking accuracy. J Med Chem 47: 1739 1749.

CHEMMEDCHEM
FULL PAPERS

ChemPubSoc Europe

DOI: 10.1002/cmdc.201300107

# Aquaporin Inhibition by Gold(III) Compounds: New Insights

Ana Paula Martins,[a, b] Antonella Ciancetta,[c] Andreia de Almeida,[d] Alessandro Marrone,[e] Nazzareno Re,[e] Graça Soveral,*[a, b] and Angela Casini*[d]

Aquaporins (AQPs) are membrane water/glycerol channels with essential roles in biological systems, as well as being promising targets for therapy and imaging. Using a stopped-flow method, a series of gold(III), platinum(II) and copper(II) complexes bearing nitrogen donor ligands, such as 1,10-phenatroline, 2,2′-bipyridine, 4,4′-dimethyl-2,2′-bipyridine, 4,4′-diamino-2,2′-bipyridine and 2,2′;6′,2″-terpyridine, were evaluated in human red blood cells expressing AQP1 and AQP3, responsible for water and glycerol movement, respectively. The results showed that the gold(III) complexes selectively modulate AQP3 over AQP1. Molecular modeling and density functional theory (DFT) calculations were subsequently performed to rationalize the observations and to investigate the possible molecular mechanism through which these gold compounds act on their putative target (AQP3). In the absence of any crystallographic data, a previously reported homology model was used for this purpose. Combined, the findings of this study show that potent and selective modulation of these solute channels is possible, however further investigation is required into the selectivity of this class of agents against all AQP isoforms and their potential therapeutic uses.

## Introduction

Aquaporins (AQPs) belong to a highly conserved group of membrane proteins that are involved in the transport of water and small solutes and that play a variety of important physiological roles. The 13 human AQP isoforms (AQP0–12) are differentially expressed in many types of cells and tissues in the body and can be divided into two major groups: those strictly selective for water (orthodox aquaporins), and those that are also permeable to other small solutes including glycerol (aquaglyceroporins). The aquaglyceroporins include isoforms AQP3, AQP7, AQP9, and AQP10.[1] Phenotype analysis of AQP-null mice and pathophysiological studies have suggested that AQPs are potential drug targets. Indeed, it has recently emerged that AQPs are implicated in various diseases, such as polycystic kidney disease, cataract, brain edema, gallstone disease, and nephrogenic diabetes insipidus, as well as in the development of obesity and cancer.[2] Moreover, analysis of AQP involvement in the life cycle of disease-causing organisms suggests additional opportunities for pharmacological intervention in the treatment of human diseases.[3]

In recent years, agents have been reported that modulate AQP-mediated water flux, including heavy metals,[4–7] quaternary ammonium salts,[8–10] and inorganic salts.[11] While these agents are valuable for gaining insight into the effect of AQP modulation at a cellular level, they are not suitable for therapeutic applications largely due to their toxic side effects and lack of selectivity. In addition, recent reports have described a few organic small-molecule AQP modulators, mainly sulfonamides[12] and some compounds containing carboxylic groups,[13] acting as inhibitors of orthodox water channels. Concerning aquaglyceroporin modulators, a few small-molecule inhibitors of AQP9 glycerol permeability have been reported; however, as their solubility in aqueous solution is very limited, these compounds are currently not suitable for in vivo experiments.[14]

Within this frame, we recently reported the potent and selective inhibition of AQP3 by a water-soluble gold(III) coordination compound, Auphen ([Au(phen)$Cl_2$]Cl, where phen is 1,10-phenatroline; Figure 1). Notably, Auphen inhibited glycerol transport in human red blood cells (hRBC) with an $IC_{50}$ value of $0.80 \pm 0.08$ μM, while only exhibiting a modest inhibitory effect on water permeability mediated by AQP1.[15]

[a] A. P. Martins, Prof. G. Soveral
Research Institute for Medicines & Pharmaceutical Sciences (iMed.UL)
Av. Prof. Gama Pinto, 1649-003 Lisbon (Portugal)
E-mail: gsoveral@ff.ul.pt

[b] A. P. Martins, Prof. G. Soveral
Dept. of Biochemistry & Human Biology
Faculty of Pharmacy, University of Lisbon
Av. das Forças Armadas, 1649-019 (Portugal)

[c] Dr. A. Ciancetta
Molecular Modeling Section (MMS)
Department of Pharmaceutical & Pharmacological Sciences
University of Padova
Via Marzolo 5, 35131 Padova (Italy)

[d] A. de Almeida, Dr. A. Casini
Dept. of Pharmacokinetics, Toxicology & Targeting
Research Institute of Pharmacy, University of Groningen
Antonius Deusinglaan 1, Groningen (The Netherlands)
E-mail: a.casini@rug.nl

[e] Dr. A. Marrone, Prof. N. Re
Department of Pharmaceutical Sciences
G. d'Annunzio University of Chieti-Pescara
Via dei Vestini, 66013 Chieti (Italy)

Supporting information for this article is available on the WWW under http://dx.doi.org/10.1002/cmdc.201300107.

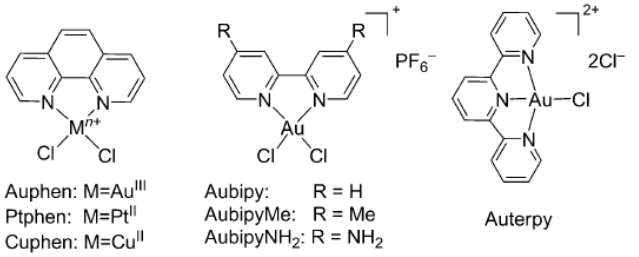


**Figure 1.** Structures of the gold(III) complexes reported in this study.

Inspired by these promising initial results, we investigated other gold-based compounds as possible AQP3 inhibitors in order to elucidate basic structure–activity relationships fundamental for drug design. Thus, we selected a series of square-planar gold(III) complexes containing functionalized bipyridine ligands of the general formula $[Au(N^N)Cl_2][PF_6]$ (Aubipys), where N^N is 2,2′-bipyridine, 4,4′-dimethyl-2,2′-bipyridine, or 4,4′-diamino-2,2′-bipyridine, as well as a compound containing the tetracoordinated gold(III) chromophore $AuN_3Cl$, $[Au(terpy)Cl]Cl_2$ (Auterpy), where terpy represents 2,2′;6′,2″-terpyridine (Figure 1). Moreover, the 1,10-phenantroline derivatives of platinum(II) and copper(II) were also included in our investigation to compare the effects of metal substitution on the AQP3 inhibitory potency. The effects of the compounds on both water and glycerol permeation were tested by stopped-flow spectroscopy on hRBC expressing large amounts of AQP1 and AQP3 accountable for membrane permeability to water and glycerol, respectively.[16] Additionally, density functional theory (DFT) and molecular modeling studies allowed the further characterization of the mechanisms of AQP3 inhibition by gold(III) coordination compounds.

## Results and Discussion

### Aquaporin inhibition studies

The effects of the metal complexes on AQP1 and AQP3 expressed in hRBC were evaluated in comparison to mercury(II) chloride, a benchmark inhibitor of aquaporin activity.[17] The compounds were tested at different concentrations until maximum inhibition was reached (for details, see the Experimental Section).[15] All of the gold(III) compounds tested exhibited a modest effect on water permeability, while drastically decreasing glycerol transport (Figure 2). The obtained results demonstrate that all of the gold(III) complexes are effective inhibitors of glycerol permeability via inhibition of AQP3 activity, with $IC_{50}$ values in the low micromolar range, comparable in potency to Auphen (Table 1). Within the metal–phenantroline series, the AQP3 inhibition potency decreased drastically in the order Auphen > Cuphen ≫ Ptphen (Figure 2, Table 1).

Moreover, the Hill slope (H) values for all compounds were determined to be greater than one (Table 1), suggesting a possible cooperative binding effect. In fact, aquaporin channels are tetrameric proteins in the membrane, with each tetramer formed by four identical monomers, and as such, a total of

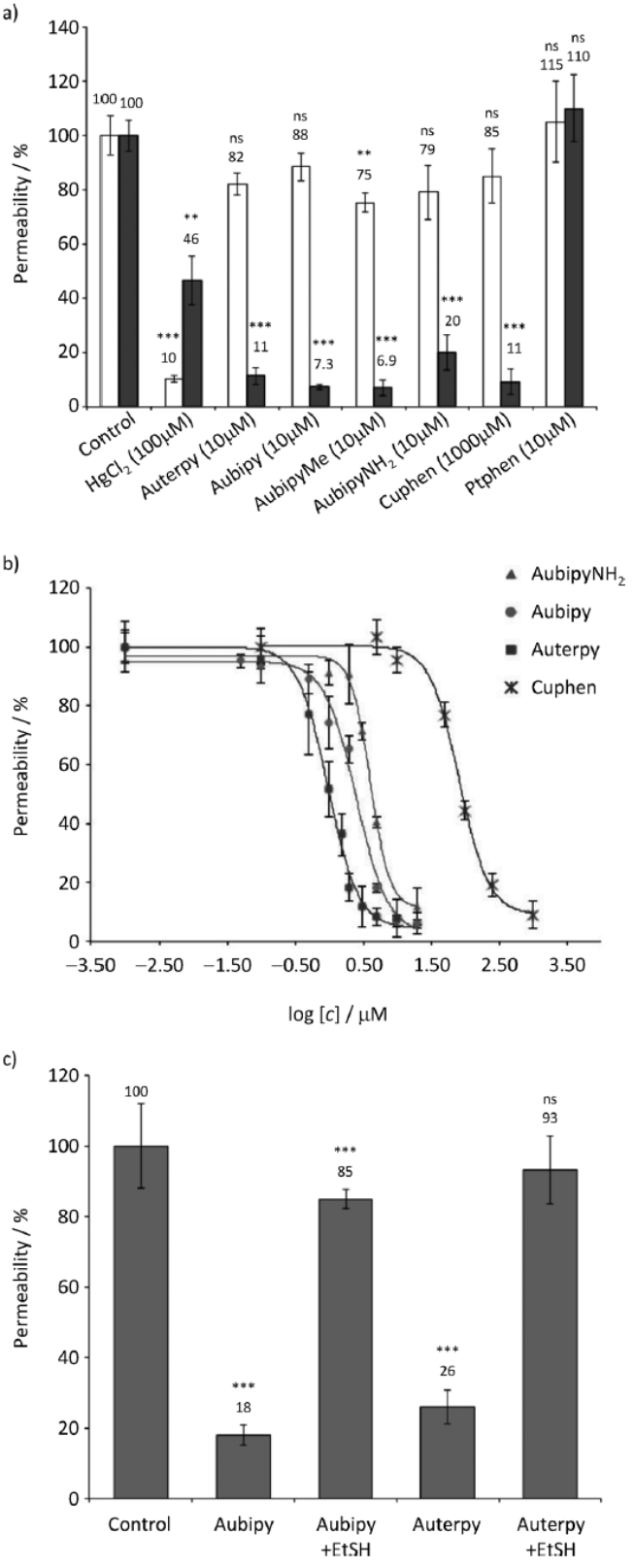


**Figure 2.** a) Inhibition of the osmoti water (AQP1; □) or glycerol (AQP3; ■) permeability in human red blood cells (hRBC) induced by different metal complexes after 30 min incubation at room temperature; b) Concentration-dependent inhibition of glycerol permeability in hRBC by representative metal compounds; c) Inhibition of glycerol permeability of hRBC after Aubipy (2 μM) and Auterpy (5 μM) treatment and incubation for 30 min at room temperature, and reversibility by incubation with 2-mercaptoethanol (1 mM for 30 min). $^{***}P < 0.001$, $^{**}P < 0.01$, ns: not statistically significant; all permeability data are expressed as the percent (%) of control.

**Table 1.** Inhibition of glycerol permeability in human red blood cells (hRBC) by metal complexes.

| Compound | $IC_{50}$[a] [μM] | H[c] |
|---|---|---|
| Aubipy | 2.3 ± 0.7 | 1.86 ± 0.4 |
| AubipyMe | 1.0 ± 0.4 | 1.76 ± 0.6 |
| $AubipyNH_2$ | 2.9 ± 1.1 | 3.08 ± 0.8 |
| Auterpy | 1.0 ± 0.2 | 2.15 ± 0.3 |
| Auphen | 0.8 ± 0.1[b] | 3.9 ± 0.3 |
| Cuphen | 81.9 ± 4.1 | 2.0 ± 0.5 |
| Ptphen | >200 | n.d. |

[a] Data represent the mean ±SE of at least three determinations. [b] Value taken from Ref. [15]. [c] Hill slope (H) values.

four Cys40 residues are available for binding. Thus, the H value for Auphen points to maximal cooperativity and correlates well with its high potency, while for the other gold compounds, with the exception of $AubipyNH_2$ that showed a slightly higher H value, all of the H values were close to two suggesting intermediary cooperativity.

The activation energy ($E_a$) for water and glycerol transport, a valuable parameter indicating the contribution of protein channels to permeation, was also estimated from an Arrhenius plot. Representative results for Auterpy are shown in Figure S1 in the Supporting Information. The observed increase in $E_a$, similar to what was previously observed for Auphen,[15] is in accordance with blockade of the AQP3 channel.

In order to obtain information on the possible binding sites of the gold complexes in AQP3, hRBC pretreated with compounds for 30 min at room temperature were subsequently washed with the reducing agent 2-mercaptoethanol (EtSH) at 1 mM according to established procedures.[18] As observed for Auphen, incubation of the compound-treated hRBC with excess EtSH resulted in almost complete recovery of glycerol permeability (~90%), suggesting that the effect of EtSH on cysteine residues is competing with gold binding to the pore. Representative results for Auterpy and Aubipy are shown in Figure 2c. These results, as well as the known affinity of gold ions for binding to sulfhydryl groups of proteins, suggest that AQP3 inhibition by gold complexes might involve direct protein binding of the gold center to cysteine residues, as it has already been described for mercury(II) chloride.[18]

### DFT calculations and molecular modeling studies

We previously reported a model for the selective inhibition of AQP3 by gold(III) channel blockers, including Auphen.[15] In this model, the metal coordinates to a specific nucleophilic site, namely the side chain of Cys40, which is located at the extracellular side of AQP3 in close proximity to the selectivity filter (SF) region, therefore, inducing the blockage of the channel upon binding (Figure S2 in the Supporting Information). In AQP1, Cys189 is also located in the protein extracellular domain and is part of the SF region, but it is deeply buried in the channel and its thiol group is poorly available for binding to the bulky gold(III) complexes.[15] In fact, our previously reported noncovalent docking studies of Auphen in AQP1 suggest that the side chain of Cys189 is distant from the gold ion (12–14 Å) and not favorably oriented for binding. Conversely, less sterically hindered $Hg^{2+}$ ions have been shown to coordinate to Cys189 in AQP1.[17] In this context, the selective inhibition of AQP3 over AQP1 is mainly related to the lack of possible gold binding sites in the extracellular pocket of AQP1 accessible to such relatively bulky metal complexes.[15]

According to the proposed inhibition mechanism, the electrophilicity of the metal center is expected to play a role in determining the reactivity of the complexes towards AQP3. Therefore, we carried out DFT calculations to characterize the electrophilicity of the considered gold(III), platinum(II) and copper(II) complexes using the perturbative approach in terms of atomic charges and frontier orbitals proposed by Klopman.[19] Mulliken and natural atomic orbital (NAO) population analyses results highlight similar charges on the metal center for all monocationic gold(III) complexes (Table 2). A higher charge is observed on the gold(III) center of Auterpy, as expected for dicationic species, while the metal of neutral Cuphen and Ptphen complexes is almost the same or less positively charged than the gold(III) center of monocationic complexes (Table 2). Thus, charge factors indicate the following order of reactivity towards nucleophiles: Auterpy > Auphen = Aubipy analogues ≥ Ptphen ≥ Cuphen.

**Table 2.** Mulliken and natural atomic orbital (NAO) charges.

| Compound | | $M^{n+}$ | Cl | N |
|---|---|---|---|---|
| Auphen | Mulliken | 0.81 | −0.17 | −0.65 |
| | NAO | 1.09 | −0.35 | −0.49 |
| $Au(bipy)Cl_2$ | Mulliken | 0.81 | −0.16 | −0.66 |
| | NAO | 1.09 | −0.35 | −0.49 |
| $Au(bipyMe)Cl_2$ | Mulliken | 0.81 | −0.17 | −0.67 |
| | NAO | 1.10 | −0.36 | −0.50 |
| $Au(bipyNH_2)Cl_2$ | Mulliken | 0.83 | −0.19 | −0.70 |
| | NAO | 1.10 | −0.37 | −0.53 |
| Auterpy | Mulliken | 1.19 | −0.14 | −0.69, −0.80[a] |
| | NAO | 1.22 | −0.38 | −0.48, −0.49[a] |
| Ptphen | Mulliken | 0.57 | −0.37 | −0.59 |
| | NAO | 0.66 | −0.44 | −0.50 |
| Cuphen | Mulliken | 0.51 | −0.44 | −0.50 |
| | NAO | 1.10 | −0.65 | −0.52 |

[a] The two values reported for Auterpy N refer to the two reciprocal *trans* and the one Cl-*trans* pyridyl nitrogens, respectively.

On the other hand, analysis of frontier orbitals shows similar LUMO energies for all monocationic gold(III) complexes (Figure S3 in the Supporting Information). Auterpy shows a significant lower LUMO energy, whereas Cuphen and Ptphen are characterized by the highest LUMO. Thus, frontier orbital factors suggest an order of reactivity towards nucleophiles substantially inverse to that indicated by charge factors: Cuphen = Ptphen > Auphen = Aubipy analogues > Auterpy. The charge and orbital factors probably compensate for each other in the gold(III) compounds, thus leading to similar reactivity towards cysteine, while the charge factors seems to prevail for the copper(II) and platinum(II) complexes, which are much less

reactive, in agreement with the observed AQP3 inhibition potency (Table 1).

The thermodynamics of the ligand exchange process leading to covalently bound $Au^{III}$–AQP3 adducts were then investigated at DFT level of theory, which has been recently shown to give good results for the reactivity of gold(III) compounds.[20] In particular, the exchange of the Cl⁻ anion by a model of the Cys40 side chain ($CH_3SH$) was analyzed (Scheme 1). As previ-

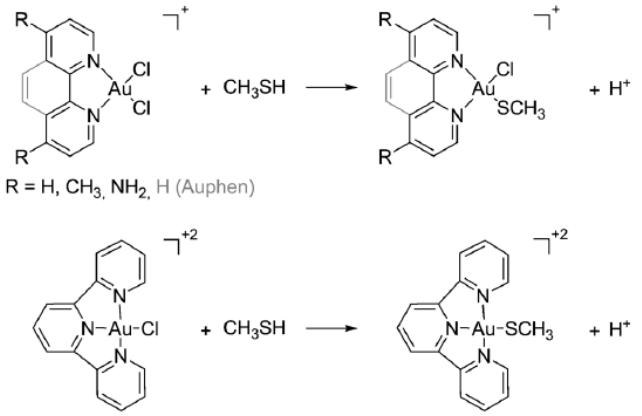


**Scheme 1.** Reaction scheme of the studied gold(III) complexes with the Cys40 side chain model leading to the final gold(III)–thiolate complexes.

ously reported, under physiological conditions (pH 7.4), the cysteine residue ($pK_a = 8.3$) is prevalently, but not exclusively, protonated, and this process can be considered a result of either the initial nucleophilic attack of the neutral cysteine with formation of an $Au^{III}$–thiol complex followed by its facile deprotonation, or the initial cysteine deprotonation followed by attack of the more nucleophilic thiolate anion giving the final $Au^{III}$–thiolate complex. In any case, the whole reaction is thermodynamically favored for all gold(III) complexes studied (Table 3), with binding energies to Cys40 similar to those previ-

**Table 3.** Calculated free energies for the reaction of the investigated gold(III) complexes with the cysteine side chain model.

| Complex | $\Delta G^{tot}$ [kJ mol$^{-1}$] |
|---|---|
| Auphen | −48 |
| Au(bipy)$Cl_2$ | −48 |
| Au(bipyMe)$Cl_2$ | −46 |
| Au(bipyNH2)$Cl_2$ | −35 |
| Auterpy | −36 |

ously calculated for Auphen[15] accounting for the good AQP3 inhibition potency observed for all these cationic gold(III) compounds.

We also considered the initial approach of the various metal complexes to the Cys40 residue in the channel pore from the periplasmatic side and the possible formation of noncovalent adducts with Cys40 itself or other neighboring residues within the active site. To this purpose, quantum mechanics/molecular mechanics (QM/MM) calculations at DFT level of theory were performed by using the previously proposed AQP3 homology model,[15] and by optimizing several possible initial poses of the complexes in the extracellular pocket around the Cys40 residue. The calculated most stable binding mode of AubipyMe at the AQP3 extracellular binding pocket is shown in Figure 3a. In this predicted binding pose, the complex lies per-

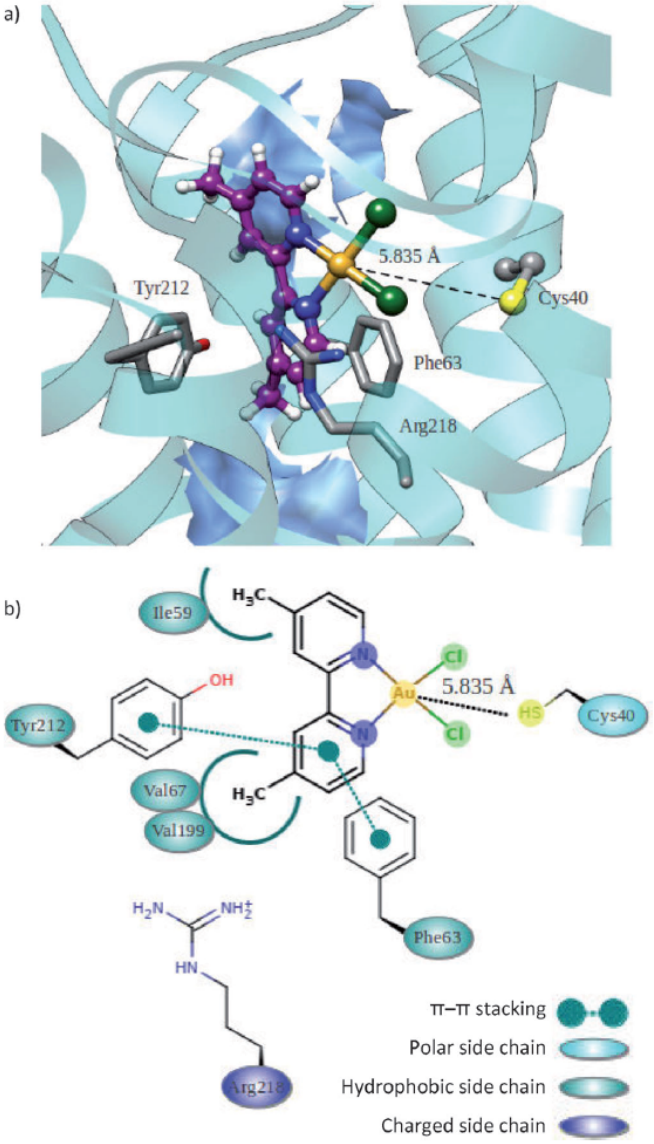


**Figure 3.** a) Hypothetical binding mode of AubipyMe in the AQP3 periplasmic pocket. The gold(III) complex and Cys40 side chain are shown in ball and sticks. Side chains of the SF domain residues are shown as grey sticks. Residues interacting with the ligand through hydrophobic contacts are displayed as surfaces. c) Interaction model of AubipyMe within the AQP3 extracellular pocket.

pendicular to the membrane plane, and the Au–S(Cys40) distance is calculated to be around 5.8 Å. As detailed in the interaction diagram (Figure 3b), in this predicted binding pose, the compound establishes π–π stacking interactions with Tyr212 and Phe63, two of the residues representing the arginine–aromatic (ar/R) constriction (SF, selectivity filter region) typical of

AQPs.[21] Along with π–π interactions, the gold(III) complex is also predicted to interact via further hydrophobic contacts between the bipy methyl substituents and residues Ile59, Val67 and Val199. It is also worth noting the predicted proximity of the complex to the Arg218 side chain, whose positive charge might play a role in the binding of the metal center to Cys40 by stabilizing the chloride leaving group. Thus, calculations showed how the placement of the metal complexes in the AQP3 extracellular pocket is potentially controlled by both covalent anchoring to Cys40 and by noncovalent interactions; the latter could be crucial in blockade of the channel via burying of the constriction region.

## Conclusions

Numerous reports have highlighted the possible areas where AQP modulators could be useful in treating human diseases. Yet, only a few pharmaceutically relevant compounds have been identified to date. We described here the selective and potent inhibitory effects on AQP3 of a series of gold(III) complexes bearing nitrogen donor ligands, which together with their high water solubility makes them suitable candidates for future in vivo studies. AQP3 has been shown to mediate the majority of glycerol movement across hRBC membranes. In addition to its expression in hRBC, AQP3 has a wide tissue distribution in epithelial cells of kidney, airways and skin, suggesting a role in water reabsorption, mucosal secretions, skin hydration, and cell-volume regulation.[23] Moreover, recent studies demonstrated aberrant AQP3 expression in tumor cells of different origins, particularly aggressive tumors,[23–26] suggesting this enhanced protein expression to be of diagnostic and/or prognostic value.

Interestingly, the gold(III) complexes described here possess antiproliferative properties in vitro,[27,28] and in recent years several gold compounds have shown promising anticancer effects related to the inhibition of different protein targets, such as thioredoxin reductases, the proteasome, and certain zinc-finger proteins.[29–33] In this context, it is possible that inhibition of AQP3 might influence the biological effects of the gold(III) compounds towards cancer cells, and further studies are ongoing in our laboratories to validate such a hypothesis. Moreover, the inhibitory properties of the compounds towards the other aquaglyceroporin isoforms involved in essential physiological pathways should be further investigated in order to optimize the design to achieve highly selective molecules with decreased risks of side effects.

## Experimental Section

**Chemistry**: Gold(III) compounds were prepared according to literature procedures.[34,35] The purity of the compounds was confirmed by elemental analysis, and all of them showed purity >98%. Copper, platinum, and 2-mercaptoethanol were purchased from Sigma.

**Ethics statement**: Venous blood samples were obtained from healthy human volunteers following a protocol approved by the Ethics Committee of the Faculty of Pharmacy of the University of Lisbon (Portugal). Informed written consent was obtained from all participants.

**Erythrocyte sampling and preparation**: Venous blood samples were collected in citrate anticoagulant (2.7% citric acid, 4.5% trisodium citrate, and 2% glucose). Fresh blood was centrifuged at 750×*g* for 5 min at 4°C, and plasma and buffy coat were discarded. Packed erythrocytes were washed three times in phosphate-buffered saline (PBS; KCl 2.7 mM, $KH_2PO_4$ 1.76 mM, $Na_2HPO_4$ 10.1 mM, NaCl 137 mM, pH 7.4), diluted to 0.5% hematocrit, and immediately used for experiments. The mean volume of hRBC in isotonic solution was determined using a CASY-1 cell counter (Schärfe System GmbH, Reutlingen, Germany) and was calculated as 82 fL.

**Stopped-flow light scattering experiments**: Stopped-flow experiments were performed on a HI-TECH Scientific PQ/SF-53 apparatus, with 2 ms dead time, temperature controlled and interfaced with a microcomputer. Experiments were performed at 23°C for glycerol permeability and at 10°C for water permeability; for activation energy measurements, temperatures ranged from 10°C to 37°C. For each experimental condition, 5–7 replicates were analyzed. For measuring the osmotic water permeability ($P_f$), a suspension of fresh erythrocytes (0.5%, 100 μL) was mixed with an equal volume of PBS containing 200 mM sucrose as a nonpermeable osmolyte to produce a 100 mM inwardly directed sucrose gradient. The kinetics of cell shrinkage were measured from the time course of 90° scattered light intensity at 400 nm until a stable light scatter signal was obtained. The $P_f$ value was estimated by $P_f - k(V_o/A)(1/V_w(osm_{out})_\infty)$, where $V_w$ is the molar volume of water, $V_o/A$ is the initial cell volume to area ratio, $(osm_{out})_\infty$ is the final medium osmolarity after the applied osmotic gradient, and $k$ is the single exponential time constant fitted to the light scattering signal of erythrocyte shrinkage.

For glycerol permeability ($P_{gly}$), a suspension of fresh erythrocytes (0.5%, 100 μL) was mixed with an equal volume of hyperosmotic PBS containing 200 mM glycerol to create a 100 mM inwardly directed glycerol gradient. After the first fast cell shrinkage due to water outflow, glycerol influx in response to the chemical gradient was followed by water influx with subsequent cell reswelling. The $P_{gly}$ value was calculated as $P_{gly} - k(V_o/A)$, where $k$ is the single exponential time constant fitted to the light scattering signal of glycerol influx in erythrocytes. For inhibition experiments, cells were incubated with different concentrations of complexes, from freshly prepared stock aqueous solutions, for various times at room temperature before stopped-flow experiments were performed. A time-dependent inhibition assay was carried out for all test compounds over several hours; incubation with hRBC showed no further increase of inhibition after 30 min at room temperature. The reversibility of inhibition was tested by incubating hRBC with test compound for 30 min followed by further incubation with 1 mM 2-mercaptoethanol (EtSH) for 30 min at room temperature. The inhibitor concentration necessary to achieve 50% inhibition ($IC_{50}$) was calculated by nonlinear regression of dose–response curves (Graph Pad Prism, Inc) according to the equation $y = y_{min} + (y_{max} - y_{min})/(1 + 10^{((LogIC50 - Log[Inh])H)})$, where $y$ is the percent inhibition obtained for each concentration of inhibitor ([Inh]) and H is the Hill slope. The activation energy ($E_a$) of water and glycerol transport was calculated from the slope of the Arrhenius plot ($\ln P_f$ or $\ln P_{gly}$ as a function of $1/T$) multiplied by the gas constant ($R$). All solution osmolarities were determined from freezing point depression on a semi-micro-osmometer (Knauer GmbH, Berlin, Germany) using standards of 100 and 400 mOsM.

**Statistic analysis**: Data are presented as the mean ± standard error of the mean (SEM) of at least four independent experiments, and were analyzed with either the paired Student's t-test or one-way analysis of variance (ANOVA) followed by a Tukey's test. A value of $P \leq 0.01$ was considered to be statistically significant.

**QM calculations**: The structures of gold(III), copper(II), and platinum(II) complexes were investigated at DFT level of theory with the B3LYP hybrid functional.[36,37] The core electrons of the chloride and metal atoms were described with the Hay and Wadt core-valence relativistic effective core-potential (ECP) leaving the outer electrons to be treated explicitly through the basis set denoted as LACVP** in Jaguar, while for the remaining atoms the 6-31G** basis set was used.[38] Each structure was optimized in the gas phase ($\varepsilon = 0$), and frequency calculations were performed to verify the correct nature of the stationary points and to estimate zero-point energy (ZPE) and vibrational entropy corrections at room temperature. Single-point energies of all stationary points were calculated by using the larger 6-311++G** set for the main group elements, and the LACV3P++** set for the metal and the chloride atoms. At this level of theory, Mulliken[39] and NAO[40] population analyses were also performed. The Poisson–Boltzmann (PB) continuum solvent method was employed to simulate the aqueous medium ($\varepsilon = 80.37$).[41] The values of $\Delta G^{II}$ for methanethiol species were calculated by using a thermodynamic cycle as previously reported.[15] The Jaguar 7.9 quantum chemistry package was used for all calculations.[42]

**QM/MM calculations**: Hybrid QM/MM calculations have been performed with the Qsite 5.8 software package.[43] Since to date no crystallographic information about AQP3 is available, we performed the studies with a previously reported AQP3 homology model,[15] built by using the crystal structure of the *Escherichia coli* glycerol facilitator (GlpF) as a template (PDB ID code: 1LDF).[44]

The starting complexes were set up manually by placing the gold(III) atom in the proximity of the Cys40 side chain, which is expected to react with the metal center. To speed up the calculations, the QM region was limited to the gold(III) complex and treated at DFT level of theory with the B3LYP functional[36,37] and the LACVP** basis set,[38] whereas the MM system, consisting of protein atoms, was described with the OPLSA_2001 force field.[45,46] Protein atoms were kept frozen at their initial coordinates, and only the side chain atoms of Cys40, Phe63, Tyr212, and Arg218 were allowed to relax during the optimization.

## Acknowledgements

*A.P. Martins received a Ph.D. fellowship from Fundação para a Ciência e Tecnologia, Portugal (SFRH/BD/65046/2009). A. Casini thanks the Rosalind Franklin program (University of Groningen, The Netherlands) for financial support. A. Ciancetta gratefully acknowledges Prof. Stefano Moro (Molecular Modeling Section, University of Padova, Italy) for scientific and technical support. COST Action CM1105 and CM0902 are acknowledged for fruitful discussion.*

**Keywords:** antitumor agents · aquaporins · cancer · glycerol · gold-containing compounds · homology models

[1] L. S. King, D. Kozono, P. Agre, *Nat. Rev. Mol. Cell Biol.* **2004**, *5*, 687–698.
[2] A. S. Verkman, *Annu. Rev. Med.* **2012**, *63*, 303–316.
[3] E. Beitz, *Biol. Cell* **2005**, *97*, 373–383.
[4] G. M. Preston, T. P. Carroll, W. B. Guggino, P. Agre, *Science* **1992**, *256*, 385–387.
[5] G. M. Preston, J. S. Jung, W. B. Guggino, P. Agre, *J. Biol. Chem.* **1993**, *268*, 17–20.
[6] Y. Yukutake, S. Tsuji, Y. Hirano, T. Adachi, T. Takahashi, K. Fujihara, P. Agre, M. Yasui, M. Suematsu, *Biol. Cell* **2008**, *100*, 355–363.
[7] M. Zelenina, S. Tritto, A. A. Bondar, S. Zelenin, A. Aperia, *J. Biol. Chem.* **2004**, *279*, 51939–51943.
[8] H. L. Brooks, J. W. Regan, A. J. Yool, *Mol. Pharmacol.* **2000**, *57*, 1021–1026.
[9] A. J. Yool, A. M. Weinstein, *News Physiol. Sci.* **2002**, *17*, 68–72.
[10] F. J. M. Detmers, B. L. De Groot, E. M. Muller, A. Hinton, I. B. M. Konings, M. Sze, S. L. Flitsch, H. Grubmuller, P. M. T. Deen, *J. Biol. Chem.* **2006**, *281*, 14207–14214.
[11] Y. Yukutake, Y. Hirano, M. Suematsu, M. Yasui, *Biochemistry* **2009**, *48*, 12059–12061.
[12] V. J. Huber, M. Tsujita, T. Nakada, *Mol. Aspects Med.* **2012**, *33*, 691–703.
[13] D. Seeliger, C. Zapater, D. Krenc, R. Haddoub, S. Flitsch, E. Beitz, J. Cerdà, B. L. de Groot, *ACS Chem. Biol.* **2013**, *8*, 249–526.
[14] S. Jelen, S. Wacker, C. Aponte-Santamaria, M. Skott, A. Rojek, U. Johanson, P. Kjellbom, S. Nielsen, B. de Groot, M. Rutzler, *J. Biol. Chem.* **2011**, *286*, 44319–44325.
[15] A. P. Martins, A. Marrone, A. Ciancetta, A. G. Cobo, M. Echevarria, T. F. Moura, N. Re, A. Casini, G. Soveral, *Plos One* **2012**, *7*, e37435.
[16] E. Campos, T. F. Moura, A. Oliva, P. Leandro, G. Soveral, *Biochem. Biophys. Res. Commun.* **2011**, *408*, 477–481.
[17] D. F. Savage, R. M. Stroud, *J. Mol. Biol.* **2007**, *368*, 607–617.
[18] C. M. Niemietz, S. D. Tyerman, *Febs Lett.* **2002**, *531*, 443–447.
[19] G. Klopman, *J. Am. Chem. Soc.* **1968**, *90*, 223–234.
[20] H. F. Dos Santos, D. Paschoal, J. V. Burda, *J. Phys. Chem. A* **2012**, *116*, 11015–11024.
[21] D. F. Savage, J. D. O'Connell III, L. J. Miercke, J. Finer-Moore, R. M. Stroud, *Proc. Natl. Acad. Sci. USA* **2010**, *107*, 17164–17169.
[22] N. Roudier, J. M. Verbavatz, C. Maurel, P. Ripoche, F. Tacnet, *J. Biol. Chem.* **1998**, *273*, 8407–8412.
[23] M. Hara-Chikuma, A. S. Verkman, *Mol. Cell Biol.* **2008**, *28*, 326–332.
[24] M. Kusayama, K. Wada, M. Nagata, S. Ishimoto, H. Takahashi, M. Yoneda, A. Nakajima, M. Okura, M. Kogo, Y. Kamisaki, *Cancer Sci.* **2011**, *102*, 1128–1136.
[25] W. Liu, K. Wang, K. Gong, X. Li, K. Luo, *Mol. Med. Rep.* **2012**, *6*, 607–610.
[26] L. Gao, Y. Gao, X. Li, P. Howell, R. Kumar, X. Su, A. V. Vlassov, G. A. Piazza, A. I. Riker, D. Sun, Y. Xi, *Mol. Oncol.* **2012**, *6*, 81–87.
[27] L. Messori, F. Abbate, G. Marcon, P. Orioli, M. Fontani, E. Mini, T. Mazzei, S. Carotti, T. O'Connell, P. Zanello, *J. Med. Chem.* **2000**, *43*, 3541–3548.
[28] A. Casini, G. Kelter, C. Gabbiani, M. A. Cinellu, G. Minghetti, D. Fregona, H. H. Fiebig, L. Messori, *J. Biol. Inorg. Chem.* **2009**, *14*, 1139–1149.
[29] A. Bindoli, M. P. Rigobello, G. Scutari, C. Gabbiani, A. Casini, L. Messori, *Coord. Chem. Rev.* **2009**, *253*, 1692–1707.
[30] E. Vergara, A. Casini, F. Sorrentino, O. Zava, E. Cerrada, M. P. Rigobello, A. Bindoli, M. Laguna, P. J. Dyson, *ChemMedChem* **2010**, *5*, 96–102.
[31] F. Mendes, M. Groessl, A. A. Nazarov, Y. O. Tsybin, G. Sava, I. Santos, P. J. Dyson, A. Casini, *J. Med. Chem.* **2011**, *54*, 2196–2206.
[32] L. Dalla Via, C. Nardon, D. Fregona, *Future Med. Chem.* **2012**, *4*, 525–543.
[33] M. Serratrice, F. Edafe, F. Mendes, R. Scopelliti, S. M. Zakeeruddin, M. Gratzel, I. Santos, M. A. Cinellu, A. Casini, *Dalton Trans.* **2012**, *41*, 3287–3293.
[34] A. Casini, M. C. Diawara, R. Scopelliti, S. M. Zakeeruddin, M. Grätzel, P. J. Dyson, *Dalton Trans.* **2010**, *39*, 2239–4225.
[35] L. S. Hollis, S. J. Lippard, *J. Am. Chem. Soc.* **1983**, *105*, 4293–4299.
[36] A. D. Becke, *J. Chem. Phys.* **1993**, *98*, 5648–5652.
[37] A. D. Becke, *Phys. Rev. A* **1988**, *38*, 3098–3100.
[38] P. J. Hay, W. R. Wadt, *J. Chem. Phys.* **1985**, *82*, 299–310.
[39] R. S. Mulliken, *J. Chem. Phys.* **1955**, *23*, 1833.
[40] Natural Bond Orbital (NBO), version 5.0; E. D. Glendening, J. K. Badenhoop, A. E. Reed, J. E. Carpenter, J. A. Bohmann, C. M. Morales, F. Weinhold, Theoretical Chemistry Institute, University of Wisconsin, Madison, USA, **2001**; http://www.chem.wisc.edu/~nbo5/.
[41] D. J. Tannor, B. Marten, R. Murphy, R. A. Friesner, D. Sitkoff, A. Nicholls, M. Ringnalda, W. A. Goddard III, B. Honig, *J. Am. Chem. Soc.* **1994**, *116*, 11875–11882.

[42] Jaguar, version 7.9, Schrödinger, LLC, New York, USA, **2012**.
[43] QSite, version 5.8, Schrödinger, LLC, New York, USA, **2012**.
[44] D. Fu, A. Libson, L. J. Miercke, C. Weitzman, P. Nollert, F. J. Krucinski, R. M. Stroud, *Science* **2000**, *290*, 481 – 486.
[45] W. L. Jorgensen, D. S. Maxwell, J. Tirado-Rives, *J. Am. Chem. Soc.* **1996**, *118*, 11225 – 11236.
[46] G. Kaminski, R. A. Friesner, J. Tirado-Rives, W. L. Jorgensen, *J. Phys. Chem. B* **2001**, *105*, 6474 – 6487.

Received: March 6, 2013
Published online on May 7, 2013

# CHAPTER 3 - Aquaporin Functional Assessment in the Yeast Cell Model

# CHAPTER 3 - Aquaporin Functional Assessment in the Yeast Cell Model

The information contained in this chapter is included in the following original publications:

*Publication 6*

Sabir F, Leandro MJ, Martins AP, Loureiro-Dias MC, Moura TF, Soveral G, Prista C.
*Exploring three PIPs and three TIPs of grapevine for transport of water and atypical substrates through heterologous expression in aqy-null yeast.*
PLoS One. 2014 Aug 11;9(8):e102087.
doi: 10.1371/journal.pone.0102087.

*Publication 7*

Noronha H, Agasse A, Martins AP, Berny MC, Gomes D, Zarrouk O, Thiebaud P, Delrot S, Soveral G, Chaumont F, Gerós H.
*The grape aquaporin VvSIP1 transports water across the ER membrane.*
J Exp Bot. 2014 Mar;65(4):981-93.
doi: 10.1093/jxb/ert448.

OPEN ACCESS Freely available online

PLOS ONE

# Exploring Three PIPs and Three TIPs of Grapevine for Transport of Water and Atypical Substrates through Heterologous Expression in *aqy-null* Yeast

**Farzana Sabir[1,2], Maria José Leandro[1], Ana Paula Martins[1,2], Maria C. Loureiro-Dias[1], Teresa F. Moura[2], Graça Soveral[2,3], Catarina Prista[1]***

**1** Centre for Botany Applied to Agriculture (CBAA), Instituto Superior de Agronomia, University of Lisbon, Lisbon, Portugal, **2** Instituto de Investigação do Medicamento (iMed.ULisboa), Faculdade de Farmácia, Universidade de Lisboa, Lisboa, Portugal, **3** Dept. de Bioquímica e Biologia Humana, Faculdade de Farmácia, Universidade de Lisboa, Lisboa, Portugal

## Abstract

Aquaporins are membrane channels that facilitate the transport of water and other small molecules across the cellular membranes. We examined the role of six aquaporins of *Vitis vinifera* (cv. Touriga nacional) in the transport of water and atypical substrates (other than water) in an *aqy-null* strain of *Saccharomyces cerevisiae*. Their functional characterization for water transport was performed by stopped-flow fluorescence spectroscopy. The evaluation of permeability coefficients ($P_f$) and activation energies (*Ea*) revealed that three aquaporins (*Vv*TnPIP2;1, *Vv*TnTIP1;1 and *Vv*TnTIP2;2) are functional for water transport, while the other three (*Vv*TnPIP1;4, *Vv*TnPIP2;3 and *Vv*TnTIP4;1) are non-functional. TIPs (*Vv*TnTIP1;1 and *Vv*TnTIP2;2) exhibited higher water permeability than *Vv*TnPIP2;1. All functional aquaporins were found to be sensitive to $HgCl_2$, since their water conductivity was reduced (24–38%) by the addition of 0.5 mM $HgCl_2$. Expression of *Vitis* aquaporins caused different sensitive phenotypes to yeast strains when grown under hyperosmotic stress generated by KCl or sorbitol. Our results also indicate that *Vitis* aquaporins are putative transporters of other small molecules of physiological importance. Their sequence analyses revealed the presence of signature sequences for transport of ammonia, boron, $CO_2$, $H_2O_2$ and urea. The phenotypic growth variations of yeast cells showed that heterologous expression of *Vitis* aquaporins increased susceptibility to externally applied boron and $H_2O_2$, suggesting the contribution of *Vitis* aquaporins in the transport of these species.

**Citation:** Sabir F, Leandro MJ, Martins AP, Loureiro-Dias MC, Moura TF, et al. (2014) Exploring Three PIPs and Three TIPs of Grapevine for Transport of Water and Atypical Substrates through Heterologous Expression in *aqy-null* Yeast. PLoS ONE 9(8): e102087. doi:10.1371/journal.pone.0102087

**Editor:** Dan Zilberstein, Technion-Israel Institute of Technology Haifa 32000 Israel, Israel

**Received** April 17, 2014; **Accepted** June 15, 2014; **Published** August 11, 2014



**Data Availability:** The authors confirm that all data underlying the findings are fully available without restriction. All gene sequences are available from GeneBank VvTnPIP1;4 accession = KJ697714, VvTnPIP2;1 accession = KJ697715, VvTnPIP2;3 accession = KJ697716, VvTnTIP1;1 accession = KJ697717, VvTnTIP2;2 accession = KJ697718, VvTnTIP4;1 accession = KJ697719.

**Funding:** This work is supported by Fundação para a Ciência e Tecnologia (FCT), Portugal (Post-Doctral grants-SFRH/BPD/89427/2012 to F. S. and SFRH/BPD/41812/2007 to M. J. L., Ciência 2007 to C. P. and project grant PTDC/AGR/AAM/099154/2008). The funders had no role in study design, data collection and analysis, decision to publish, or preparation of the manuscript.

**Competing Interests:** The authors have declared that no competing interests exist.

* Email: cprista@isa.ulisboa.pt

## Introduction

Aquaporins play a crucial role in maintaining water and ion homeostasis of plants, essential for plant cell integrity, growth and survival in their ever-changing environment. These water channels can provide rapid and reversible changes to cells hydraulic conductance by modulating membrane water permeability [1]. Aquaporins belong to Major Intrinsic Proteins (MIPs) family and based on their sequence similarity and sub-cellular localization, plant aquaporins are divided in seven subfamilies: the plasma membrane intrinsic proteins (PIPs), the tonoplast intrinsic proteins (TIPs), the nodulin-26-like intrinsic proteins (NIPs), the small intrinsic proteins (SIPs), the GlpF-like intrinsic proteins (GIPs), the hybrid intrinsic proteins (HIPs) and the uncategorized X intrinsic proteins (XIPs) [2]. Studies on plant aquaporins revealed their role far beyond the membrane water transport. Besides water, they are reported to transport also other small molecules and/or gases of physiological importance (reviewed by [3]), suggesting their versatile functions in plants. Putative substrate specificities of aquaporins are generally assigned by the presence of specific amino acid residues at well-defined positions in the sequences [4].

Since aquaporins establish a tight association between water transport and plant development and adaptation under stress conditions, a rigorous regulation of aquaporin activity is essential to fine-tune the overall hydraulic conductivity in plants [5]. Expression of aquaporin genes can be altered under various environmental conditions as well as according to cell/tissue type and plant developmental stages [6]. Besides these initial regulatory steps of gene expression, the activity of translated and targeted aquaporin proteins can be further regulated by various post-translational modifications such as methylation, glycosylation, phosphorylation, membrane trafficking, heteromerization, and their gating can also be regulated by pH, divalent ions and membrane tension [7]. Various stress conditions like anoxia, salt and water stress have also been reported to affect the activity of aquaporins in plants (reviewed by [3,6]).

*Vitis vinifera* cv. Touriga nacional is an important Portuguese cultivar. This variety is a key ingredient in both dry red and fortified wines (particularly, Port wine). Grapevines are known to be extremely stress-tolerant plants, especially for dry environment [8]. In fact, deficit irrigation techniques are commonly used to achieve high fruit quality [9]. Since the water status of the plant greatly influences the fruit quality and hence the characteristics of wine [10], it is significant to study the molecular cell entry point of water, i.e. aquaporins in these plants. Release of full genomic sequence of grapevine revealed the occurrence of 28 genes encoding putative aquaporins in *V. vinifera* [11]. Comprehensive phylogenetic analyses of the deduced amino acid sequences suggest that the *V. vinifera* (cv. Cabernet Sauvignon and cv. Pinot Noir) aquaporins can be distributed in the four main subfamilies: PIPs (8 genes), TIPs (10 genes), NIPs (8 genes) and SIPs (2 genes) [12]. Despite being a very important economical plant, only few reports are available on *Vitis* aquaporins, explaining their quantitative expression in various rootstocks [13], during water stress [14,15] and their cloning and expression *in planta* [8,16] or in heterologous systems, such as *Xenopus* oocytes [1,12] and *S. cerevisiae* [17,18]. Although from a molecular point of view the presence of aquaporins can be easily recognized in a genome, their physiological role *in planta* is still difficult to understand. At transcript level, plant aquaporins respond variedly to stress, depending on the plant tissue/organ, cultivars/species and types/degree of stress [1], impairing the interpretation of the role of an individual aquaporin. To study the physiological role of each aquaporin, we used *S. cerevisiae* as a simple and well-characterized heterologous expression system [19]. The evaluation of water transport activity in intact yeast cells through stopped-flow fluorescence spectroscopy is already well-established [17,20].

The present work is focused on the cloning and expression of putative aquaporins (three PIPs and three TIPs) of *Vitis vinifera* (cv. Touriga nacional) in an *aqy-null* strain of *S. cerevisiae*. Their functional characterization for water transport was performed through stopped-flow spectroscopy. Further, tolerance/sensitivity of these aquaporins expressing strains was tested under hyperosmotic stress exerted by KCl or sorbitol. This study also includes the analysis of signature sequences for transport of atypical substrates and growth assays of yeast strains expressing *Vitis* aquaporins in the presence of these substrates, to explore their putative route of transport.

## Materials and Methods

### Yeast strain, plasmid and growth conditions

*Saccharomyces cerevisiae* 10560-6B *MATα leu2::hisG trp1::hisG his3::hisG ura3-52 aqy1::KanMX4 aqy2::HIS3* (from now on designated as *aqy-null*) was used as host strain for heterologous expression of putative aquaporins from *V. vinifera* cv. Touriga nacional. The centromeric plasmid pUG35 was used for cloning, conferring C-terminal GFP tagging, MET25 promoter and CYC1-T terminator [21]. For propagation of these plasmids, *Escherichia coli* DH5α strain was used as host [22]. *E. coli* transformants were grown in Luria-Bertani (LB) medium supplemented with ampicillin (100 μg $ml^{-1}$), at 37°C. The host *S. cerevisiae* strain (*aqy-null*) was maintained in YPD medium (5 g $l^{-1}$ yeast extract, 10 g $l^{-1}$ peptone, 20 g $l^{-1}$ glucose and 20 g $l^{-1}$ agar). Transformed yeast strains were grown and maintained in YNB medium without amino acids (DIFCO) with 2% (w/v) glucose supplemented with the adequate requirements for prototrophic growth [23].

### Cloning and heterologous expression of *Vitis vinifera* aquaporins in *S. cerevisiae*

To clone the putative aquaporins from *V. vinifera* cv. Touriga nacional, their cDNA (kindly provided by Dr. Luísa Carvalho, ISA-ULisboa) amplification, cloning and expression in *S. cerevisiae* were performed according to previously described methods [17]. Primers used in this study are listed in Table S1.

### Sequence analysis

Nucleotide sequences identified in the present study are submitted to National Center for Biotechnological Information (NCBI) (http://www.ncbi.nlm.nih.gov). These sequences were translated by ExPASy translate tool (http://web.expasy.org/translate/). Deduced amino acid sequences were analysed and compared with database sequences of *V. Vinifera* cv. Pinot noir, available at Grape Genome Browser (http://www.genoscope.cns.fr/externe/Genome Browser/Vitis/) and NCBI. Multiple protein sequence alignments were generated by using the ClustalX [24] and BioEdit [25] programs. Phylogenetic tree was constructed from the alignment of deduced amino acid sequences obtained from the present study and our previous study [17] with twenty-eight amino acid sequences of aquaporins of *V. vinifera* cv. Pinot noir, by MEGA5.1 software using neighbor-joining method [26]. Topology and hydrophobicity of deduced amino acid sequences were predicted by using various ExPASy tools e.g. TMHMM [27], HMMTOP [28] and TMPred [29].

All gene sequences are available from at GeneBank VvTnPIP1;4 accession = KJ697714, VvTnPIP2;1 accession = KJ697715, VvTnPIP2;3 accession = KJ697716, VvTnTIP1;1 accession = KJ697717, VvTnTIP2;2 accession = KJ697718, VvTnTIP4;1 accession = KJ697719.

To search the signature sequences for transport of atypical substrates, obtained amino acid sequences were grouped with reference sequences as per their reported substrates for transport, described by [4] and were aligned using ClustalX. Conserved amino acid residues at NPA, ar/R constriction and P1 P5 regions were determined from the alignment and matched with reference sequences of transporters of various substrates. Based on the conserved residues at these positions, selectivity profiles of cloned aquaporins were predicted.

### Water transport assays of *Vitis* aquaporins expressed in *S. cerevisiae*

Functional analyses of heterologously expressed *Vitis* aquaporins for water conductivity were performed by stopped-flow fluorescence spectroscopy as previously described [17]. Briefly, yeast strains grown in liquid YNB medium were harvested at mid exponential phase ($OD_{640\ nm} \approx 1.0$) (Ultrospec 2100 pro, Amersham Biosciences) and incubated for 1 hour at 28°C in YPD medium (6 g $l^{-1}$ wet weight). Further, cells were washed and re-suspended in ice-cold 1.4 M sorbitol (3 ml $g^{-1}$ wet weight) and incubated on ice for at least 90 minutes. Cells were pre-loaded with the membrane permeable nonfluorescent precursor 5-(and-6)-carboxyfluorescein diacetate (CFDA), which is intracellularly hydrolyzed releasing the membrane impermeable fluorescent form. For water transport assays, hyperosmotic shocks were applied on stopped-flow apparatus (HI-TECH Scientific PQ/SF-53). Cells equilibrated with 1.4 M sorbitol were mixed with an equal volume of 2.1 M sorbitol. The resulting cell shrinkage caused a quenching of the fluorescence intensity. Signals were fitted to a single exponential, from which the rate constant ($k$) was calculated. Permeability coefficient ($P_f$) and activation energy ($Ea$) were estimated as described by [17,20].

Inhibition of water transport in *Vitis* aquaporins expressing yeast strains was tested with mercury chloride ($HgCl_2$), a well-known inhibitor of aquaporins. Yeast strains expressing functional *Vitis* aquaporins were incubated with $HgCl_2$ (0.5 and 1 mM, in 50 mM potassium citrate buffer, pH 5.0) for 15 and 30 minutes before the osmotic shock at 23°C. The yeast strain with the empty plasmid was treated in the same way and considered as control. Osmotic shocks were applied without and after incubation with $HgCl_2$ and the signals obtained were compared and used to calculate the $P_f$ in both conditions.

### Growth assays under osmotic stress and sensitivity tests on atypical substrates

*S. cerevisiae* strains harboring *Vitis* aquaporins were tested for their ability to grow under osmotic stress. Moreover, possibility to transport atypical substrates, such as ammonia, boron, hydrogen peroxide ($H_2O_2$) and urea was also investigated. Growth assays were performed on solid YNB medium (pH 5.0) supplemented with 2% (w/v) glucose. NaCl (0.5, 1.0 and 1.5 M), KCl (0.5, 1.0 and 1.5 M) and osmoequivalent concentration of sorbitol (0.84, 1.4 and 2.1 M) were added to growth media for osmotic stress experiments. Hydrogen peroxide (0.5, 0.75, 1.0, 1.5 and 2.0 mM) and boron (as boric acid, 20, 40, 50 and 60 mM), were used as atypical substrates for transport. Media with $H_2O_2$ was freshly prepared at the time of inoculation. Moreover, in order to test the putative transport of ammonia (1.0, 2.0 and 3.0 mM) and urea (1.0, 2.0, 2.5 and 3.5 mM), either of them was used as sole nitrogen source. Yeast strains were initially grown in liquid YNB medium supplemented with 2% (w/v) glucose, with orbital shaking (180 rpm) at 28°C, up to $OD_{640\ nm} \approx 1.0$ corresponding to $1 \times 10^7$ cells/ml. Cells were centrifuged and washed in sterile distilled water and re-suspended to $OD_{640\ nm} \approx 10$. Multi-well plates were prepared with serial 10-fold dilutions of the original concentrated culture, 3 µl suspensions was spotted with replica platter for 96-well plates device on plates containing YNB solid medium with ammonia, boric acid, $H_2O_2$ and urea, separately and incubated at 28°C. Strain with the empty plasmid (pUG35) was considered as control. Differences in growth phenotypes of yeast strains were recorded after 1 and 2 weeks of incubation.

### Microscopy

For the localization of GFP-tagged proteins in *S. cerevisiae*, mid-exponential phase cells were observed under Leitz Wetzlar Germany 513558 epifluorescence microscope equipped with a Leitz Wetzlar Germany Type 307-148002 514687 mercury bulb and BP 340 380; BP 450 490 (for GFP visualizing); BP 515 560 filter sets. Images were obtained with a digital camera Axiocam Zeiss using AxioVision Rel. 4.8.2 Software.

### Statistical analysis

All the data were collected from at least three independent experiments. For stopped-flow experiments, usually five runs at each temperature and ten runs for $P_f$ at 23°C were stored and analyzed in each experiment. Student's t test was used for statistical analysis. $P<0.05$ (marked as *) was considered to be statistically significant. Data are presented as mean ± standard deviation (SD).

## Results

### Cloning and heterologous expression of *Vitis vinifera* aquaporins in *S. cerevisiae*

Specific primers designed from the sequences of aquaporins of *Vitis vinifera* (cv. Pinot Noir) were able to amplify six full-length cDNAs of putative aquaporins from *V. vinifera* (cv. Touriga nacional). The predicted amino acid sequences were aligned and compared with the Pinot noir variety (Figure S1), all of them shared high identity (>96%) in both varieties. As expected, the six amino acids sequences corresponding to the cDNAs cloned from *V. vinifera* cv. Touriga nacional in this study were clearly identified in the genome of Pinot noir variety and three of them were clustered in their subsequent groups of PIPs, while other three in TIPs subfamilies (Figure 1). Based on BLASTN (http://blast.ncbi.nlm.nih.gov/Blast.cgi) alignment, sequences were classified as *PIP1;4* (858 bp), *PIP2;1* (852 bp), *PIP2;3* (861 bp) and *TIP1;1* (753 bp), *TIP2;2* (750 bp), *TIP4;1* (759 bp) and their encoded proteins were named as *Vv*TnPIP1;4 (286 aa), *Vv*TnPIP2;1 (284 aa), *Vv*TnPIP2;3 (287 aa) and *Vv*TnTIP1;1 (251 aa), *Vv*TnTIP2;2 (250 aa), *Vv*TnTIP4;1 (253 aa) following the nomenclature proposed for plant aquaporins [30]. *Vv*TnPIP1;4 has 96.5% identity with nine substitution of amino acids (Figure S1A), while *Vv*TnPIP2;1 is 98.6% identical with difference at four positions (Figure S1B). *Vv*TnTIP2;2 shares 99.2% identity of amino acids with substitution at two positions (Figure S1C), similarly *Vv*TnTIP1;1 has 99.6% identity with substitution at only one amino acid position (Figure S1D). On the other hand, *Vv*TnPIP2;3 and *Vv*TnTIP4;1 were 100% identical to their respective proteins of the other variety (Figures S1E and S1F, respectively).

Expression and localization of these cloned proteins in selected yeast transformants were verified by GFP tagging under fluorescent microscopy. Most of the GFP-tagged aquaporins were localized in the plasma membrane of *S. cerevisiae* (Figure 2). Besides plasma membrane, some of the GFP-tagged proteins were also observed retained inside the cell, probably in the endoplasmic reticulum or vesicles of the secretory pathway.

### Topology prediction and analysis of conserved sequences of *Vitis vinifera* aquaporins

The hypothetical transmembrane topology of deduced amino acid sequences revealed that, as expected, all cloned aquaporins exhibit typical features common to orthodox plant aquaporins (Figure 3): (i) six transmembrane-spanning hydrophobic α-helices (TMH1 TMH6) connected with five alternating extracellular and intracellular loops (LA-LE), (ii) intracellular facing amino and carboxyl terminals, (iii) two highly conserved NPA (Asn-Pro-Ala) motifs on LB and LE loops important for configuration of aqueous pore in aquaporins [31], and (iv) a Serine residue near the second NPA motif (GXXXNPAR(S/D)XG), specific for water transport [32,33].

Besides the general characteristics of aquaporins, special features attributed to the PIP aquaporin family and subfamilies (PIP1s and PIP2s) of *Vitis* aquaporins were found, such as: (i) longer N-terminal in *Vv*TnPIP1;4 (PIP1 subfamily) than *Vv*TnPIP2;1 and *Vv*TnPIP2;3 (PIP2 subfamily) (Figures 3 and S2A), (ii) longer C-terminal in *Vv*TnPIP2;1 and *Vv*TnPIP2;3 than *Vv*TnPIP1;4 [12,34] (Figures 3 and S2B), (iii) methylation site (K3/4 and E6) [35] and diacidic motif (D/E-I/X-E/D) [36] at N-terminal (*Vv*TnPIP1;4, *Vv*TnPIP2;1 and *Vv*TnPIP2;3) (Figures 3 and S3A), (iv) His residue for pH sensitivity in loop D (*Vv*TnPIP1;4-$H^{206}$, *Vv*TnPIP2;1-$H^{196}$, *Vv*TnPIP2;3-$H^{199}$) [37] (Figures 3 and S4B), (v) multiple conserved Ser residues for phosphorylation in loop B, loop D and C-terminal positions, such as 1) in loop B (*Vv*TnPIP1;4-$S^{128}$, *Vv*TnPIP2;1-$S^{118}$ and *Vv*TnPIP2;3-$S^{121}$) (Figures 3 and S4A), 2) in loop D two positions of conserved Ser in consensus sequence N/SARDSHVP, in which the first Ser is present only in *Vv*TnPIP2;1 ($S^{191}$) [38], while second Ser is present in all cloned PIPs (*Vv*TnPIP1;4-$S^{205}$,

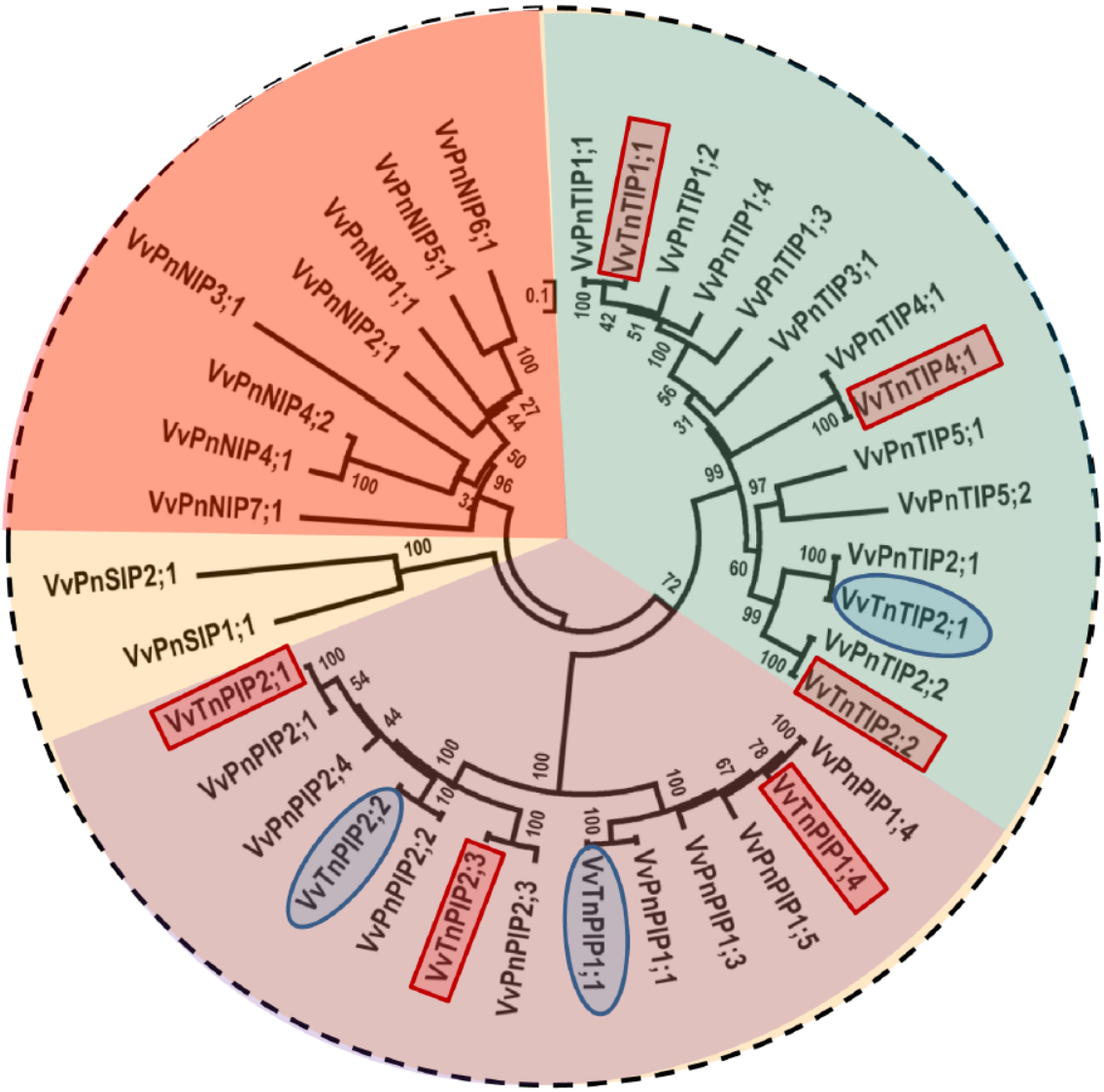


**Figure 1. Phylogenetic tree based on protein sequences of aquaporins from *V. vinifera* cv. Pinot noir and cv. Touriga nacional.** Dendrogram depicting the phylogenetic relationship between the aquaporins of Touriga nacional variety cloned in this study (framed in rectangular shape), previous study (oval shape frame) [17] with the aquaporins of Pinot noir variety. Dendogram was generated by neighbor-joining method (applied to 1000 bootstrap data sets) using the MEGA5.1 program [26]. Accession numbers of presented protein sequences are: *Vv*PnPIP1;1 (CAO41326, GSVIVT00029248001), *Vv*PnPIP1;3 (CAO62835, GSVIVT00000433001), *Vv*PnPIP1;4 (CAO39626, GSVIVT00026881001), *Vv*PnPIP1;5 (CAO39627, GSVIVT00026882001), *Vv*PnPIP2;1 (CAN75442), *Vv*PnPIP2;2 (CAO47394, GSVIVT00036133001), *Vv*PnPIP2;3 (CAO18152, GSVIVT00023192001), *Vv*PnPIP2;4 (CAO21844, GSVIVT00024536001), *Vv*PnTIP1;1 (CAO69259, GSVIVT00018548001), *Vv*PnTIP1;2 (CAO63006, GSVIVT00000605001), *Vv*PnTIP1;3 (CAO16745, GSVIVT00022146001), *Vv*PnTIP1;4 (CAO21720, GSVIVT00024394001), *Vv*PnTIP2;1 (CAO45860, GSVIVT00034350001), *Vv*PnTIP2;2 (CAO23095, GSVIVT00012703001), *Vv*PnTIP3;1 (CAO62035, GSVIVT00013854001), *Vv*PnTIP4;1 (CAO44039, GSVIVT00032441001), *Vv*PnTIP5;1 (CAO42713, GSVIVT00029946001), *Vv*PnTIP5;2 (CAO70596, GSVIVT00019170001), *Vv*PnNIP1;1 (CAO48005, GSVIVT00035815001), *Vv*PnNIP2;1 (CAO15462, GSVIVT00011149001), *Vv*PnNIP3;1 (CAO17108, GSVIVT00022377001), *Vv*PnNIP4;1 (CAO70192, GSVIVT00007127001), *Vv*PnNIP4;2 (CAO43338, GSVIVT00003903001), *Vv*PnNIP5;1 (CAO62847, GSVIVT00000446001), *Vv*PnNIP6;1 (CAO45476, GSVIVT00033750001), *Vv*PnNIP7;1 (CAO71103, GSVIVT00019910001), *Vv*PnSIP1;1 (CAO23510, GSVIVT00025504001) and *Vv*PnSIP2;1 (CAO18284, GSVIVT00023346001) (for Pinot noir cultivar sequences) and *Vv*TnPIP1;1 (HQ913643), *Vv*TnPIP1;4 (KJ697714), *Vv*TnPIP2;1 (KJ697715), *Vv*TnPIP2;2 (HQ913642), *Vv*TnPIP2;3 (KJ697716), *Vv*TnTIP1;1 (KJ697717), *Vv*TnTIP2;1 (HQ913640), *Vv*TnTIP2;2 (KJ697718) and *Vv*TnTIP4;1 (KJ697719) (for Touriga nacional cultivar sequences).
doi:10.1371/journal.pone.0102087.g001

*Vv*TnPIP2;1-$S^{195}$ and *Vv*TnPIP2;3-$S^{198}$) [39] (Figures 3 and S4B), 3) at C-terminal, consensus phosphorylation site (Lys-x-x-x-Ser-x-Arg) is conserved only in PIP2 subfamily members (*Vv*TnPIP2;1-$S^{277}$ and $S^{280}$, *Vv*TnPIP2;3-$S^{280}$ and $S^{283}$) [40,41] (Figures 3 and S4C).

Distinct characteristics found in cloned TIPs were: (i) shorter N-terminals than PIPs (Figures 3 and S2A) (ii) slightly longer C-terminal than PIP1s, but shorter than PIP2s subfamily members (Figures 3 and S2B) [34] (iii) Cys residue for mercury sensitive site (*Vv*TnTIP1;1-$C^{118}$, *Vv*TnTIP2;2-$C^{116}$ and *Vv*TnTIP4;1- $C^{113}$) [42] (Figures 3 and S5A), (iv) His residue for pH sensitive site (*Vv*TnTIP2;2-$H^{131}$ and *Vv*TnTIP4;1-$H^{128}$) (Figures 3 and S5B) [17]. (viii) Thr residue for putative phosphorylation site (*Vv*TnTIP1;1-$T^{99}$, *Vv*TnTIP2;2-$T^{97}$ and *Vv*TnTIP4;1-$T^{94}$) (Figures 3 and S4A) [40,43].

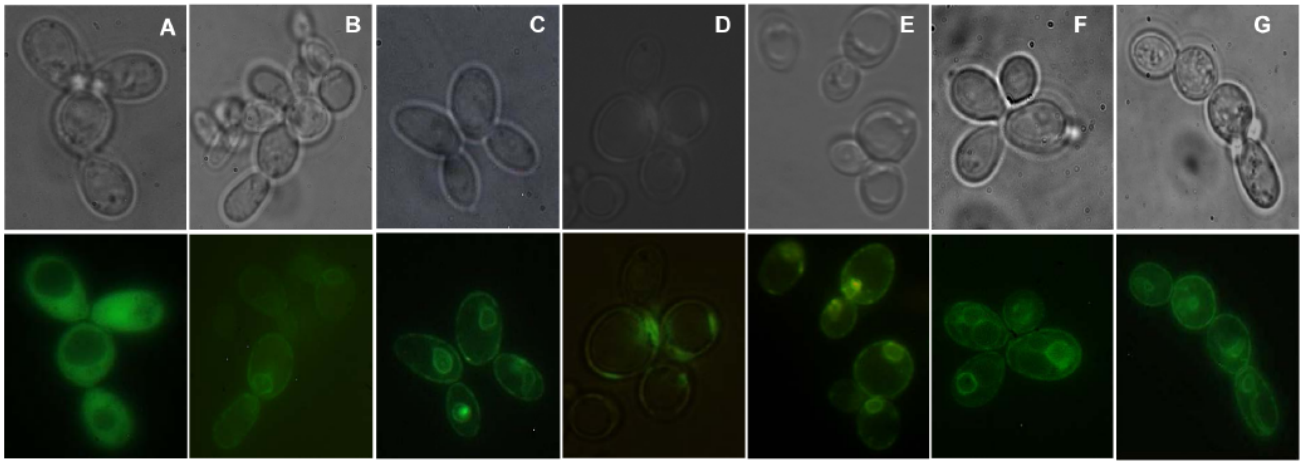


**Figure 2. Localization of GFP-tagged aquaporins from *V. Vinifera* expressed in *S. cerevisiae* strains.** Cytosolic GFP localization in (A) control cells (transformed with empty plasmid pUG35) and in the membrane of cells expressing (B) *Vv*TnPIP1;4, (C) *Vv*TnPIP2;1, (D) *Vv*TnPIP2;3, (E) *Vv*TnTIP1;1, (F) *Vv*TnTIP2;2, (G) *Vv*TnTIP4;1. Images were taken under phase contrast (upper panel) and fluorescence (lower panel) microscopy.
doi:10.1371/journal.pone.0102087.g002

## Presence of signature sequences for transport of substrates other than water

Signature sequences for transport of atypical substrates in all cloned aquaporins were explored according to [4] (Table 1), in particular the ar/R (aromatic/Arginine) constriction (filter 2) that consists of four residues (one in the second and one in the fifth helix (TMH2 and TMH5) and two in the fifth loop (LE1 and LE2 or R)) and P1 P5 positions (P1 in the third loop (LC), P2 and P3 in the fifth loop (LE), P4 and P5 in sixth helix (TMH6)) (Figure 3). The analysis showed the presence of signature sequences deciphered for boron (filter 2: F/A/G-H/I/S-T/G/A-R and P1 P5 residues: Q/F/I-S/T-A-F/Y-W/L) (Figure S6A) and $CO_2$ (filter 2: F-H-T-R and P1 P5 residues: Q/M-S-A-F-W) (Figure S6B) transport in all cloned PIPs: *Vv*TnPIP1;4 (filter 2: $F^{94}$-$H^{223}$-$T^{232}$-$R^{238}$ and P1 P5: $Q^{154}$-$S^{239}$-$A^{243}$-$F^{258}$-$W^{259}$), *Vv*TnPIP2;1 (filter 2: $F^{84}$-$H^{213}$-$T^{222}$-$R^{228}$ and P1 P5: $Q^{144}$-$S^{229}$-$A^{233}$-$F^{248}$-$W^{249}$) and *Vv*TnPIP2;3 (filter 2: $F^{87}$-$H^{216}$-$T^{225}$-$R^{231}$ and P1 P5: $Q^{147}$-$S^{232}$-$A^{236}$-$F^{251}$-$W^{252}$) (Table 1). Whereas, sequences for ammonia transport (filter 2: H/W-I/V-G/A-R and P1 P5 residues: T/F-S-A-Y-W/L) (Figure S7) were found in all the TIPs: *Vv*TnTIP1;1 (filter 2: $H^{65}$-$I^{187}$-$A^{196}$-$V^{202}$ and P1 P5 residues: $T^{125}$-$S^{203}$-$A^{207}$-$V^{219}$-$W^{220}$), *Vv*TnTIP2;2 (filter 2: $H^{63}$-$I^{185}$-$G^{194}$-$R^{20}0$ and P1 P5 residues: $T^{123}$-$S^{201}$-$A^{205}$-$V^{217}$-$W^{218}$ and *Vv*TnTIP4;1 (filter 2: $H^{60}$-$V^{183}$-$A^{192}$-$R^{198}$ and P1 P5 residues: $T^{120}$-$S^{199}$-$A^{203}$-$V^{215}$-$W^{216}$) (Table 1). On the other hand, all cloned aquaporins exhibited the signature sequences for $H_2O_2$ transport (filter 2: H/F/W-I/H/V-A/T/G-R/V and P1 P5 residues: T/Q/F-S/A-A-Y/F-W/I) (Figure S8A) and urea transport (filter 2: F/H/G/A/N-I/H/S/V-T/A/G-R/V and P1 P5 residues: M/T/Q/L/F/V/I-S/A/T-A-F/Y-W/F/L) (Figure S8B) (Table 1).

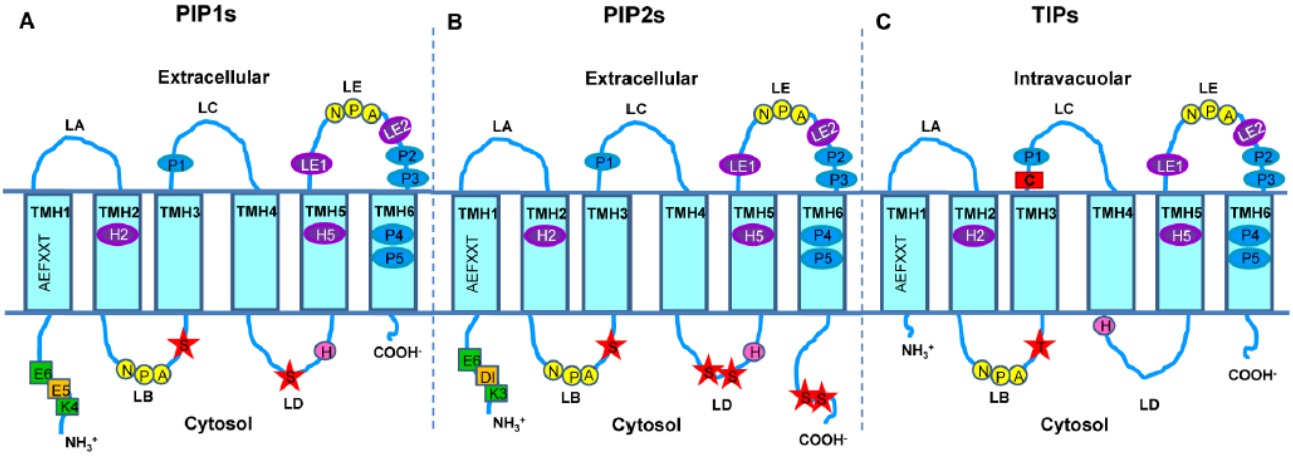


**Figure 3. Schematic representation of predicted topology of *V. vinifera* aquaporins (PIP1s, PIP2s and TIPs) obtained in this study.** These aquaporins consist of six transmembrane domains (TMH1–TMH6), five connecting loops (LA–LE) and N- and C-terminal extremities. The conserved NPA motifs (filter 1) are shown in yellow circles, while residues for ar/R constriction (filter 2) and P1–P5 positions for selectivity of atypical substrates (according to [4]) are shown in purple and blue ovals, respectively. Putative phosphorylation sites are marked as red stars, pH regulation sites are shown as pink rounds, green and yellow rectangles represent methylation and sorting signals. (A) PIP1s subfamily consisting of longer N-terminal with methylation and sorting signals, two putative phosphorylation sites in loop B and D, conserved His in loop D for pH regulation site and shorter C-terminal. (B) PIP2s subfamily having slightly shorter N-terminal with methylation and sorting signals conserved His in loop D for pH regulation, four Ser for putative phosphorylation: one in loop B, two in loop D and two in long C-terminal. (C) TIPs with very short N-terminal without sorting or methylation signals, only one conserved Thr residue instead of Ser residue for putative phosphorylation in loop B, Cys residue (red rectangle) in TMH4 for mercury sensitivity and His residue in loop D for pH regulation.
doi:10.1371/journal.pone.0102087.g003

**Table 1.** Specific amino acid residues for atypical substrates at ar/R constrictions and P1–P5 positions (based on [4]).

| Aquaporins | Putative substrates | ar/R constrictions (filter 2) | | | | P1–P5 positions | | | | | |
|---|---|---|---|---|---|---|---|---|---|---|---|
| | | TMH2 | TMH5 | LE1 | LE2 | P1 | P2 | P3 | P4 | P5 |
| *Vv*TnPIP1;4 | Boron, $CO_2$, $H_2O_2$, urea | $F^{94}$ | $H^{223}$ | $T^{232}$ | $R^{238}$ | $Q^{154}$ | $S^{239}$ | $A^{243}$ | $F^{258}$ | $W^{259}$ |
| *Vv*TnPIP2;1 | Boron, $CO_2$, $H_2O_2$, urea | $F^{84}$ | $H^{213}$ | $T^{222}$ | $R^{228}$ | $Q^{144}$ | $S^{229}$ | $A^{233}$ | $F^{248}$ | $W^{249}$ |
| *Vv*TnPIP2;3 | Boron, $CO_2$, $H_2O_2$, urea | $F^{87}$ | $H^{216}$ | $T^{225}$ | $R^{231}$ | $Q^{147}$ | $S^{232}$ | $A^{236}$ | $F^{251}$ | $W^{252}$ |
| *Vv*TnTIP1;1 | Urea, $NH_3$, $H_2O_2$ | $H^{65}$ | $I^{187}$ | $A^{196}$ | $V^{202}$ | $T^{125}$ | $S^{203}$ | $A^{207}$ | $V^{219}$ | $W^{220}$ |
| *Vv*TnTIP2;2 | Urea, $NH_3$, $H_2O_2$ | $H^{63}$ | $I^{185}$ | $G^{194}$ | $R^{200}$ | $T^{123}$ | $S^{201}$ | $A^{205}$ | $V^{217}$ | $W^{218}$ |
| *Vv*TnTIP4;1 | Urea, $NH_3$, $H_2O_2$ | $H^{60}$ | $V^{183}$ | $A^{192}$ | $R^{198}$ | $T^{120}$ | $S^{199}$ | $A^{203}$ | $V^{215}$ | $W^{216}$ |

doi:10.1371/journal.pone.0102087.t001

## Functional characterization of water transport in yeast strains expressing *V. vinifera* aquaporins

Water transport activity of heterologously expressed *Vitis* aquaporins in yeast strains was assayed by stopped-flow fluorescence spectroscopy. The shrinking rate of yeast cells upon a sorbitol hyperosmotic shock was monitored as change in fluorescence signals (Figure 4A). The strain with empty plasmid (pUG35), devoid of water channels, was used as control ($P_f = 4.30\pm0.28\times10^{-4}$ cm $s^{-1}$). Water permeability ($P_f$) of yeast cells was not affected by the expression of *Vv*TnPIP1;4 ($4.0\pm0.35\times10^{-4}$ cm $s^{-1}$), *Vv*TnPIP2;3 ($5.30\pm0.63\times10^{-4}$ cm $s^{-1}$) and *Vv*TnTIP4;1 ($3.3\pm0.08\times10^{-4}$ cm $s^{-1}$) (Table 2, Figure 4B). Thus, these strains were considered as non-functional for water transport. On the other hand, heterologous expression of *Vv*TnPIP2;1 ($7.43\pm0.64\times10^{-4}$ cm $s^{-1}$), *Vv*TnTIP1;1 ($8.06\pm0.34\times10^{-4}$ cm $s^{-1}$) and *Vv*TnTIP2;2 ($9.65\pm0.026\times10^{-4}$ cm $s^{-1}$) (Table 2, Figure 4B) led to 73%, 88% and 125%, respectively, higher water permeability and were stated as functional for water transport. Among all cloned *Vitis* aquaporins, TIPs (*Vv*TnTIP1;1, *Vv*TnTIP2;2) exhibited higher water conductivity as compared to *Vv*TnPIP2;1.

To evaluate the activation energy for water transport, $P_f$ values of all yeast strains were analyzed in a range of temperatures (9 37°C) and Arrhenius plots were drawn (Figure 5A). As expected, transport of water was strongly dependent on temperature in control yeast strain, as reflected by higher activation energy *Ea* ($14.05\pm0.01$ kcal $mol^{-1}$) (Figure 5B and Table 2). Arrhenius plots for *Vv*TnPIP1;4, *Vv*TnPIP2;3 and *Vv*TnTIP4;1 expressing yeast strains exhibited parallel steep slopes, overlapped with control strain (Figure 5A) and almost similar activation energies ($14.74\pm0.62$, $14.53\pm0.55$, $14.86\pm0.22$ kcal $mol^{-1}$, respectively) (Figure 5B and Table 2). On the other hand, expression of *Vv*TnPIP2;1, *Vv*TnTIP1;1 and *Vv*TnTIP2;2 led to drastic reduction in the activation energies to $10.84\pm0.83$, $8.8\pm0.77$ and $8.77\pm0.62$ kcal $mol^{-1}$, respectively (Figure 5B and Table 2), demonstrating that transport of water was majorly mediated by aquaporins in these yeast strains.

To examine the dose and time dependent effects of mercurial inhibition, yeast strains expressing functional *Vitis* aquaporins (*Vv*TnPIP2;1, *Vv*TnTIP1;1 and *Vv*TnTIP2;2) as well as the control strain were pretreated with various concentrations (0.5 and 1.0 mM) of $HgCl_2$ for 15 to 30 minutes at room temperature, before hyperosmotic shock. Figure 6A compares the stopped-flow signals of yeast cells expressing *Vv*TnTIP2;2, obtained after hyperosmotic shock either in the absence or presence of mercury chloride (0.5 mM) after 15 minutes of incubation. It is clear from the signals that $HgCl_2$ reduced the shrinking rates of the cells. All the functional aquaporins tested were mercury sensitive. TIPs were more sensitive than PIP. $P_f$ was markedly decreased when cells were incubated with 0.5 mM $HgCl_2$ for 15 minutes before the osmotic shock. $P_f$ of *Vv*TnPIP2;1 expressing strain was reduced by 24% while *Vv*TnTIP1;1 and *Vv*TnTIP2;2 expressing strains exhibited 38% and 36% reduction (Figure 6B). Water transport in control cells was not affected by 0.5 mM $HgCl_2$, even after 30 minutes of incubation, while higher concentration (1 mM) reduced the $P_f$ of all yeast strains including the control strain, indicating a general toxicity at this concentration (data not shown).

## Growth assays under osmotic stress and in the presence of atypical substrates

Expression of *Vitis* aquaporins in *S. cerevisiae* was not deleterious to yeast cells, since neither the specific growth rate nor the final biomass of the yeast were affected during growth in standard YNB media. Accordingly, all the strains showed

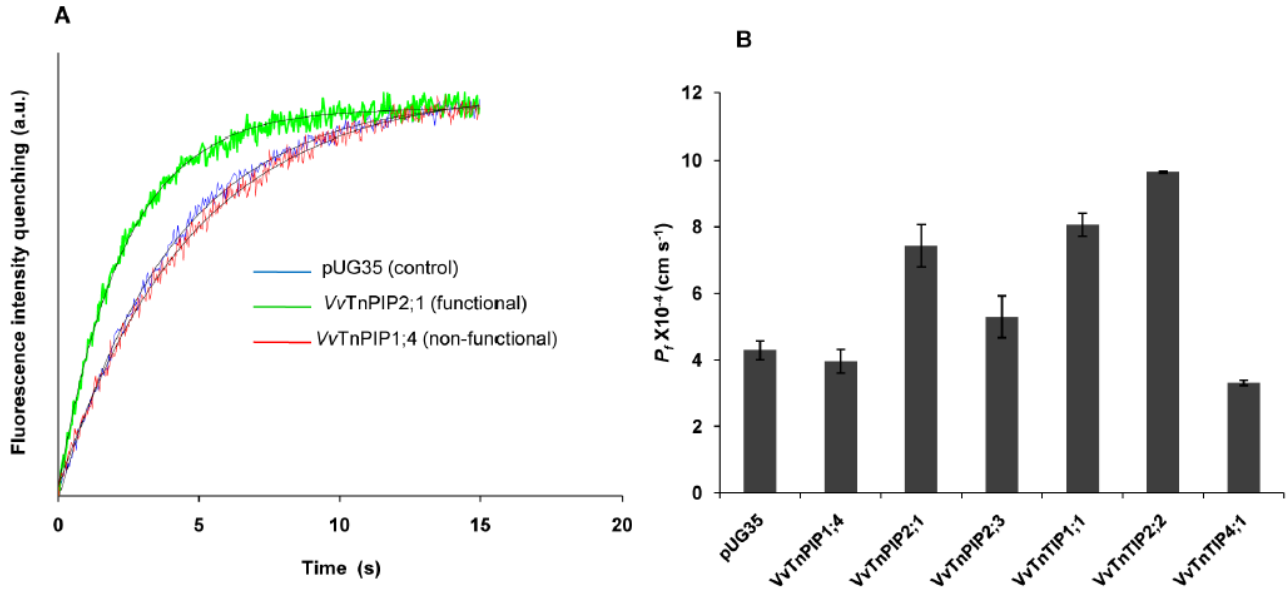


**Figure 4. Stopped-flow assays for measurement of water transport activity of *V. vinifera* aquaporins expressed in yeast.** (A) Typical traces obtained from stopped-flow spectroscopy after hyperosmotic shock. Presented signals are illustrative of ten traces at 23°C obtained from strains expressing functional (*Vv*TnPIP2;1) and non-functional (*Vv*TnTIP4;1) aquaporins for water transport, and control (transformed with empty plasmid pUG35). (B) Water permeability coefficients ($P_f$ at 23°C) of *Vv*TnPIP2;1, *Vv*TnTIP1;1 and *Vv*TnTIP2;2 were higher than control strain. Expression of *Vv*TnPIP1;4, *Vv*TnPIP2;3 and *Vv*TnTIP4;1 did not increase water permeability in yeast cells. Data are mean + SD of three independent experiments with at least ten traces.
doi:10.1371/journal.pone.0102087.g004

approximately 3.5 hours of doubling time and grew up to similar final biomass in liquid YNB media (data not shown).

**Expression of Vitis aquaporins affects the growth of yeast cells under osmotic stress.** Osmotic tolerance/susceptibility of heterologously expressed *Vitis* aquaporins was examined in the presence of NaCl, KCl and sorbitol. When exposed to hyperosmotic stress, yeast cells expressing *Vitis* aquaporins exhibited decreased growth to a variable degree, depending on the types of aquaporins expressed (Figure 7). Growth of all yeast strains (including empty plasmid strain) was equally inhibited in the presence of NaCl, even at lower concentration (0.5 M) (data not shown). At the highest concentration of KCl (1.5 M), cells expressing *Vv*TnTIP4;1 were least inhibited by KCl, while growth of *Vv*TnTIP2;2 and *Vv*TnPIP1;4 expressing cells displayed a clear osmosensitive phenotype followed by *Vv*TnTIP1;1, *Vv*TnPIP2;3 and *Vv*TnPIP2;1 (Figure 7). Growth of these strains was reduced under osmoequivalent concentration of sorbitol (2.1 M), but did not show any clear phenotype (Figure 7).

**Expression of *V. vinifera* aquaporins increases the sensitivity of yeast to $H_2O_2$ and boron.** Ability of *Vitis* aquaporins to facilitate the transport of $H_2O_2$ and boron was examined by drop test assays in the presence of these substrates on solid YNB (pH 5.0). Impaired growth of yeast strains due to the expression *Vitis* aquaporins was tested in the presence of these substrates.

Growth of *Vitis* aquaporins (*Vv*TnPIP1;4, *Vv*TnPIP2;1, *Vv*TnPIP2;3, *Vv*TnTIP1;1 and *Vv*TnTIP2;2) expressing strains was affected by externally supplied $H_2O_2$ in a dose dependent manner (Figure 8). Impaired growth of *Vitis* aquaporins expressing strains was observed at higher concentration of $H_2O_2$ (0.75 mM) (Figure 8), while the control strain was able to grow up to the last dilution at 1.0 mM $H_2O_2$. Growth of the strain expressing *Vv*TnTIP2;2 was most severely inhibited, followed by *Vv*TnTIP1;1, *Vv*TnPIP2;3, *Vv*TnPIP1;4 and *Vv*TnPIP2;1 expressing strains (Figure 8). Cells expressing *Vv*TnTIP4;1 were least sensitive toward $H_2O_2$ and exhibited similar growth as the control strain.

The ability of *Vitis* aquaporins to facilitate boron transport was tested in the same way as $H_2O_2$. Yeast transformants were spotted

**Table 2.** Water transport activity in *V. vinifera* aquaporins expressed in *S. cerevisiae*.

| Yeast strains expressing *Vitis* aquaporins | Permeability coefficient ($P_f$) (cm s$^{-1}$)×10$^{-4}$ | Activation energy (*Ea*) (kcal mol$^{-1}$) |
|---|---|---|
| pUG35 | 4.3±0.28 | 14.05±0.01 |
| *Vv*TnPIP1;4 | 4.0±0.35 | 14.74±0.62 |
| *Vv*TnPIP2;1 | 7.43±0.64 | 10.84±0.83 |
| *Vv*TnPIP2;3 | 5.30±0.63 | 14.53±0.55 |
| *Vv*TnTIP1;1 | 8.06±0.34 | 8.79±0.77 |
| *Vv*TnTIP2;2 | 9.65±0.03 | 8.77±0.62 |
| *Vv*TnTIP4;1 | 3.31±0.08 | 14.86±0.22 |

Data are mean ± SD of three independent experiments with at least ten traces.
doi:10.1371/journal.pone.0102087.t002

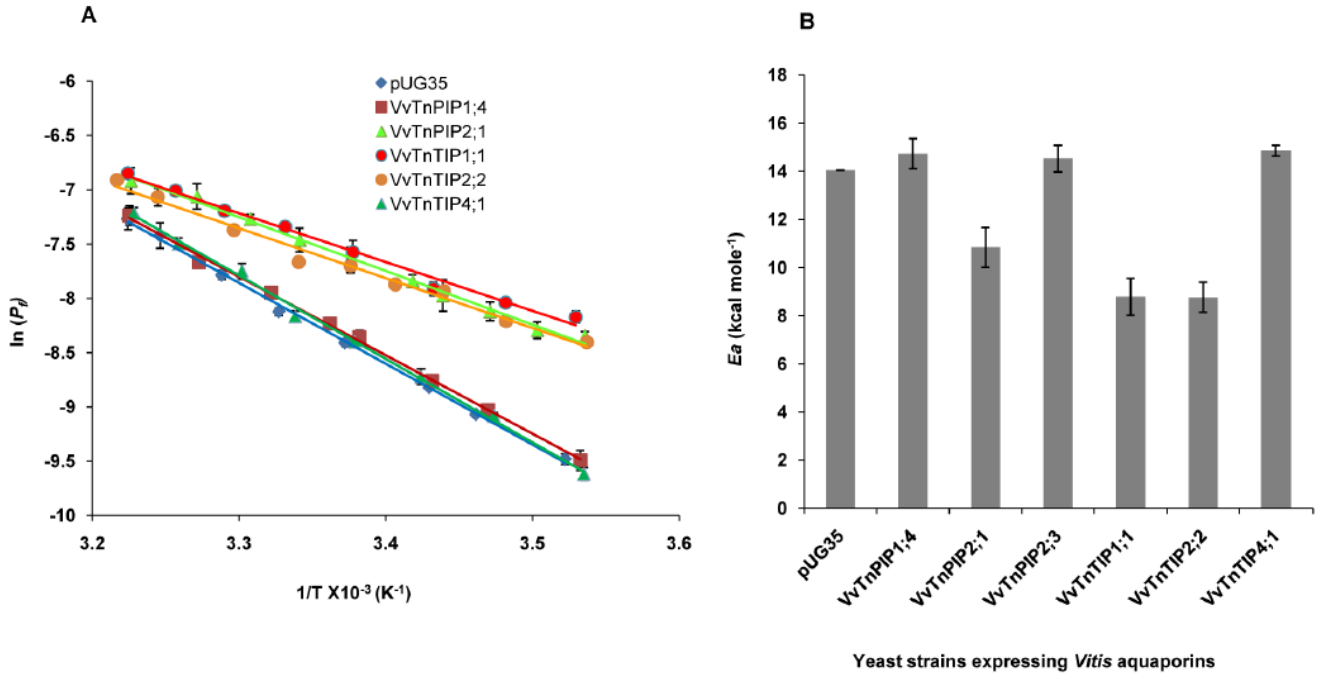


**Figure 5. Activation energies (*Ea*) of water transport in *V. vinifera* aquaporins expressed in yeast.** (A) Arrhenius plot of $P_f$ at temperature range (9–37°C), where T is temperature in Kelvin. *Ea* was evaluated from the slopes. Strains expressing *Vv*TnPIP1;4, *Vv*TnTIP4;1 and empty plasmid (pUG35) showed steeper slope, while strains expressing *Vv*TnPIP2;1, *Vv*TnTIP1;1 and *Vv*TnTIP2;2 exhibited shallow slope. (B) Calculated *Ea* from the slope showed that *Vv*TnPIP2;1, *Vv*TnTIP1;1 and *Vv*TnTIP2;2 expressing strains exhibited lower *Ea*, while *Vv*TnPIP1;4, *Vv*TnPIP2;3 and *Vv*TnTIP4;1 expressing strains showed were almost equal to control strain (pUG35). Data are mean + SD of three independent experiments with at least five traces (ten traces in case of $P_f$ at 23°C) at each temperature.
doi:10.1371/journal.pone.0102087.g005

on YNB plates containing various concentrations of boron as boric acid (Figure 9). The exposure to boric acid (40 mM) caused reduced growth of strains expressing *Vitis* aquaporin. Interestingly, at 40 mM boric acid, cells transformed with *Vv*TnTIP4;1 grew better in comparison to control strain, but these cells showed clear sensitivity toward boric acid when exposed to higher concentration (60 mM) of boric acid. Heterologous expression of all cloned *Vitis* aquaporins, except *Vv*TnPIP2;1, showed increased sensitivity to 60 mM boric acid. *Vv*TnPIP2;1 expressing strain was the most tolerant to externally supplied boric acid and was able to grow as the control strain. Growth of *Vv*TnTIP2;2 expressing strain was severely inhibited by boric acid exposure (Figure 9).

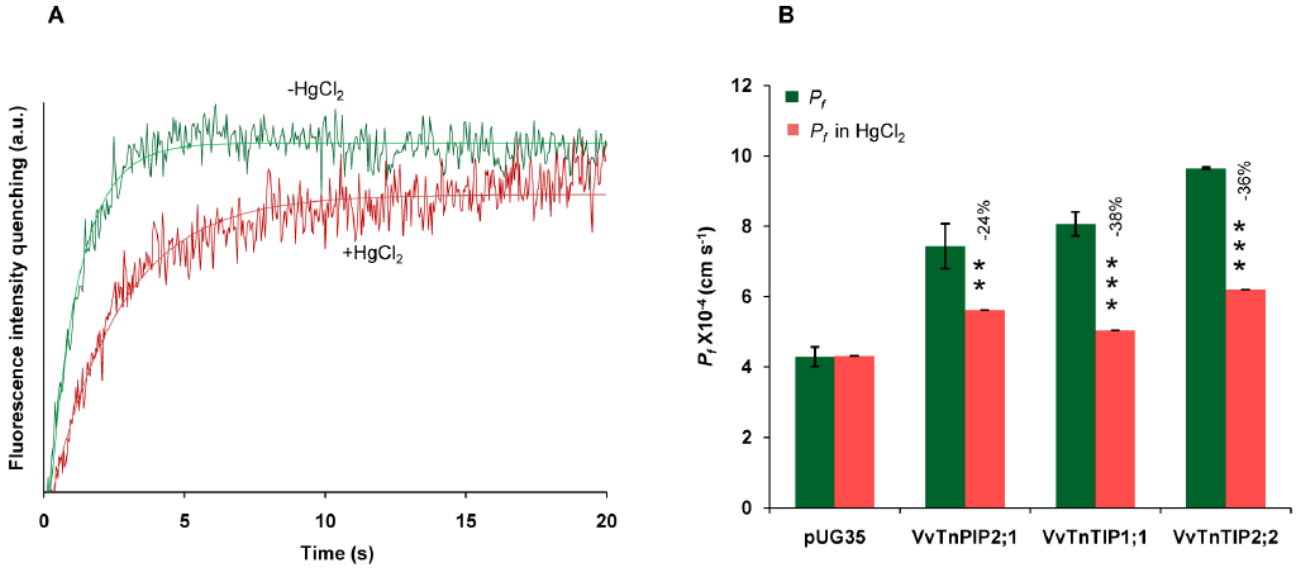


**Figure 6. Inhibition of water permeability by mercury chloride ($HgCl_2$) in yeast strains expressing *V. vinifera* aquaporins.** (A) Inhibition of water permeability in yeast cells expressing functional aquaporin (*Vv*TnTIP2;2) by $HgCl_2$. The green signal represents water permeability without $HgCl_2$ and the red signal shows the lower permeability when cells were incubated with 0.5 mM $HgCl_2$ for 15 minutes prior to osmotic shock. (B) Water permeability coefficients ($P_f$ at 23°C) of *Vv*TnPIP2;1, *Vv*TnTIP1;1 and *Vv*TnTIP2;2 were reduced by 0.5 mM $HgCl_2$. Data are mean + SD of three independent experiments with at least five traces. The data were analyzed by *t-test* and asterisks above bars indicate statistically significant differences, where **p<0.01, ***p<0.001.
doi:10.1371/journal.pone.0102087.g006

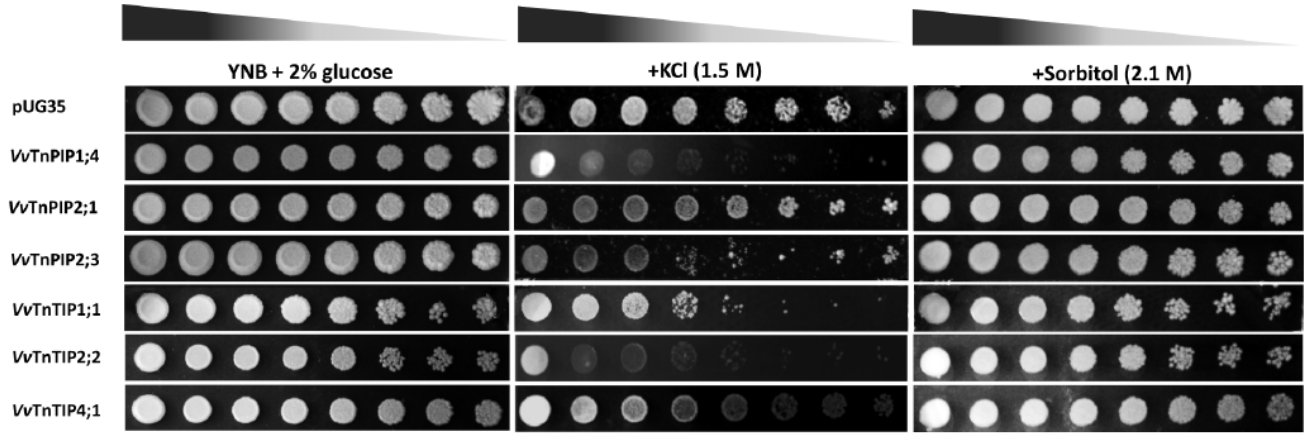


**Figure 7. Growth assays of *S. cerevisiae* strains expressing *V. vinifera* aquaporins under osmotic stress.** Hyperosmotic stress was exerted by osmo-equivalent concentration of either KCl or sorbitol. Yeast strain transformed with empty pUG35 plasmid was used as control (pUG35). Yeast suspensions were spotted in 10-fold dilution on solid YNB plates without or with 1.5 M KCl or 2.1 M sorbitol. Growth was recorded after two weeks at 28°C. Photographs shown are representative of three independent experiments with consistent results.
doi:10.1371/journal.pone.0102087.g007

We also performed the growth assays of yeast strains expressing *Vitis* aquaporins in the presence of ammonia and urea, to explore their possible transport by aquaporins. We observed that growth of yeast strains was not affected by these substrates at any tested concentrations, since no distinct growth phenotypes were observed (results not shown).

## Discussion

In this study we have cloned and characterized three plasma membrane (PIPs) and three tonoplast (TIPs) aquaporins from *Vitis vinifera* cv. Touriga nacional, an important Portuguese cultivar, widely believed to produce the finest red wines of Portugal.

All the cloned full length aquaporin genes from *V. vinifera* (cv. Touriga nacional) encoding three PIPs (*Vv*TnPIP1;4, *Vv*TnPIP2;1 and *Vv*TnPIP2;3) and TIPs (*Vv*TnTIP1;1, *Vv*TnTIP2;2 and *Vv*TnTIP4;1) proteins showed obvious similarity with the same proteins of the database variety of *V. vinifera* (cv. Pinot noir). Their plasma membrane localization was confirmed by GFP-tagging, although we observed a partial retention in intracellular structures, probably in endoplasmic reticulum or in vesicles of secretory pathway (reviewed by [6]). Several reports suggest that a fraction of intracellular plant aquaporins (TIPs) is generally "miss-targeted" to the plasma membrane of heterologous models, which enabled the researchers to measure their water transport activity in *Xenopus* and yeast (reviewed by [44]).

Their sequence analysis for topological prediction revealed all the characteristics of typical aquaporin subfamilies. Specific residues for transport of ammonia (filter 2: H/W-I/V-G/A-R and P1 P5 residues: T/F-S-A-Y-W/L), boron (filter 2: F/A/G-H/I/S-T/G/A-R and P1 P5 residues: Q/F/I-S/T-A-F/Y-W/L), $CO_2$ (filter 2: F-H-T-R and P1 P5 residues: Q/M-S-A-F-W), $H_2O_2$ (filter 2: H/F/W-I/H/V-A/T/G-R/V and P1 P5 residues: T/Q/F-S/A-A-Y/F-W/I) and urea (filter 2: F/H/G/A/N-I/H/S/V-T/A/G-R/V and P1 P5 residues: M/T/Q/L/F/V/I-S/A/T-A-F/Y-W/F/L) were present at ar/R constriction and P1 P5 positions [4] of the cloned *Vitis* aquaporins, depending on their subfamilies (Table 1).

Expression of functional aquaporins *Vv*TnPIP2;1, *Vv*TnTIP1;1 and *Vv*TnTIP2;2 increased the water permeability coefficient ($P_f$) and reduced the activation energy (*Ea*) required for water transport in yeast cells, while expression of non-functional aquaporins *Vv*TnPIP1;4, *Vv*TnPIP2;3 and *Vv*TnTIP4;1 expression exhibited higher *Ea* and did not affect $P_f$. The obtained

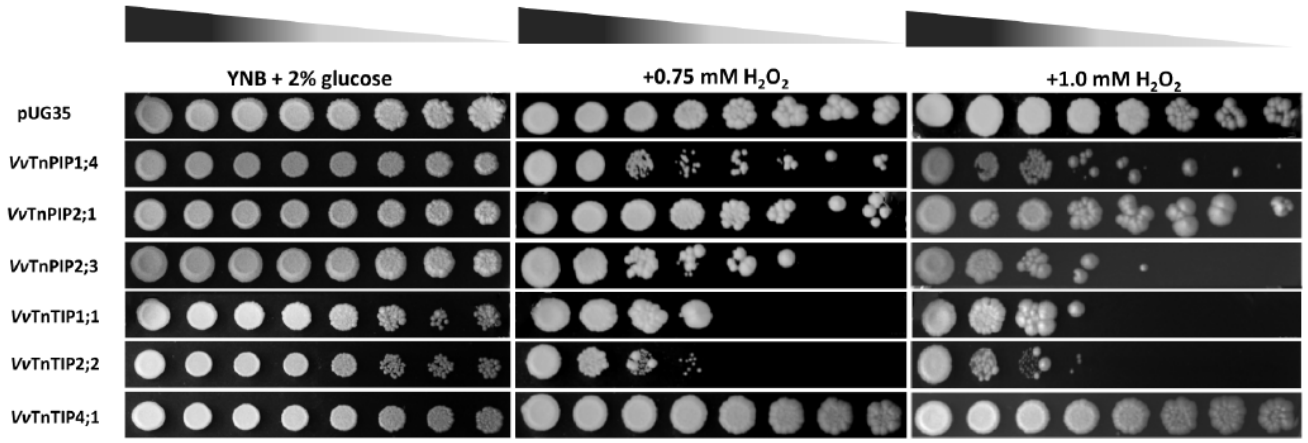


**Figure 8. Growth assays of *S. cerevisiae* strains expressing *V. vinifera* aquaporins on $H_2O_2$ containing minimal media.** Yeast strain transformed with empty pUG35 plasmid was used as control (pUG35). Yeast suspensions were spotted in 10-fold dilution on solid YNB plates without or with 0.75 mM and 1.0 mM $H_2O_2$. Growth was recorded after two weeks at 28°C. Photographs shown are representative of three independent experiments with consistent results.
doi:10.1371/journal.pone.0102087.g008

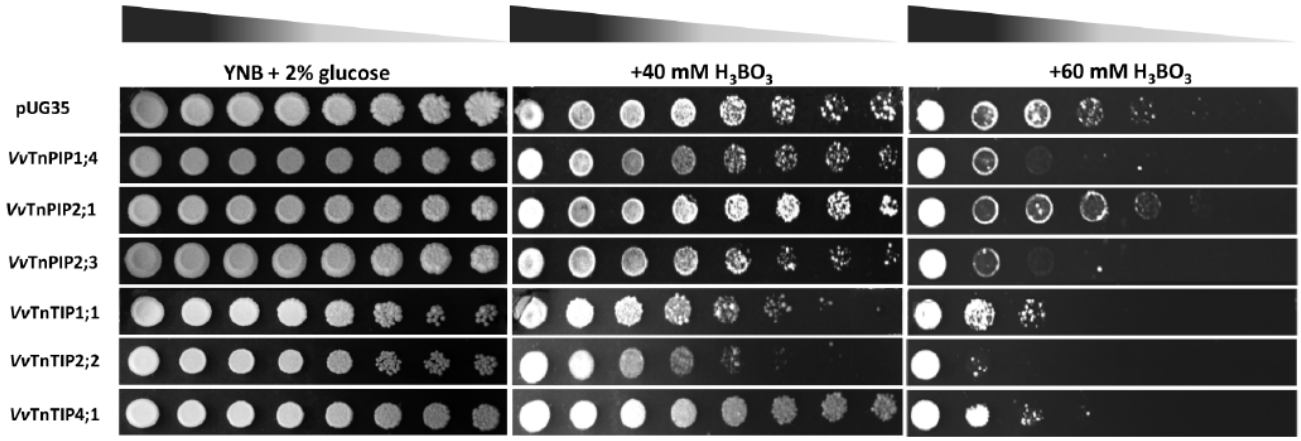


**Figure 9. Growth assays of *S. cerevisiae* strains expressing *V. Vinifera* aquaporins on minimal medium containing boric acid.** Yeast strain transformed with empty pUG35 plasmid was the control (pUG35). Yeast suspensions were spotted in 10-fold dilution on solid YNB plates without or with 40 mM and 60 mM boric acid. Growth was recorded after two weeks at 28°C. Photographs shown are representative of three independent experiments with consistent results.
doi:10.1371/journal.pone.0102087.g009

higher *Ea* and lower $P_f$ can not be correlated with their lower plasma membrane expression since all the functional aquaporins were also partially retained at various subcellular regions and, on the other hand, one of the aquaporins (*Vv*TnTIP4;1) showed to be localized at the plasma membrane of *S. cerevisiae* and exhibited low water transport.

TIPs (*Vv*TnTIP1;1 and *Vv*TnTIP2;2) exhibited higher water conductivity in comparison to PIP (*Vv*TnPIP2;1). This finding is in agreement with previous reports of heterologously expressed plant aquaporins [41,45,46]. Higher water permeability of TIPs may be required for the central role of vacuole in osmoregulation of the cytoplasm. Constitutively higher water permeability of tonoplast aquaporins may allow the cells to use the vacuolar space to maintain the cellular integrity, in case of osmotic fluctuations caused by rapid water exchange during stress or developmental stages of plants (reviewed in [43,45]).

All functional *Vitis* aquaporins were found to be mercury-sensitive, as their $P_f$ was reduced by mercury chloride. Many plant aquaporins have been inhibited by mercurial reagents, which bind to a conserved cysteine residue located downstream to first NPA motif, subsequently blocking the pore and shutting-down the aqueous pathway (reviewed in [3]). Notably all cloned TIPs showed the conserved cysteine residue responsible for mercury sensitivity (Figure S5A). Although PIPs (except *Vv*TnPIP2;3) did not have the conserved cysteine at the same position of alignment, they have four conserved cysteine residues in second and third transmembrane helices and one of these residues may represent the mercury sensitive site [47].

Transport of solutes of physiological significance, such as $CO_2$, $H_2O_2$, boron or silicic acid is now well established and has linked aquaporins to many functions, including carbon metabolism, oxidative stress responses, and plant mineral nutrition [3]. We performed a broad screening of growth sensitivity test of all cloned *Vitis* aquaporins on $H_2O_2$ and boric acid containing plates to investigate their ability to transport these atypical substrates. The phenotypic growth variations showed that heterologous expression of all cloned *Vitis* aquaporins (except *Vv*TnTIP4;1) caused more susceptibility to externally applied $H_2O_2$, indicating their putative role in $H_2O_2$ transport. In principle, increased level of $H_2O_2$ can disturb the cellular metabolism in an unidentified manner, which may lead to reduced or impaired growth of yeast cells. A higher permeability of $H_2O_2$ by heterologously expressed aquaporins might have increased the influx of $H_2O_2$ into yeast cells and eventually triggered the cell death or growth inhibition. $H_2O_2$, a long-lived reactive oxygen species (ROS) shares molecular properties with water, it can form hydrogen bonds and has similar permeability as water [48,49]. Based on the sensitivity of yeast cells expressing *Vitis* aquaporins, we assume that both *Vitis* PIPs and TIPs may permeate $H_2O_2$. Similar results were previously reported in heterologously expressed *Arabidopsis* [50 52] and maize aquaporins [53] expressed in *S. cerevisiae*. It is noteworthy that putative amino acids for $H_2O_2$ transport were found at ar/R constriction of all cloned *Vitis* aquaporins. Besides a potential threat to biological components, $H_2O_2$ also acts as a physiologically important molecule to activate $Ca^{2+}$ channels for NADPH oxidase activity required during root hair growth and stomatal movement [54]. Under stress, $H_2O_2$ can be compartmentalized in various intracellular organelles as well as outside of the cells in apoplastic regions [55]. Further, the extracellular accumulated $H_2O_2$ can act as a regulator of water homeostasis by triggering the PIP internalization in *Arabidopsis* roots and consequently reduces the water permeability in roots under stress [56]. The role of *Vitis* PIPs may be involved in apoplastic exclusion of excess $H_2O_2$. Our results indicate that not only plasma membrane aquaporins (PIPs), but also tonoplast aquaporins (TIPs) are involved in $H_2O_2$ transport. Results of growth assays suggest that the cells expressing TIPs were more sensitive as compared with the cells expressing PIPs. TIPs are reported to be more diverse transporters and can conduct many solutes other than water due to having relatively weak selectivity (reviewed in [52,57]). Under elevated stress conditions, plant TIPs are suggested to transport high amounts of $H_2O_2$ into vacuoles, resulting in their further detoxification by vacuolar peroxidases using vacuole stored flavanoids as an electron donors [50]. Expression level of TIPs was found to be affected by $H_2O_2$ in tulip flowers [58] and it was suggested that TIPs triggered the ROS translocation into the vacuoles for their detoxification [57].

When exposed to $H_2O_2$, all yeast cells exhibited fluffy and larger colony morphology with rough edges (results not shown). $H_2O_2$ induces aging of the cells by releasing free radicals, leading to higher number of old cells which are bigger in size in comparison to young cells and eventually make the larger colonies with mature

cells [59]. Fluffy and rough surface colonies may represent a metabolic strategy of growth under unfavorable conditions [60].

Growth assays in the presence of boric acid showed that strains expressing *Vitis* aquaporins were more sensitive in comparison to control strain. Heterologous expression of plant aquaporins either in *Xenopus laevis* oocytes or *S. cerevisiae*, suggests that besides other routes, boron can be transported through PIPs [61,62] and NIPs [63 66]. NIP5;1 and NIP6;1 of *Arabidopsis thaliana* were identified as boric acid channels and were up-regulated under limited boron supply to accomplish the demand of boric acid [63,64]. Although boron is an essential micronutrient for plants, when accumulated at higher concentration it leads to toxicity. Being a non-charged molecule, boric acid can passively diffuse across lipid bilayer, but only significantly at high concentration gradient caused by high boron supply [67]. In plants, urea (*DUR3*) and glycerol (*FPS1*) transporters were identified as boron importers, while *BOR1* and its homolog *ScBOR1* of *S. cerevisiae* were characterized as boron exporters, exporting boron and protecting the cells from boron toxicity [68]. In this work, all the yeast strains expressing *Vitis* aquaporins have the same background for passive diffusion or importers and exporters of boric acid in their native membrane. Since different levels of toxicity were detected (Figure 9), we can speculate the putative transport of boron by *Vitis* aquaporins resulting in growth inhibition. Similarly, heterologously expressed barley *Hv*NIP2;1 [66], *Hv*PIP1;3 and *Hv*PIP1;4 [62] displayed sensitive growth phenotype in the presence of boron and were identified as boron transporters. Interestingly, all PIPs exhibited the signature sequences for boron transport and showed sensitivity (except *Vv*TnPI2;1) to boric acid. On the contrary, these conserved residues were not present in TIPs, although yeast strains expressing TIPs also exhibited increased sensitivity toward boron.

Although these studies are based on the molecular analysis of ar/R regions of *Vitis* aquaporins and indirect yeast based sensitivity growth assays on these substrates, transport of $H_2O_2$ and boron by *Vitis* aquaporins can be hypothesized.

In conclusion, we have cloned six PIPs and TIPs aquaporins from grapevine (cv. Touriga nacional) in *S. cerevisiae*, and have shown that three of them facilitate the transport of water. Reduced growth and survival of *Vitis* aquaporins expressing yeast cells in the presence of $H_2O_2$ and boron, indicates their probable role in transport of these non-aqua substrates. Additionally, expression of three aquaporins in yeast, which were found non-functional for water transport, exhibited sensitive phenotype when grown in the presence of these substrates, suggests their possible role in transport of substrates other than water. The combined use of molecular analysis of their sequences and functional investigation of growth sensitivity assays provided the initial insight on the selectivity profiles of *Vitis* aquaporins. Further studies are required to ascertain the role of *Vitis* aquaporins in transport of $H_2O_2$ and boron. Moreover, co-expression of aquaporins in *S. cerevisiae* may represent the next step for better understanding their interaction and regulation in plants.

## Supporting Information

**Figure S1 Comparison of *V. vinifera* aquaporins from Pinot noir and Touriga nacional cultivars.** Alignment of deduced amino acid sequences of *Vv*TnPIP1;4 (A), *Vv*TnPIP2;1 (B), *Vv*TnPIP2;3 (C), *Vv*TnTIP1;1 (D), *Vv*TnTIP2;2 (E), *Vv*TnTIP4;1 (F) obtained from the present study (Touriga nacional) with the database variety (Pinot noir). Accession numbers of presented protein sequences are: *Vv*PnPIP1;4 (CAO39626), *Vv*TnPIP1;4 (KJ697714), *Vv*PnPIP2;1 (CAN75442), *Vv*TnPIP2;1 (KJ697715), *Vv*PnPIP2;3 (CAO18152), *Vv*TnPIP2;3 (KJ697716), *Vv*PnTIP1;1 (CAO69259), *Vv*TnTIP1;1 (KJ697717), *Vv*PnTIP2;2 (CAO23095), *Vv*TnTIP2;2 (KJ697718), *Vv*PnTIP4;1 (CAO44039), *Vv*TnTIP4;1 (KJ697719).
(PDF)

**Figure S2 Comparison of N- (A) and C- (B) terminals of PIP1s, PIP2s and TIPs aquaporins.** Aquaporins cloned in the present study are marked with red arrows. Accession numbers of presented protein sequences are: *At*PIP2;1 (P43286), *At*-deltaTIP2 (CAB10515), *At*-gammaTIP3 (AAC62778), *At*-epsilon-TIP (AAC42249), *Fa*PIP2;1 (ADJ67992), *Pv*-alphaTIP (CAA44669), *So*PIP2;1 (4JC6_N), *Vv*PnPIP1;1 (CAO41326), *Vv*TnPIP1;1 (HQ913643), *Vv*PnPIP1;4 (CAO39626), *Vv*TnPIP1;4 (KJ697714), *Vv*PnPIP2;1 (CAN75442), *Vv*TnPIP2;1 (KJ697715), *Vv*PnPIP2;2 (CAO47394), *Vv*TnPIP2;2 (HQ913642), *Vv*PnPIP2;3 (CAO18152), *Vv*TnPIP2;3 (KJ697716), *Vv*PnTIP1;1 (CAO69259), *Vv*TnTIP1;1 (KJ697717), *Vv*PnTIP2;1 (CAO45860), *Vv*TnTIP2;1 (HQ913640), *Vv*PnTIP2;2 (CAO23095), *Vv*TnTIP2;2 (KJ697718), *Vv*PnTIP4;1 (CAO44039), *Vv*TnTIP4;1 (KJ697719), *Zm*PIP2;1 (Q84RL7), *Zm*PIP2;5 (Q9XF58). *At*: *Arabidopsis thaliana*, *Fa*: *Fragaria*×*ananassa*, *Pv*: *Phaseolus vulgaris*, *So*: *Spinacia oleracea*, *Vv*Pn: *Vitis vinifera* cv. Pinot noir, *Vv*Tn: *V. vinifera* cv. Touriga nacional.
(PDF)

**Figure S3 Presence of methylation and sorting signal sequences (D/E-X-D/E) at N-terminal (A) and pH regulation site (His residue) for gating (B) of PIPs aquaporins.** Consensus sequences are framed and conserved residues are indicated as red triangle. Aquaporins cloned in the present study are marked with red arrows. Accession numbers of presented protein sequences are: *At*PIP2;1 (P43286), *At*PIP1;2 (Q06611), *At*PIP1;4 (Q39196), *Fa*PIP2;1 (ADJ67992), *So*PIP2;1 (4JC6_N), *Vv*PnPIP1;1 (CAO41326), *Vv*TnPIP1;1 (HQ913643), *Vv*PnPIP1;4 (CAO39626), *Vv*TnPIP1;4 (KJ697714), *Vv*PnPIP2;1 (CAN75442), *Vv*TnPIP2;1 (KJ697715), *Vv*PnPIP2;2 (CAO47394), *Vv*TnPIP2;2 (HQ913642), *Vv*PnPIP2;3 (CAO18152), *Vv*TnPIP2;3 (KJ697716), *Zm*PIP2;1 (Q84RL7), *Zm*PIP2;5 (Q9XF58), *Zm*PIP2;4 (Q9ATM6). *At*: *Arabidopsis thaliana*, *Fa*: *Fragaria*×*ananassa*, So: *Spinacia oleracea*, *Vv*Pn: *Vitis vinifera* cv. Pinot noir, *Vv*Tn: *V. vinifera* cv. Touriga nacional, *Zm*: *Zea mays*.
(PDF)

**Figure S4 Putative phosphorylation sites in aquaporins.** Ser residue in PIPs and Thr residue in TIPs aquaporins in loop B (A), loop D (B) and C-terminal (C) are tentative phosphorylation sites. Consensus sequences are framed and conserved residues are indicated as red triangle. Aquaporins cloned in the present study are marked with red arrows. Accession numbers of presented protein sequences are: *At*PIP1;2 (Q06611), *At*PIP1;4 (Q39196), *At*PIP2;1 (P43286), *At*-deltaTIP2 (CAB10515), *At*-gammaTIP3 (AAC62778), *At*-alphaTIP (AAC42249), *Fa*PIP2;1 (ADJ67992), *So*PIP2;1 (4JC6_N), *Vv*PnPIP1;1 (CAO41326), *Vv*TnPIP1;1 (HQ913643), *Vv*PnPIP1;4 (CAO39626), *Vv*TnPIP1;4 (KJ697714), *Vv*PnPIP2;1 (CAN75442), *Vv*TnPIP2;1 (KJ697715), *Vv*PnPIP2;2 (CAO47394), *Vv*TnPIP2;2 (HQ913642), *Vv*PnPIP2;3 (CAO18152), *Vv*TnPIP2;3 (KJ697716), *Vv*PnTIP1;1 (CAO69259), *Vv*TnTIP1;1 (KJ697717), *Vv*PnTIP2;1 (CAO45860), *Vv*TnTIP2;1 (HQ913640), *Vv*PnTIP2;2 (CAO23095), *Vv*TnTIP2;2 (KJ697718), *Vv*PnTIP4;1 (CAO44039), *Vv*TnTIP4;1 (KJ697719), *Zm*PIP2;1 (Q84RL7), *Zm*PIP2;4 (Q9ATM6), *Zm*PIP2;5 (Q9XF58). *At*: *Arabidopsis*

*thaliana*, *Fa*: *Fragaria*×*ananassa*, *Pv*: *Phaseolus vulgaris*, *So*: *Spinacia oleracea*, *Vv*Pn: *Vitis vinifera* cv. Pinot noir, *Vv*Tn: *V. vinifera* cv. Touriga nacional, *Zm*: *Zea mays*.
(PDF)

**Figure S5 Mercury sensitive site and pH regulation site in TIPs.** Alignment of TIPs aquaporins for (A) mercury sensitive site (Cys residue) and (B) pH regulation site (His residue) for gating. Consensus sequences are framed and conserved residues are indicated as red triangle. TIPs cloned in the present study are marked with red arrows. Accession numbers of presented protein sequences are: *At*-deltaTIP2 CAB10515), *At*-gammaTIP3 (AAC62778), *At*-alphaTIP (AAC42249), *Pv*-alphaTIP (CAA44669), *Vv*PnTIP1;1 (CAO69259), *Vv*TnTIP1;1 (KJ697717), *Vv*PnTIP2;1 (CAO45860), *Vv*TnTIP2;1 (HQ913640), *Vv*PnTIP2;2 (CAO23095), *Vv*TnTIP2;2 (KJ697718), *Vv*PnTIP4;1 (CAO44039), *Vv*TnTIP4;1 (KJ697719). *At*: *Arabidopsis thaliana*, *Pv*: *Phaseolus vulgaris*, *Vv*Pn: *Vitis vinifera* cv. Pinot noir, *Vv*Tn: *V. Vinifera* (cv. Touriga nacional).
(PDF)

**Figure S6 Consensus sequences for transport of boron and $CO_2$.** Alignment of putative amino acids of aquaporins of *V. Vinifera* (cv. Touriga nacional) obtained from present study and previous study [17] with the sequences of aquaporins reported to transport (A) boron and (B) $CO_2$. ar/R constrictions and P1 P5 positions are shown to demonstrate the conserved amino acid residue. Accession numbers of presented protein sequences are: *At*PIP1;2 (Q06611), *At*NIP5;1 (NP_192776), *Hv*PIP1;3 (BAA23745), *Hv*PIP2;1 (BAA23744), *Nt*AQP1 (O24662), *Os*-NIP2;1 (Q6Z2T3), *Vv*TnPIP1;1 (HQ913643), *Vv*TnPIP1;4 (KJ697714), *Vv*TnPIP2;1 (KJ697715), *Vv*TnPIP2;2 (HQ913642), *Vv*TnPIP2;3 (KJ697716), *Vv*TnTIP1;1 (KJ697717), *Vv*TnTIP2;1 (HQ913640), *Vv*TnTIP2;2 (KJ697718), *Vv*TnTIP4;1 (KJ697719), *Zm*PIP1;1 (Q41870). *At*: *Arabidopsis thaliana*, *Hv*: *Hordeum vulgare*, *Vv*Tn: *V. vinifera* (cv. Touriga nacional), *Zm*: *Zea mays*.
(PDF)

**Figure S7 Consensus sequences for transport of ammonia.** Alignment of putative amino acids of aquaporins of *V. Vinifera* (cv. Touriga nacional) obtained from present study and previous study [17] with sequences of aquaporins reported to transport ammonia. ar/R constrictions and P1 P5 positions are shown to demonstrate the conserved amino acid residue. Accession numbers of presented protein sequences are: *At*TIP2;1 (Q41951), *At*TIP2;3 (Q9FGL2), *Gm*NOD26 (P08995), *Ta*TIP2;1 (AAS19468),*Vv*TnPIP1;1 (HQ913643), *Vv*TnPIP1;4 (KJ697714), *Vv*TnPIP2;1 (KJ697715), *Vv*TnPIP2;2 (HQ913642), *Vv*TnPIP2;3 (KJ697716), *Vv*TnTIP1;1 (KJ697717), *Vv*TnTIP2;1 (HQ913640), *Vv*TnTIP2;2 (KJ697718), *Vv*TnTIP4;1 (KJ697719). *At*: *Arabidopsis thaliana*, *Gm*: *Glycine max*, *Ta*: *Triticum aestivum*, *Vv*Tn: *V. Vinifera* (cv. Touriga nacional).
(PDF)

**Figure S8 Consensus sequences for transport of $H_2O_2$ and urea.** Alignment of putative amino acids of aquaporins of *V. Vinifera* (cv. Touriga nacional) obtained from present study and previous study [17] with sequences of aquaporins reported to transport (A) $H_2O_2$ and (B) urea. ar/R constrictions and P1 P5 positions are shown to demonstrate the conserved amino acid residue. Accession numbers of presented protein sequences are: *At*TIP1;1 (P25818), *At*TIP1;2 (Q41963), *At*TIP1;3 (NP_192056), *At*TIP2;1 (Q41951), *At*TIP2;3 (Q9FGL2), *At*PIP2;4 (Q9FF53), *Cp*NIP1 (CAD67694), *Nt*AQP1 (O24662), *Nt*TIPa (Q9XG70), *Os*NIP2;1 (Q6Z2T3), *Vv*TnPIP1;1 (HQ913643), *Vv*TnPIP1;4 (KJ697714), *Vv*TnPIP2;1 (KJ697715), *Vv*TnPIP2;2 (HQ913642), *Vv*TnPIP2;3 (KJ697716), *Vv*TnTIP1;1 (KJ697717), *Vv*TnTIP2;1 (HQ913640), *Vv*TnTIP2;2 (KJ697718), *Vv*TnTIP4;1 (KJ697719), *Zm*PIP1;5 (Q9AR14). *At*: *Arabidopsis thaliana*, *Cp*: *Cucurbita pepo*, *Nt*: *Nicotiana tabacum*, *Os*: *Oryza sativa*, *Vv*Tn: *Vitis vinifera* (cv. Touriga nacional), *Zm*: *Zea mays*.
(PDF)

**Table S1 Primers used in this work (restriction sites are underlined).**
(PDF)

## Acknowledgments

We thank Sara Amâncio and Luísa Carvalho, ISA-ULisboa for providing cDNAs of *V. vinifera* cv. Touriga nacional.

## Author Contributions

Conceived and designed the experiments: FS MJL MCD TFM GS CP. Performed the experiments: FS MJL APM CP. Analyzed the data: FS APM MCD TFM GS CP. Contributed reagents/materials/analysis tools: MCD GS. Contributed to the writing of the manuscript: FS MJL APM MCD TFM GS CP.

## References

1. Vandeleur RK, Mayo G, Shelden MC, Gilliham M, Kaiser BN, et al. (2009) The role of plasma membrane intrinsic protein aquaporins in water transport through roots: diurnal and drought stress responses reveal different strategies between isohydric and anisohydric cultivars of grapevine. Plant Physiol 149: 445 460.
2. Danielson JA, Johanson U (2008) Unexpected complexity of the aquaporin gene family in the moss *Physcomitrella patens*. BMC Plant Biol 8: 45.
3. Maurel C, Verdoucq L, Luu DT, Santoni V (2008) Plant aquaporins: membrane channels with multiple integrated functions. Annu Rev Plant Biol 59: 595 624.
4. Hove RM, Bhave M (2011) Plant aquaporins with non-aqua functions: deciphering the signature sequences. Plant Mol Biol 75: 413 430.
5. Maurel C, Chrispeels MJ (2001) Aquaporins. A molecular entry into plant water relations. Plant Physiol 125: 135 138.
6. Chaumont F, Moshelion M, Daniels MJ (2005) Regulation of plant aquaporin activity. Biol Cell 97: 749 764.
7. Soveral G, Madeira A, Loureiro-Dias MC, Moura TF (2008) Membrane tension regulates water transport in yeast. Biochim Biophys Acta 1778: 2573 2579.
8. Baiges I, Schäffner A, Mas A (2001) Eight cDNA encoding putative aquaporins in *Vitis* hybrid Richter-110 and their differential expression. J Exp Bot 52: 1949 1951.
9. Flexas J, Galmés J, Gallé A, Gulías J, Pou A, et al. (2010) Improving water use efficiency in grapevines: potential physiological targets for biotechnological improvement. Aust J Grape and Wine 16: 106 121.
10. Hayes MA, Davies C, Dry IB (2007) Isolation, functional characterization, and expression analysis of grapevine (*Vitis vinifera* L.) hexose transporters: differential roles in sink and source tissues. J Exp Bot 58: 1985 1997.
11. Jaillon O, Aury JM, Noel B, Policriti A, Clepet C, et al. (2007) The grapevine genome sequence suggests ancestral hexaploidization in major angiosperm phyla. Nature 449: 463 467.
12. Shelden MC, Howitt SM, Kaiser BN, Tyerman SD (2009) Identification and functional characterisation of aquaporins in the grapevine, *Vitis vinifera*. Funct Plant Biol 36: 1065 1078.
13. Gambetta G, Manuck C, Drucker S, Shaghasi T, Fort K, et al. (2012) The relationship between root hydraulics and scion vigour across *Vitis* rootstocks: what role do root aquaporins play? J Exp Bot 63: 6445 6455.
14. Galmés J, Pou A, Alsina MM, Tomàs M, Medrano H, et al. (2007) Aquaporin expression in response to different water stress intensities and recovery in Richter-110 (*Vitis* sp.): relationship with ecophysiological status. Planta 226: 671 681.
15. Pou A, Medrano H, Flexas J, Tyerman SD (2013) A putative role for TIP and PIP aquaporins in dynamics of leaf hydraulic and stomatal conductances in grapevine under water stress and re-watering. Plant Cell Environ 36: 828 843.
16. Fouquet R, Leon C, Ollat N, Barrieu F (2008) Identification of grapevine aquaporins and expression analysis in developing berries. Plant Cell Rep 27: 1541 1550.

17. Leitão L, Prista C, Moura TF, Loureiro-Dias MC, Soveral G (2012) Grapevine aquaporins: gating of a tonoplast intrinsic protein (TIP2;1) by cytosolic pH. PLoS One 7: e33219.
18. Noronha H, Agasse A, Martins AP, Berny MC, Gomes D, et al. (2014) The grape aquaporin VvSIP1 transports water across the ER membrane. J Exp Bot 65: 981 993.
19. Pettersson N, Hagstrom J, Bill RM, Hohmann S (2006) Expression of heterologous aquaporins for functional analysis in *Saccharomyces cerevisiae*. Curr Genet 50: 247 255.
20. Soveral G, Madeira A, Loureiro-Dias MC, Moura TF (2007) Water transport in intact yeast cells as assessed by fluorescence self-quenching. Appl Environ Microbiol 73: 2341 2343.
21. Güldener U, Hegemann J (1998) A second generation of GFP-vectors for subcellular localization studies in budding yeast. Technical report, Heinrich-Heine Universität, Inst. für Mikrobiologie. Available: http://mips.helmholtz-muenchen.de/proj/yeast/info/tools/hegemann/gfp.html Accessed 2014 April 16.
22. Hanahan D (1985) Techniques for transformation of *E. coli*. In DNA cloning: A Practical Approach. (ed DM Glover) 1: 109 135.
23. Pronk JT (2002) Auxotrophic yeast strains in fundamental and applied research. Appl Environ Microbiol 68: 2095 2100.
24. Thompson JD, Gibson TJ, Plewniak F, Jeanmougin F, Higgins DG (1997) The CLUSTAL_X windows interface: flexible strategies for multiple sequence alignment aided by quality analysis tools. Nucleic Acids Res 25: 4876 4882.
25. Hall TA (1999) BioEdit: a user-friendly biological sequence alignment editor and analysis program for Windows 95/98/NT 41: 95 98.
26. Tamura K, Peterson D, Peterson N, Stecher G, Nei M, et al. (2011) MEGA5: molecular evolutionary genetics analysis using maximum likelihood, evolutionary distance, and maximum parsimony methods. Mol Biol Evol 28: 2731 2739.
27. Krogh A, Larsson B, von Heijne G, Sonnhammer EL (2001) Predicting transmembrane protein topology with a hidden Markov model: application to complete genomes. J Mol Biol 305: 567 580.
28. Tusnady GE, Simon I (2001) The HMMTOP transmembrane topology prediction server. Bioinformatics 17: 849 850.
29. Hofmann K, Stoffel W (1993) TMbase - A database of membrane spanning proteins segments. Biol Chem Hoppe-Seyler 374: 166.
30. Johanson U, Karlsson M, Johansson I, Gustavsson S, Sjövall S, et al. (2001) The complete set of genes encoding major intrinsic proteins in *Arabidopsis* provides a framework for a new nomenclature for major intrinsic proteins in plants. Plant Physiol 126: 1358 1369.
31. Forrest KL, Bhave M (2007) Major intrinsic proteins (MIPs) in plants: a complex gene family with major impacts on plant phenotype. Funct Integr Genomics 7: 263 289.
32. Froger A, Tallur B, Thomas D, Delamarche C (1998) Prediction of functional residues in water channels and related proteins. Protein Sci 7: 1458 1468.
33. Heymann JB, Engel A (2000) Structural clues in the sequences of the aquaporins. J Mol Biol 295: 1039 1053.
34. Johansson I, Karlsson M, Johanson U, Larsson C, Kjellbom P (2000) The role of aquaporins in cellular and whole plant water balance. Biochim Biophys Acta 1465: 324 342.
35. Santoni V, Verdoucq L, Sommerer N, Vinh J, Pflieger D, et al. (2006) Methylation of aquaporins in plant plasma membrane. Biochem J 400: 189 197.
36. Zelazny E, Miecielica U, Borst JW, Hemminga MA, Chaumont F (2009) An N-terminal diacidic motif is required for the trafficking of maize aquaporins ZmPIP2;4 and ZmPIP2;5 to the plasma membrane. Plant J 57: 346 355.
37. Tournaire-Roux C, Sutka M, Javot H, Gout E, Gerbeau P, et al. (2003) Cytosolic pH regulates root water transport during anoxic stress through gating of aquaporins. Nature 425: 393 397.
38. Nyblom M, Frick A, Wang Y, Ekvall M, Hallgren K, et al. (2009) Structural and functional analysis of SoPIP2;1 mutants adds insight into plant aquaporin gating. J Mol Biol 387: 653 668.
39. Van Wilder V, Miecielica U, Degand H, Derua R, Waelkens E, et al. (2008) Maize plasma membrane aquaporins belonging to the PIP1 and PIP2 subgroups are *in vivo* phosphorylated. Plant Cell Physiol 49: 1364 1377.
40. Prak S, Hem S, Boudet J, Viennois G, Sommerer N, et al. (2008) Multiple phosphorylations in the C-terminal tail of plant plasma membrane aquaporins role in subcellular trafficking of AtPIP2; 1 in response to salt stress. Mol Cell Proteomics 7: 1019 1030.
41. Johansson I, Karlsson M, Shukla VK, Chrispeels MJ, Larsson C, et al. (1998) Water transport activity of the plasma membrane aquaporin PM28A is regulated by phosphorylation. The Plant Cell Online 10: 451 459.
42. Daniels MJ (1996) Characterization of a new vacuolar membrane aquaporin sensitive to mercury at a unique site. Plant Cell 8: 587 599.
43. Kjellbom P, Larsson C, Johansson I, Karlsson M, Johanson U (1999) Aquaporins and water homeostasis in plants. Trends Plant Sci 4: 308 314.
44. Wudick MM, Luu DT, Maurel C (2009) A look inside: localization patterns and functions of intracellular plant aquaporins. New Phytol 184: 289 302.
45. Maurel C, Reizer J, Schroeder J, Chrispeels M (1993) The vacuolar membrane protein gamma-TIP creates water specific channels in *Xenopus* oocytes. The EMBO Journal 12: 2241 2247.
46. Daniels MJ, Mirkov TE, Chrispeels MJ (1994) The plasma membrane of *Arabidopsis thaliana* contains a mercury-insensitive aquaporin that is a homolog of the tonoplast water channel protein TIP. Plant Physiol 106: 1325 1333.
47. Suga S, Maeshima M (2004) Water channel activity of radish plasma membrane aquaporins heterologously expressed in yeast and their modification by site-directed mutagenesis. Plant Cell Physiol 45: 823 830.
48. Neill S, Desikan R, Hancock J (2002) Hydrogen peroxide signalling. Curr Opin Plant Biol 5: 388 395.
49. Antunes F, Cadenas E, Brunk U (2001) Apoptosis induced by exposure to a low steady-state concentration of $H_2O_2$ is a consequence of lysosomal rupture. Biochem J 356: 549 555.
50. Bienert GP, Schjoerring JK, Jahn TP (2006) Membrane transport of hydrogen peroxide. Biochim Biophys Acta - Biomembranes 1758: 994 1003.
51. Bienert GP, Møller ALB, Kristiansen KA, Schulz A, Møller IM, et al. (2007) Specific aquaporins facilitate the diffusion of hydrogen peroxide across membranes. J Biol Chem 282: 1183 1192.
52. Dynowski M, Schaaf G, Loque D, Moran O, Ludewig U (2008) Plant plasma membrane water channels conduct the signalling molecule $H_2O_2$. Biochem J 414: 53 61.
53. Bienert GP, Heinen RB, Berny MC, Chaumont F (2014) Maize plasma membrane aquaporin ZmPIP2;5, but not ZmPIP1;2, facilitates transmembrane diffusion of hydrogen peroxide. Biochim Biophys Acta 1838: 216 222.
54. Mori IC, Schroeder JI (2004) Reactive oxygen species activation of plant $Ca^{2+}$ channels. A signaling mechanism in polar growth, hormone transduction, stress signaling, and hypothetically mechanotransduction. Plant Physiol 135: 702 708.
55. Foyer CH, Noctor G (2003) Redox sensing and signalling associated with reactive oxygen in chloroplasts, peroxisomes and mitochondria. Physiol Plant 119: 355 364.
56. Boursiac Y, Boudet J, Postaire O, Luu DT, Tournaire-Roux C, et al. (2008) Stimulus-induced downregulation of root water transport involves reactive oxygen species-activated cell signalling and plasma membrane intrinsic protein internalization. Plant J 56: 207 218.
57. Azad AK, Yoshikawa N, Ishikawa T, Sawa Y, Shibata H (2012) Substitution of a single amino acid residue in the aromatic/arginine selectivity filter alters the transport profiles of tonoplast aquaporin homologs. Biochim Biophys Acta 1818: 1 11.
58. Azad A, Ishikawa T, Ishikawa T, Sawa Y, Shibata H (2008) Intracellular energy depletion triggers programmed cell death during petal senescence in tulip. J Exp Bot 59: 2085 2095.
59. Canetta E, Walker GM, Adya AK (2009) Nanoscopic morphological changes in yeast cell surfaces caused by oxidative stress: an atomic force microscopic study. J Microbiol Biotechnol 19: 547 555.
60. Kuthan M, Devaux F, Janderová B, Slaninová I, Jacq C, et al. (2003) Domestication of wild *Saccharomyces cerevisiae* is accompanied by changes in gene expression and colony morphology. Mol Microbiol 47: 745 754.
61. Dordas C, Chrispeels MJ, Brown PH (2000) Permeability and channel-mediated transport of boric acid across membrane vesicles isolated from squash roots. Plant Physiol 124: 1349 1362.
62. Fitzpatrick KL, Reid RJ (2009) The involvement of aquaglyceroporins in transport of boron in barley roots. Plant Cell Environ 32: 1357 1365.
63. Takano J, Wada M, Ludewig U, Schaaf G, von Wiren N, et al. (2006) The *Arabidopsis* major intrinsic protein NIP5;1 is essential for efficient boron uptake and plant development under boron limitation. Plant Cell 18: 1498 1509.
64. Tanaka M, Wallace IS, Takano J, Roberts DM, Fujiwara T (2008) NIP6;1 is a boric acid channel for preferential transport of boron to growing shoot tissues in *Arabidopsis*. Plant Cell 20: 2860 2875.
65. Mitani N, Yamaji N, Ma JF (2008) Characterization of substrate specificity of a rice silicon transporter, Lsi1. Pflugers Arch, EJP 456: 679 686.
66. Schnurbusch T, Hayes J, Hrmova M, Baumann U, Ramesh SA, et al. (2010) Boron toxicity tolerance in barley through reduced expression of the multifunctional aquaporin HvNIP2;1. Plant Physiol 153: 1706 1715.
67. Tanaka M, Fujiwara T (2008) Physiological roles and transport mechanisms of boron: perspectives from plants. Pflugers Arch 456: 671 677.
68. Nozawa A, Takano J, Kobayashi M, von Wiren N, Fujiwara T (2006) Roles of *BOR1*, *DUR3*, and *FPS1* in boron transport and tolerance in *Saccharomyces cerevisiae*. FEMS Microbiol Lett 262: 216 222.

*Journal of Experimental Botany*
doi:10.1093/jxb/ert448

Journal of Experimental Botany
www.jxb.oxfordjournals.org

RESEARCH PAPER

# The grape aquaporin VvSIP1 transports water across the ER membrane

**Henrique Noronha[1,2], Alice Agasse[2], Ana Paula Martins[3], Marie C. Berny[4], Dulceneia Gomes[2], Olfa Zarrouk[5], Pierre Thiebaud[6], Serge Delrot[7], Graça Soveral[3], François Chaumont[4] and Hernâni Gerós[1,2,*]**

[1] Centro de Investigação e de Tecnologias Agro-ambientais e Biológicas CITAB, Portugal
[2] Grupo de Investigação em Biologia Vegetal Aplicada e Inovação Agroalimentar (AgroBioPlant), Departamento de Biologia, Escola de Ciências, Universidade do Minho, Braga, Portugal
[3] Research Institute for Medicines and Pharmaceutical Sciences (iMed.UL) and Department of Biochemistry and Human Biology, Faculty of Pharmacy, University of Lisbon, Lisbon, Portugal
[4] Institut des Science de la Vie, Université catholique de Louvain, Croix du Sud 4-L7.07.14, B-1348 Louvain-la-Neuve, Belgium
[5] Instituto de Tecnologia Química e Biológica, Apartado 127, 2781–901 Oeiras, Portugal
[6] CNRS UMR 5164, Bordeaux, France
[7] Université de Bordeaux, INRA, ISVV, Ecophysiologie et Génomique Fonctionnelle de la Vigne, UMR 1287, F-33140 Villenave d'Ornon, France

* To whom correspondence should be addressed. E-mail: geros@bio.uminho.pt

Received 3 July 2013; Revised 21 November 2013; Accepted 26 November 2013

## Abstract

**Water diffusion through biological membranes is facilitated by aquaporins, members of the widespread major intrinsic proteins (MIPs). In the present study, the localization, expression, and functional characterization of a small basic intrinsic protein (SIP) from the grapevine were assessed. *VvSIP1* was expressed in leaves and berries from field-grown vines, and in leaves and stems from *in vitro* plantlets, but not in roots. When expressed in tobacco mesophyll cells and in *Saccharomyces cerevisiae*, fluorescent-tagged VvSIP1 was localized at the endoplasmic reticulum (ER). Stopped-flow spectroscopy showed that VvSIP1-enriched ER membrane vesicles from yeast exhibited higher water permeability and lower activation energy for water transport than control vesicles, indicating the involvement of protein-mediated water diffusion. This aquaporin was able to transport water but not glycerol, urea, sorbitol, glucose, or inositol. VvSIP1 expression in *Xenopus* oocytes failed to increase the water permeability of the plasma membrane. *VvSIP1-His-tag* was solubilized and purified to homogeneity from yeast ER membranes and the reconstitution of the purified protein in phosphatidylethanolamine liposomes confirmed its water channel activity. To provide further insights into gene function, the expression of *VvSIP1* in mature grapes was studied when vines were cultivated in different field conditions, but its transcript levels did not increase significantly in water-stressed plants and western-exposed berries. However, the expression of the aquaporin genes *VvSIP1*, *VvPIP2;2*, and *VvTIP1;1* was up-regulated by heat in cultured cells.**

**Key words:** Aquaporin, protein purification, proteoliposomes, *Vitis vinifera*, VvSIP1, water transport.

## Introduction

The physiological role of intracellular aquaporins (AQPs) in plants is not yet clear and remains a stimulating matter of debate (for reviews, see Ishibashi, 2006; Nozaki *et al.*, 2008; Maeshima and Ishikawa, 2008; Gomes *et al.*, 2009; Wudick *et al.*, 2009; Conde *et al.*, 2010). Intracellular AQPs may play important roles in organelle water transport and intracellular water homeostasis, but they may also transport small solutes important for cell signalling (Gomes *et al.*, 2009).

In comparison with other organisms, plants appear to have a remarkably large number of ubiquitously expressed AQPs (Javot and Maurel, 2002; Javot *et al.*, 2003). Following the identification of *Arabidopsis thaliana* AtTIP1;1 as the first plant water channel (Höfte *et al.*, 1992; Maurel *et al.*, 1993), several intracellular AQPs have been described, particularly at the tonoplast (reviewed by Wudick *et al.*, 2009). However, three SIPs (small basic intrinsic protein) and one NIP (nodulin-like intrinsic protein) from *Arabidopsis* have shown to localize at the endoplasmic reticulum (ER) (Ishikawa *et al.*, 2005; Mituzani *et al.*, 2006). Also, an AQP able to transport $CO_2$, NtAQP1, was shown to be localized at the chloroplast membranes (Uehlein *et al.*, 2003, 2008). AQP8 and AQP9 from mammals were localized in the membrane system of the mitochondria (Calamita *et al.*, 2005; Amiry-Moghaddam *et al.*, 2005) and, more recently, *Arabidopsis* AtTIP5;1 was specifically found in the mitochondria of pollen tubes (Soto *et al.*, 2010).

SIPs constitute a subfamily of major intrinsic proteins (MIPs) that was identified for the first time by database mining and phylogenetic analyses (Johanson and Gustavsson, 2002), and are related to mammalian AQP11 and AQP12 in their intracellular localization and function (reviewed by Ishibashi, 2006). Each SIP member may exhibit a particular pattern of expression in the plant and play a role specific to each cell. *Arabidopsis thaliana* AtSIP1;1 is expressed in the roots and flowers, especially in stamens, and pollen, and in trichomes of rosette leaves. AtSIP1;2 is expressed in the cotyledon and hydathode tissue of rosette leaves. AtSIP2;1 is expressed in the vascular tissue of roots and the leaf veins, and in flowers, pollen, and siliques (Ishikawa *et al.*, 2005).

Regarding key distinctive structural characteristics of SIPs, the first NPA motif of loop B, which participates in the formation of an essential constriction region, is changed to NPT, NPC, or NPL in AtSIP1;1, AtSIP1;2, and AtSIP2;1, respectively, and to NPC or NPT in the human AQPs AQP11 and AQP12, respectively. The two NPA motifs are involved in the selection of substrate through hydrogen bond formation between a water molecule and the asparagine residue. Thus, any variation of the NPA motif might directly reflect the substrate specificity and/or velocity of water transport (reviewed by Ishibashi, 2006; Maeshima and Ishikawa, 2008; Gomes *et al.*, 2009). The SIP members are also relatively rich in basic residues such as lysine, and their isoelectric points are higher than in AQPs from other subfamilies.

Grape berries are sophisticated biochemical factories of major economic importance. They import and accumulate water, minerals, sugars, and amino acids, and synthesize organic acids, tannins, and anthocyanins, as well as flavour and aroma compounds. The development and maturation of grape berries have received considerable scientific scrutiny because of both the uniqueness of such processes to plant biology and the importance of these fruits as a significant component of the human diet and wine industry (Conde *et al.*, 2007). The grape genome has only two SIP genes, *VvSIP1* and *VvSIP2*, encoding a SIP1 and SIP2 subtype, respectively. The present study investigates the expression of *VvSIP1* in leaves and grape berries throughout the season and the subcellular localization of the protein fused to a fluorescent tag both in tobacco leaves and in yeast. Expression of *VvSIP1* in *Xenopus* oocytes did not increase the water permeability of the plasma membrane. In contrast, when expressed in yeast, VvSIP1-enriched ER membrane vesicles exhibited higher water permeability than control vesicles, as determined by stopped-flow spectroscopy, and the protein was unable to accept other substrates, including glycerol, urea, sorbitol, glucose, and inositol. VvSIP1 protein was also purified to homogeneity and its water transport activity was reconstituted in phosphatidylethanolamine artificial vesicles. The potential role of *VvSIP1* in stress response was studied in field-grown grapevines and grape cell cultures.

## Materials and methods

### *Plant material*

Field-grown grapevines (*Vitis vinifera* L.) of cv. Aragonez and Vinhão were used in the present study. Cv. Aragonez vines were collected from commercial vineyards in Reguengos de Monsaraz and Estremoz (south of Portugal) and cv. Vinhão from a commercial vineyard in Guimarães (north of Portugal). Rows were oriented north–south. Expression studies were also performed in 3-month-old grapevine plantlets of the cv. Trincadeira growing *in vitro*.

The cv. Aragonez vines cultivated in Reguengos de Monsaraz were subjected to RDI (regulated deficit irrigation) and SDI (sustained deficit irrigation), within the scope of the European Project Innovine. RDI vines were supplied with 50% less water than SDI vines, and berries from SDI vines were collected from the green to mature phase to study *VvSIP1* expression during maturation. At the mature stage, the following values for leaf water potential were measured: –0.7 MPa (RDI) and –0.5 MPa (SDI). Also, the oscillations in berry temperature were continuously monitored. Average daily maximum temperatures in grapes from clusters exposed to the west (RDI-W and SDI-W) were 4–5 °C higher than in east-exposed clusters (RDI-E and SDI-E) because ambient temperatures are higher after mid-day. The expression of *VvSIP1* was also studied in berries from SDI-E, RDI-E, SDI-W, and RDI-W vines.

The cv. Aragonez vines in Estremoz were subjected to full irrigation (100% evapotranspiration) and non-irrigation (rain-fed only). Watering was applied according to crop evapotranspiration and soil water content.

Grape berry clusters from 4–6 plants, located in three different rows, were collected, and grapes from three different berry clusters per plant were harvested and immediately frozen in liquid nitrogen. Berries and leaves were sampled at green [4 weeks after flowering (WAF)], veraison (9 WAF), and mature (15 WAF) stages of berry development and ripening.

Cells of *V. vinifera* L. (CSB, Cabernet Sauvignon Berry) were cultivated in liquid medium according to Descendit *et al.* (1996), and maintained in 250 ml flasks on a rotatory shaker at 100 rpm in the dark, at 25 °C. The mineral medium was supplemented with 2% (w/v) sucrose. Cells were subcultured weekly by transferring 10 ml aliquots into 40 ml of fresh medium. In order to study the effect of different treatments on *VvSIP1* expression, 5 ml aliquots were incubated overnight with 100 mM NaCl, polyethylene glycol (PEG) 2% (w/v), 150 µM abscisic acid (ABA) (Gagné *et al.*, 2011), and 150 µM salicylic acid (SA) (Laura *et al.*, 2007) at 23 °C. The effect of heat was evaluated after an overnight incubation at 38 °C. Cells were immediately frozen in liquid nitrogen and stored at –80 °C.

### *In silico studies*

SIP sequences were obtained from the database of the National Center of Biotechnology (NCBI). Protein alignment was performed

by Prankster and the result was visualized in Genedoc (Nicholas *et al.*, 1997). The 3D representation was performed by I-TASSER (Zhang, 2008) using SoPIP2;1 as a template (Törnroth-Horesfiel *et al.*, 2006). The resulting 3D model was visualized using the PyMol software (DeLano, 2002).

### *RNA isolation from grape berries and leaves*

Total RNA was isolated from grape berries and leaves with a QIAGEN RNeasy Plant Mini Kit following the manufacturer's instructions, except that the extraction buffer was changed to 2% cetyltrimethyl ammonium bromide (CTAB), 2% soluble polyvinylpyrrolidone (PVP) K-30, 300 mM TRIS-HCl (pH 8.0), 25 mM EDTA, 2.0 M NaCl, and 2% (v/v) β-mercaptoethanol. After an in-column DNase treatment, the RNA integrity was checked in a 1% agarose gel, and first-strand cDNA synthesis was performed with the LongRange 2Step RT-PCR (Qiagen), following the manufacturer's instructions.

### *Subcellular localization of VvSIP1*

The *pH7RWG2-VvSIP1-RFP* construct was obtained using Gateway (Qiagen) recombination technology. Briefly, the recombination sequences (forward, GGG GAC AAG TTT GTA CAA AAA AGC AGG CT; and reverse, GGG GAC CAC TTT GTA CAA GAA AGC TGG GT) were introduced by PCR (primers are shown in Supplementary Table S1 available at *JXB* online) in the *VvSIP1* cDNA without a stop codon and the fragment was recombined into the entry vector *pDONR221* using the BP clonase enzyme. The *VvSIP1* cDNA was recombined into the *pH7RWG2* vector by the LR clonase enzyme, introduced in *Agrobacterium tumefaciens* (GV3101), and transient transformation of tobacco (*Nicotiana tabacum*) leaf epidermal cells constitutively expressing green fluorescent protein (GFP)–HDEL (Batoko *et al.*, 200) was performed according to Sparkes *et al.* (2006). Bacterial cells were cultivated overnight in liquid LB medium up to the exponential–stationary phase and then diluted to $OD_{600nm}$=0.1 with infiltration buffer (50 mM MES pH 5.6, 2 mM $Na_3PO4$, 0.5% glucose, and 100 μM acetosyringone). Diluted cells were cultivated again until the culture reached an $OD_{600nm}$=0.2. Four-week-old tobacco plants were infiltrated with the bacterial cultures and leaf discs were examined under the confocal microscope 3 d later.

*VvSIP1* was cloned into *pUG35-GFP* behind the cDNA encoding GFP. Restriction sites for *Bam*HI were introduced by PCR (primers are shown in Supplementary Table S1 at *JXB* online), and the fragment was cloned into *pUG35-GFP* vector after digestion with *Bam*HI. *VvSIP1* expression was regulated by the inducible MET25 promoter. *Saccharomyces cerevisiae* strain CEN.PK 135-5D (ura–) was transformed with the *pUG35-SIP1-GFP* vector with the LiAc/SS-DNA/PEG method (Gietz and Woods, 2002). To study fluorescence localization, transformed yeast cells were cultivated overnight in YNB minimal medium without methionine and uracil, washed with deionized water, and observed with a Zeiss 710 confocal microscope (Carl Zeiss, Jena, Germany), with excitation at 488 nm and detection between 506 nm and 538 nm.

### *Real-time PCR studies*

Quantitative real-time PCRs were prepared with a QuantiTect SYBR Green PCR Kit (Qiagen) and were performed in a CFX96 Real-Time Detection System (Bio-Rad), at an annealing temperature of 50 °C. RNA and cDNA were obtained as detailed above. Experiments were done in triplicate (biological replicates) with the software Bio-Rad CFX Manager (Bio-Rad), using *VvGAPDH* as internal control. After each run, melting curves were performed to check for unspecific and primer dimer amplification. The primers used to study the expression of *VvSIP1*, *VvGAPDH*, and *VvGPT* are shown in Supplementary Table S1 at *JXB* online.

### *Semi-quantitative PCR studies*

Semi-quantitative PCR was performed with HotStarTaq DNA Polymerase (Qiagen) to study the effect of heat on AQP expression. Briefly, all the primers used were previously tested to determine the exponential phase of the amplification curve for each condition. Three reactions for each condition were run in the same gel and quantified with the software Quantity One (Biorad). The primers used for *VvHT1*, *VvPIP2;2*, *VvTIP1;1*, and *VvACT1* are shown in Supplementary Table S1 at *JXB* online.

### *Isolation of yeast endoplasmic reticulum*

The recombination sequences of Gateway technology were introduced in the *VvSIP1* cDNA with the stop codon with the primers shown in Supplementary Table S1 at *JXB* online. The fragment was introduced in the vector *pDONR221*, recombined with *pYES-DEST52*, and the resulting vector *pYES-DEST52-VvSIP1* introduced into yeast cells by the method described above. ER-enriched vesicles were obtained following the method of Wuestehube and Schekman (1992), which has been routinely used to purify ER membranes from yeasts. Briefly, yeast cells were cultivated overnight in YNB medium without uracil supplemented with 2% galactose, and spheroplasts were obtained by digestion with zymolyase 20T (Rodrigues *et al.*, 2013) dissolved in digestion buffer (1.35 M sorbitol, 10 mM citric acid, 30 mM $Na_2HPO_4$, 1 mM EGTA, pH 7.4). After 45 min digestion, the spheroplasts were lysed in a Dounce tissue homogenizer in HEPES-lysis buffer [20 mM HEPES, 50 mM potassium acetate, 100 mM sorbitol, 2 mM EDTA, 1 mM phenylmethylsulphonyl fluoride (PMSF), 1 mM dithiothreitol (DTT), pH 6.8], and a crude membrane fraction was obtained by centrifugation at 18 000 *g* for 15 min at 4 °C. This membrane fraction was resuspended in HEPES-lysis buffer, layered on top of a 1.2/1.5 M discontinuous sucrose gradient, and centrifuged at 100 000 *g* for 1 h at 4 °C. The enriched ER membrane fraction was collected from the 1.2/1.5 M sucrose interface, centrifuged at 18 000 *g* for 15 min at 4 °C, and the pellet was resuspended in 100 mM mannitol, 10 mM TRIS-HEPES (pH 7.5), and stored at –80 °C. The protein amount was estimated by the Lowry method (Lowry *et al.*, 1951). The purity of the ER fraction was checked by immunoblot with an anti-calreticulin antibody.

### *Functional characterization by stopped-flow spectroscopy*

Water permeability of membrane vesicles was assessed with the stopped-flow technique (HI-TECH Scientific PQ/SF-53). Experiments were performed at 10–37 °C to study activation energies. Five runs were usually stored and analysed in each experimental condition, as described by Soveral *et al.* (1997). Briefly, vesicles resuspended in 100 mM mannitol, 10 mM TRIS-HEPES (pH 7.5) (0.1 ml, 0.4 mg protein $ml^{-1}$) were mixed with an equal amount of hyperosmotic mannitol solutions at 23 °C to produce an inwardly directed gradient of impermeant solute (osmotic gradient 120 mOsmol). The kinetics of vesicle shrinkage were measured from the time course of 90 ° scattered light intensity at 400 nm until a stable light scatter signal was attained. The osmotic water permeability coefficient ($P_f$) was estimated by fitting the light scatter signal to a single exponential curve with the equation $P_f = k(V_o/A)$ $[1/V_w/(osm_{out})_\infty]$, where $V_w$ is the molar volume of water, $V_o/A$ is the initial volume to area ratio of the vesicle population, and $(osm_{out})_\infty$ is the final medium osmolarity after the application of the osmotic gradient. The osmolarity of each solution was determined from freezing point depression by a semi-micro-osmometer (Knauer GmbH, Germany). The activation energy ($E_a$) of water transport was obtained from the slope of an Arrhenius plot (ln $P_f$ as a function of 1/T) multiplied by the gas constant R. Vesicle size (initial volume) was determined by quasi-elastic light scattering (QELS) by a particle sizer (BI-90 Brookhaven Instruments) as described by Soveral *et al.* (1997). To determine VvSIP1 specificity for water, mannitol was replaced by several solutes (glycerol, urea, glucose, sorbitol, and inositol) with

the same osmotic potential, and solute uptake was measured as stated above.

### *VvSIP1 purification and reconstitution into phosphatidylethanolamine liposomes*

The construct *pYES-DEST52-VvSIP1-His-tag* was obtained by Gateway recombination. Briefly, the *pDONR221-VvSIP1* without a stop codon (see above) was recombined with *pYES-DEST52-His-tag* in front of the *GAL1* promoter, and behind six histidines. This vector was used to transform *S. cerevisiae*, and purified ER membranes were obtained as described above. The sample was diluted to 0.2 mg protein $ml^{-1}$ in $Na_2CO_3$, incubated for 30 min at 4 °C, and centrifuged for 40 min at 50 000 *g*. The pellet was washed with ice-cold water and resuspended in purification buffer [20 mM imidazole, 100 mM KCl, 10% (w/v) glycerol, pH 7.5] before protein solubilization. Three detergents were tested at different concentrations [1 and 2% (w/v)] and protein:lipid ratios (1/10 and 1/20): octyl-glucoside (OTG), *n*-dodecyl β-D-maltoside (DDM), and lysophosphatidylcholine (LPC). The best results were obtained with 2% LPC at a 1/10 protein:lipid ratio after incubation for 2 h at 42 °C under shaking. Non-digested proteins were pelleted at 100 000 *g* for 30 min at 4 °C. The purification step was started by mixing the supernatant with Ni-NTA agarose (Qiagen), and, after incubation for 2 h at 37 °C under shaking, the mixture was loaded into an empty Bio-Spin Chromatography Column (Bio-Rad). The column was sequentially eluted with the following buffers: purification buffer supplemented with 0.05% (w/v) LPC, 40 mM imidazole buffer [40 mM imidazole, 10% glycerol (v/v), 100 mM KCl, 0.05% (w/v) LPC, pH 7.5], and 300 mM imidazole buffer [300 mM imidazole, 10% glycerol (v/v), 100 mM KCl, 0.05% (w/v) LPC, pH 7.5]. In each eluate, the purity of VvSIP1 was checked by western blot with an anti-ZmSIP1 antibody raised in maize against the C-terminal peptide of ZmSIP1;1 (FLPPAPKPKTKKA). To reconstitute VvSIP1 in artificial vesicles, phosphatidylethanolamine lipids were mixed by sonication in a buffer with 100 mM mannitol, 10 mM TRIS-HEPES (pH 7.5), and 2% (w/v) OTG before addition of the purified protein (protein:lipid ratio of 1/50). After 30 min incubation on ice, the mixture was dialysed against 100 mM mannitol, 10 mM TRIS-HEPES (pH 7.5) to remove LPC, and the proteoliposomes were frozen in liquid nitrogen and stored at –80 °C until used (Gerós *et al.*, 1996).

### *Western blot analysis*

Protein samples obtained as described above were separated on 10% acrylamide gels as described by Laemmli (1970). Proteins were transferred to a nitrocellulose membrane during 1 h 30 min at 100 V, and were blocked during 1 h in TRIS-buffered saline containing 0.1% (v/v) Tween-20 (TBS-T) with 5% (w/v) skimmed milk powder, 1% (w/v) bovine serum albumin (BSA), 0.1% goat serum, and 0.05% (v/v) Tween-20. The membranes were probed against ZmSIP1 (1:1000 dilution) and calreticulin (1:10 000) (Carqueijeiro *et al.*, 2013) during 1 h at room temperature in blocking solution, followed by an incubation with an anti-rabbit peroxidase-conjugated antibody (Sigma) at 1:160 000 dilution in TBS-T, for 45 min. The immunodetection was accomplished with the chemiluminescent ECL detection substrate (Biorad).

### *Oocyte injection and permeability assays*

*NtPIP2;1* and *VvSIP1* cDNAs were cloned into the oocyte expression vector *pXT7* with the primers shown in Supplementary Table S1 at *JXB* online, and *in vitro* complementary RNAs (cRNAs) were obtained with the Transcript Aid T7 High Yield Transcription Kit (Fisher, Thermo Scientific). *Xenopus laevis* oocytes were isolated and defolliculated by digestion at room temperature for 1.5 h with 4 mg $ml^{-1}$ collagenase A in Barth's solution [88 mM NaCl, 1 mM KCl, 2.4 mM $NaHCO_3$, 10 mM HEPES-NaOH, 0.33 mM $Ca(NO_3)_2$, 0.41 mM $CaCl_2$, 0.82 mM $MgSO_4$, pH 7.4, and 200 mOsm $kg^{-1}$]. *In vitro* transcripts or distilled water (50 nl) were injected and the oocytes were incubated at 18 °C in Barth's solution for 2 d. Oocyte swelling was measured by transferring the oocytes to 5-fold diluted Barth's solution, and the changes in the cell volume were calculated as described before (Fetter *et al.*, 2004).

### *Flow cytometry*

Flow cytometry analysis of proteoliposomes was performed in an Epics XL Beckman Coulter flow cytometer equipped with an argon-ion laser with a beam emitting at 488 nm at 15 mW. Green fluorescence was collected through a 525 nm band-pass filter. Data were analysed with Flowing Software 2.0 (Rodrigues *et al.*, 2013).

### *Statistical analysis*

The results were statistically analysed by Student's *t*-test and by analysis of variances tests (one-way and two-way ANOVA) using Prism v. 5 (GraphPad Software, Inc.). Post-hoc multiple comparisons were performed using the HSD Tukey test. For each condition, differences between mean values are identified with different letters or asterisks.

### *Sequence accession numbers*

VvSIP1(DQ086835), VvGPT (GSVIVT00006900001), VvPIP2;2 (EF364436), VvTIP1;1 (DQ834701), MtSIP1;1 (G7JDK7), MtSIP1;2 (G7KYE4), AtSIP1;1 (Q9M8W5), AtSIP1;2 (Q9FK43), ZmSIP1;1 (Q9ATM3), ZmSIP1;2 (Q9ATM2), OeSIP1;1 (B0L1W3), OeSIP1;2 (B5KGP0), OsSIP1;1 (Q5VR89), PpSIP1;1 (A9RDU1), PpSIP1;2 (A9U3Q2).

## Results

### *Analysis of SIP1 protein sequences*

The amino acid sequence of *V. vinifera* VvSIP1 was compared with that of SIP1 AQPs from *A. thaliana*, *Zea mays* (maize), *Olea europaea* (olive), *Oryza sativa* (rice), *Medicago truncatula*, and the moss *Physcomitrella patens* (Fig. 1). All proteins share six transmembrane domains and two intracellular and extracellular loops that fold into the membrane and interact with each other through two 'NPA' motifs. A 3D computer simulation of VvSIP1 using SoPIP2;1 as a template (Törnroth-Horesfiel *et al.*, 2006) confirmed that these 'NPA' motifs form a central constriction (Supplementary Fig. S1 at *JXB* online). Except for MtSIP1;1 and AtSIP1;2, the first 'NPA' motif is changed to NPT (Fig. 1). The R1 (I, L,V, or N), R2 (I, L, or V), R3 (P), and R4 (I or N) residues, which form the Ar/R filter, meet proximal to the central constriction formed by the two 'NPA' motifs (Supplementary Fig. S1). In contrast to most PIPs, TIPs, and NIPs, which contain an arginine (R) in R4 residues, the SIP1 proteins analysed show a conserved asparagine (N), except in the case of AtSIPs. In SIP1 sequences, the R3 residue is a conserved proline (P), which seems to be a characteristic of SIP1 members. Furthermore, a highly conserved AFGWAYI motif is present in loop E of all SIP1s.

### *Expression studies of* VvSIP1

To study the expression of *VvSIP1*, total RNA was isolated from cv. Vinhão leaves and berries and from grape berries of cv. Aragonez at three different developmental stages. RNAs

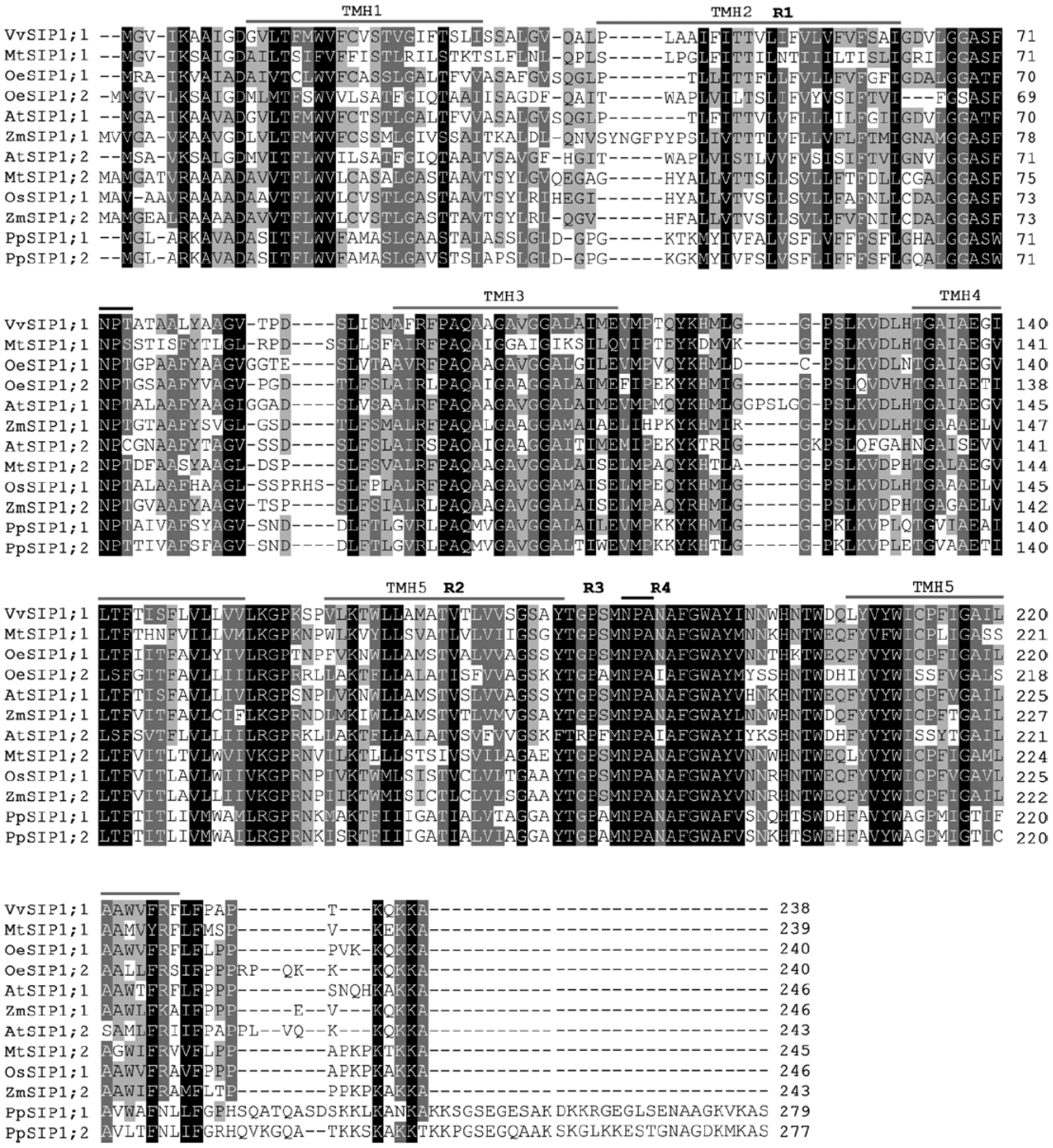


**Fig. 1.** Alignment of seven SIP1 proteins showing six transmembrane domains (TMH1–TMH6) and two intracellular and extracellular loops containing the conserved 'NPA' motifs (black lines) and the four amino acids corresponding to the Ar/R filter (R1–R4).

from grapevine plantlets growing *in vitro* and from liquid-cultured cells were also isolated to study the transcript levels of *VvSIP1*. In cv. Vinhão, *VvSIP1* transcripts were detected in all samples, but were more abundant at the end of the season, both in leaves and in mature grapes (Fig. 2A, B). Conversely, in berries from cv. Aragonez, *VvSIP1* expression decreased during maturation (Fig. 2C). In 3-month-old grapevine plantlets growing *in vitro VvSIP1* transcripts were very abundant in leaves and stem but were not detected in roots (data not shown).

Aragonez vines cultivated under field conditions were also used to study *VvSIP1* expression in berries in response to water deficit and different sun exposures (Fig. 2D, E). As described in the Materials and methods, grapevines subjected to RDI were irrigated with 50% less water than those subjected to SDI. In addition, average daily maximum temperatures were 4–5 °C higher in grapes exposed to the west (RDI-W and SDI-W) than in those exposed to the east (RDI-E and SDI-E). The results showed that transcript levels of *VvSIP1* did not increase significantly in berries from water-stressed plants

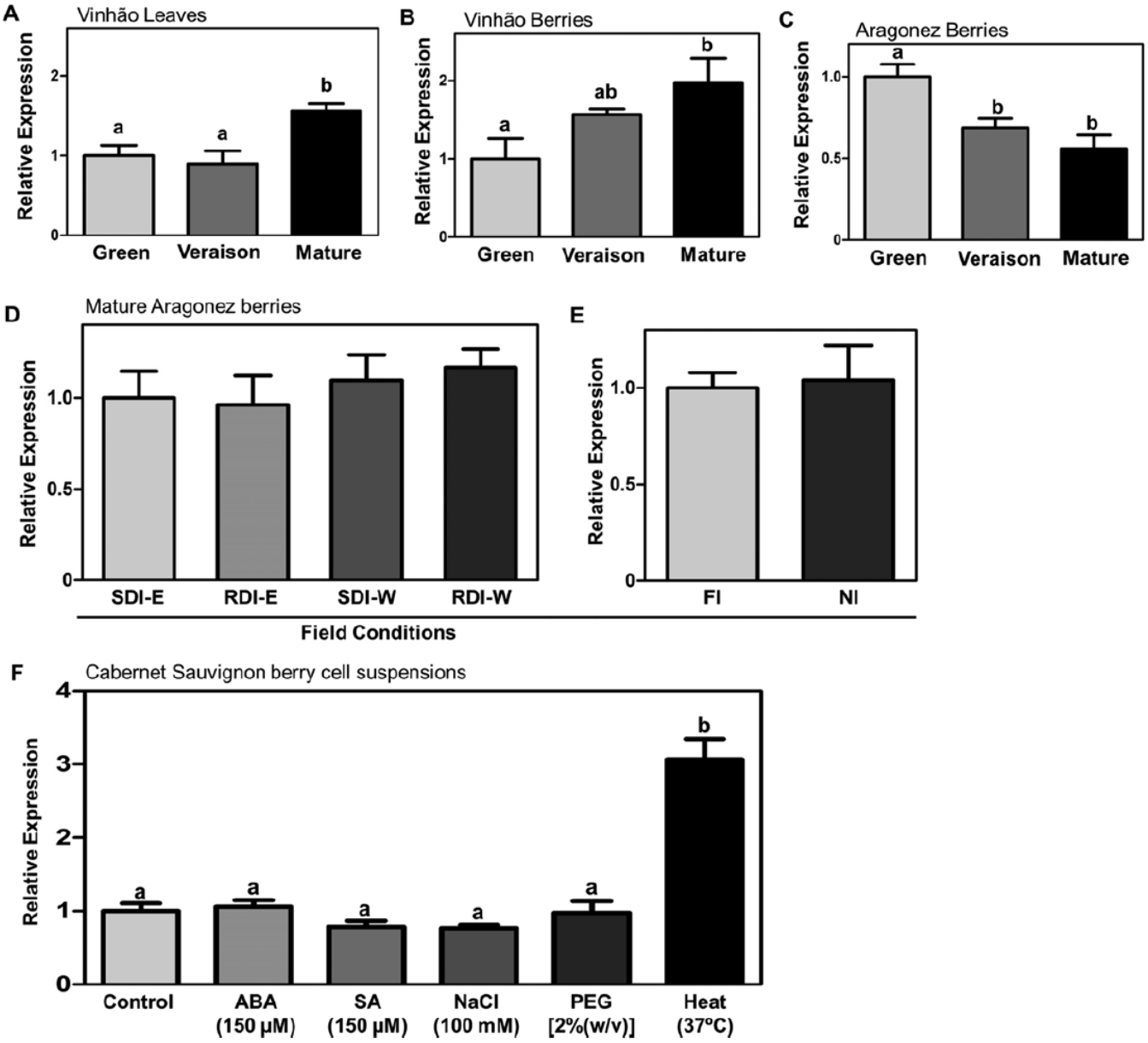


**Fig. 2.** *VvSIP1* expression determined by quantitative real-time PCR. Transcript levels in leaves (A) and berries (B) from cv. Vinhão and cv. Aragonez (C) during development. *VvSIP1* expression in mature berries from cv. Aragonez under different irrigation regimes and sun exposures (D, E). Expression of *VvSIP1* in cultured cells in response to ABA and SA, and salt, osmotic, and heat stresses. Results indicate the mean ±SD of three independent experiments. Letters denote significant differences.

and in berries from western-exposed clusters. The expression of *VvSIP1* was also studied in mature berries from vines cultivated under more pronounced water deficit conditions (non-irrigation), but again the expression of *VvSIP1* did not increase significantly (Fig. 2E).

In suspension-cultured cells (CSB, Cabernet Sauvignon Berry), *VvSIP1* expression (Fig. 2F) did not change after treatments with salt (150mM NaCl) and osmotic stresses [2% (w/v) PEG], nor did it change after elicitation with the stress-related hormones ABA (150 µM) and SA (150 µM). These stress conditions have been reported to induce physiological changes in plant cells. In contrast, *VvSIP1* transcript levels were significantly increased after an overnight incubation at 37 °C, while the expression of *VvGPT* (*Vitis vinifera* Glucose-Pi Transporter) decreased in the same experimental conditions (Supplementary Fig. S2 at *JXB* online; negative control). Heat seems to be a positive signal for the expression of AQPs, because plasma membrane *VvPIP2;2* and tonoplast *VvTIP1;1* were also up-regulated (Supplementary Fig. S3).

### *Subcellular localization of VvSIP1*

The subcellular localization of VvSIP1–red fluorescent protein (RFP) was studied after transient expression in tobacco epidermal cells. Figure 3 shows that VvSIP1–RFP co-localized with the ER marker GFP–HDEL (Batoko *et al.*, 2000). This reticular nature of the ER of tobacco cells has been clearly shown in other reports (Más and Beachy, 1999). VvSIP1 also localized in yeast internal membranes resembling the ER after transformation with VvSIP1–GFP (Fig. 4A). Western

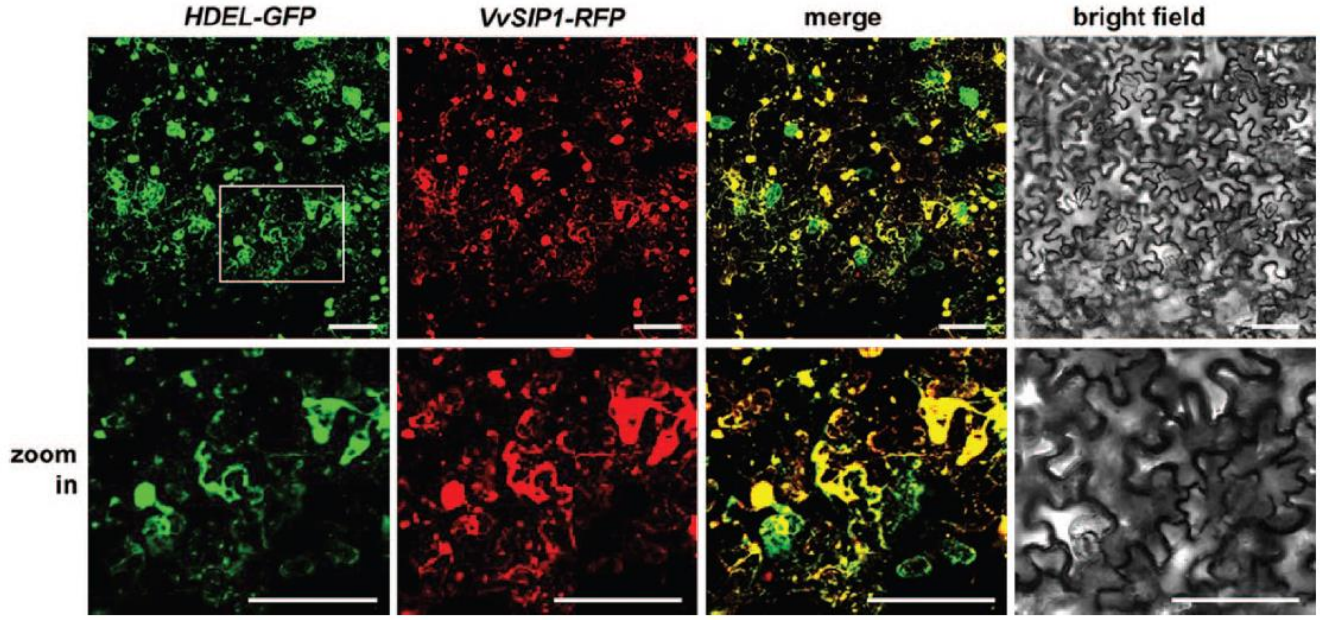


**Fig. 3.** Subcellular localization of VvSIP1;1 in tobacco. Transgenic plants expressing the ER marker GFP–HDEL (Batoko *et al.*, 2000) were infiltrated with *Agrobacterium* strains containing the pH7RWG2-VvSIP1-RFP plasmid. Images were acquired 2 d after infiltration using a confocal microscope and showed the fluorescence of GFP–HDEL and VvSIP1;1–RFP, and the overlap of fluorescence signals (merge). The white box shows a close up; bar=100 μm. (This figure is available in colour at *JXB* online.)

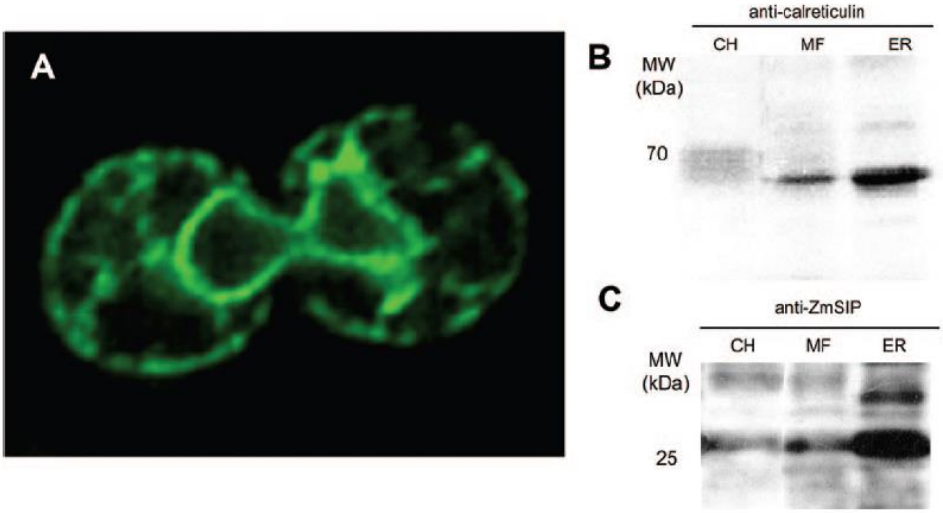


**Fig. 4.** Subcellular localization of VvSIP1 in yeast. Cells were transformed with the pUG35-VvSIP1-GFP plasmid and observed under a confocal microscope (A). Membrane fractions from the crude homogenate (CH), microsomal fraction (MF), and endoplasmic reticulum (ER) were subjected to immunoblot with anti-calreticulin (B) and anti-ZmSIP (C) antibodies to study both ER and VvSIP1 enrichment. (This figure is available in colour at *JXB* online.)

blot analysis with anti-ZmSIP and anti-calreticulin antibodies confirmed that VvSIP1 co-purified with the marker calreticulin, further corroborating that VvSIP1 is localized at the ER of transformed yeast.

### *Water transport by VvSIP1*

The osmotic permeability coefficient ($P_f$) of *Xenopus* oocytes injected with *VvSIP1* cRNA did not increase, in contrast to the $P_f$ of the positive control cells injected with tobacco *NtPIP2;1* cRNA (Fig. 5). These results suggest that VvSIP1 is not correctly targeted to the plasma membrane of oocytes or that it is inactive.

To study VvSIP1 function, ER vesicles were isolated from yeast cells expressing *VvSIP1*, and its water permeability monitored by stopped-flow light-scattering spectrophotometry. QELS analysis showed that the vesicle size in all batches was homogeneous. Unimodal distributions were observed, with a mean hydrodynamic diameter of $379 \pm 65$ nm ($n$=8) (data not shown). To analyse VvSIP1

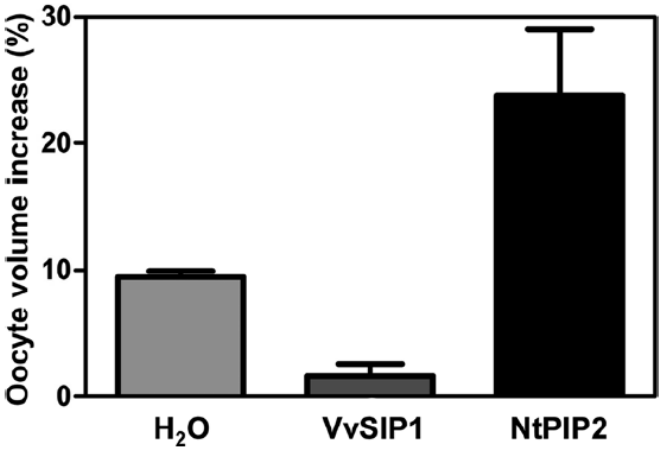


**Fig. 5.** Study of aquaporin transport activity in *Xenopus* oocytes 2 d after injection of *NtPIP2;1* and *VvSIP1 cRNAs*. Volume changes for individual oocytes were recorded after immersion in hyposmotic solutions. Control oocytes were injected with water. Results are the means ±SD of at least five cells.

activity, vesicles were challenged with a hypertonic mannitol solution. The change in the light scatter signal due to water efflux was used to calculate the $P_f$ and the $E_a$ of water transport. As shown in Fig. 6A, the shrinking rate of ER vesicles from *VvSIP1*-expressing yeast cells was twice as high as that of the control (Table 1). The increase in water permeability was consistent with the decrease in $E_a$ (Fig. 6B; Table 1), clearly indicating the involvement of protein-mediated water diffusion.

To purify VvSIP1, yeast cells were transformed with the construct *pYesDes52-VvSIP1-6-His-tag* followed by the purification of the ER fraction. Approximately 7 mg of total ER protein was obtained from 1.5 litres of yeast culture at $OD_{640}$=1.5. After solubilization with 2% LPC at a 1/10 protein to detergent ratio, VvSIP1 was eluted from the Ni-NTA column with 300 mM imidazole. Western blot analysis with the anti-ZmSIP1 antibody confirmed that VvSIP1 was purified to homogeneity (Fig. 7). In addition to a main band with a molecular mass of ~26 kDa, corresponding to the AQP monomer, a second band of ~52 kDa was detected, which probably corresponds to a VvSIP1 dimeric assembly (Bienert *et al.*, 2012). Finally, a smaller band (~20 kDa) was also detected in fractions #3 and #4 that could correspond to partially degraded VvSIP1. The preparation of phosphatidylethanolamine proteoliposomes was optimized for low protein to lipid ratios (1/50 lipid to protein ratio) to avoid the use of high amounts of purified protein.

Flow cytometry analysis showed that proteoliposomes formed a homogenous population and stained positively when loaded with the fluorescent sugar 2-NBDG, suggesting that sealed vesicles were formed, which is a prerequisite for transport experiments (Supplementary Fig. S4 at *JXB* online). To confirm the water transport activity mediated by VvSIP1, the shrinkage rate of proteoliposomes resuspended in a hypertonic medium was assayed by stopped-flow. These proteoliposomes displayed higher water transport activity and lower $E_a$ than empty liposomes (Table 1), confirming that VvSIP1 is able to facilitate water diffusion.

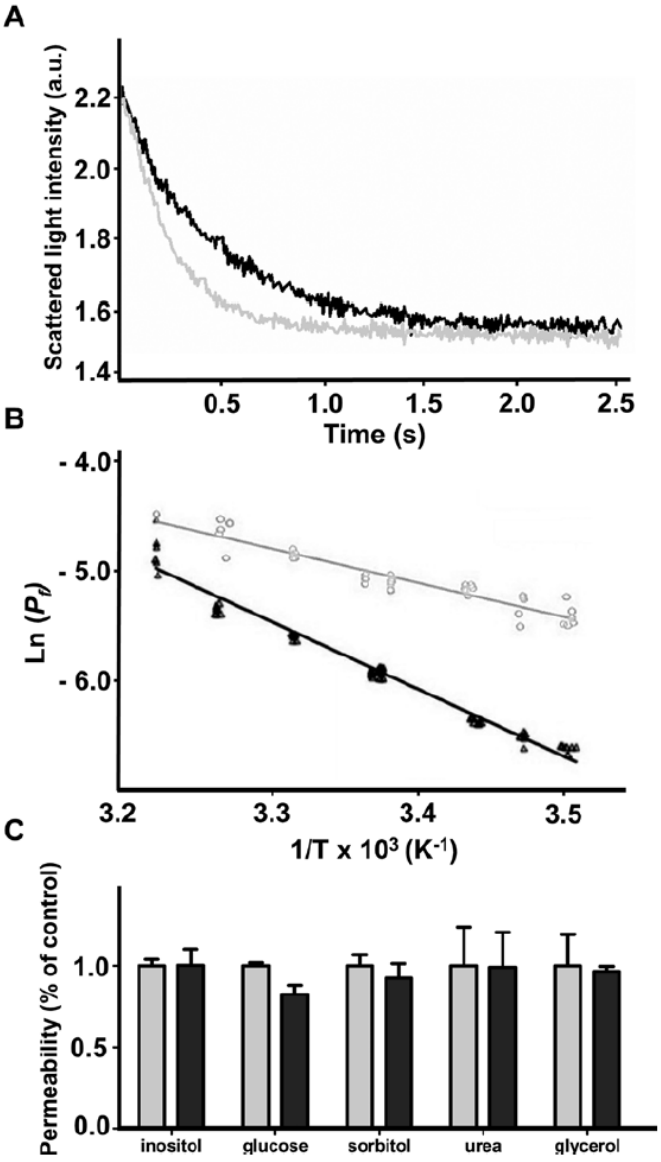


**Fig. 6.** Stopped-flow experiment for evaluation of the water permeability in ER vesicles. Normalized scattered light intensity obtained from stopped-flow experiments with ER vesicles purified from yeast cells transformed with *pYESDES52-VvSIP1* (grey) or the empty vector (black) and suddenly exposed to an osmotic gradient of 120 mOsm with an impermeant solute (A) and the corresponding Arrhenius plots (B) used to calculate $E_a$. To test VvSIP1 specificity for water (C), mannitol was replaced by several solutes (glycerol, urea, glucose, sorbitol, and inositol) with the same osmotic potential.

**Table 1.** *Permeability ($P_f$) and activation energy ($E_a$) for water transport in ER membranes and liposomes obtained by stopped flow (for details see the Materials and methods)*

| | | $P_f$ ($10^{-3}$ cm $s^{-1}$) | $E_a$ (kcal $mol^{-1}$) |
|---|---|---|---|
| ER vesicles | Empty vector | 1.99 ± 0.23 | 13.7 ± 2.6 |
| | VvSIP1 | 5.09 ± 0.77* | 6.4 ± 1.5* |
| Liposomes | Empty | 3.8 ± 0.1 × $10^{-1}$ | 16.6 ± 0.5 |
| | Proteoliposomes (1/50) | 5.0 ± 0.4 × $10^{-1}$* | 12.2 ± 0.7* |

Asterisks denote significant differences compared with the control: *$P \leq 0.01$.

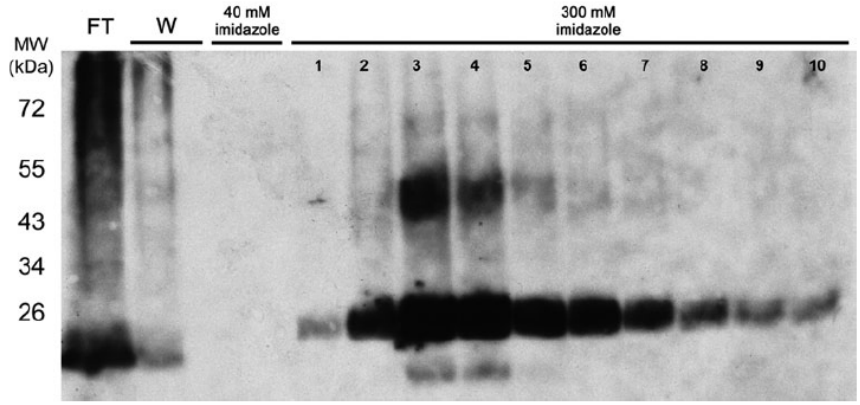


**Fig. 7.** Purification of VvSIP1 from *S. cerevisiae*. ER membranes from yeast transformed with *pYESDES52-VvSIP1-6-His* were isolated, solubilized with 2% LPC (w/v) at a protein:detergent ratio of 1/10, and purified in an Ni-NTA agarose column (for details see the Materials and methods). VvSIP1 monomeric (~26 kDa) and dimeric (~52 kDa) assembly can be observed. FT, flow-through of the column; W, eluates after washing the column. Eluates after addition of 300 mM imidazole (1–10).

## Discussion

### *Comparison of VvSIP1 with other SIP1 aquaporins*

Three members of the SIP subfamily were found in *Arabidopsis* (*SIP1;1*, *SIP1;2*, and *SIP2;1*) (Johanson *et al.*, 2001) and maize (Chaumont *et al.*, 2001), and two in rice (*OsSIP1;1* and *OsSIP2;1*) (Sakurai *et al.*, 2005) and grape (*VvSIP1;1* and *VvSIP2;1*) (Fouquet *et al.*, 2008). SIPs have also been described in *Populus trichocarpa* (Gupta and Sankararamakrishnan, 2009), the moss *P. patens* (Danielson and Johanson, 2008), and a putative ER AQP was described for the first time in the arbuscular mycorrhizal fungi *Glomus intraradices* (Aroca *et al.*, 2009). As shown in Fig. 1, the VvSIP1 amino acid sequence has a high degree of similarity with SIP1 AQPs from monocots, dicots, and moss. In particular, all the sequences analysed share R3 and R4 residues of the Ar/R filter, except AtSIP1;1 and AtSIP1;2 where asparagine is replaced by isoleucine in R4, and all the sequences contain the motif AFGWAYI in loop E. The importance of loop E for the oligomerization of AQPs has already been shown (Duchesne *et al.*, 2002; Fetter *et al.*, 2003), and a single amino acid substitution in loop E of AQP11 is responsible for a mice lethal phenotype (Tchekneva *et al.*, 2008). Nonetheless, there is still little information on the oligomerization of intracellular AQPs.

Three types of ER retention signals were identified at the C-termini of transmembrane proteins: dihydrophobic, diacidic, and dibasic (reviewed by Barlowe, 2003; Giraudo and Maccioni, 2003). Interestingly, a dihydrophobic motif (LF) and a dibasic signal (KQKK) are present in the C-terminus of VvSIP1, but their role in ER retention remains to be determined. The presence of a sequence rich in positively charged amino acids is a common feature of SIP AQPs (reviewed by Gomes *et al.*, 2009).

### *VvSIP1 co-localizes at the ER*

So far, only one experimental study was dedicated to SIP localization and function (Ishikawa *et al.*, 2005). AtSIP1;1, AtSIP1;2, and AtSIP2;1 are localized at the ER of *Arabidopsis* protoplasts. Likewise, VvSIP1 clearly co-localized at the ER of tobacco epidermal cells (Fig. 3). This ER localization was further demonstrated in yeast cells expressing VvSIP1–GFP and by ER purification followed by western blotting with an anti-ZmSIP1 (Fig. 4). A similar approach was used to localize AtSIPs (Ishikawa *et al.*, 2005) and mouse AQP11 and AQP12 (Itoh *et al.*, 2005; Morishita *et al.*, 2005) at the ER.

### *VvSIP1 facilitates membrane water diffusion in ER vesicles and in proteoliposomes*

Oocytes have often been used as a tool to study the water channel activity of AQPs, especially PIPs and TIPs (Gomes *et al.*, 2009), but, in the present study, oocytes injected with *VvSIP1;1* cRNA did not show increased membrane water permeability (Fig. 5). This could be due to a failure in VvSIP1 protein expression or trafficking to the plasma membrane, which might indicate that this cell model is not suitable to study SIP AQPs. However, it cannot be excluded that VvSIP1 was targeted to the plasma membrane but the protein was inactive or was able to facilitate the diffusion of other substrates rather than water. In agreement, oocytes injected with the intracellular AQP11 did not show water transport although the protein was apparently targeted to the plasma membrane (Gorelick *et al.*, 2006), in contrast to what was observed previously (Morishita *et al.*, 2005).

To clarify the function of VvSIP1 further, water transport activity was monitored by stopped-flow light-scattering spectrophotometry in ER membrane vesicles isolated from yeast cells expressing *VvSIP1* (Fig. 6). The observed increase in water permeability, together with the decrease in activation energy for water permeation, strongly supports that VvSIP1 mediates water fluxes. Furthermore, it was shown that VvSIP1 does not transport other solutes, including urea, glycerol, glucose, inositol, and sorbitol, suggesting that it is specific for water. In crude membranes from *AtSIP*-expressing yeast cells, AtSIP1;1 and AtSIP1;2, but not AtSIP2;1, also displayed water transport activity (Ishikawa *et al.*, 2005).

However, it was not excluded that AtSIP2;1 could facilitate water diffusion after heterodimerization with other SIPs.

Some AQPs, but no SIP members, were purified to homogeneity and reconstituted in liposomes (Zeidel *et al.*, 1992; Liu *et al.*, 2006; Yakata *et al.*, 2007; Tanimura *et al.*, 2009). Recently, the intracellular AQP11 from mouse was shown to exhibit water channel activity after its reconstitution in proteoliposomes followed by stopped-flow measurements (Yakata *et al.*, 2006). Here, the solubilization of VvSIP1-His-tag from yeast ER membranes using LPC, its purification to homogeneity through an Ni-NTA column, and its incorporation into phosphatidylethanolamine proteoliposomes by detergent dialysis were reported (Fig. 7). As observed in ER vesicles, stopped-flow studies with proteoliposomes (Table 1) suggested that VvSIP1 plays a role as an intracellular water channel.

### VvSIP1 *is not responsive to different vine water regimes and berry sun exposures*

As already mentioned, *AtSIP1;1* and *AtSIP1;2* are expressed in a variety of *Arabidopsis* tissues, but low expression levels were detected in leaves and fruits (Ishikawa *et al.*, 2005). In grapevine, expression of *VvSIP1* in leaves and berries of cv. Vinhão increased during development, peaking at the mature phase (Fig. 2A, B). In contrast, *VvSIP1* expression in cv. Aragonez decreased during berry development (Fig. 2C), suggesting that the *VvSIP1* expression pattern may depend on the variety or be affected by the terroir.

It has been shown that water deficit is one of many environmental conditions that regulate plant aquaporins (Tyerman *et al.*, 2002; Hachez *et al.*, 2008). This is particularly relevant since grape berries are higly susceptible to excessive sun exposure and their quality is affected by temperature and water availability (Kliewer and Torres, 1972; Spayd *et al.*, 2002; Pillet *et al.*, 2012). Generally, plants modulate the expression of plasma membrane and tonoplast AQPs in response to drought (Tyerman *et al.*, 2002). In the present study, the transcript levels of *VvSIP1* did not increase significantly in berries from vines subjected to water stress and in berries from western-oriented clusters (Fig. 2D, E), suggesting that *VvSIP1* does not play an important role in stress response under the field conditions tested. In contrast, in *in vitro* cultures the expression of *VvSIP1* (Fig. 2D), *VvPIP2:2*, and *VvTIP1;1* (Supplementary Fig. S3 at *JXB* online) was up-regulated after an overnight incubation at 37 °C. This treatment did not affect the viability of the cells and induced heat-shock proteins. However, the cells kept their morphology substantially unchanged, with a prominent central vacuole (not shown). Thus, the observed transcription profile of AQPs could be involved in the regulation of the intracellular water status under heat stress. In agreement with this, it cannot be excluded that more extreme temperature conditions in the field can also promote the increase of *VvSIP1* expression and that of other AQP members in grapevine tissues.

Besides regulation at the transcriptional level, several factors may affect the gating of AQPs, including phosphorylation, heteromerization, pH, $Ca^{2+}$, pressure, solute gradients, and temperature (Chaumont *et al.*, 2005). Post-transcriptional regulation of AQPs by protonation was shown in AtPIP2;2 in response to anoxia (Tournaire-Roux *et al.*, 2003). In this regard, the possible involvement of post-transcriptional regulation of VvSIP1 deserves further investigation.

Much work is also needed to clarify the specific physiological role of SIPs in the ER membrane. In mammals, it was observed that AQP11-knockout mice died before weaning due to advanced renal failure, and two important abnormalities were detected: vacuolization and cyst formation in the kidney proximal tubule. Because the observed vacuoles apparently originated from the ER, it was suggested that AQP11 might have some role in vesicle homeostasis (Morishita *et al.*, 2005). In plants, the analysis of *Arabidopsis* mutants followed by complementation experiments is a major tool for the assignment of a physiological role to a gene from a non-model plant. However, in preliminary experiments with T-DNA insertion mutants of AtSIP1;1 and AtSIP2;1, visible modifications in growth, morphology, and stress responses were not observed (Maeshima and Ishikawa, 2008). In this regard, a thorough exploitation of phenotypes at the cellular level, including the study of ER ultrastructure, could provide important information on the role of SIPs.

## Supplementary data

Supplementary data are available at *JXB* online.

Figure S1. Lateral (A) and top (B) views of the VvSIP1 3D structure predicted by I-Tasser software using SoPIP2;1 as template.

Figure S2. *VvGPT* expression determined by quantitative real-time PCR in CSB (Cabernet Sauvignon Berry) suspension cells incubated overnight at 37 °C and in control cells incubated at 23 °C.

Figure S3. *VvPIP2;2* and *VvTIP1;1* expression determined by real-time PCR in Cabernet Sauvignon Berry suspension cells incubated overnight at 37 °C and in control cells incubated at 23 °C.

Figure S4. Flow cytometry analysis of phosphatidylethanolamine liposomes showing a homogeneous population (A) able to accumulate the fluorescent sugar analogue 2-NBDG (B).

Table S1. Primers used for PCR.

## Acknowledgements

This work is supported by European Union Funds (FEDER/COMPETE-Operational Competitiveness Programme and INNOVINE, ref. 311775), by Portuguese national funds [Portuguese Foundation for Science and Technology (FCT)] under the project FCOMP-01-0124-FEDER-022692, the research projects PTDC/AGR-AAM/099154/2008 and PTDC/AGR-ALI/100636/2008, the Belgian National Fund for Scientific Research (FNRS), the Interuniversity Attraction Poles Programme-Belgian Science Policy, the 'Communauté française de Belgique-Actions de Recherches Concertées', and the Francqui Fundation. HN was supported by a PhD

grant no. SFRH/BD/74257/2010 from the FCT, and MCB was a Research Fellow at the 'Fonds pour la Formation à la Recherche dans l'Industrie et dans l'Agriculture'. This work also benefited from the networking activities within the European funded COST ACTION FA1106 QualityFruit'.

## References

**Amiry-Moghaddam M, Lindland H, Zelenin S, Roberg BA, Gundersen BB, Petersen P, Rinvik E, Torgner IA, Ottersen OP.** 2005. Brain mitochondria contain aquaporin water channels: evidence for the expression of a short AQP9 isoform in the inner mitochondrial membrane. *FASEB Journal* **9,** 1459–1467.

**Aroca R, Bago A, Sutka M, Paz JA, Cano C, Amodeo G, Ruiz-Lozano JM.** 2009. Expression analysis of the first arbuscular mycorrhizal fungi aquaporin described reveals concerted gene expression between salt-stressed and nonstressed mycelium. *Molecular Plant-Microbe Interactions* **22,** 1169–1178.

**Barlowe C.** 2003. Signals for COPII-dependent export from the ER: what's the ticket out? *Trends in Cell Biology* **13,** 295–300.

**Batoko H, Zheng HQ, Hawes C, Moore I.** 2000. A Rab1 GTPase is required for transport between the endoplasmic reticulum and Golgi apparatus and for normal Golgi movement in plants. *The Plant Cell* **12,** 2201–2217.

**Bienert GP, Cavez D, Besserer A, Berny MC, Gilis D, Rooman M, Chaumont F.** 2012. A conserved cysteine residue is involved in disulfide bond formation between plant plasma membrane aquaporin monomers. *Biochemical Journal* **445,** 101–111.

**Calamita G, Ferri D, Gena P, Liquori GE, Cavalier A, Thomas D, Svelto M.** 2005. The inner mitochondrial membrane has Aquaporin-8 water channels and is highly permeable to water. *Journal of Biological Chemistry* **280,** 17149 –17153.

**Carqueijeiro I, Noronha H, Duarte P, Gerós H, Sottomayor M.** 2013. Vacuolar transport of the medicinal alkaloids from *Catharantus roseus* is mediated by a proton driven antiport. *Plant Physiology* **162,** 1486–1496.

**Chaumont F, Barrieu F, Wojcik E, Chrispeels MJ, Jung R.** 2001. Aquaporins constitute a large and highly divergent protein family in maize. *Plant Physiology* **125,** 1206–1215.

**Chaumont F, Moshelion M, Daniels MJ.** 2005. Regulation of plant aquaporin activity. *Biology of the Cell* **97,** 749–764.

**Conde A, Diallinas G, Chaumont F, Chaves M, Gerós H.** 2010. Transporters, channels or simple diffusion? Dogmas, atypical roles and complexity in transport systems. *International Journal of Biochemistry and Cell Biology* **42,** 857–868.

**Conde C, Silva P, Fontes N, Dias ACP, Tavares RM, Sousa MJ, Agasse A, Delrot S, Gerós H.** 2007. Biochemical changes throughout grape berry development and fruit and wine quality. *Food* **1,** 1–22.

**Danielson J, Johanson U.** 2008. Unexpected complexity of the aquaporin gene family in the moss *Physcomitrella patens*. *BMC Plant Biology* **8,** 45.

**DeLano WL.** 2002. The PyMOL molecular graphics system. DeLano Scientific, San Carlos, CA, USA. http://www.pymol.org.

**Descendit A, Ramawat KG, Waffo P, Deffieux G, Badoc A, Merillon JM.** 1996. Anthocyanins, catechins, condensed tannins and piceid production in Vitis vinifera cell bioreactor cultures. *Biotechnology Letters* **18,** 659–662.

**Duchesne L, Pellerin I, Delemarche C, Deschamps S, Lagrée V, Froger A, Bonnec G, Thomas D, Hubert JF.** 2002. Role of C-terminal domain and transmembrane helices 5 and 6 in function and quaternary structure of major intrinsic proteins. *Journal of Biological Chemistry* **277,** 20598–20604.

**Fetter K, Van Wilder V, Moshelion M, Chaumont F.** 2004. Interactions between plasma membrane aquaporins modulate their water channel activity. *The Plant Cell* **16,** 215–228.

**Fouquet R, Leon C, Ollat N, Barrieu F.** 2008. Identification of grapevine aquaporins and expression analysis in developing berries. *Plant Cell Reports* **27,** 1541–1550.

**Gagné S, Cluzet S, Mérillon J, Gény L.** 2011. ABA initiates anthocyanin production in grape cell cultures. *Journal of Plant Growth Regulation* **30,** 1–10.

**Gerós H, Cássio F, Leão C.** 1996. Reconstitution of lactate proton symport activity in plasma membrane vesicles from the yeast *Candida utilis*. *Yeast* **12,** 1263–1272.

**Gietz RD, Woods RA.** 2002. Transformation of yeast by the Liac/SS carrier DNA/PEG method. *Methods in Enzymology* **350,** 87–96.

**Giraudo GC, Maccioni HJF.** 2003. Endoplasmic reticulum export of glycosyl transferases depends on interaction of a cytoplasmic dibasic motif with Sar1. *Molecular Biology of the Cell* **14,** 3753–3766.

**Gomes D, Agasse A, Thiébaud P, Delrot S, Gerós H, Chaumont F.** 2009. Aquaporins are multifunctional water and solute transporters highly divergent in living organisms. *Biochimica et Biophysica Acta* **1788,** 1213–1228.

**Gorelick DA, Praetorius J, Tsunerari T, Nielsen S, Agre P.** 2006. Aquaporin-11: a channel protein lacking apparent transport function expressed in brain. *BMC Biochemistry* **7,** 14.

**Gupta AB, Sankararamakrishnan R.** 2009. Genome-wide analysis of major intrinsic proteins in the tree plant *Populus trichocarpa*: characterization of XIP subfamily of aquaporins from evolutionary perspective. *BMC Plant Biology* **9,** 134.

**Hachez C, Heinen RB, Draye X, Chaumont F.** 2008. The expression pattern of plasma membrane aquaporins in maize leaf highlights their role in hydraulic regulation. *Plant Molecular Biology* **68,** 337–353.

**Hofte H, Hubberd L, Reizer J, Ludevid D, Herman EM, Chrispeels MJ.** 1992. Vegetative and seed-specific forms of tonoplast intrinsic protein in the vacuolar membrane of *Arabidopsis thaliana*. *Plant Physiology* **99,** 561–570.

**Ishibashi K.** 2006. Aquaporin subfamily with unusual NPA boxes. *Biochimica et Biophysica Acta* **1758,** 989–993.

**Ishikawa F, Suga S, Uemura T, Sato MH, Maeshima M.** 2005. Three SIP aquaporins of Arabidopsis are localized in the ER membrane and expressed in a tissue- and cell-specific manner. *FEBS Letters* **579,** 5814–5820.

**Itoh T, Rai T, Kuwahara M, Ko SBH, Uchida S, Sasaki S, Ishibashi K.** 2005. Identification of a novel aquaporin, AQP12,

expressed in pancreatic acinar cells. *Biochemical and Biophysical Research Communications* **330,** 832–838.

**Javot H, Lauvergeat V, Santoni V, *et al.*** 2003. Role of a single aquaporin isoform in root water uptake. *The Plant Cell* **15,** 509–522.

**Javot H, Maurel C.** 2002. The role of aquaporins in root water uptake. *Annals of Botany* **90,** 301–313.

**Johanson U, Gustavsson S.** 2002. A new subfamily of major intrinsic proteins in plants. *Molecular Biology and Evolution* **19,** 456–461.

**Johanson U, Karlsson M, Johansson I, Gustavsson S, Sjovall S, Fraysse L, Weig AR, Kjellbom P.** 2001. The complete set of genes encoding major intrinsic proteins in Arabidopsis provides a framework for a new nomenclature for major intrinsic proteins in plants. *Plant Physiology* **126,** 1358–1369.

**Kliewer WM, Torres RE.** 1972. Effect of controlled day and night temperatures on grape coloration. *American Journal of Enology and Viticulture* **23,** 71–77.

**Laemmli UK.** 1970. Cleavage of structural proteins during the assembly of the head of bacteriophage T4. *Nature* **227,** 680–685.

**Laura R, Franceschetti M, Ferri M, Tassoni A, Bagni N.** 2007. Resveratrol production in Vitis vinifera cell suspensions treated with several elicitors. *Caryologia* **60,** 169–171.

**Liu K, Nagasse H, Huang CG, Calamita G, Agre P.** 2006. Purification and functional characterization of aquaporin-8. *Biology of the Cell* **98,** 153–161.

**Lowry OH, Rosebrough NJ, Farr AJ, Randall RJ.** 1951. Protein measurement with the Folin reagent. *Journal of Biological Chemistry* **193,** 265–275.

**Maeshima M, Ishikawa F.** 2008. ER membrane aquaporins in plants. *European Journal of Physiology* **456,** 709–716.

**Más P, Beachy RN.** 1999. Replication of tobacco mosaic virus on endoplasmic reticulum and role of the cytoskeleton and virus movement protein in intracellular distribution of viral RNA. *Journal of Cell Biology* **147,** 945–958.

**Maurel C, Reizer J, Schroeder JI, Chrispeels MJ.** 1993. The vacuolar membrane protein gamma-TIP creates water specific channels in Xenopus oocytes. *EMBO Journal* **12,** 2241–2247.

**Mituzani M, Watanabe S, Nakagawa T, Maeshima M.** 2006. Aquaporin NIP2;1 is mainly localized to the ER membrane and shows root-specific accumulation in *Arabidopsis thaliana*. *Plant and Cell Physiology* **47,** 1420–1426.

**Morishita Y, Matsuzaki T, Hara-Chikuma M, *et al.*** 2005. Disruption of aquaporin-11 produces polycystic kidneys following vacuolization of the proximal tubule. *Molecular and Cellular Biology* **25,** 7770–7779.

**Nicholas KB, Nicholas HB Jr, Deerfield DW II**. 1997. GeneDoc: analysis and visualization of genetic variation. *EMBNET.NEWS* **4,** 14.

**Nozaki K, Ishii D, Ishibashi K.** 2008. Intracellular aquaporins: clues for intracellular water transport? *European Journal of Physiology* **456,** 701–707.

**Pillet J, Egert A, Pieri P, Lecourieux F, Kappel C, Charon J, Gomès E, Keller F, Delrot S, Lecourieux D.** 2012. VvGOLS1 and VvHsfA2 are involved in the heat stress responses in grapevine berries. *Plant and Cell Physiology* **53,** 1776–1792.

**Rodrigues J, Silva RD, Noronha H, Pedras A, Gerós H, Côrte-Real M.** 2013. Flow cytometry as a novel tool for structural and functional characterization of isolated yeast vacuoles. *Microbiology* **159,** 848–856.

**Sakurai J, Ishikawa F, Yamaguchi T, Uemura M, Maeshima M.** 2005. Identification of 33 rice aquaporin genes and analysis of their expression and function. *Plant and Cell Physiology* **46,** 1568–1577.

**Soto G, Fox R, Ayub N, Alleva K, Guaimas F, Erijman EJ, Mazzella A, Amodeo G, Muschietti J.** 2010. TIP5;1 is an aquaporin specifically targeted to pollen mitochondria and is probably involved in nitrogen remobilization in Arabidopsis thaliana. *The Plant Journal* **64,** 1038–1047.

**Soveral G, Macey RI, Moura TF.** 1997. Water permeability of brush border membrane vesicles from kidney proximal tubule. *Journal of Membrane Biology* **158,** 219–228.

**Sparkes IA, Runions J, Kearns A, Hawes C.** 2006. Rapid, transient expression of fluorescent fusion proteins in tobacco plants and generation of stably transformed plants. *Nature Protocols* **1,** 2019–2025.

**Spayd SE, Tarara JM, Mee DL, Ferguson JC.** 2002. Separation of sunlight and temperature effects on the composition of *Vitis vinifera* cv. Merlot berries. *American Journal of Enology and Viticulture* **53,** 171–182.

**Tanimura Y, Hiroaki Y, Fujiyoshi Y.** 2009. Acetazolamide reversibly inhibits water conduction by aquaporin-4. *Journal of Structural Biology* **166,** 16–21.

**Tchekneva EE, Khuchua Z, Davis LS, *et al.*** 2008. Single amino acid substitution in aquaporin 11 causes renal failure. *Journal of the American Society of Nephrology* **19,** 1955–1964.

**Törnroth-Horsefield S, Wang Y, Hedfalk K, Johanson U, Karlsson M, Tajkhorshid E, Neutze R, Kjellbom P.** 2006. Structural mechanism of plant aquaporin gating. *Nature* **439,** 688–694.

**Tournaire-Roux C, Sutka M, Javot H, Gout E, Gerbeau P, Luu D, Bligny R, Maurel C.** 2003. Cytosolic pH regulates root water transport during anoxic stress through gating of aquaporins. *Nature* **425,** 393–397.

**Tyerman SD, Niemietz CM, Bramley H.** 2002. Plant aquaporins: multifunctional water and solute channels with expanding roles. *Plant, Cell and Environment* **25,** 173–194.

**Uehlein N, Lovisolo C, Siefritz F and Kaldenhoff R.** 2003. The tobacco aquaporin NtAQP1 is a membrane CO2 pore with physiological functions. *Nature* **425,** 734–737.

**Uehlein N, Otto B, Hanson TD, Fischer M, MacDowell N, Kaldenhoff R.** 2008. Function of *Nicotiana tabacum* aquaporins as chloroplast gas pores challenges the concept of membrane $CO_2$ permeability. *The Plant Cell* **20,** 648–657.

**Wudick MM, Luu DT, Maurel C.** 2009. A look inside: localization patterns and functions of intracellular plant aquaporins. *New Phytologist* **184,** 289–302.

**Wuestehube LJ, Schekman RW.** 1992. Reconstitution of transport from endoplasmic reticulum to Golgi complex using endoplasmic

reticulum-enriched membrane fraction from yeast. *Methods in Enzymology* **219,** 124–136.

**Yakata K, Hiroaki Y, Ishibashi K, Sohara E, Sasaki S, Mitsuoka K, Fujiyoshi Y.** 2007. Aquaporin-11 containing a divergent NPA motif has normal water channel activity. *Biochimica et Biophysica Acta* **1768,** 688–693.

**Zeidel ML, Ambudkar SV, Smith BL, Agre P.** 1992. Reconstitution of functional water channels in liposomes containing purified red cell CHIP28 protein. *Biochemistry* **31,** 7436–7440.

**Zhang Y.** 2008. I-TASSER server for protein 3D structure prediction. *BMC Bioinformatics* **9,** 40.

# GENERAL DISCUSSION AND CONCLUSIONS

# GENERAL DISCUSSION AND CONCLUSIONS

The work presented in this thesis encompasses different aspects of biological membranes features. Membranes are barriers that assure the selective communication of the internal media with the external environment; membrane components, lipids and proteins, are key players responsible its selective permeability and regulation.

Part I of this thesis is dedicated to the study of the influence of dietary conditions in membrane biophysical properties, namely fluidity and permeability. In collaboration with the Veterinary School of Lisbon University, we used animal models and designed experiments where the effects of dietary FAs (PUFA and CLA) and reduced protein diets (RPD) on membrane composition, fluidity and permeability were analysed. In addition, since the animal genetic background is known to have an important contribution for the regulation of several biochemical pathways resulting in different phenotypes, this variable was included in the study.

One aspect of these experiments is the observation that, despite the significant changes in dietary components, we can only observe relatively small variations on FAs membrane composition. This probably reflects that, besides the complex set of processes that FAs face after ingestion (e.g. digestion, absorption, transport, metabolizing and finally incorporation into membranes), regulatory mechanisms accurately control membrane composition ensuring optimized cellular function[30].

In this work we studied CLA effects in obese Zucker rats fed a hyperlipidic (high fat) and atherogenic (high cholesterol) diet, a trial aiming to mimic an obese human sub-population with severe metabolic problems that consumes CLA supplements (publication 1). We observed that the FA composition of adipose membranes of Zucker rats is highly dependent on diet's lipid composition. It must be noted that animals were fed with fat from different origins - palm oil (rich in saturated fats) or ovine fat (rich in unsaturated fats) and that additionally, diets were supplemented with CLA. It was found that the lipid deposition on membranes was highly dependent on the specific dietary fat and in particular, CLA was found incorporated into adipose membranes reflecting relative patterns of CLA intake. Furthermore, in palm oil group the total sum of *n-3* FA was highly dependent on the fat origin. This was correlated to the fact that compared with ovine fat, palm oil has less alpha-linolenic acid[227], an essential omega-3 FA, precursor of these *n-3* PUFA classes that cannot be synthetized *de novo*. Thus, in the case of Zucker rats, the type of dietary lipids clearly influenced the lipid membrane composition.

Regarding the membrane biophysical properties, we were able to correlate a decrease in membrane fluidity and the concomitant decrease on permeability to water and glycerol with the specific incorporation of t10,c12 CLA isomer into adipose membranes of Zucker rats. Interestingly, this same isomer has been suggested to have fat lowering properties in several animal studies[228].

In publication 2, bovines were fed with silage (similar to natural feeding) or concentrate. In ruminants the FAs metabolization profile is completely different from

other species. In this specie unsaturated FAs undergo an extensive biohydrogenation in the rumen, with consequently high levels of SFA being absorbed in the intestine and deposited in the tissues[229]. As consequence, dietary lipids do not directly affect the FA composition of ruminant adipose tissues, as they do in non-ruminants[230]. In this case, neither breed nor diet affected fluidity and permeability of adipose plasma membranes.

Under reduced protein diet conditions, lower contents of linoleic (18:2*n-6*) and arachidonic acids (20:4*n-6*) were detected in pigs (publication 3), with a subsequent lower PUFA sum, in particular from the *n-6* family. This results from the fact that dietary linoleic acid is the precursor for the synthesis of arachidonic acid, thus predicting a proportional variation in the content of both FAs.

The genetic background in obese pigs was found to play a determinant role on the fluidity of adipose membranes by increasing membrane fluidity (publication 3) in accordance with the reported for a wide variety of other cell membranes from obese mice and rats.

To correlate the outcome of different dietary conditions on membrane composition and biophysical properties from different biological systems can be an intimidating puzzle. By one side, membrane lipid composition tends to be conserved, one the other hand, several biological conditionings may contribute for adaptive responses, which may have several consequences, including altered membrane lipid composition. Relatively small changes in the concentration of membrane lipids, in the order of 10%, are significant enough to alter biophysical properties of the membrane[231]. Thus we can speculate that even minor concentrations of some FA, may affect lipid packing within cellular membranes thus contributing to alterations in membrane fluidity and permeability. Additionally, Biological membranes are extremely complex. Thousands of different lipids interacts with each other, where phospholipids, cholesterol and other membrane components are not only organized in several different domains but also distributed in an asymmetric pattern in both sheets of the bilayer. Certainly, this heterogeneity implies also heterogeneity in the biophysical properties of the membrane. Although these aspects were not taken into account, our results enabled to correlate dietary components with membrane lipid composition and with membrane biophysical properties, namely fluidity and permeability. As discussed above in the context of membrane composition (general introduction of part I), these findings likely reflect membrane adaptation pointing to compensatory mechanisms that maintain membrane biophysical properties preserving optimal cellular function.

One consideration goes to the animal models used in this study. Rodent is a model wildly used in biomedical research. In particular, obese Zucker rats used in this study are models for investigation of human obesity. The pig is also emerging rapidly as a biomedical model for studying energy metabolism and obesity in humans. This results from the fact that pigs are devoid of postnatal brown fat, have similar cardiovascular system and proportional organ sizes and metabolic features[65]. Additionally, porcine is also a model for animal production studies. Bovines are solely models for animal production, moreover they have a different digestive metabolism where FA undergoes an extensive biohydrogenation in the rumen[229]; despite not being comparable with the previous species, investigation of dietary effects on membrane composition and adipose

tissue features can contribute to the improvement of ruminant feeding with possible outcomes in meat quality.

An interesting observation is that, within the same animal species all adipose membranes were found richer in SFA independently of their genetic background or diet. The distribution pattern of the main FAs follows the trend SFA > MUFA > PUFA. These results suggest a consistent FA pattern in the adipocyte membrane of the different species tested, coherent with a conservation of the lipid bilayer structure adapted to the specialized functions of these cells. The general pattern observed is in contradiction with the current idea that membranes are richer in PUFAs than in SFA.

Part II of this thesis is devoted to the study of membrane protein channels, AQPs, aiming at identifying new modulators with potential pharmacological use. Additionally, building an experimental cell model able to characterize individual AQP activity and selectivity, as well as to validate modulators effect and potency, was another goal of this work.

AQPs are important membrane proteins that control fluxes of water, glycerol and other small solutes through biological membranes. They are now recognized as important players in several physiological and pathological processes. Taking into account their broad distribution in the body and the extensive spectrum of pathologies where AQPs are involved, they are predicted to be of broad utility in the treatment of several diseases both as therapeutic targets and diagnostic agents. However, only a small number of AQP inhibitors suitable for clinical trials has been described so far. With this in mind, and taking into account that AQPs activity is inhibited by some metal salts, we decided to explore the properties of coordination metal complexes as possible inhibitors.

Using human RBCs that express one orthodox aquaporin (AQP1) and one aquaglyceroporin (AQP3) as a screening system we reported on the potent and selective inhibition of AQP3 by a water-soluble Au(III) coordination compound, Auphen (publication 4). The selectivity towards AQP3 was confirmed using transfected PC12 cell lines with overexpression of either AQP1 or AQP3. Based on the recovery of AQP3 activity after mercaptoethanol addition and knowing that Au(III) has affinity for sulfhydryl groups, we proposed a mechanistic hypotheses where AQP3 inhibition would occur through direct biding of Cys residues to the gold centre of the metal compounds. Thus Auphen inhibitory mechanism was investigated using molecular modelling studies together with analysis of non-covalent binding of Auphen to AQP1 and AQP3 by docking approaches. Since no human glycerol channel has a resolved structure yet, we built a homology model of human AQP3 using the crystal structure of E. coli's glycerol facilitator (GlpF) as reference. This approach allowed us to propose Cys40 as the likeliest candidate for binding to gold(III) complexes via a direct Au-thiol bond. In AQP3, the thiol group of Cys40 is projected towards the extracellular space approaching the channel pore. Contrariwise,

in AQP1 none of the cysteine, methionine or histidine residues present in the extracellular surface appear to be accessible for gold binding (residues with sulphur-donor groups, with which gold(III) ions are prone to interact).

Indeed, these results were later confirmed by our group using site directed mutagenesis in which Cys40 was replaced by a serine residue (Ser40)[232], confirming our initial proposal that for Auphen mechanism of action.

The potent and selective inhibitory effect of Auphen prompted us to further investigate other gold-based compounds as possible AQP3 inhibitors (publication 5). We selected a series of square planar Au(III) complexes containing functionalised bipyridine or terpyridine ligands. Moreover, to compare the effects of metal substitution on the AQP3 inhibition potency, phenantroline derivatives of Pt(II) and Cu(II) were also used. The effects of these compounds on both water and glycerol permeation were also tested on human RBCs. Au(III) was shown to be the most effective inhibitor of glycerol permeability, comparable in potency to Auphen.

Given the diversity of pathologies associated with dysfunction of the different AQPs, these proteins are now emergent drug targets. AQP-based modulator drugs are predicted to be of broad potential utility in the treatment of several diseases including cancer and others, as well as diagnostic agents. The identification of selective inhibitors for different AQP isoforms is a first step towards this avenue. One important question to be addressed is the effect of these compounds on other AQP isoforms. Additionally, a better understanding of AQP regulation and gating would allow its manipulation facilitating the identification of new putative modulators. However, it should be noted that cells and tissues frequently express more than one AQP isoform in the plasma membrane and, unless a specific isoform is mutated or overexpressed, its function is not easily discriminated. To this end we needed to develop a heterologous system for expression and functional assessment of AQP isoforms.

Such a cell system expressing individual AQPs would also be very useful for analysis of function and regulation of AQPs from the plant kingdom. Plant performance is highly dependent on the tight regulation of water permeation across cellular membranes and tissues. An important role for plant AQPs, more than to promote paths for water movements, is to provide regulation of water flow triggered by environmental modifications, an essential funtion under stress conditions. Plants express numerous AQP isoforms, but for most their physiological relevance is still unclear.

Heterologous expression in yeast is considered an excellent model for the study of proteins in general, because there is a large library of available strains and their genetic manipulation is easy and inexpensive when compared with cultures of animal cells. *S. cerevisiae* is an appropriate heterologous expression system for AQPs due to the intrinsic low water permeability of the yeast plasma membrane. Moreover, contrary to animal cells, yeast cells can survive in severe external environments allowing establishing experimental conditions where AQP selectivity and gating can be evaluated.

Thus, we used a strain of *S. cerevisiae* silenced in endogenous AQPs for the expression and functional characterization of pant AQPs (publication 6). The grapevine *Vitis vinifera* is a plant usually withstanding hostile drought conditions essential for the quality of berries and wine. Using GFP as a gene reporter, *V. vinifera* PIPs and TIPs AQP expression and localization in the yeast plasma membranes was confirmed by

fluorescence microscopy. Subsequently, yeast were functionally analysed using a methodology previously developed by our group[220] that uses intact yeast cells in their native physiological status to evaluate water and glycerol transport.

Using this approach, we showed that three AQPs from *V. vinifera* (VvTnPIP2;1, VvTnTIP1;1 and VvTnTIP2;2) are functional for water transport, while other three (VvTnPIP1;4, VvTnPIP2;3 and VvTnTIP4;1) are non-functional, and that functional AQPs were found to be sensitive to $HgCl_2$, a well-known but unselective inhibitor of AQP activity. Our results also indicate that *V. vinifera* AQPs are putative transporters of other small molecules of physiological importance (publication 6). Their sequence analyses revealed the presence of signature sequences for transport of ammonia, boron, $CO_2$, hydrogen peroxide and urea.

To clarify the function of VvSIP1, an intracellular AQP localized in the ER, ER membrane vesicles expressing VvSIP1 were isolated and purified from yeast cells and water transport activity was monitored. In parallel, proteoliposomes containing purified VvSIP1 were also tested for AQP activity. Both ER vesicles and proteoliposomes displayed higher water transport activity and lower activation energy for water transport, confirming that VvSIP1 is able to facilitate water diffusion. Importantly, this is also the first experimental evidence that VvSIP1 is able to transport water but not glycerol, urea, sorbitol, glucose, or inositol (publication 7).

One longer-term goal of our research is to identify human AQP inhibitors. The results obtained herein validate the yeast cell model as a useful and simple heterologous expression system to characterize the activity of individual AQPs. In addition, this cell model can be used to screen for compounds with pharmacological potential as well as to study gating mechanisms and pH regulation of AQP permeation.

# FUTURE PRESPECTIVES

# FUTURE PRESPECTIVES

During the work developed and herein presented, many ideas arose that could bring new insights into the field of membrane properties modulation by dietary components. The techniques optimized are now available to assess particular aspects of membrane composition. Moreover, other biochemical tools could be used to analyse membrane lipid composition in more detail (e.g., phospholipid content) giving valuable information to interpret changes in membrane biophysical properties.

The results obtained in this work regarding gold compounds as inhibitors of aquaglyceroporins unveiled numerous other issues to be addressed, such as their effect on other human AQPs as well as more insights to their modulation mechanisms. To assist these questions, we have now a yeast cell model as a valuable tool to investigate individual AQP modulation. In this way, the effect of the compounds described in this thesis as AQP3 inhibitors can be investigated on other human AQPs as well as in other from diverse origin. For example, non-mammalian AQPs from pathogenic organisms responsible for human diseases (bacteria, fungi, parasites) could be investigated using the yeast cell model. In particular, parasite AQPs are involved in crucial functions for parasite physiology, suggesting that they can be targets for human parasitosis therapeutics.

This model will also enable to screen for new modulators as well as to study AQP regulation mechanisms including pH regulation and gating. Additionally, it would allow site directed mutagenesis in order to study inhibition and regulatory mechanism.

# REFERENCES

# REFERENCES


1. Estadella, D. *et al.* Lipotoxicity: effects of dietary saturated and transfatty acids. *Mediators Inflamm.* **2013,** 137579 (2013).

2. Soveral, G. *et al.* Effect of dietary conjugated linoleic acid isomers on water and glycerol permeability of kidney membranes. *Biochem. Biophys. Res. Commun.* **383,** 108–12 (2009).

3. Verkman, A. S., Anderson, M. O. & Papadopoulos, M. C. Aquaporins: important but elusive drug targets. *Nat. Rev. Drug Discov.* **13,** 259–77 (2014).

4. Nicolson, G. L. The Fluid-Mosaic Model of Membrane Structure: still relevant to understanding the structure, function and dynamics of biological membranes after more than 40 years. *Biochim Biophys Acta* **1838,** 1451–1466 (2014).

5. Ibarguren, M., López, D. J. & Escribá, P. V. The effect of natural and synthetic fatty acids on membrane structure, microdomain organization, cellular functions and human health. *Biochim. Biophys. Acta* **1838,** 1518–28 (2014).

6. Alberts, B. *et al.* in *Molecular Biology of the Cell - capter 10* available online at: http://www.ncbi.nlm.nih.gov/b (Garland Science, 2002). at <http://www.ncbi.nlm.nih.gov/books/NBK26871/>

7. Van Meer, G., Voelker, D. R. & Feigenson, G. W. Membrane lipids: where they are and how they behave. *Nat. Rev. Mol. Cell Biol.* **9,** 112–24 (2008).

8. Shevchenko, A. & Simons, K. Lipidomics: coming to grips with lipid diversity. *Nat. Rev. Mol. Cell Biol.* **11,** 593–8 (2010).

9. Muranushi, N., Takagi, N., Muranishi, S. & Sezaki, H. Effect of fatty acids and monoglycerides on permeability of lipid bilayer. *Chem. Phys. Lipids* **28,** 269–279 (1981).

10. Marsh, D., Watts, A. & Knowles, P. F. Evidence for phase boundary lipid. Permeability of tempo-choline into dimyristoylphosphatidylcholine vesicles at the phase transition. *Biochemistry* **15,** 3570–3578 (1976).

11. Ehringer, W., Belcher, D., Wassall, S. R. & Stillwell, W. A comparison of the effects of linolenic (18:3Ω3) and docosahexaenoic (22:6Ω3) acids on phospholipid bilayers. *Chem. Phys. Lipids* **54,** 79–88 (1990).

12. Stillwell, W., Ehringer, W. & Jenski, L. J. Docosahexaenoic acid increases permeability of lipid vesicles and tumor cells. *Lipids* **28,** 103–8 (1993).

13. Lee, A. How lipids affect the activities of integral membrane proteins. *Biochim. Biophys. Acta (BBA)-Biomembranes* **1666,** 62–87 (2004).

14. Lapshina, E. A., Zavodnik, I. B. & Bryszewska, M. Effect of free fatty acids on the structure and properties of erythrocyte membrane. *Scand. J. Clin. Lab. Invest.* **55,** 391–7 (1995).

15. Zavodnik, I. B., Zaborowski, A., Niekurzak, A. & Bryszewska, M. Effect of free fatty acids on erythrocyte morphology and membrane fluidity. *Biochem. Mol. Biol. Int.* **42,** 123–33 (1997).

16. Zavodnik, I. B., Lapshina, E. A., Palecz, D. & Bryszewska, M. The effects of palmitate on human erythrocyte membrane potential and osmotic stability. *Scand. J. Clin. Lab. Invest.* **56,** 401–7 (1996).

17. López, D. J. *et al.* Accumulated bending energy elicits neutral sphingomyelinase activity in human red blood cells. *Biophys. J.* **102,** 2077–85 (2012).

18. Keren, K. Cell motility: the integrating role of the plasma membrane. *Eur. Biophys. J.* **40,** 1013–27 (2011).

19. Simons, K. & Ikonen, E. Functional rafts in cell membranes. *Nature* **387,** 569–72 (1997).

20. Lingwood, D. & Simons, K. Lipid rafts as a membrane-organizing principle. *Science* **327,** 46–50 (2010).

21. Stillwell, W. The role of polyunsaturated lipids in membrane raft function. *Scand. J. Food Nutr.* **50,** 107–113 (2006).

22. Wassall, S. R. & Stillwell, W. Polyunsaturated fatty acid-cholesterol interactions: domain formation in membranes. *Biochim. Biophys. Acta* **1788,** 24–32 (2009).

23. Harroun, T. a, Katsaras, J. & Wassall, S. R. Cholesterol hydroxyl group is found to reside in the center of a polyunsaturated lipid membrane. *Biochemistry* **45,** 1227–33 (2006).

24. Harroun, T. a, Katsaras, J. & Wassall, S. R. Cholesterol is found to reside in the center of a polyunsaturated lipid membrane. *Biochemistry* **47,** 7090–6 (2008).

25. Mally, M., Peterlin, P. & Svetina, S. Partitioning of oleic acid into phosphatidylcholine membranes is amplified by strain. *J. Phys. Chem. B* **117,** 12086–94 (2013).

26. Ibarguren, M. *et al.* Partitioning of liquid-ordered/liquid-disordered membrane microdomains induced by the fluidifying effect of 2-hydroxylated fatty acid derivatives. *Biochim. Biophys. Acta* **1828,** 2553–63 (2013).

27. Chakravarthy, B. R., Spence, M. W. & Cook, H. W. Turnover of phospholipid fatty acyl chains in cultured neuroblastoma cells: involvement of deacylation-reacylation and de novo synthesis in plasma membranes. *Biochim. Biophys. Acta* **879,** 264–77 (1986).

28. Igarashi, M., Chang, L., Ma, K. & Rapoport, S. I. Kinetics of eicosapentaenoic acid in brain, heart and liver of conscious rats fed a high n-3 PUFA containing diet. *Prostaglandins. Leukot. Essent. Fatty Acids* **89,** 403–12 (2013).

29. Martin, M. L. *et al.* The role of membrane fatty acid remodeling in the antitumor mechanism of action of 2-hydroxyoleic acid. *Biochim. Biophys. Acta* **1828,** 1405–13 (2013).

30. Hagen, R. M., Rodriguez-Cuenca, S. & Vidal-Puig, A. An allostatic control of membrane lipid composition by SREBP1. *FEBS Lett.* **584,** 2689–98 (2010).

31. Goldstein, J. L., DeBose-Boyd, R. a & Brown, M. S. Protein sensors for membrane sterols. *Cell* **124,** 35–46 (2006).

32. Horton, J. D., Goldstein, J. L. & Brown, M. S. Critical review SREBPs : activators of the complete program of cholesterol and fatty acid synthesis in the liver. **109,** 1125–1131 (2002).

33. Hulbert, A. J., Turner, N., Storlien, L. H. & Else, P. L. Dietary fats and membrane function : implications for metabolism and disease. 155–169 (2005).

34. Calder, P. C. n-3 Fatty acids and cardiovascular disease: evidence explained and mechanisms explored. *Clin. Sci. (Lond).* **107,** 1–11 (2004).

35. Smith, W. & Mukhopadhyay, R. Essential fatty acids: the work of George and Mildred Burr. *J. Biol. Chem.* **287,** 35439–41 (2012).

36. Kapoor, R. & Huang, Y.-S. Gamma linolenic acid: an antiinflammatory omega-6 fatty acid. *Curr. Pharm. Biotechnol.* **7,** 531–4 (2006).

37. Calder, P. C. n-3 polyunsaturated fatty acids, inflammation, and inflammatory diseases. *Am. J. Clin. Nutr.* **83,** 1505S–1519S (2006).

38. Healy, D. A., Wallace, F. A., Miles, E. A., Calder, P. C. & Newsholm, P. Effect of low-to-moderate amounts of dietary fish oil on neutrophil lipid composition and function. *Lipids* **35,** 763–8 (2000).

39. Abbott, S. K., Else, P. L., Atkins, T. A. & Hulbert, A. J. Fatty acid composition of membrane bilayers: importance of diet polyunsaturated fat balance. *Biochim. Biophys. Acta* **1818,** 1309–17 (2012).

40. Baum, S. J. *et al.* Fatty acids in cardiovascular health and disease: a comprehensive update. *J. Clin. Lipidol.* **6,** 216–34 (2012).

41. Das, U. N. Essential fatty acids: biochemistry, physiology and pathology. *Biotechnol. J.* **1,** 420–39 (2006).

42. Yang, Q., Alemany, R., Lanier, S. M. & Escrib, P. V. Influence of the Membrane Lipid Structure on Signal Processing via G Protein-Coupled Receptors. **68,** 210–217 (2005).

43. Terés, S. *et al.* Oleic acid content is responsible for the reduction in blood pressure induced by olive oil. *Proc. Natl. Acad. Sci. U. S. A.* **105,** 13811–6 (2008).

44. Lavie, C. J., Milani, R. V, Mehra, M. R. & Ventura, H. O. Omega-3 polyunsaturated fatty acids and cardiovascular diseases. *J. Am. Coll. Cardiol.* **54,** 585–94 (2009).

45. Faloia, E. *et al.* Physicochemical and functional modifications induced by obesity on human erythrocyte membranes. *Eur. J. Clin. Invest.* **29,** 432–7 (1999).

46. Matsuo, T., Sumida, H. & Suzuki, M. Beef tallow diet decreases beta-adrenergic receptor binding and lipolytic activities in different adipose tissues of rat. *Metabolism.* **44,** 1271–7 (1995).

47. Sehat, N. *et al.* Identification of conjugated linoleic acid isomers in cheese by gas chromatography, silver ion high performance liquid chromatography and mass spectral reconstructed ion profiles. Comparison of chromatographic elution sequences. *Lipids* **33,** 963–71 (1998).

48. Banni, S. Conjugated linoleic acid metabolism. *Curr. Opin. Lipidol.* **13,** 261–6 (2002).

49. Domeneghini, C., Di Giancamillo, A. & Corino, C. Conjugated linoleic acids (CLAs) and white adipose tissue: how both in vitro and in vivo studies tell the story of a relationship. *Histol. Histopathol.* **21,** 663–72 (2006).

50. Kennedy, A., Martinez, K., Schmidt, S., Mandrup, S. & Mcintosh, M. Antiobesity mechanisms of action of conjugated linoleic acid. *J. Nutr. Biochem.* **21,** 171–179 (2011).

51. Kelly, G. S. Conjugated Linoleic Acid: A Review. *Altern. Med. Rev.* **6,** 367–382 (2001).

52. Oleszczuk, J., Oleszczuk, L., Siwicki, a. & Skopińska-Różewska, E. Biological effects of conjugated linoleic acids supplementation. *Pol. J. Vet. Sci.* **15,** 403–408 (2012).

53. Kramer, J. K. *et al.* Distributions of conjugated linoleic acid (CLA) isomers in tissue lipid classes of pigs fed a commercial CLA mixture determined by gas chromatography and silver ion-high-performance liquid chromatography. *Lipids* **33,** 549–58 (1998).

54. Pond, W. G., Yen, J. T., Mersmann, H. J. & Haschek, W. M. Comparative effects of dietary protein and cholesterol-fat content on genetically lean and obese pigs. *J. Nutr.* **116,** 1116–24 (1986).

55. Hornick, J. L., Van Eenaeme, C., Gérard, O., Dufrasne, I. & Istasse, L. Mechanisms of reduced and compensatory growth. *Domest. Anim. Endocrinol.* **19,** 121–32 (2000).

56. Wood, J. D. *et al.* Effects of breed, diet and muscle on fat deposition and eating quality in pigs. *Meat Sci.* **67,** 651–67 (2004).

57. Doran, O. *et al.* A reduced protein diet induces stearoyl-CoA desaturase protein expression in pig muscle but not in subcutaneous adipose tissue: relationship with intramuscular lipid formation. *Br. J. Nutr.* **95,** 609–17 (2006).

58. Cristancho, A. G. & Lazar, M. a. Forming functional fat: a growing understanding of adipocyte differentiation. *Nat. Rev. Mol. Cell Biol.* **12,** 722–734 (2011).

59. Cinti, S. The adipose organ at a glance. *Dis. Model. Mech.* **5,** 588–94 (2012).

60. Cushman, S. W. & Rizack, M. A. Structure-function relationships in the adipose cell. 3. Effects of bovine serum albumin on the metabolism of glucose and the release of nonesterified fatty acids and glycerol by the isolated adipose cell. *J. Cell Biol.* **46,** 354–61 (1970).

61. Virtue, S. & Vidal-Puig, A. It's not how fat you are, it's what you do with it that counts. *PLoS Biol.* **6,** e237 (2008).

62. Gray, S. L. *et al.* Leptin deficiency unmasks the deleterious effects of impaired peroxisome proliferator-activated receptor gamma function (P465L PPARgamma) in mice. *Diabetes* **55,** 2669–77 (2006).

63. Medina-Gomez, G. *et al.* PPAR gamma 2 prevents lipotoxicity by controlling adipose tissue expandability and peripheral lipid metabolism. *PLoS Genet.* **3,** e64 (2007).

64. Pietiläinen, K. H. *et al.* Association of lipidome remodeling in the adipocyte membrane with acquired obesity in humans. *PLoS Biol.* **9,** e1000623 (2011).

65. Spurlock, M. E. & Gabler, N. K. The development of porcine models of obesity and the metabolic syndrome. *J. Nutr.* **138,** 397–402 (2008).

66. Kurtz, T. W., Morris, R. C. & Pershadsingh, H. A. The Zucker fatty rat as a genetic model of obesity and hypertension. *Hypertension* **13,** 896–901 (1989).

67. Zucker, L. M. & Zucker, T. F. Fatty , a new mutation in the rat. *J. Hered.* **52,** 275–278 (1961).

68. Bray, G. A. The Zucker-fatty rat: a review. *Fed. Proc.* **36,** 148–53 (1977).

69. Macey, R. I., Karan, D. M. & Farmer, R. E. Properties of water channels in human red cells. *Biomembranes* **3,** 331–340 (1972).

70. Farmer, R. & Macey, R. Perturbation of red cell volume: rectification of osmotic flow. *Biochim. Biophys. Acta - Biomembr.* **196,** 53–65 (1970).

71. Paganelli, C. V & Solomon, A. K. The rate of exchange of tritiated water across the human red cell membrane. *J. Gen. Physiol.* **41,** 259–277 (1957).

72. Vieira, F. L., Sha'afi, R. I. & Solomon, A. K. The state of water in human and dog red cell membranes. *J. Gen. Physiol.* **55,** 451–466 (1970).

73. Whittembury, G. Ion and Water Transport in the Proximal Tubules of the Kidney of Necturus maculosus. *J. Gen. Physiol.* **43,** 43–56 (1960).

74. Sidel, V. W. & Solomon, A. K. Entrance of water into human red cells under an osmotic pressure gradient. *J. Gen. Physiol.* **41,** 243–257 (1957).

75. Finkelstein, A. & Felix, B. in *Current Topics in Membranes and Transport - Volume 21 - Ion Channels: Molecular and psysiological aspects* 295–308 (Academic Press, 1984).

76. Moura, T. F., Macey, R. I., Chien, D. Y., Karan, D. & Santos, H. Thermodynamics of all-or-none water channel closure in red cells. *J. Membr. Biol.* **81,** 105–11 (1984).

77. Gorin, M. B., Yancey, S. B., Cline, J., Revel, J.-P. & Horwitz, J. The major intrinsic protein (MIP) of the bovine lens fiber membrane: Characterization and structure based on cDNA cloning. *Cell* **39,** 49–59 (1984).

78. Preston, G., Carroll, T., Guggino, W. & Agre, P. Appearance of water channels in Xenopus oocytes expressing red cell CHIP28 protein. *Science (80-. ).* **256,** 385–7 (1992).

79. Denker, B. M., Smith, B. L., Kuhajda, P. & Agre, P. Identification , Purification , and Partial Characterization of a Novel Mr 28 , 000 Integral Membrane Protein from Erythrocytes and Renal Tubules *. *J. Biol. Chem.* **263,** 15634–15642 (1988).

80. Tani, K. & Fujiyoshi, Y. Water channel structures analysed by electron crystallography. *Biochim. Biophys. Acta* **1840,** 1605–13 (2014).

81. Tanghe, A., Van Dijck, P. & Thevelein, J. M. Why do microorganisms have aquaporins? *Trends Microbiol.* **14,** 78–85 (2006).

82. Soveral, G., Prista, C., Moura, T. F. & Loureiro-Dias, M. C. Yeast water channels: an overview of orthodox aquaporins. *Biol. Cell* **103,** 35–54 (2010).

83. Maurels, C., Reizer, J., Schroeder, J. I., Chrispeels, J. & Milton, H. Functional Characterization of the Escherichia coli Glycerol Facilitator , GlpF , in Xenopus Oocytes. *J. Biol. Chemestry* **269,** 11869–11872 (1994).

84. Calamita, G., Bishai, W. R., Preston, G. M., Guggino, W. B. & Agre, P. Molecular Cloning and Characterization of AqpZ, a Water Channel from Escherichia coli. *J. Biol. Chem.* **270,** 29063–29066 (1995).

85. Johanson, U. *et al.* The complete set of genes encoding major intrinsic proteins in Arabidopsis provides a framework for a new nomenclature for major intrinsic proteins in plants. *Plant Physiol.* **126,** 1358–69 (2001).

86. Rojek, A., Praetorius, J., Frøkiaer, J., Nielsen, S. & Fenton, R. A. A current view of the mammalian aquaglyceroporins. *Annu. Rev. Physiol.* **70,** 301–27 (2008).

87. Wu, B. & Beitz, E. Aquaporins with selectivity for unconventional permeants. *Cell. Mol. Life Sci.* **64,** 2413–21 (2007).

88. Gorelick, D. a, Praetorius, J., Tsunenari, T., Nielsen, S. & Agre, P. Aquaporin-11: a channel protein lacking apparent transport function expressed in brain. *BMC Biochem.* **7,** 14 (2006).

89. Ishibashi, K. *et al.* Molecular cloning and expression of a member of the aquaporin family with permeability to glycerol and urea in addition to water expressed at the basolateral membrane of kidney collecting duct cells. *Proc. Natl. Acad. Sci. U. S. A.* **91,** 6269–73 (1994).

90. Ishibashi, K. *et al.* Cloning and Functional Expression of a New Water Channel Abundantly Expressed in the Testis Permeable to Water, Glycerol, and Urea. *J. Biol. Chem.* **272,** 20782–20786 (1997).

91. Ko, S. B. *et al.* Cloning and functional expression of rAOP9L a new member of aquaporin family from rat liver. *Biochem. Mol. Biol. Int.* **47,** 309–18 (1999).

92. Ishibashi, K., Morinaga, T., Kuwahara, M., Sasaki, S. & Imai, M. Cloning and identification of a new member of water channel (AQP10) as an aquaglyceroporin. *Biochim. Biophys. Acta - Gene Struct. Expr.* **1576,** 335–340 (2002).

93. Liu, Z. *et al.* Arsenite transport by mammalian aquaglyceroporins AQP7 and AQP9. *Proc. Natl. Acad. Sci. U. S. A.* **99,** 6053–8 (2002).

94. Tsukaguchi, H. *et al.* Molecular Characterization of a Broad Selectivity Neutral Solute Channel. *J. Biol. Chem.* **273,** 24737–24743 (1998).

95. Yasui, M. *et al.* Rapid gating and anion permeability of an intracellular aquaporin. *Nature* **402,** 184–7 (1999).

96. Ikeda, M. *et al.* Characterization of aquaporin-6 as a nitrate channel in mammalian cells. Requirement of pore-lining residue threonine 63. *J. Biol. Chem.* **277,** 39873–9 (2002).

97. Miller, E. W., Dickinson, B. C. & Chang, C. J. Aquaporin-3 mediates hydrogen peroxide uptake to regulate downstream intracellular signaling. *Proc. Natl. Acad. Sci. U. S. A.* **107,** 15681–6 (2010).

98. Musa-Aziz, R., Chen, L., Pelletier, M. F. & Boron, W. F. Relative CO2/NH3 selectivities of AQP1, AQP4, AQP5, AmtB, and RhAG. *Proc. Natl. Acad. Sci. U. S. A.* **106,** 5406–11 (2009).

99. Wang, Y. & Tajkhorshid, E. Nitric oxide conduction by the brain aquaporin AQP4. *Proteins* **78,** 661–70 (2010).

100. Kaldenhoff, R., Kai, L. & Uehlein, N. Aquaporins and membrane diffusion of CO2 in living organisms. *Biochim. Biophys. Acta* **1840,** 1592–5 (2014).

101. Hub, J. S., Grubmüller, H. & de Groot, B. L. Dynamics and energetics of permeation through aquaporins. What do we learn from molecular dynamics simulations? *Handb. Exp. Pharmacol.* **190,** 57–76 (2009).

102. Murata, K. *et al.* Structural determinants of water permeation through aquaporin-1. *Nature* **407,** 599–605 (2000).

103. Lee, J. K. *et al.* Structural basis for conductance by the archaeal aquaporin AqpM at 1 . 68 Å. *Proc. Natl. Acad. Sci. U. S. A.* **102,** 18932–7 (2005).

104. Fu, D. *et al.* Structure of a Glycerol-Conducting Channel and the Basis for Its Selectivity. *Science (80-. ).* **290,** 481–486 (2000).

105. Savage, D. F., Egea, P. F., Robles-colmenares, Y., Iii, J. D. O. C. & Stroud, R. M. Architecture and Selectivity ˚ X-Ray Structure in Aquaporins 2 . 5 : A of Aquaporin Z. *PLOS Biol.* **1,** E72 (2003).

106. Fischer, G. *et al.* Crystal structure of a yeast aquaporin at 1.15 angstrom reveals a novel gating mechanism. *PLoS Biol.* **7,** e1000130 (2009).

107. Newby, Z. Crystal structure of the aquaglyceroporin PfAQP from the malarial parasite Plasmodium falciparum. *Nat. Struct. …* **15,** 619–25 (2008).

108. Törnroth-Horsefield, S. *et al.* Structural mechanism of plant aquaporin gating. *Nature* **439,** 688–94 (2006).

109. Sui, H., Han, B.-G., Lee, J. K., Walian, P. & Jap, B. K. Structural basis of water-specific transport through the AQP1 water channel. *Nature* **414,** 872–8 (2001).

110. Harries, W. E. C., Akhavan, D., Miercke, L. J. W., Khademi, S. & Stroud, R. M. The channel architecture of aquaporin 0 at a 2 . 2-Å resolution. *Proc. Natl. Acad. Sci. U. S. A.* **101,** 14045–14050 (2004).

111. Gonen, T. *et al.* Lipid-protein interactions in double-layered two-dimensional AQP0 crystals. *Nature* **438,** 633–638 (2006).

112. Fellert, M. *et al.* High-resolution x-ray structure of human aquaporin 5. *Proc. Natl. Acad. Sci. U. S. A.* **105,** 13327–32 (2008).

113. Smith, B. L. & Agre, P. Erythrocyte Mr 28,000 transmembrane protein exists as a multisubunit oligomer similar to channel proteins. *J. Biol. Chem.* **266,** 6407–15 (1991).

114. Preston, G. M., Jung, J. S., Gugginoll, W. B. & Agre, P. The mercury-sensitive residue at cysteine 189 in the CHIP28 water channel. *J. Biol. Chem.* **268,** 17–20 (1993).

115. Jung, J. S., Preston, G. M., Smith, B. L., Guggino, W. B. & Agre, P. Molecular structure of the water channel through aquaporin CHIP. The hourglass model. *J. Biol. Chem.* **269,** 14648–14654 (1994).

116. Soveral, G., Trincão, J. & Moura, T. F. in *Canal BQ Nº8 - Biomembranes and transport (Journal of the Portiguese Biochemical Society)* **8,** 36–43 (2011).

117. Wang, Y., Cohen, J., Boron, W. F., Schulten, K. & Tajkhorshid, E. Exploring gas permeability of cellular membranes and membrane channels with molecular dynamics. *J. Struct. Biol.* **157,** 534–44 (2007).

118. Hub, J. S. & de Groot, B. L. Mechanism of selectivity in aquaporins and aquaglyceroporins. *Proc. Natl. Acad. Sci. U. S. A.* **105,** 1198–203 (2008).

119. Yool, A. J. & Weinstein, A. M. New Roles for Old Holes : Ion Channel Function in Aquaporin-1. *News Physiol. Sci.* **17,** 68–72 (2002).

120. Boassa, D., Stamer, W. D. & Yool, A. J. Ion channel function of aquaporin-1 natively expressed in choroid plexus. *J. Neurosci.* **26,** 7811–9 (2006).

121. Ishibashi, K., Hara, S. & Kondo, S. Aquaporin water channels in mammals. *Clin. Exp. Nephrol.* **13,** 107–17 (2009).

122. Preston, G. M. & Agre, P. Isolation of the cDNA for erythrocyte integral membrane protein of 28 kilodaltons : Member of an ancient channel family. *Proc. Natl. Acad. Sci. U. S. A.* **88,** 11110–11114 (1991).

123. Walz, T., Fujiyoshi, Y. & Engel, A. The AQP structure and functional implications. *Handb. Exp. Pharmacol.* 31–56 (2009). doi:10.1007/978-3-540-79885-9_2

124. De Groot, B. L., Frigato, T., Helms, V. & Grubmüller, H. The Mechanism of Proton Exclusion in the Aquaporin-1 Water Channel. *J. Mol. Biol.* **333,** 279–293 (2003).

125. Mitsuoka, K. *et al.* The Structure of Aquaporin-1 at 4.5-Å Resolution Reveals Short α-Helices in the Center of the Monomer. *J. Struct. Biol.* **128,** 34–43 (1999).

126. Preston, G. M., Jungh, J. S., Gugginoll, W. B. & Agres, P. Membrane topology of aquaporin CHIP. Analysis of functional epitope-scanning mutants by vectorial proteolysis. *J. Biol. Chem.* **269,** 1668–1673 (1994).

127. De Groot, B. L. & Grubmüller, H. Water permeation across biological membranes: mechanism and dynamics of aquaporin-1 and GlpF. *Science (80-. ).* **294,** 2353–7 (2001).

128. Burykin, A. & Warshel, A. What Really Prevents Proton Transport through Aquaporin ? Charge Self-Energy versus Proton Wire Proposals. *Biophys. J.* **85,** 3696–3706 (2003).

129. Kato, M., Pisliakov, A. V. & Warshel, A. The barrier for proton transport in aquaporins as a challenge for electrostatic models: the role of protein relaxation in mutational calculations. *Proteins* **64,** 829–44 (2006).

130. Tajkhorshid, E. *et al.* Control of the selectivity of the aquaporin water channel family by global orientational tuning. *Science (80-. ).* **296,** 525–30 (2002).

131. Borgnia, M. J. & Agre, P. Reconstitution and functional comparison of purified GlpF and AqpZ, the glycerol and water channels from Escherichia coli. *Proc. Natl. Acad. Sci. U. S. A.* **98,** 2888–93 (2001).

132. Savage, D. F. & Stroud, R. M. Structural basis of aquaporin inhibition by mercury. *J. Mol. Biol.* **368,** 607–17 (2007).

133. Wang, Y., Schulten, K. & Tajkhorshid, E. What makes an aquaporin a glycerol channel? A comparative study of AqpZ and GlpF. *Structure* **13,** 1107–18 (2005).

134. Jensen, M. Ø., Park, S., Tajkhorshid, E. & Schulten, K. Energetics of glycerol conduction through aquaglyceroporin GlpF. *Proc. Natl. Acad. Sci. U. S. A.* **99,** 6731–6 (2002).

135. Törnroth-Horsefield, S., Hedfalk, K., Fischer, G., Lindkvist-Petersson, K. & Neutze, R. Structural insights into eukaryotic aquaporin regulation. *FEBS Lett.* **584,** 2580–2588 (2010).

136. Alleva, K., Chara, O. & Amodeo, G. Aquaporins: another piece in the osmotic puzzle. *FEBS Lett.* **586,** 2991–9 (2012).

137. Soveral, G., Madeira, A., Loureiro-Dias, M. C. & Moura, T. F. Membrane tension regulates water transport in yeast. *Biochim. Biophys. Acta* **1778,** 2573–9 (2008).

138. Ozu, M., Dorr, R. a, Gutiérrez, F., Politi, M. T. & Toriano, R. Human AQP1 is a constitutively open channel that closes by a membrane-tension-mediated mechanism. *Biophys. J.* **104,** 85–95 (2013).

139. Soveral, G., Macey, R. I. & Moura, T. F. Membrane stress causes inhibition of water channels in brush border membrane vesicles from kidney proximal tubule. *Biol. cell* **89,** 275–82 (1997).

140. Hedfalk, K. *et al.* Aquaporin gating. *Curr. Opin. Struct. Biol.* **16,** 447–56 (2006).

141. Gonen, T., Sliz, P., Kistler, J., Cheng, Y. & Walz, T. Aquaporin-0 membrane junctions reveal the structure of a closed water pore. *Nature* **429,** 193–7 (2004).

142. Kortenoeven, M. L. A. & Fenton, R. A. Renal aquaporins and water balance disorders. *Biochim. Biophys. Acta* **1840,** 1533–49 (2014).

143. Badaut, J., Fukuda, A. M., Jullienne, A. & Petry, K. G. Aquaporin and brain diseases. *Biochim. Biophys. Acta* **1840,** 1554–65 (2014).

144. Delporte, C. Aquaporins in salivary glands and pancreas. *Biochim. Biophys. Acta* **1840,** 1524–32 (2014).

145. Boury-Jamot, M. *et al.* Skin aquaporins: function in hydration, wound healing, and skin epidermis homeostasis. *Handb. Exp. Pharmacol.* 205–17 (2009). doi:10.1007/978-3-540-79885-9_10

146. Papadopoulos, M. C. & Saadoun, S. Key roles of aquaporins in tumor biology. *Biochim. Biophys. Acta* (2014). doi:10.1016/j.bbamem.2014.09.001

147. Hara, M. & Verkman, A. S. Glycerol replacement corrects defective skin hydration, elasticity, and barrier function in aquaporin-3-deficient mice. *Proc. Natl. Acad. Sci. U. S. A.* **100,** 7360–5 (2003).

148. Ma, T., Hara, M., Sougrat, R., Verbavatz, J.-M. & Verkman, a S. Impaired stratum corneum hydration in mice lacking epidermal water channel aquaporin-3. *J. Biol. Chem.* **277,** 17147–53 (2002).

149. Hara-Chikuma, M. & Verkman, a S. Aquaporin-3 facilitates epidermal cell migration and proliferation during wound healing. *J. Mol. Med. (Berl).* **86,** 221–31 (2008).

150. Kang, S. K. *et al.* Role of human aquaporin 5 in colorectal carcinogenesis. *Am. J. Pathol.* **173,** 518–25 (2008).

151. Zhang, Z. *et al.* Expression of aquaporin 5 increases proliferation and metastasis potential of lung cancer. *J. Pathol.* **221,** 210–20 (2010).

152. Lebeck, J. Metabolic impact of the glycerol channels AQP7 and AQP9 in adipose tissue and liver. *J. Mol. Endocrinol.* **52,** R165–78 (2014).

153. Verkman, a S. Aquaporins: translating bench research to human disease. *J. Exp. Biol.* **212,** 1707–15 (2009).

154. Huber, V. J., Tsujita, M. & Nakada, T. Aquaporins in drug discovery and pharmacotherapy. *Mol. Aspects Med.* **33,** 691–703 (2012).

155. De Almeida, A., Soveral, G. & Casini, A. Gold compounds as aquaporin inhibitors: new opportunities for therapy and imaging. *Med. Chem. Commun* **5,** 1444–1453 (2014).

156. Ishibashi, K. *et al.* Immunolocalization and effect of dehydration on AQP3, a basolateral water channel of kidney collecting ducts. *Am. J. Physiol.* **272,** F235–41 (1997).

157. Murillo-Carretero, M. I., Ilundáin, A. A. & Echevarria, M. Regulation of aquaporin mRNA expression in rat kidney by water intake. *J. Am. Soc. Nephrol.* **10,** 696–703 (1999).

158. Ma, T. *et al.* Nephrogenic diabetes insipidus in mice lacking aquaporin-3 water channels. *Proc. Natl. Acad. Sci. U. S. A.* **97,** 4386–91 (2000).

159. Niu, D. *et al.* Expression of aquaporin3 in human neoplastic tissues. *Histopathology* **61,** 543–551 (2012).

160. Hara-Chikuma, M. & Verkman, a S. Prevention of skin tumorigenesis and impairment of epidermal cell proliferation by targeted aquaporin-3 gene disruption. *Mol. Cell. Biol.* **28,** 326–32 (2008).

161. Verkman, A. S. A cautionary note on cosmetics containing ingredients that increase aquaporin-3 expression. *Exp. Dermatol.* **17,** 871–2 (2008).

162. Hamann, S. *et al.* Aquaporins in complex tissues: distribution of aquaporins 1-5 in human and rat eye. *Am. J. Physiol.* **274,** C1332–45 (1998).

163. Karasawa, K. *et al.* Patterns of aquaporin expression in the canine eye. *Vet. J.* **190,** e72–7 (2011).

164. Levin, M. H. & Verkman, a S. Aquaporin-3-dependent cell migration and proliferation during corneal re-epithelialization. *Invest. Ophthalmol. Vis. Sci.* **47,** 4365–72 (2006).

165. Schey, K. L., Wang, Z., L Wenke, J. & Qi, Y. Aquaporins in the eye: expression, function, and roles in ocular disease. *Biochim. Biophys. Acta* **1840,** 1513–23 (2014).

166. Fischbarg, J. Water channels and their roles in some ocular tissues. *Mol. Aspects Med.* **33,** 638–41 (2012).

167. Moore, M., Ma, T., Yang, B. & Verkman, A. S. Tear secretion by lacrimal glands in transgenic mice lacking water channels AQP1, AQP3, AQP4 and AQP5. *Exp. Eye Res.* **70,** 557–62 (2000).

168. Tsubota, K., Hirai, S., King, L. S., Agre, P. & Ishida, N. Defective cellular trafficking of lacrimal gland aquaporin-5 in Sjögren's syndrome. *Lancet* **357,** 688–9 (2001).

169. Hara-Chikuma, M. *et al.* Chemokine-dependent T cell migration requires aquaporin-3-mediated hydrogen peroxide uptake. *J. Exp. Med.* **209,** 1743–52 (2012).

170. Guttman-Yassky, E., Nograles, K. E. & Krueger, J. G. Contrasting pathogenesis of atopic dermatitis and psoriasis--part I: clinical and pathologic concepts. *J. Allergy Clin. Immunol.* **127,** 1110–8 (2011).

171. Zhu, N. *et al.* Defective macrophage function in aquaporin-3 deficiency. *FASEB J.* **25,** 4233–9 (2011).

172. Ikarashi, N. The elucidation of the function and the expression control mechanism of aquaporin-3 in the colon. *Yakugaku Zasshi* **133,** 955–61 (2013).

173. Thiagarajah, J. R., Zhao, D. & Verkman, a S. Impaired enterocyte proliferation in aquaporin-3 deficiency in mouse models of colitis. *Gut* **56,** 1529–35 (2007).

174. Roudier, N. Evidence for the Presence of Aquaporin-3 in Human Red Blood Cells. *J. Biol. Chem.* **273,** 8407–8412 (1998).

175. Liu, Y. *et al.* Aquaporin 9 is the major pathway for glycerol uptake by mouse erythrocytes, with implications for malarial virulence. *Proc. Natl. Acad. Sci. U. S. A.* **104,** 12560–4 (2007).

176. Guo, X. *et al.* Prognostic value of combined aquaporin 3 and aquaporin 5 overexpression in hepatocellular carcinoma. *Biomed Res. Int.* **2013,** 206525 (2013).

177. Liu, S., Zhang, S., Jiang, H., Yang, Y. & Jiang, Y. Co-expression of AQP3 and AQP5 in esophageal squamous cell carcinoma correlates with aggressive tumor progression and poor prognosis. *Med. Oncol.* **30,** 636 (2013).

178. Kafé, H., Verbavatz, J.-M., Cochand-Priollet, B., Castagnet, P. & Vieillefond, A. Collecting duct carcinoma: an entity to be redefined? *Virchows Arch.* **445,** 637–40 (2004).

179. Macey, R. L. & Farmer, R. E. L. Inhibition of water and solute permeability in human red cells. *Biochim. Biophys. Acta - Biomembr.* **211,** 104–106 (1970).

180. Tissues, W. Molecular cloning of a mercurial-insensitive water channel expressed in selected water-transporting tissues. *J. Biol. Chem.* **269,** 5497–500 (1994).

181. Hirano, Y. *et al.* Molecular mechanisms of how mercury inhibits water permeation through aquaporin-1: understanding by molecular dynamics simulation. *Biophys. J.* **98,** 1512–9 (2010).

182. Niemietz, C. C. M. & Tyerman, S. D. S. New potent inhibitors of aquaporins : silver and gold compounds inhibit aquaporins of plant and human origin. *FEBS Lett.* **531,** 443–447 (2002).

183. Yukutake, Y., Hirano, Y., Suematsu, M. & Yasui, M. Rapid and reversible inhibition of aquaporin-4 by zinc. *Biochemistry* **48,** 12059–61 (2009).

184. Brooks, H. L., Regan, J. W. & Yool, A. J. Inhibition of aquaporin-1 water permeability by tetraethylammonium : involvement of the loop E pore region. *Mol. Pharmacol.* **57,** 1021–1026 (2000).

185. Detmers, F. J. M. *et al.* Quaternary ammonium compounds as water channel blockers. Specificity, potency, and site of action. *J. Biol. Chem.* **281,** 14207–14 (2006).

186. Yang, B., Kim, J. K. & Verkman, A. S. Comparative efficacy of HgCl2 with candidate aquaporin-1 inhibitors DMSO, gold, TEA+ and acetazolamide. *FEBS Lett.* **580,** 6679–6684 (2006).

187. Søgaard, R. & Zeuthen, T. Test of blockers of AQP1 water permeability by a high-resolution method: no effects of tetraethylammonium ions or acetazolamide. *Pflugers Arch.* **456,** 285–92 (2008).

188. Ma, B. *et al.* Effects of acetazolamide and anordiol on osmotic water permeability in AQP1-cRNA injected Xenopus oocyte. *Acta Pharmacol. Sin.* **25,** 90–97 (2004).

189. Gao, J. *et al.* Acetazolamide inhibits osmotic water permeability by interaction with aquaporin-1. *Anal. Biochem.* **350,** 165–70 (2006).

190. Tanimura, Y., Hiroaki, Y. & Fujiyoshi, Y. Acetazolamide reversibly inhibits water conduction by aquaporin-4. *J. Struct. Biol.* **166,** 16–21 (2009).

191. Huber, V. J., Tsujita, M., Yamazaki, M., Sakimura, K. & Nakada, T. Identification of arylsulfonamides as Aquaporin 4 inhibitors. *Bioorg. Med. Chem. Lett.* **17,** 1270–3 (2007).

192. Huber, V. J., Tsujita, M., Kwee, I. L. & Nakada, T. Inhibition of aquaporin 4 by antiepileptic drugs. *Bioorg. Med. Chem.* **17,** 418–24 (2009).

193. Yang, B., Zhang, H. & Verkman, A. S. Lack of aquaporin-4 water transport inhibition by antiepileptics and arylsulfonamides. *Bioorg. Med. Chem.* **16,** 7489–93 (2008).

194. Migliati, E. *et al.* Inhibition of Aquaporin-1 and Aquaporin-4 Water Permeability by a Derivative of the Loop Diuretic Bumetanide Acting at an Internal Pore-Occluding Binding Site. *Mol. Pharmacol.* **76,** 105–112 (2009).

195. Ozu, M., Dorr, R. A., Politi, M. T., Parisi, M. & Toriano, R. Water flux through human aquaporin 1: inhibition by intracellular furosemide and maximal response with high osmotic gradients. *Eur. Biophys. J.* **40,** 737–746 (2011).

196. Yool, A. J. *et al.* AqF026 is a pharmacologic agonist of the water channel aquaporin-1. *J. Am. Soc. Nephrol.* **24,** 1045–52 (2013).

197. Hinson, S. R. *et al.* Molecular outcomes of neuromyelitis optica (NMO)-IgG binding to aquaporin-4 in astrocytes. *Proc. Natl. Acad. Sci. U. S. A.* **109,** 1245–50 (2012).

198. Rossi, A., Ratelade, J., Papadopoulos, M. C., Bennett, J. L. & Verkman, A. S. Neuromyelitis Optica IgG Does Not Alter Aquaporin-4 Water Permeability, Plasma Membrane M1/M23 Isoform Content, or Supramolecular Assembly. *Glia* **60,** 2027–2039 (2013).

199. Nicchia, G. P. *et al.* Aquaporin-4 orthogonal arrays of particles are the target for neuromyelitis optica autoantibodies. *Glia* **57,** 1363–73 (2009).

200. Huber, V. J., Tsujita, M. & Nakada, T. Identification of aquaporin 4 inhibitors using in vitro and in silico methods. *Bioorg. Med. Chem.* **17,** 411–7 (2009).

201. Igarashi, H., Huber, V. J., Tsujita, M. & Nakada, T. Pretreatment with a novel aquaporin 4 inhibitor, TGN-020, significantly reduces ischemic cerebral edema. *Neurol. Sci.* **32,** 113–6 (2011).

202. Nakamura, Y. *et al.* Development of a Novel Ligand, [C]TGN-020, for Aquaporin 4 Positron Emission Tomography Imaging. *ACS Chem. Neurosci.* **2,** 568–571 (2011).

203. Seeliger, D. *et al.* Discovery of novel human aquaporin-1 blockers. *ACS Chem. Biol.* **8,** 249–56 (2013).

204. Mola, M. G., Nicchia, G. P., Svelto, M., Spray, D. C. & Frigeri, A. Automated cell-based assay for screening of aquaporin inhibitors. *Anal. Chem.* **81,** 8219–8229 (2010).

205. Haddoub, R., Rützler, M., Robin, A. & Flitsch, S. L. Design, synthesis and assaying of potential aquaporin inhibitors. *Handb. Exp. Pharmacol.* 385–402 (2009). doi:10.1007/978-3-540-79885-9_19

206. Jelen, S. *et al.* Aquaporin-9 protein is the primary route of hepatocyte glycerol uptake for glycerol gluconeogenesis in mice. *J. Biol. Chem.* **286,** 44319–25 (2011).

207. Gomes, D. *et al.* Aquaporins are multifunctional water and solute transporters highly divergent in living organisms. *Biochim. Biophys. Acta* **1788,** 1213–28 (2009).

208. Danielson, J. A. & Johanson, U. Unexpected complexity of the aquaporin gene family in the moss Physcomitrella patens. *BMC Plant Biol.* **8,** 45 (2008).

209. Johanson, U. & Gustavsson, S. A New Subfamily of Major Intrinsic Proteins in Plants. *Mol. Biol. Evol.* **19,** 456–461 (2000).

210. Wallace, I. S. & Roberts, D. M. Homology Modeling of Representative Subfamilies of Arabidopsis Major Intrinsic Proteins . Classification Based on the Aromatic / Arginine Selectivity Filter. *Plant Physiol.* **135,** 1059–1068 (2004).

211. Wudick, M. M., Luu, D.-T. & Maurel, C. A look inside: localization patterns and functions of intracellular plant aquaporins. *New Phytol.* **184,** 289–302 (2009).

212. Hove, R. M. & Bhave, M. Plant aquaporins with non-aqua functions: deciphering the signature sequences. *Plant Mol. Biol.* **75,** 413–30 (2011).

213. Maurel, C., Verdoucq, L., Luu, D.-T. & Santoni, V. Plant aquaporins: membrane channels with multiple integrated functions. *Annu. Rev. Plant Biol.* **59,** 595–624 (2008).

214. Maurel, C. & Chrispeels, M. J. Aquaporins . A Molecular Entry into Plant Water Relations. *Plant Physiol.* **125,** 135–138 (2001).

215. Chaumont, F., Moshelion, M. & Daniels, M. J. Regulation of plant aquaporin activity. *Biol. Cell* **97,** 749–64 (2005).

216. Outeiro, T. F. & Giorgini, F. Yeast as a drug discovery platform in Huntington's and Parkinson's diseases. *Biotechnol. J.* **1,** 258–69 (2006).

217. Pettersson, N., Hagström, J., Bill, R. M. & Hohmann, S. Expression of heterologous aquaporins for functional analysis in Saccharomyces cerevisiae. *Curr. Genet.* **50,** 247–55 (2006).

218. Shinbo, I. *et al.* Functional analysis of aquaporin-2 mutants associated with nephrogenic diabetes insipidus by yeast expression. *Am. J. Physiol.* **277,** F734–41 (1999).

219. Delamarche, C. *et al.* Visualization of AqpZ-mediated water permeability in Escherichia coli by cryoelectron microscopy. (1999).

220. Soveral, G., Madeira, A., Loureiro-Dias, M. C. & Moura, T. F. Water transport in intact yeast cells as assessed by fluorescence self-quenching. *Appl. Environ. Microbiol.* **73,** 2341–3 (2007).

221. Madeira, A. *et al.* Effect of ethanol on fluxes of water and protons across the plasma membrane of Saccharomyces cerevisiae. *FEMS Yeast Res.* **10,** 252–8 (2010).

222. Dobbs, L. G. *et al.* Highly water-permeable type I alveolar epithelial cells confer high water permeability between the airspace and vasculature in rat lung. *Proc. Natl. Acad. Sci. U. S. A.* 95, 2991–6 (1998).

223. Coury, L. A. *et al.* Water transport across yeast vacuolar and plasma membrane-targeted secretory vesicles occurs by passive diffusion. *J. Bacteriol.* 181, 4437–40 (1999).

224. Calamita, G. *et al.* The inner mitochondrial membrane has aquaporin-8 water channels and is highly permeable to water. *J. Biol. Chem.* 280, 17149–53 (2005).

225. Mollajew, R. *et al.* Routes of epithelial water flow: aquaporins versus cotransporters. *Biophys. J.* 99, 3647–56 (2010).

226. Soveral, G., Macey, R. I. & Moura, T. F. Water permeability of brush border membrane vesicles from kidney proximal tubule. *J. Membr. Biol.* 158, 219–28 (1997).

227. Martins, S. V *et al.* Serum adipokine profile and fatty acid composition of adipose tissues are affected by conjugated linoleic acid and saturated fat diets in obese Zucker rats. *Br. J. Nutr.* 103, 869–78 (2010).

228. Park, Y. & Pariza, M. W. Mechanisms of body fat modulation by conjugated linoleic acid (CLA). *Food Res. Int.* 40, 311–323 (2007).

229. Wachira, A. M. *et al.* Effects of dietary fat source and breed on the carcass composition, n-3 polyunsaturated fatty acid and conjugated linoleic acid content of sheep meat and adipose tissue. *Br. J. Nutr.* 88, 697–709 (2002).

230. Sarkkinen, E. S., Agren, J. J., Ahola, I., Ovaskainen, M. L. & Uusitupa, M. I. Fatty acid composition of serum cholesterol esters, and erythrocyte and platelet membranes as indicators of long-term adherence to fat-modified diets. *Am. J. Clin. Nutr.* 59, 364–70 (1994).

231. Oresic, M., Hänninen, V. A. & Vidal-Puig, A. Lipidomics: a new window to biomedical frontiers. *Trends Biotechnol.* 26, 647–52 (2008).

232. Serna, A. *et al.* Functional inhibition of aquaporin-3 with a gold-based compound induces blockage of cell proliferation. *J. Cell. Physiol.* 229, 1787–801 (2014).

# Acknowledgments

Esta tese não seria possível sem o esforço e dedicação destas e muitas outras pessoas que, de diversas formas, permitiram que chega-se até aqui com um sentimento imenso de realização e prazer pessoais. Assim quero agradecer:

This thesis would not be possible without the efforts and dedication of many other people that, in several ways, allowed me to reach this point of my life with an immense sense of achievement and personal pleasure. So I want to thank:

À Faculdade de Ciências e Tecnologia da Universidade Nova de Lisboa, a minha primeira casa, onde grande parte deste trabalho foi realizado.

À Faculdade de Farmácia da Universidade de Lisboa que tão bem me acolheu nestes últimos dois anos e por todos os meios materiais e humanos que têm permitido dar continuidade ao meu trabalho.

Ao Instituto Superior de Agronomia da Universidade de Lisboa que me acolheu durante boa parte deste período.

À Paula Lopes e Susana Martins da Faculdade de Medicina Veterinária da Universidade de Lisboa pela importante colaboração no capítulo 1 deste trabalho e pela pronta disponibilidade sempre que foi necessário tirar dúvidas e discutir resultados ou para qualquer outro assunto relacionado com este trabalho.

Ao Nuno Santos do Instituto de Medicina Molecular onde foram realizados os estudos de fluidez apresentados no capítulo 1 desta tese, obrigada por me ter acolhido e proporcionado todos os meios para a realização destes ensaios.

To Angela Casini from University of Groningen for her pivotal role in chapter 2 of this thesis, for her dynamism and focus during laboratorial work and for her joviality and excellent mood.

Ao Henrique Noronha e ao Hernâni Gerós da Escola de Ciências da Universidade do Minho pela importante colaboração para o trabalho apresentado no capítulo 3.

To Farzana Sabir from Institute of Agronomy from University of Lisbon for carrying out important part of the work presented in chapter 3, for friendship and for the unforgettable moments spent at the lab.

Á professora Mané do Instituto Superior de agronomia por me ter acolhido no seu grupo e proporcionado todos os meios necessários à realização do meu trabalho.

À Catarina Prista minha co-orientadora, por todo o acompanhamento durante o trabalho realizado no Instituto Superior de Agronomia, pela pronta disponibilidade na supervisão do trabalho e por me ter proporcionado todos os meios necessários à realização do mesmo.

Às professoras Teresa Moura e Graça Soveral, tantos agradecimentos. Em primeiro lugar por me terem acolhido no seio do vosso grupo, pelos conselhos mas acima de tudo por todo o apoio que me têm dado ao longo destes anos e que por vezes transcende largamente qualquer espectativa que se possa ter em relação a um orientador, o meu sincero obrigada.

À professora Graça Soveral, minha orientadora ao longo destes anos, um agradecimento especial pelo papel decisivo que teve em todo este trabalho, e ainda um agradecimento muito pessoal, por todo o apoio, dinamismo, oportunidades, amizade, confiança, por me aturar e tantas outras coisas que não caberiam aqui.

To my colleagues at the Institute of Agronomy from University of Lisbon, whom I miss so much, Madalena, Sara, Maria Jose, Tiago and Farzana. Thank you all for friendship, empathy, companionship, madness and for sharing with me simple moments, but ones I keep among the best of my life.

Aos meus colegas do Instituto Superior de Agronomia, de quem tenho tantas saudades, Madalena, Sara, Maria José, Tiago e Farzana. Obrigada a todos pela amizade, empatia, companheirismo, loucura, e por terem partilhado comigo momentos simples mas que guardo como uns dos melhores da minha vida.

Aos meus colegas de grupo na Faculdade de Farmácia, um beijinho muito especial a todas, à Ana que me acompanha há tantos anos, à Cláudia e à Andreia, um obrigada pela amizade, bom ambiente, companheirismo e boa disposição.

À D. Graça e ao Sr. António por todo o apoio durante o período de redação desta tese e sem o qual teria sido impossível escrevela.

Ao Rui, um beijo cheio de carinho, obrigada pela revisão de partes desta tese, pelo carro ;) (quando é que vais outra vez?) e claro! pela Inês e pela Beatriz ☺.

E finalmente à minha família, pelo apoio incondicional ao longo da minha vida e que me permitiu chegar até aqui. Ao meu pai por toda a ajuda que mesmo de longe tem proporcionado. À minha mãe um obrigada muito especial pelo apoio e disponibilidade incondicional, sem ela nada disto seria possível. À minha querida avó por todo o apoio, amor e ajuda que tem dado ao longo destes anos e que continua a ser importante. E finalmente aos meus queridos filhos, Hugo, Inês e Beatriz, obrigada por darem um sentido especial à vida ☺. Um obrigada especial ao Hugo por toda a paciência e concessões que teve de fazer ao longo destes anos e sem as quais também não me teria sido possível chegar aqui.

Obrigado ainda a todos aqueles que de alguma forma contribuíram para a realização deste trabalho mas que não figuram nesta lista de agradecimentos pelo simples facto ser impossível enumera-los a todos. Bem hajam.